Removal of herbicides using hybrid membrane technologies

Zur Erlangung des akademischen Grades einer
DOKTORIN DER INGENIEURWISSENSCHAFTEN

von der KIT-Fakultät für Chemieingenieurwesen und Verfahrenstechnik des
Karlsruher Instituts für Technologie (KIT)
genehmigte

DISSERTATION

von

Phuong Bich Trinh, M.Sc.
aus Hanoi, Vietnam

Tag der mündlichen Prüfung: 27.03.2026

Erstgutachterin: Prof. Dr. Andrea Iris Schäfer

Zweitgutachter: Prof. Dr. Graham Gagnon

“Science should not be about faith, but about questioning cherished beliefs.”

John Gribbin, *Seven pillars of science*

Kurzfassung

Glyphosat (GLY) ist das weltweit am häufigsten verwendeten Herbizid, und Aminomethylphosphonsäure (AMPA) ist sein Hauptmetabolit. Ihr Vorkommen in Grund- und Oberflächengewässern verursacht Krankheiten beim Menschen, während komplexe physikalisch-chemische Eigenschaften die Erkennung und wirksame Entfernung erschweren. Zur Entfernung von GLY und AMPA wurden verschiedene Technologien wie Adsorption, Filtration und Abbau mit unterschiedlicher Wirksamkeit eingesetzt. Die derzeitigen Entfernungstechnologien konnten GLY und AMPA jedoch nicht effektiv und nachhaltig aus dem Wasser entfernen. Die „Effektivität" bezieht sich auf die Entfernungseffizienz der Technologien, während die „Nachhaltigkeit" sich auf die für die Wasseraufbereitung verwendete Energie und die produzierte Wassermenge bezieht. Daher ist die Entwicklung von Wasseraufbereitungstechnologien zur Entfernung von GLY und AMPA aus dem Wasser dringend erforderlich.

In dieser Dissertation wurden vier verschiedene Technologien hinsichtlich ihrer Entfernungseffizienz von GLY und AMPA untersucht. Diese Technologien sind: Adsorption durch polymerbasierte sphärische Aktivkohle (PBSAC, Kapitel 4), ein hybrides Adsorptions-Membranfiltrationssystem (Ultrafiltration mit permeatseitiger polymerbasierter kugelförmiger Aktivkohle, UF–PBSAC, Kapitel 5), Nanofiltrationsmembran (NF, Kapitel 6), und eine photokatalytische Membran (TiO_2-beschichtete Poly(vinylidenfluorid)-Membran, PVDF-TiO_2, Kapitel 7).

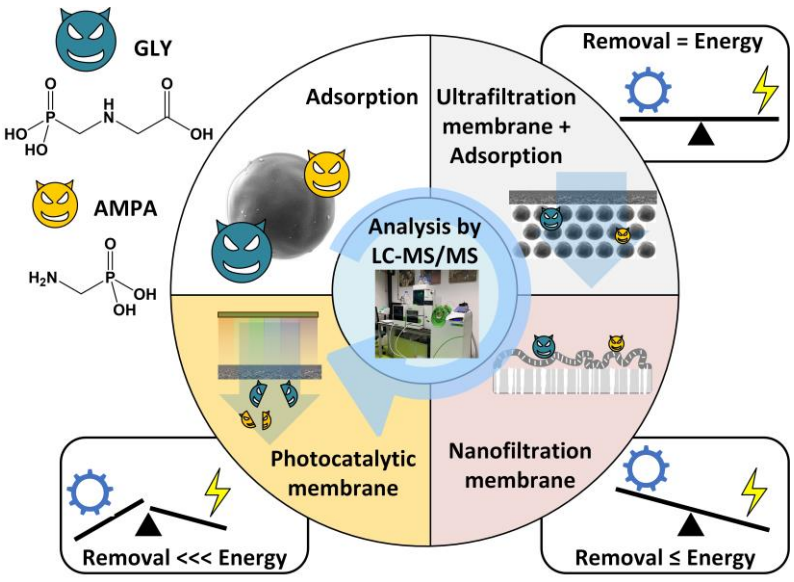

Vor der Untersuchung von Entfernungstechnologien muss die Analysemethode für GLY und AMPA in umweltrelevanten Konzentrationen entwickelt werden. Aufgrund ihrer komplexen physikalisch-chemischen Eigenschaften sind GLY und AMPA schwer zu analysieren und aus Wasser zu entfernen. Das Ziel besteht darin, GLY und AMPA in Wasser in niedri-

ger Konzentration zu analysieren, wobei ein geringes Injektionsvolumen und kein Derivatisierungsschritt erforderlich sind. Für die Analyse der beiden Herbizide wurde die Flüssigkeitschromatographie mit Tandem-Massenspektrometrie gewählt. Um eine zuverlässige Analysemethode mit reproduzierbaren Ergebnissen zu erzielen, wurde die Ionenunterdrückung auf dem LC-MS/MS bewertet. Nach einer systematischen Überprüfung hat die entwickelte Analysemethode eine Nachweisgrenze von 10 ng/L, erfordert ein Injektionsvolumen von 100 µL und keinen Derivatisierungsschritt. Die entwickelte Analysemethode wird in Kapitel 3 erläutert.

Die statische Adsorption (ohne Membran) wurde in einem Inkubatorschüttler durchgeführt, um die Adsorptionsleistung ohne Begrenzung der Verweildauer zu bestimmen. Filtrationsversuche mit NF und UF–PBSAC wurden mit einer Dead-End-Rührzelle mit einer Membranfläche von 38 cm^2 durchgeführt. Die Filtration der PVDF-TiO_2-Membran wurde in einem Mikro-Crossflow-Filtrationssystem mit einer Filtrationsfläche von 2 cm^2 unter einem Sonnensimulator in Durchflussanordnung durchgeführt.

Jede Technologie wurde hinsichtlich ihrer Entfernungseffizienz für GLY und AMPA sowie hinsichtlich der begrenzenden Faktoren für die Entfernung untersucht. Zu den begrenzenden Faktoren gehörten die Eigenschaften der Membran/des Adsorbens, die Betriebsparameter und die Wasserbedingungen. Mit dem Verständnis des Mechanismus der Technologie wurde das Experiment schließlich unter den optimierten Bedingungen zur Bewertung der Entfernung von GLY und AMPA durchgeführt. Die wichtigsten Ergebnisse dieser Dissertation sind:

- Die statische Adsorption von GLY und AMPA in umweltrelevanten Konzentrationen aus Wasser durch PBSAC war mit einer Entfernung von 95% für GLY und 57% für AMPA möglich, wobei die Außen- und Innenfläche von PBSAC den begrenzenden Faktor für die Adsorption darstellte.
- UF-PBSAC kann unter optimierten Bedingungen (Verringerung der PBSAC-Größe, Erhöhung der PBSAC-Schichtdicke und Erhöhung der hydraulischen Verweildauer) 98% GLY und 95% AMPA entfernen, wodurch die EU-Richtlinien für Herbizide erfüllt werden.
- Die NF-Membran kann GLY und AMPA durch Größenausschluss, Ladungsausschluss und dielektrische Interaktionen teilweise entfernen, erfordert jedoch einen hohen Druck.
- Die photokatalytische Membran kann unter optimierten Bedingungen (Erhöhung der hydraulischen Verweildauer, Erhöhung der Lichtintensität) 95% GLY und 80% AMPA aus Wasser entfernen, was jedoch einen hohen Energieaufwand für die Lichtbestrahlung erfordert.

Es wurde ein Vergleich zwischen verschiedenen Wasseraufbereitungstechnologien anhand der Kriterien GLY- und AMPA-Entfernungseffizienz und der Betriebsparameter durchgeführt.

Abstract

Glyphosate (GLY) is the most commonly used herbicide worldwide, and aminomethylphosphonic acid (AMPA) is its main metabolite. These herbicides in ground and surface waters cause diseases in humans, while complex physico-chemical properties hinder detection and effective removal. Several technologies have been applied to remove GLY and AMPA, including adsorption, filtration, and degradation, with varying efficiencies. However, current removal technologies cannot effectively and sustainably remove GLY and AMPA in water. In this context, the "effectiveness" refers to the removal efficiency of the technologies; meanwhile, the "sustainability" relates to the energy used in water treatment and the amount of water produced. The development of water treatment technologies for GLY and AMPA removal in water is urgently needed.

In this dissertation, four different technologies were investigated for the removal efficiency of GLY and AMPA, including: adsorption by polymer-based spherical activated carbon (PBSAC, Chapter 4), hybrid adsorption–membrane filtration system (ultrafiltration with permeate-side polymer-based spherical activated carbon, UF–PBSAC, Chapter 5), nanofiltration membrane (NF, Chapter 6), and photocatalytic membrane (TiO_2-coated poly(vinylidene fluoride) membrane, PVDF-TiO_2, Chapter 7).

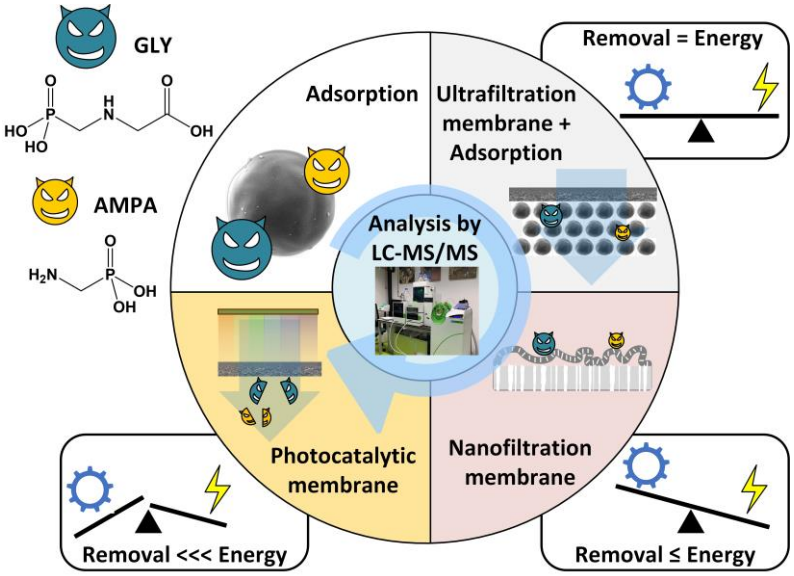

Before investigating the removal technologies, the analytical method needs to be developed for GLY and AMPA at environmentally relevant concentrations. Due to the complex physicochemical properties, GLY and AMPA are challenging to analyze and remove from water. The target is to analyze GLY and AMPA in water at low concentration, with low injection volume, and without derivatization step. Liquid chromatography with tandem mass spectrometry (LC-MS/MS) was chosen for the analysis of the two herbicides. To achieve a reliable analytical method with reproducible results, ion suppression in the LC-MS/MS was evaluated. After a

systematic review, the developed analytical method had the LOD of 10 ng/L, with the injection volume of 100 µL, and required no derivatization step. The analytical method development is explained in Chapter 3.

The static adsorption (without any membrane) was performed in an incubator shaker to determine the adsorption performance without the limitation of residence time. Filtration experiments with NF and UF–PBSAC were performed with a dead-end stirred cell with membrane area of 38 cm^2. The filtration of PVDF-TiO_2 membrane was performed in a micro-crossflow filtration system with a filtration area of 2 cm^2 under solar simulator in a flow-through configuration.

Each technology was studied on the GLY and AMPA removal efficiency, and the limiting factors on the removal. The limiting factors included membrane/ adsorbent characteristics, operational parameters, and water conditions. With the understanding of the mechanism of the technology, the experiment was finally conducted at the optimized conditions for the evaluation of GLY and AMPA removal.

The key findings from this dissertation are:

- The static adsorption of GLY and AMPA at environmentally relevant concentrations from water by PBSAC was achievable, with the removal of 95% for GLY and 57% for AMPA, where the external and internal surface of PBSAC were the limiting factors of the adsorption.
- UF–PBSAC could remove 98% GLY and 95% AMPA at optimized conditions (decreasing PBSAC size, increasing PBSAC layer thickness, and increasing hydraulic residence time), which achieved the EU guidelines for herbicides.
- NF membrane could partially remove GLY and AMPA via size exclusion, charge exclusion, and dielectric exclusion, but required high pressure.
- Photocatalytic membrane could remove 95% GLY and 80% AMPA in water at optimized conditions (increasing hydraulic residence time, increasing light irradiance), which required high energy for light irradiation.

A comparison between different water treatment technologies took place with the criteria of GLY and AMPA removal efficiency and the operating parameters.

Table of contents

Acknowledgements

First of all, I would like to send my deep gratitude to my supervisor, Professor Andrea Iris Schäfer, for the scientific knowledge that she gifted me, and for the continuous guidance, encouragement, trust, and support throughout my PhD. I have learnt a lot at work, from all meetings, discussions, to Team days, teaching courses, and conferences. I also learnt a lot about life from her. Thank you for being so patient with me and picking me up at the right time. I always said she was like a "mama" at the lab. But for me, Andrea, as a female professor, is very inspiring for my future career and for the future woman that I will become.

I would like to acknowledge my Scholarship providers, DAAD, for providing me with the funding for research under the Research Grant programme. Thank you, Anna Katharina Rusche, Natalie Bursinski, and everyone else at ST34 for granting me the scholarship and several extensions. Thank you again, Dr. Holger Finken and ST43, for selecting me for the DAAD Travel Grant to Ho Chi Minh City, Vietnam, to attend an international conference (GTSW 2019).

I am also thankful for the financial support in this dissertation: Helmholtz Recruitment Initiative for the IAMT laboratory and project funding. For the photocatalytic project, the Bundesministerium für Bildung und Forschung (BMBF) project NEMWARE is thanked for project funding of Prof. Andrea I. Schäfer (02WIL1555) in collaboration with Prof. Daniel Mandler (HUIJ, Israel) and Prof. Rafael Semiat (Technion, Israel).

I would like to thank my colleagues at IAMT. A very sincere thanks to Dr. Minh Nhat Nguyen, from my supervisor to my colleague and friend. He has given me lots of help, instructions, and comments during my PhD. He is the most trustworthy person to ask when I have a problem. Special thanks to Dr. Matteo Tagliavini, who always started our conversation with "What do you want to ask today?", for all of your knowledge on PBSAC and the filtration system. Special thanks to Dr. Youssef Amine Boussouga, Dr. Alessandra Imbrogno, Dr. Jennifer Quiros-Jimenez, Dr. Akhil Gopalakrishnan, for all of the insightful discussions on the membrane and mechanism; Dr. Siqi Liu for the great discussion and collaboration on photocatalytic membrane, and all the fun we had; Dr. Martyna Krajewska for assisting with the concentration polarization. I want to thank the fellow PhD candidates who have helped me during my PhD: Dr. Roman Lyubimenko and Dr. Camilla Raota for assisting with the analytical questions; Dr. Yang-Hui Cai, James Joseph, Mohammad Allouzi, Nurul Himma, and Hanya Lin for the scientific discussion. Thanks to Master student Harsha Philips for giving me the opportunity to learn about supervision and her contribution to the fugacity model. And everyone at IAMT is thanked for all of your support; none of you can be excluded from this acknowledgement for the various discussions and a lot of fun we had.

Special thanks to all colleagues at Perkin Elmer who have continuously supported me in solving problems, developing and adapting methods, lots of hardware replacements, and installation: Guido Lohkamp-Schmitz, Thomas Becker, Derek Mattern, Adam Kycia, Frank Weide, and Patrick Schmidt. I am thankful to be one of the first users of the new technology. Thank you for

supporting me during the process of method adaptation and problem-solving. Thanks to you guys, this PhD can happen.

I greatly appreciate my thanks to everyone who has helped during the development of the analytical method: Dr. Frank Kirschhöfer (IFG, KIT) for introducing me to the analytical world, Professor Damià Barceló and the colleagues at Catalan Institute for Water Research (ICRA-CERCA, Spain) for advising on the problem-solving solution.

All of the collaborators whose name on the publications are thanked for all of your support and scientific discussion: Prof. Poul B. Peterson, Prof. Babak Minofar, Prof. Zdenek Futera, Dr. Marco Personeni, and Prof. Béla Fiser.

Dr. Andrey Turshatov and Dr. Eduard Madirov (IMT) are thanked for the FTIR measurement of PBSAC (Chapter 4). Prof. Ben Corry is thanked for the discussion on the hydration layer (Chapter 6). Prof Bryce Richards (MIT-IMT) is thanked for providing the solar simulator methodology and ongoing collaboration with photocatalysis. Dr Kristina Fischer and Dr Agnes Schulze (IOM Leipzig, Germany) are thanked for membrane modification and provision of TiO_2-coated membranes and for the continued collaboration.

A big thank you to Blücher GmbH for supplying PBSAC and continuous cooperation with material modification; Millipore company (Merck group), DuPont Water Solutions, and Hydranautics, Nitto for supplying membranes for this project.

I would like to thank the Mitacs Globalink Research Award for giving me a chance for the short research trip during my PhD in Canada in 2024. Although the results of the research trip are not included in this dissertation, I have learnt a lot during a three-month trip in Canada. It was also a confirmation of what I have learnt during my PhD. Thank you to Prof. Graham Gagnon, Rayleen MacDonald, Dr. Jessica Bennett, Heather Daurie, and everyone at Dalhousie University; my landlord Mike Tanner, who has treated me like his daughter, he had passed away a week before my final examination; and everyone in Canada for having me there.

Last but not least, I would like to send my deepest thanks to my family for their unconditional love and support throughout my life. Thanks to my mom, who started to use technology to call me, and to my dad, who is always curious about my research and makes our call like a conference. A big thanks to my brother and his small family for always supporting me. Finally, this project is dedicated to two of the strongest women I have ever met in my life, my grandmother and my aunt, who always supported and encouraged me. I will always remember you and your last words.

Karlsruhe, in March 2026

Phuong Bich Trinh

List of publications

Dissertation-related publications:

The following publications were produced from this study. The contributions of co-authors in the core papers are indicated in the opening of each corresponding chapter.

[1] **P.B. Trinh**, A.I. Schäfer, **Adsorption of glyphosate and metabolite aminomethylphosphonic acid (AMPA) from water by polymer-based spherical activated carbon (PBSAC)**, Journal of Hazardous Materials, (2023) 131211.

Contribution of authors:

Phuong B. Trinh: performing experiments; samples analysis; data analysis and interpretation; validation; methodology; visualization; writing – original draft

Andrea I. Schäfer: conceptualization; methodology; funding acquisition; project administration; resources; supervision; validation; writing – review & editing

Other contribution:

Dr. Eduard Madirov, Dr. Andrey Turshatov (Institute of Micro-structure Technology (IMT-KIT)): adsorbent characterization.

[2] **P.B. Trinh**, A.I. Schäfer, **Removal of glyphosate (GLY) and aminomethylphosphonic acid (AMPA) by ultrafiltration with permeate-side polymer-based spherical activated carbon (UF–PBSAC)**, Water Research, 250 (2024) 121021.

Phuong B. Trinh: performing experiments; samples analysis; data analysis and interpretation; validation; methodology; visualization; writing – original draft

Andrea I. Schäfer: conceptualization; methodology; funding acquisition; project administration; resources; supervision; validation; writing – review & editing

[3] **P.B. Trinh**, M.N. Nguyen, Z. Futera, B. Minofar, M. Personeni, P.B. Petersen, A.I. Schäfer, **The role of hydration in the removal of glyphosate (GLY) and aminomethylphosphonic acid (AMPA) by nanofiltration membranes**, Nature Communications, 17 (2026) 3741.

Phuong B. Trinh: conceptualization; performing experiments; samples analysis; data analysis and interpretation; methodology; validation; visualization; writing – original draft

Minh N. Nguyen: conceptualization; data analysis and interpretation; methodology; supervision; validation; visualization; writing – review & editing

Zdenek Futera: performing molecular dynamics simulation, data analysis and interpretation; funding acquisition; methodology; validation; visualization; writing – review & editing

Babak Minofar: performing molecular dynamics simulation, data interpretation; funding acquisition; methodology; validation; writing – review & editing

Marco Personeni: FTIR measurement and the hydration layer characterization; data analysis; formal analysis; investigation; methodology; validation; visualization; writing – review & editing

Poul B. Petersen: conceptualization; data interpretation; funding acquisition; methodology; supervision; validation; writing – review & editing

Andrea I. Schäfer: conceptualization, funding acquisition; project administration; resources; supervision; validation; writing – review & editing

[4] **P.B. Trinh**, S. Liu, N.F. Himma, B. Fiser, A.I. Schäfer, **Continuous-flow photocatalytic degradation of glyphosate and aminomethylphosphonic acid under simulated sunlight with TiO_2-coated poly(vinylidene fluoride) membrane**, Advanced Functional Materials, *Cover*, 36, no. 21 (2026) e11431.

Phuong B. Trinh: conceptualization; performing experiments; samples analysis; data analysis and interpretation; methodology; validation; visualization; writing – original draft

Siqi Liu: conceptualization; data interpretation; methodology; supervision; validation; visualization; writing – review & editing

Nurul F. Himma: performing experiments; sample preparation; data analysis; visualization

Béla Fiser: data curation; formal analysis; funding acquisition; investigation; methodology; validation; visualization; writing – review & editing

Andrea I. Schäfer: conceptualization, funding acquisition; project administration; resources; supervision; validation; writing – review & editing

[5] **P.B. Trinh**, D.J. Mattern, A.I. Schäfer, **Determination of glyphosate (GLY) and aminomethylphosphonic acid (AMPA) in water by direct injection liquid chromatography tandem mass spectrometry (LC-MS/MS)**, submitted to Scientific Reports, (2026).

Phuong B. Trinh: conceptualization; performing sample analysis; trouble shooting; data analysis and interpretation; methodology; validation; visualization; writing – original draft

Derek J. Mattern: trouble shooting; methodology; resources; writing – review & editing

Andrea I. Schäfer: funding acquisition; project administration; resources; supervision; writing – review & editing

Scientific Contribution at Conferences

The parts of the thesis have been presented at international scientific conferences:

20–24 Nov 2022	Euromembrane 2022, Sorrento, Italy Oral presentation: “Removal of glyphosate and AMPA by ultrafiltration membrane integrated polymer-based activated carbon”
10–11 Oct 2022	18th Annual workshop on emerging high-resolution mass spectrometry (HRMS) and LC-MS/MS applications in environmental analysis and food safety, Barcelona, Spain Oral presentation: “Determination of glyphosate (GLY) and aminomethylphosphonic acid (AMPA) in real water by liquid chromatography with tandem mass spectrometry (LC-MS/MS)”
26–30 June 2022	Nanofiltration 2022: Principals, Applications and New Materials, Achalm, Germany Poster presentation: “Removal of glyphosate (GLY) by polymer-based spherical activated carbon (PBSAC)”
15–16 Oct 2020	16th Annual workshop on emerging high-resolution mass spectrometry (HRMS) and LC-MS/MS applications in environmental analysis and food safety, Online, ***Poster prize*** Poster presentation: “Determination of glyphosate (GLY) and aminomethylphosphonic acid (AMPA) in water by liquid chromatography with tandem mass spectrometry (LC-MS/MS)”
01–05 Dec 2019	Green Technologies for Sustainable Water (GTSW) 2019, HCM City, Vietnam Oral presentation: “Removal of glyphosate (GLY) and its metabolite aminomethylphosphonic acid (AMPA) by polymer based spherical activated carbon (PBSAC) in water treatment”

1 Introduction

The first chapter provides a broad context and the major challenges that this project is solving. The water contamination and the incomplete removal of current water treatment technologies are discussed, highlighting the need to remove herbicide micropollutants from water.

The last part outlines the research objectives and overall structure of the dissertation.

1.1 Pesticide and herbicide micropollutants

Water contamination causes an imbalance in life and sustainable development, where its impacts extend far beyond ecological degradation. At its core, water pollution violates one of the most basic human needs and rights, which is access to safe drinking water. 2.2 billion people still lacked access to safe drinking water, and 1.2 billion people lacked access to drinking water [1]. The domino effect leads to short- and long-term impacts on public health (physical and mental), energy, the economy, livelihoods, and culture, as well as equity and justice [1]. Water stress increased by 3% globally from 2015 to 2021, particularly in Africa and Asia [1], posing additional stress on low-income communities. Women and girls around the world who are most likely responsible for collecting water in families walk on average 6 kilometers daily to carry water that is often contaminated, reducing their access to education. More than 1000 children under 5 years old die from diseases related to lack of clean water and sanitation every day [2]. Despite all efforts to achieve the goal of "Clean water and sanitation" [3], water contamination remains unsolved, not only in low-income countries where low water quality is often attributed to inadequate water treatment facilities, but also in high-income countries due to agricultural runoff and industrial discharge [4, 5].

Micropollutants are contaminants that occur at low concentrations in water (ng/L to µg/L), but can cause adverse effects on the environment and human health [6]. Micropollutants, including pesticides, biocides, pharmaceuticals, and per- and polyfluoroalkyl substances (PFAS), are persistent and continuously discharged from diverse sources [7]. In a study of 258 rivers worldwide, over 25% of the detected micropollutants were found at concentrations exceeding safe limits for aquatic organisms [8]. Among all micropollutants, pesticides and herbicides are "old topics" but remain a concern worldwide [15, 16], causing an annual economic loss of 78 million euros in Europe [9]. Over the past 20 years, the use of chemicals in agriculture has increased by more than 40 %. Over 4.1 million tons of pesticides are used worldwide each year, with herbicides accounting for 48%, insecticides (30%), fungicides (17%), and others (5%) [10] (Figure 1.1). Despite the well-managed water system, different pesticides were found in European streams at concentrations ranging from 10 ng/L to 20 µg/L [7, 11], some hot spots with the concentration of mg/L, which was much higher than European Union (EU) guidelines for herbicides in water (100 ng/L for each pesticide, and 500 ng/L for total pesticides [12, 13]).

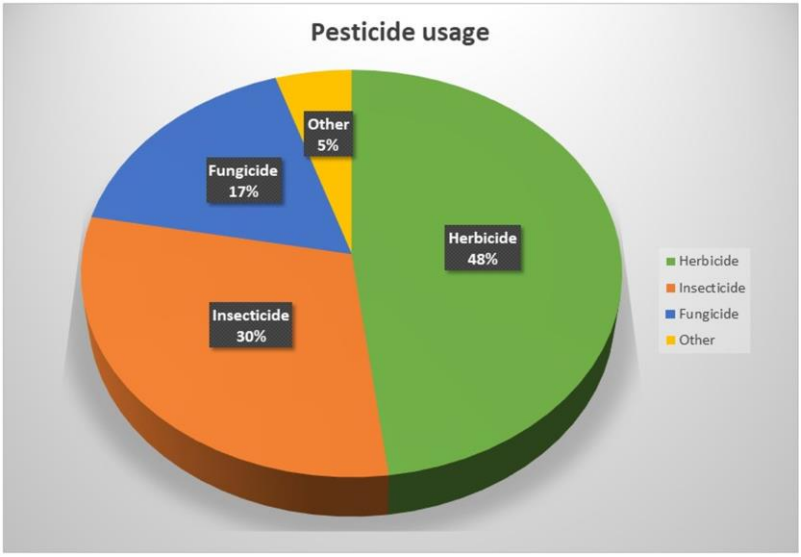

Figure 1.1. Pesticide usage in agriculture

1.2 Glyphosate and aminomethylphosphonic acid

Glyphosate (N-(phosphonomethyl) glycine) (GLY), also known as Roundup, is an organophosphate herbicide. GLY is the most widely used herbicide, which accounts for 30% of total herbicide use worldwide [14-17]. With the extensive annual usage of 600–750 thousand tonnes in agriculture alone, which is estimated to increase to 740–920 thousand tonnes by 2025 [16]. Only in 2024, 1.2 million tonnes of GLY were produced for the market [18]. Therefore, the concentrations of GLY and its main metabolite, aminomethylphosphonic acid (AMPA), in the water environment (surface water, groundwater, and seawater [19, 20]) are expected to continue increasing in the future, which is a global problem (Figure 1.2) [21, 22]. In Figure 1.2, it is noted that the areas with low GLY inputs into rivers do not represent low contamination, but might be due to the lack of data collection and processing.

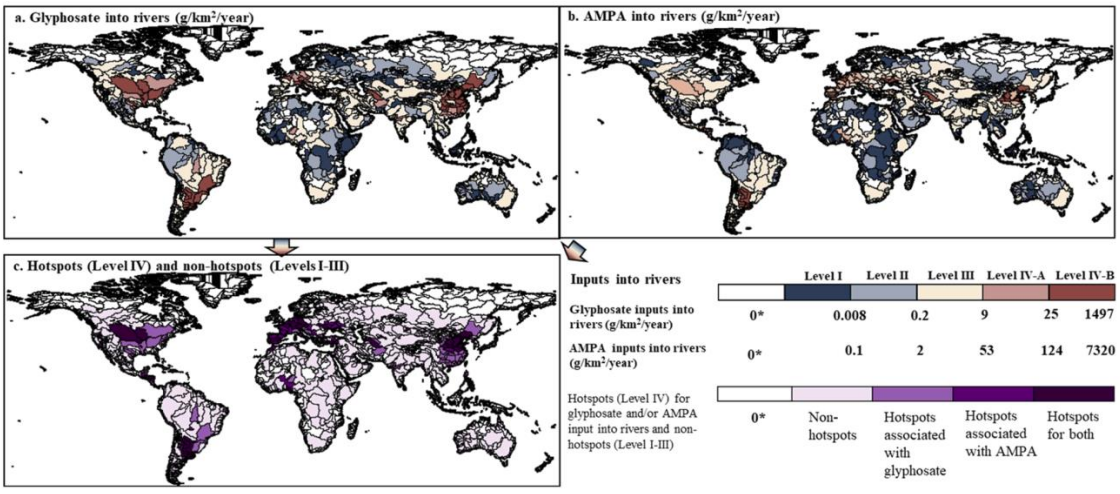

Figure 1.2. River pollution with GLY and AMPA from crop production (Reprinted from Zhang et al. [21]).

The exposure to GLY and AMPA has been linked to DNA damage, cytotoxic effects, reduced male fertility, cancer, and endocrine disruption [23-26]. GLY was classified as a potential carcinogen by the World Health Organization (WHO) [25, 27, 28]. 100 ng/L as individual herbicides and 500 ng/L for total herbicides are the maximum concentrations of GLY and AMPA in water according to EU guidelines [13]. Because of the health effects caused by GLY, around 200,000 lawsuits have been filed against Roundup. Monsanto (now Bayer) needs to pay nearly $16 billion for settlements [29]. Nevertheless, the GLY market is still expanding with annual growth at 6.32%, and is expected to reach 17 billion Euros by the end of 2031 [30]. Due to the massive market and the lack of alternative products, the ban on GLY in agriculture has been discussed and postponed for several years in Europe [31]. In 2023, the European Commission authorized the GLY market for 10 more years until 2033 despite its impact on the environment and public health [32], leaving a continuing water contamination issue. GLY and AMPA were still detected in surface and groundwater at concentrations ranging from nanograms to milligrams per liter [37-41] (higher than EU guidelines), which require advanced water treatment technologies for effective removal from water sources [32, 33]. The challenge of balancing economic benefits and environmental protection remains unresolved.

1.3 GLY and AMPA problem: from farm to home

From the farm, GLY and AMPA used in agriculture can directly reach the surface and groundwater by surface runoff [34, 35] (Figure 1.3).

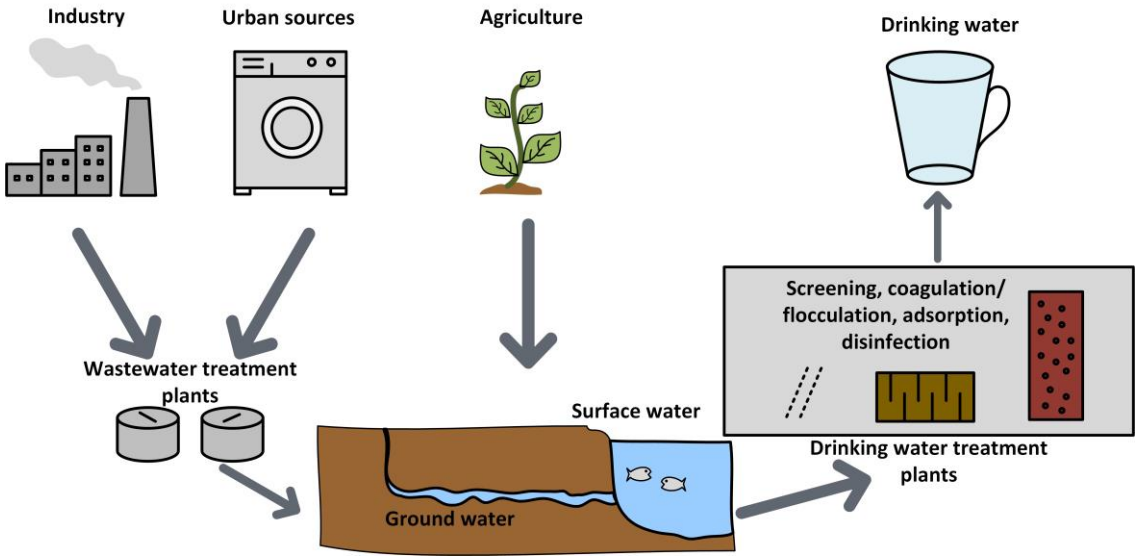

Figure 1.3. Schematic of conventional water treatment plants

Other sources of GLY/AMPA include urban runoff and industrial activities, where micropollutants can be discharged from the conventional wastewater treatment process due to incomplete removal or bypass treatment *via* stormwater overflows [36, 37], and can reach surface, ground, and seawater [19, 20]. Most current water treatment plants have integrated sorption and/or ozonation to enhance the organic matter removal capacity and partially remove micropollutants

[38, 39]. In the state of Baden−Württemberg, Germany, 33 wastewater treatment plants use PAC, GAC, ozonation, and a combined ozonation and GAC system for micropollutant removal (Figure 1.4) [40]. As of May 2025, 30 wastewater treatment plants are planned, including one plant that will adopt PAC and ultrafiltration (UF) membrane technology [40]. However, GLY and AMPA cannot be removed by current technologies, leading to the discharge of the herbicides into the water environments from industrial and urban sources, besides agricultural sources.

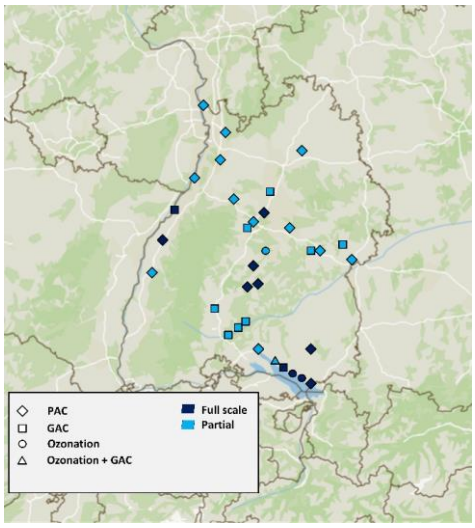

Figure 1.4. Map of active WWTPs with micropollutant removal technologies (granular/powdered activated carbon (GAC/PAC) adsorption, and ozonation) in Baden−Württemberg (BW). Data were taken from the BW websites in May 2025 [40]. The map was created by P.T.

After entering surface and groundwater, GLY and AMPA can reach drinking water treatment plants, as 30% and 70% of drinking water comes from surface water and groundwater, respectively [41]. As GLY and AMPA cannot be removed by conventional treatment technologies, these herbicides can finally enter housing and be consumed by humans.

To reduce contamination of GLY and AMPA in water, different approaches can be considered, including controlling contamination sources or improving water treatment technologies. With extensive use, expansion, and continued growth of the GLY market, controlling the sources is necessary but very challenging. Therefore, research on water treatment technologies for GLY and AMPA is extremely essential and needs more investigation.

1.4 Objective of the dissertation

The research objective is to **investigate and compare different water treatment technologies** for removing herbicides, **glyphosate (GLY)** and its main metabolite, **aminomethylphosphonic acid (AMPA)**, from water.

Being one of the common technologies in current water treatment plants, adsorption is chosen as the first technique. More advanced technologies, such as membrane filtration processes

(nanofiltration (NF) and reverse osmosis (RO)), can efficiently remove micropollutants and herbicides, but they require more energy than adsorption and ozonation [42, 43]. Different membrane technologies are applied to remove GLY and AMPA, including adsorption–membrane hybrid system, nanofiltration membrane, and photocatalytic membrane. With each technology, the research objectives are addressed and answered:

1) Determine the removal potential of each technology at lab-scale and evaluate the removal to meet EU guidelines for herbicides in water.
2) Identify the limiting factors for GLY and AMPA removal.
3) Investigate the mechanisms of GLY and AMPA removal and evaluate removal at optimized conditions.

At last, a comprehensive comparison among adsorption, adsorption–membrane hybrid system, nanofiltration membrane technology, and photocatalytic membrane is presented in this dissertation, with the following criteria in consideration.

- Evaluation of "effectiveness": the removal efficiency of each technology and whether the EU guidelines for herbicides in water can be achieved at lab-scale systems.
- Evaluation of "sustainability": the estimated energy consumption of each technology at the optimized filtration conditions.

Although this dissertation does not include real water interferences or the upscaling of the filtration system, the long-term goal is to design herbicide treatment processes that effectively remove herbicides to water guidelines with little or no chemicals added, low energy, and low risk to the environment.

1.5 Structure of the dissertation

The structure of this thesis is illustrated in Figure 1.5.

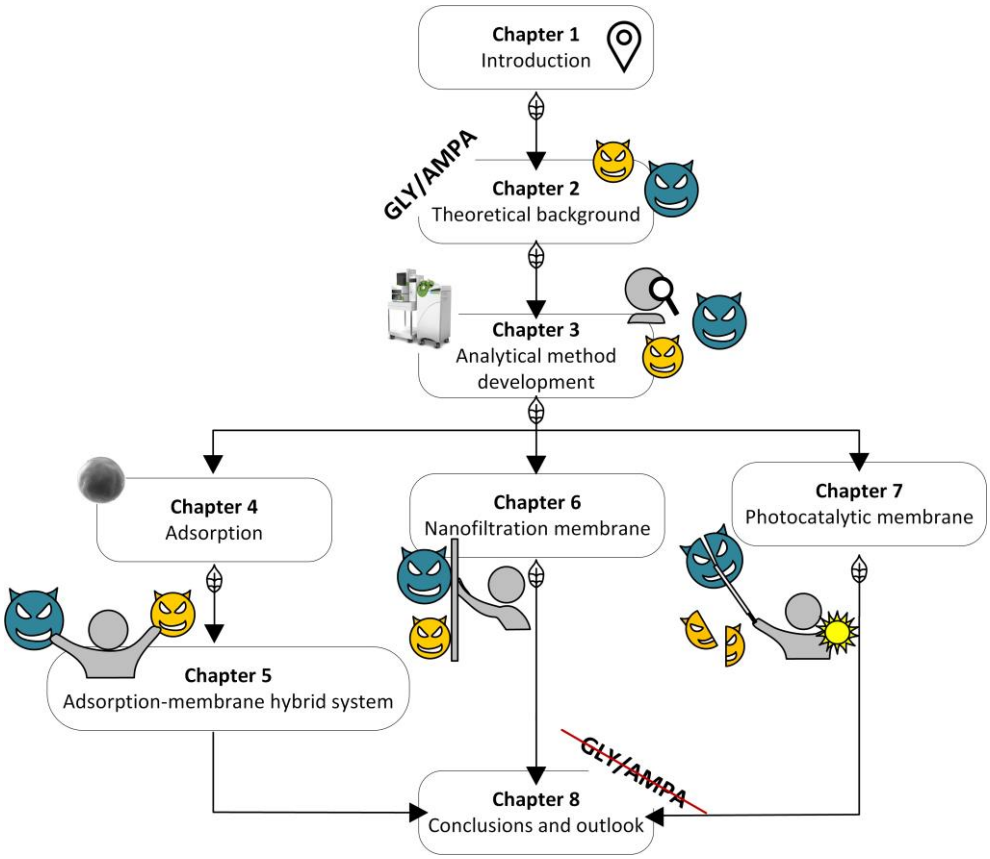

Figure 1.5. Schematic of the dissertation structure

The theoretical background is explained in **Chapter 2**, following the structure of a literature review paper on the occurrence and removal technologies of GLY and AMPA. The chapter includes the occurrence and fate of GLY and AMPA in the environment, in which part of this section was the result of the study project of M.Sc. Harsha Philips, under P.T. supervision, challenges the detection and removal of GLY and AMPA, reviews current GLY and AMPA removal technologies, and conducts research.

Chapter 3 presents the analytical method development for quantifying GLY and AMPA, as well as the problem identification and solving.

> Related publication: "P.B. Trinh, D.J. Mattern, A.I. Schäfer, Determination of glyphosate (GLY) and aminomethylphosphonic acid (AMPA) in water by direct injection liquid chromatography tandem mass spectrometry (LC-MS/MS), submitted to Scientific Reports, (2026)".

Chapter 4 examines the removal of GLY and AMPA using polymer-based spherical activated carbon (PBSAC) with varying adsorbent properties (size, activation level, oxygen content) and water conditions.

> Related publication: "P.B. Trinh, A.I. Schäfer, Adsorption of glyphosate and metabolite aminomethylphosphonic acid (AMPA) from water by polymer-based spherical activated carbon (PBSAC), Journal of Hazardous Materials, (2023) 131211".

PBSAC, studied in **Chapter 5**, is then integrated with an ultrafiltration (UF) membrane for GLY and AMPA removal. The hybrid UF–PBSAC system is investigated, and the mass transfer limitation is discussed in the context of the short hydraulic residence time.

> Related publication: "P.B. Trinh, A.I. Schäfer, Removal of glyphosate (GLY) and aminomethylphosphonic acid (AMPA) by ultrafiltration with permeate-side polymer-based spherical activated carbon (UF–PBSAC), Water Research, 250 (2024) 121021".

Chapter 6 presents the results of experiments on GLY and AMPA removal by nanofiltration (NF) membrane and discusses the herbicide transport in the membrane and removal efficiency.

> Related publication: "P.B. Trinh, M.N. Nguyen, Z. Futera, B. Minofar, M. Personeni, P.B. Petersen, A.I. Schäfer, The role of hydration in the removal of glyphosate (GLY) and aminomethylphosphonic acid (AMPA) by nanofiltration membranes, Nature Communications, 17 (2026) 3741".

Chapter 7 presents the experimental results of GLY and AMPA degradation by photocatalytic membrane under simulated sunlight. The limiting factor to the degradation process is studied, and the degradation pathway is discussed.

> Related publication: "P.B. Trinh, S. Liu, N.F. Himma, B. Fiser, A.I. Schäfer, Continuous-flow photocatalytic degradation of glyphosate and aminomethylphosphonic acid under simulated sunlight with TiO_2-coated poly(vinylidene fluoride) membrane, Advanced Functional Materials, Cover, 36, no. 21 (2026) e11431".

Chapter 8 summarizes and compares the results from different water treatment technologies to evaluate the removal efficiency of GLY and AMPA.

2 Theoretical background

The chapter gives a brief literature review on glyphosate (GLY) and aminomethylphosphonic acid (AMPA) micropollutants in water bodies.

After a brief introduction to the properties of GLY and AMPA, the fate and occurrence of these compounds in water are reviewed. The fate of GLY and AMPA in the environment was supported by the fugacity model, which was done by Harsha Philips, a Master student, under the supervision of P.T.

Subsequently, a review of the analytical methods and challenges in GLY and AMPA analysis is presented.

Based on the understanding of GLY and AMPA, four different water treatment technologies will be reviewed: (1) current research on GLY/AMPA removal; (2) challenges in improving the removal efficiency. The four water treatment technologies include adsorption, hybrid adsorption–membrane filtration process, membrane filtration, and advanced oxidation technologies.

The last part of this chapter highlights the comparison between four technologies. This comparison is the key to the final conclusions of this project.

2.1 GLY and AMPA properties

Glyphosate (N-(phosphonomethyl) glycine) (GLY) is a polar and hydrophilic compound with a molecular weight (MW) of 169 g/mol (Table 2.1) [44, 45]. Aminomethylphosphonic acid (AMPA), the primary metabolite of GLY, is frequently detected in surface waters alongside GLY [36, 37]. AMPA, with a molecular weight of 111 g/mol, exhibits similar toxicity to GLY [46, 47]. Physically, GLY and AMPA are odorless, crystalline, white powders with a water solubility of 12 g/L and 50 g/L, respectively, at 20 °C [48, 49]. Being non-volatile compounds, GLY and AMPA volatilization from land to the atmosphere is unfavorable, and inhalation exposure is not expected to be significant [50]. However, these compounds can be dissolved and transported easily in water due to the high solubility in water [44, 51, 52].

Table 2.1: Chemical properties of GLY and AMPA [48, 49, 53, 54]

Chemical	GLY	AMPA
Chemical name	N-(phosphonomethyl) glycine	Aminomethylphosphonic acid
Structure	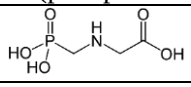	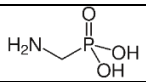
MW (g/mol)	169.07	111.04
Log K_{OW}	−3.4	−2.2
Solubility in water (g/L) at 20 °C	12	50
pKa	0.8, 2.6, 5.6, 10.6	1.8, 5.4, 10.2
Polarity	High	High
H-donors/ acceptors	4/6	3/4

GLY contains three polar functional groups: –COOH, $–NH_2$, and $–PO_3H_2$ (Figure 2.1) [44, 45]. These functional groups can be protonated or deprotonated, making the charge of GLY strongly dependent on pH. GLY has four pKa: 0.8, 2.6, 5.8, and 10.8, with the charge of GLY ranging from +1 to –3 with an increase in pH [45, 55].

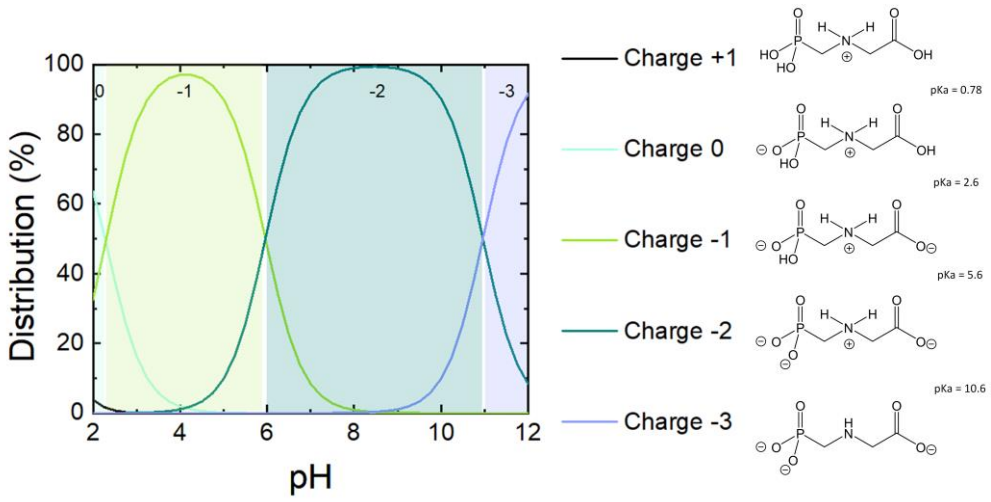

Figure 2.1. Speciation of GLY at pH 2–12 (calculated by Visual MINTEQ (v 3.1, KTH, Sweden) at the corresponding water matrix using the input parameters described in section 2.2)

AMPA, which is formed via C–N bond cleavage of GLY [62], contains two functional groups: $–NH_2$ and $–PO_3H_2$ (Figure 2.2) [56]. There are three pKa values for AMPA (1.8, 5.4, and 10.2) [45, 55], making the charge of AMPA range from +1 to –2 [45, 55].

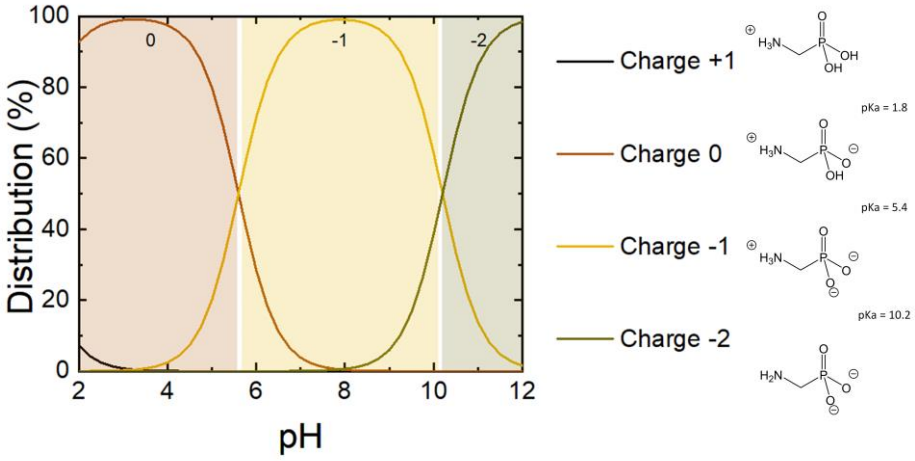

Figure 2.2. Speciation of AMPA at pH 2–12 (calculated by Visual MINTEQ (v 3.1, KTH, Sweden) at the corresponding water matrix using the input parameters described in section 2.2)

At neutral pH 8, the charge of GLY is –2 and AMPA is –1 [54].

Due to the complex physicochemical properties, GLY and AMPA are challenging to detect and remove from water [44, 45, 57, 58]. For analysis, the non-volatile nature of GLY and AMPA makes them difficult to analyze consistently by gas chromatography compared to other pesticides, such as atrazine [59]. Additionally, GLY and AMPA are polar and hydrophilic, with high solubility, making these compounds easily soluble in water and difficult to separate from the water matrix for quantification [48]. GLY and AMPA can also form complexes with colloids and metal ions (Ca^{2+}, Mg^{2+}, Fe^{3+}, and Al^{3+})[61, 62], which are more challenging to analyze [48, 60]. For removal, GLY and AMPA are small molecules with the hydrodynamic diameter of 0.62 nm for GLY and 0.49 nm for AMPA [61]. Therefore, GLY and AMPA can be transported easily in water. In addition, as GLY and AMPA are highly soluble in water [54], it is difficult to remove them from water using conventional water treatment technologies [65], which are also dependent on water chemistry and speciation [62, 63].

2.2 GLY and AMPA fate and occurrence in the environment

The main sources of GLY and AMPA in the environment are agriculture and industry. The direct exposure of GLY in the environment is related to air spray in agricultural activities [64]. There has been a lot of debate over whether GLY from agriculture can contaminate water. In previous studies, GLY could be strongly adsorbed by soil, and the concentration was predicted to be low in water [65, 66]. Some stated that GLY cannot reach water; however, GLY was

detected in water at the range of µg/L to mg/L [67]. To determine whether GLY and AMPA contamination is an issue, the fugacity model would be studied.

Fugacity model

To understand the fate of GLY in the environment and the possibility of GLY contamination in water, a fugacity model was applied. The fugacity model of GLY fate in the environment was done by Harsha Philips, a Master student, under P.T. supervision.

A fugacity-based approach was used to model the chemical fate of GLY in the environment. The fugacity approach, developed by group of Mackay in the early 1980s, has been described as the tendency of a chemical to escape from one medium to another [68-70]. Fugacity models account for partitioning and degradation of a chemical in a phase to predict steady-state concentrations. Conversion of equilibrium from concentration units to fugacity units makes it easy to use in mass-balance equations to simulate the distribution of chemicals within different media. While the chemical potential within a particular compartment is logarithmically related to the concentration, the equilibrium criterion of fugacity is linearly related to concentration [71]. Equilibrium between two phases is attained when the chemical in both phases has the same escaping tendency (fugacity), considering that all the environmental media are fully mixed. Fugacity is related to the concentration by a proportionality constant, the fugacity capacity. The fugacity capacity (Z) is dependent on pressure, temperature, nature of the substance and the medium [68, 69]. Z value depends on physical-chemical parameters, partition coefficient, and the compartment characteristics.

Fugacity capacity for air: $$Z_a = 1/RT \quad (2.1)$$

Fugacity capacity for water: $$Z_w = \frac{1}{H} = C^s/P^s \quad (2.2)$$

Fugacity capacity for soil: $$Z_s = K_{sw}.\rho_s/H \quad (2.3)$$

where, R is the universal gas constant [Pa.L^3/K.m], T is the absolute temperature [K], H is Henry's law constant [Pa.L^3/m], C^s is the saturation concentration [m/L^3], K_{sw} is the solid–water partition coefficient [L^3/m], and ρ_s is solids density [m/L^3] [69, 72].

The fugacity approach is classified into four levels with increasing complexity (Level I, Level II, Level III, EQC, QWASI) (Table 2.2). In the four levels, level II fits as GLY is being used continuously. Therefore, Level II will be used for modelling GLY fate in the environment.

Table 2.2. Classification of fugacity models into four levels of complexity [68]

Levels	Assumption	Levels	Assumption
Level I	Equilibrium One-time input No flow, no degradation	Level III	Steady-state (non-equilibrium) Different fugacity in phases Flow, degradation Resistance in phase transfer Different inputs in compartments
Level II	Equilibrium Flow, degradation Phase transfer occurs fast	Level IV	Unsteady state (input rate, concentration and fugacity vary with time)

For simplicity, the evaluative environment is chosen for this chapter. The definition of evaluative environment follows the same assumptions as those used by Mackay et al. (1985) [73] in defining the "unit world", which includes:

- The environment is divided up to six compartments: air, water, soil, bottom sediment, suspended sediment, and aquatic biota.
- All phases are homogeneous. Soil and sediment are not stratified with respect to concentration.
- Only aquatic biota considered are fish [69, 73].

Volumes and densities of the environmental compartments are given in Table 2.3.

Table 2.3. Volumes and densities of units considered [74]

Volumes and densities for the unit world	Volume (m^3)	Density (kg/m^3)	Fraction of organic content
Air	10^{14}	1.19	NA
Water	$2 \cdot 10^{11}$	1000	NA
Soil	$9 \cdot 10^{9}$	1500	0.02
Sediment	10^{8}	2400	0.04

The level II model simulates the fate of a chemical when continuously emitted into the environment at a constant rate and reaches a steady-state equilibrium once the input rate and combined rate of output become equal [68, 69]. The rate of outflow, including advection (air, water, and sediment) and degradation (across all compartments), will affect fugacity [75]. In addition, the half-lives of the chemical in each medium need to be provided so that the overall persistence time can also be estimated [76]. The model input values were chosen from the International Union of Pure and Applied Chemistry (IUPAC) pesticide properties database under the A5 category. These properties are listed in Table 2.4.

Table 2.4. Model input values based on the Pesticides Properties Database [77]

Parameter	Unit	GLY
Molar mass	g/mol	169
Data temperature	ºC	20
Melting point	ºC	189
Vapor pressure	Pa	$1.3 \cdot 10^{-2}$
Solubility in water	g/m^3	10500
Henry's law constant	$Pa.m^3/mol$	$2.1 \cdot 10^{-7}$
Log octanol-water partition coefficient (log K_{ow})		-3.2
Organic carbon partition coefficient (K_{oc})		1424
Emission rate for Level II *	kg/h	16
Reaction half-life in soil	days	23
Reaction half-life in air	days	10^{11} (stable)
Reaction half-life in water	days	10
Reaction half-life in water-sediment	days	74

* The emission rate was calculated from the normal usage in agriculture [78].

In this chapter, GLY is modelled using two spreadsheet-based freeware models developed by the Canadian Environmental Modelling Centre.

The results from the fugacity model are shown in Table 2.5.

Table 2.5. The partitioning of GLY into different environmental compartments

Phase	Concentration	Concentration unit	Quantity (%)
Air	$9 \cdot 10^{-6}$	ng/m^3	~ 0
Water	105	ng/L	24
Suspended solid	29	ng/g	0.1
Fish	$3 \cdot 10^{-6}$	ng/g	~ 0
Soil	3	ng/g	74
Sediment	6	ng/g	1.9

It was shown that 74% of GLY can reach the soil, where it can be adsorbed and degraded into AMPA [79, 80]. Meanwhile, 24% GLY can reach the water, resulting in a concentration of 105 ng/L. Only a small amount of GLY can reach suspended solids and sediment (0.1% and 1.9%, respectively). Meanwhile, GLY does not stay long in the air, which is also due to its low volatility. The residence time is 22 days (530 h), with reaction persistence of 25 days and advection persistence of 172 days. The reaction in soil and water includes the degradation of GLY into different by-products (with AMPA being the main metabolite [53]).

In conclusion, even though GLY can be adsorbed by soil, a high amount of GLY can still reach the water environment at high concentration. Moreover, GLY in soil can also be biodegraded into by-products, including AMPA. Therefore, GLY and AMPA contamination in water is indeed an issue that has been raised in research on the detection of these micropollutants.

Fate of GLY and AMPA in the environment

The overall fate of GLY and AMPA in the water environment is summarized in Figure 2.3.

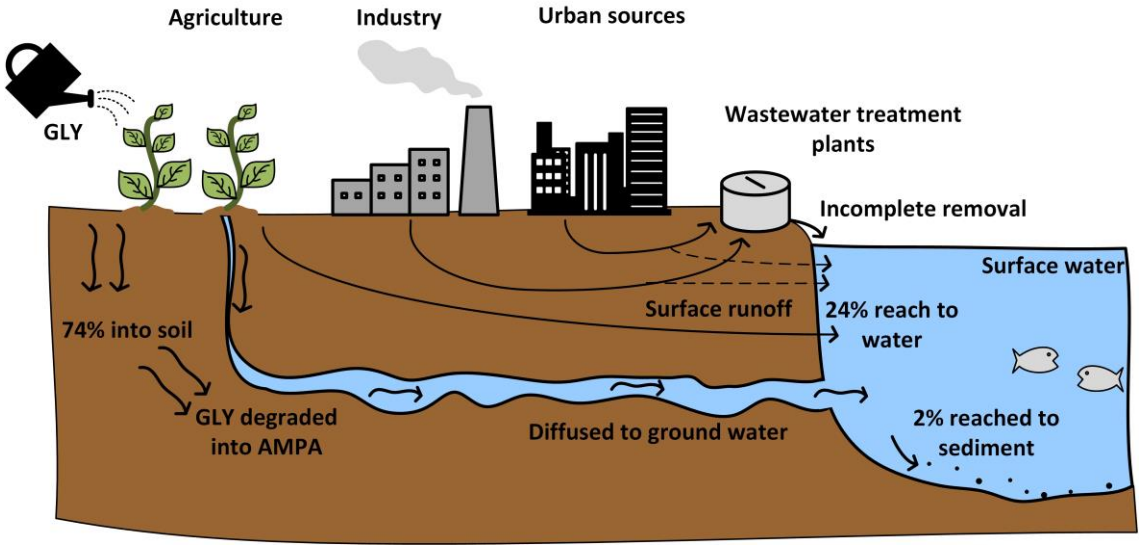

Figure 2.3: Fate of GLY and AMPA in the water environment

As mentioned before, the main sources of GLY and AMPA in the environment are agriculture and industry [64]. In addition, GLY is not only confined to agricultural sources, but also comes from urban roads and railways, as found in the Orge basin (France) [81]. Torstensson *et al.*

showed that railway maintenance was a major source of GLY contamination in Sweden, as GLY residues were found in railway drainage and nearby groundwater [82]. Hanke *et al.* found that GLY leached with fast runoff from hard surfaces, wastewater treatment plants, sewer system overflows, and separate sewer systems, accounting for 60% of GLY in surface water [83]. In a recent study by Schwientek *et al.*, the main source of GLY in European rivers was found not to be from agriculture, but rather from phosphonates used as antiscalants and bleach stabilizers in urban applications, such as laundry [84]. This study has raised a controversial debate among farmers, researchers, and industry over the sources and impacts of GLY and AMPA [85]. Some claimed that the final results were overestimated because the impact of water hardness on the analysis was not considered. In later research, Engelbart *et al.* and Röhnelt *et al.* provided experimental evidence, along with analytical methods, to support the findings reported in previous studies [86, 87]. As GLY and AMPA cannot be removed by current technologies, resulting in the discharge of GLY/AMPA into the water environment from industrial, urban, and agricultural sources [88-90]. After entering the environment, GLY undergoes physical, chemical, and biological processes that affect its degradation and persistence, forming AMPA [91]. Hence, GLY and AMPA always appear together in the environment.

GLY and AMPA occurrence in the water environment

GLY and its metabolite AMPA occur at the concentration of 0.2 to 370 μg/L in groundwater and surface water [30, 92-94], although GLY concentration can be in the range of milligrams per liter in some water bodies [67]. Sanchis *et al.* reported GLY concentrations as high as 2.6 μg/L in Catalonia, Spain, which is higher than the EU limit for surface and ground water [95]. Carles *et al.* reported that GLY and AMPA were the two most commonly detected herbicides in rivers across Europe [96]. Torstensson *et al.* reported GLY occurrence above 50 ng/L in groundwater in Swedish railway embankments [82]. A study by Campbell *et al.* reported that GLY and AMPA concentrations did not change or increased after WWTP, and the 11-year data showed an increasing GLY trend, with concentrations ranging from 0.4 to 370 μg/L [90]. In Germany, GLY and AMPA were detected in surface and groundwater at around 1 μg/L [97, 98]. Table 2.6 summarizes GLY occurrence in the water environment in previous studies.

Table 2.6. Review of GLY occurrence studies in water

Location	Compartment	Max GLY levels detected	Reference
Cordoba, Argentina	Water	125 μg/L	[99]
Mai Po Nature Reserve, Hong Kong	Estuarine water Freshwater pond	2191 μg/L 216 μg/L	[100]
Mississippi	Water	290 μg/L	[101]
Rouffach, France	Runoff water	86 μg/L	[101]
Hopelchen, Mexico	Groundwater	1.41 μg/L	[102]
Baden-Württemberg, Germany	Surface water	0.33 μg/L 1.2 μg/L	[103]

Because of the low concentrations in water and the persistence of GLY and AMPA, detecting, monitoring, assessing impacts, and removing these herbicides are challenging.

2.3 GLY and AMPA analysis in water

Analytical methods used to analyze GLY and AMPA are typically based on chromatography. Table 2.7 summarizes the analytical methods for GLY and AMPA in water.

Table 2.7: An overview of analytical methods for the determination of GLY and AMPA in water

Analyte	Matrix (sample amount)	Sample treatment	LOD (ng/L)	Detection technique	Ref
GLY and AMPA	Surface water (10 mL)	Derivatization SPE	100 (GLY) 220 (AMPA)	GC-FPD[1]	[104]
GLY	Surface water (25 mL)	Derivatization SPE	200	ESI[2]-MS/MS	[105]
GLY and AMPA	Environmental water (4 mL)	Derivatization Online SPE as a preconcentration step	1000 (GLY) 2000 (AMPA)	ESI-MS/MS	[106]
GLY and AMPA	Water (30 mL)	SPE	1000 (GLY) 290 (AMPA)	ICP[3]-MS/MS	[107]
GLY and AMPA	Water (2 mL)	Direct injection Large volume injection	250	ESI-MS/MS	[108]
GLY and AMPA	Water (0.2 mL)	Derivatization	200 (GLY) 50 (AMPA)	ESI-MS/MS	[109]
GLY and AMPA	Sea water (500 mL)	Derivatization SPE	120 (GLY) 220 (AMPA)	ESI-MS/MS	[110]

[1] flame photometry detector [2] electrospray ionization [3] inductively coupled plasma

Gas chromatography with mass spectrometry (MS) or flame photometry detectors [104, 111] can analyze GLY and AMPA with LOD of 50 ng/L [104, 111, 112]. As GLY and AMPA are non-volatile, sample treatment and derivatization are required to convert these micropollutants into sufficiently volatile, thermally stable derivatives that can be detected by mass spectrometry (MS) [113-115]. Ion chromatography (IC) with tandem MS (IC-MS/MS) was studied but required the addition of ethylenediaminetetraacetic acid (EDTA) to improve the recovery of GLY/AMPA [116]. Liquid chromatography with MS or tandem MS (LC-MS or LC-MS/MS) using an electrospray ionization source (ESI) could analyze GLY and AMPA. In previous studies, reverse-phase liquid chromatography (LC) has been applied to detect GLY and AMPA using ESI-MS or UV detection [122, 123], with a LOD of 50 ng/L. However, solid-phase extraction and derivatization steps using solvents such as p-toluenesulfonyl chloride and FMOC-Cl were required [117, 118]. The derivatization enhances hydrophobicity, improves separation and ionization [124], and increases sensitivity [119, 120]. Nevertheless, the residual FMOC-Cl or byproducts could interfere with the analysis, which requires further cleanup, maintenance, and careful optimization [121]. In addition, extraction and derivatization are time-consuming and can increase analytical errors, especially for GLY and AMPA in environmental samples at environmentally relevant concentrations [122]. The direct analytical method was studied for

GLY and AMPA in water. Okada *et al.* investigated a direct injection method using an ion exchange column for GLY and AMPA in environmental water samples with the LOD of 250 ng/L [108]. Another direct injection method for analysis of GLY and AMPA using charged-surface LC-MS/MS was developed for drinking water and surface waters, which achieved LOD of 110 ng/L [123]. However, the investigated method could not reach the desired LOD of 10 ng/L for further studies on water treatment.

Table 2.8 summarizes analytical challenges for GLY and AMPA in water.

Table 2.8. Analytical challenges for GLY and AMPA in water

Challenges	Description
Solubility	GLY and AMPA are highly soluble in water but insoluble in organic solvents, making them difficult to extract from water matrices [124].
pH dependent	GLY and AMPA properties are dependent on water chemistry [44, 125] with multiple pKa values [119, 126].
Low concentration	GLY and AMPA occur in water at concentrations in the range of µg/L [30, 67, 92-94].
Low volume samples	Environmental samples and water samples from water treatment experiments in research often have low volumes (2–10 mL), which are not suitable for pre-treatment steps.
High error	Due to the sample preparation and low concentration, the analytical error is high.

Ion suppression can affect the performance of chromatography and spectrometry. Ion suppression can be caused by endogenous substances (ionic or highly polar compounds in the sample) and exogenous substances (substances introduced during sample preparation) [127, 128]. Ion suppression causes inconsistent analyte signals (gain or loss), low repeatability, and poor quantification [129]. Due to these difficulties, research is often carried out at spiked concentrations that exceed realistic micropollutant levels (in the range of mg/L) [130]. For example, Naghdi *et al.* investigated the adsorption of GLY by metal–organic frameworks from a feed concentration of 5 mg/L [136], which exceeds environmentally relevant concentrations in real water. Song *et al.* studied GLY removal by a hollow fiber NF membrane, using UV-Vis spectrophotometry for GLY analysis in the feed at a concentration of 500 mg/L [63], requiring careful consideration of safety hazards in a laboratory. In addition, sample preparation for analysis often requires a high volume for extraction, which is not realistic for water samples from lab-scale water treatment experiments, where the sample volume ranges from 2–10 mL. With the requirement for analysis at environmentally relevant low concentrations (in the range of ng/L to µg/L) and low sample volumes, studies on analytical method development are needed to support further investigation of treatment technologies.

2.4 GLY and AMPA removal from water

Several approaches have been developed to remove GLY and AMPA from water, including physical/ physiochemical, biological, and advanced oxidation processes (AOPs) [131, 132] (Figure 2.4). Physical/physiochemical includes coagulation/flocculation, adsorption, and membrane filtration. Biological involves the degradation of GLY and AMPA by microorganisms, such as bacteria and fungi. Meanwhile, AOPs include ozonation, Fenton oxidation, electro-

chemical oxidation, and photochemical oxidation. The newer approach is a hybrid process that combines different water treatment technologies. The "connections" between different points in Figure 2.4 will be introduced later.

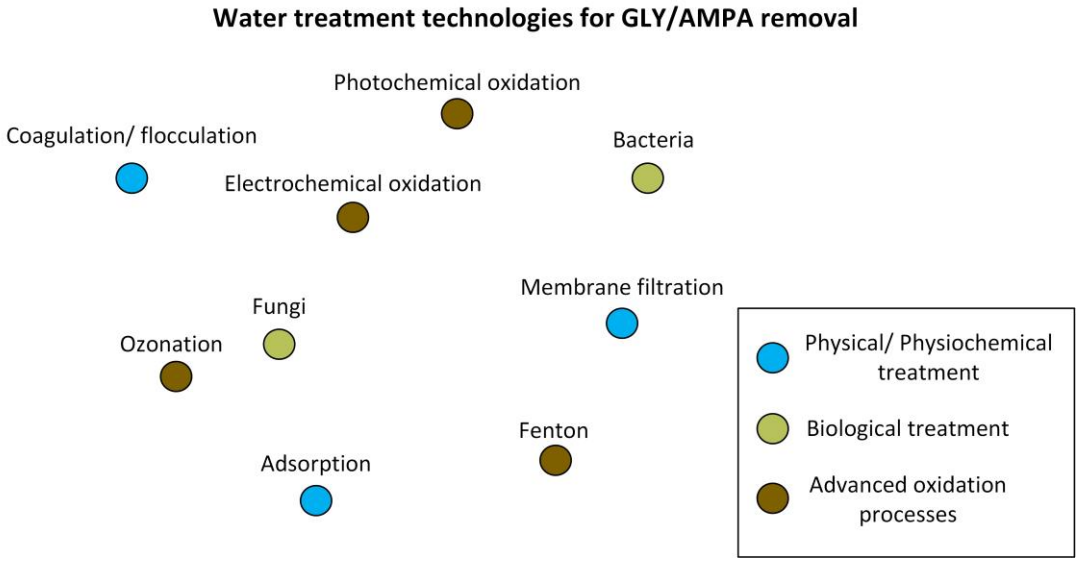

Figure 2.4. Water treatment technologies for GLY and AMPA removal in the water environment

Physical/physiochemical processes

Physical/physiochemical processes include coagulation/flocculation, adsorption, and membrane filtration (Figure 2.5).

Coagulation and flocculation are commonly used in water treatment plants. Even though GLY and AMPA can bind with metals such as (Ca^{2+}, Mg^{2+}, Fe^{3+}, and Al^{3+}), the small molecular weight of GLY (169 g/mol) and AMPA (111 g/mol) hinders the reaction. Moreover, the interaction between GLY/AMPA and the coagulant is strongly dependent on coagulant dose and pH [61, 62], leading to poor removal (< 20%) of GLY and AMPA by coagulation/flocculation [133]. To improve the removal efficiency, coagulation was combined with other technologies [134]. Daniel Villalobos-Lara *et al.* studied GLY removal in an electrocoagulation reactor, achieving 30–40% removal from an initial concentration of 270 mg/L [134]. The removal was slightly improved, but the electrocoagulation time was limited (reaching hours). Another approach to reduce the hydraulic residence time (HRT) was microsand ballasted flocculation [133]. The HRT was reduced to 19–28 min; however, the removal was still low, 34–58% for GLY and 25–63% for AMPA, from a feed concentration of 5–10 µg/L.

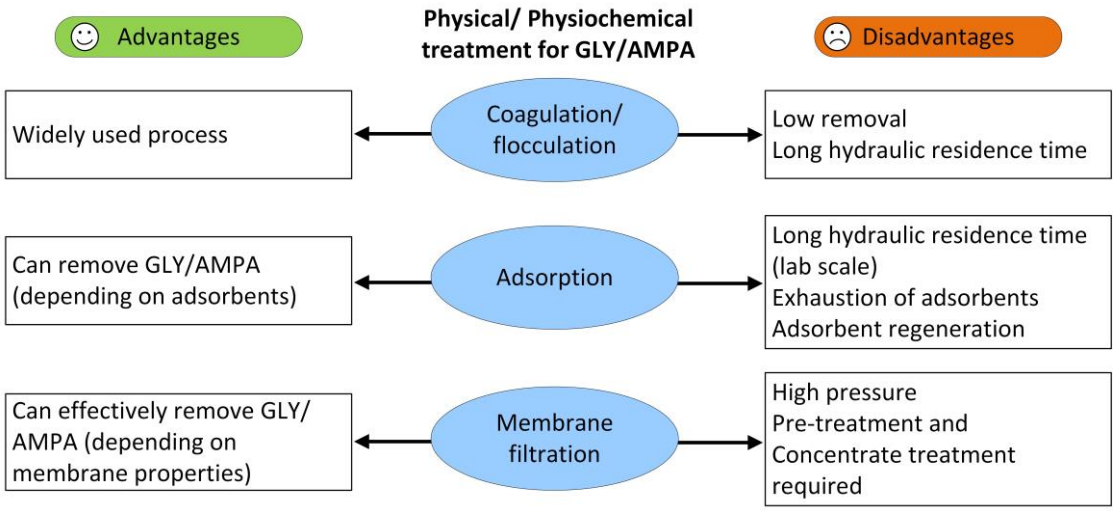

Figure 2.5. Physical/ physiochemical technologies for GLY and AMPA removal in water

Adsorption is a common technology to remove herbicides that has been applied in pilot and full-scale plants for micropollutant removal [135-139] due to its low cost, ease of operation, flexibility, and absence of by-product formation [140]. Some adsorbents for GLY removal include industrial residues [147], biochar [148, 149], ion-exchange resins [141, 142], metal–organic frameworks (MOFs) [143, 144], magnetite nanoparticles [145], and activated carbon (AC) [146, 147]. Goethite has been studied for the removal of GLY and AMPA, achieving 20–80% removal from 0.8 M salt GLY in batch experiments [148, 149]. Ion exchange in a batch reactor could remove 90% GLY from an initial concentration of 400 mg/L [142], but can only adsorb charged pollutants and ions. Interference from other water components can reduce the number of adsorption sites [150, 151]. Industrial residues and biochar could remove 60–80% GLY from 1 µg/L–100 mg/L in batch [152-154]. Metal-organic frameworks (MOFs) and metal oxide nanoparticles [155, 156] could remove > 80% GLY and AMPA, but raised toxicological concerns due to the penetration of nanoparticles into treated water [156]. Compared to other adsorbents, AC still has advantages, such as non-selective adsorption and a safe material. At the lab scale, most experiments were conducted in static adsorption, leaving the challenge of dynamic adsorption. Another drawback of adsorption is the exhaustion of the adsorbent, which will inhibit long-term operation and require adsorbent regeneration [157].

Membrane filtration acts as a physical barrier that rejects micropollutants. While microfiltration (MF) and ultrafiltration (UF) cannot remove GLY and AMPA due to the large pore size (100–10000 nm, and 2–100 nm, respectively), nanofiltration (NF, pore size 0.5–2 nm) and reverse osmosis (RO, pore size <0.5 nm) can do so due to the smaller pore size [158-161]. NF and RO membranes with a low molecular weight cut-off (MWCO, indicating the molecular weight of solutes that are at least 90% retained by the membranes) of 100–300 Da can partially remove GLY and AMPA from water [130, 162, 163]. DOW XLE and Toray THM (RO membrane, MWCO 100 Da [164, 165]) in a pilot system removed 97% AMPA from 0.7 µg/L feed under pressure of 5.8 bar [163]. A more permeable membrane, NF 300 (MWCO 180 Da), can reject 95% GLY from 48 mg/L under pressure 10 bar [162]. Looser pore NF membranes (MWCO 150–300 Da) could only remove 80% GLY and 70% AMPA from an initial concentration of 50 µg/L at 25 bar [130]. Under such high pressure (up to 25 bar for NF and up to 120 bar for RO),

GLY/AMPA removal was still incomplete due to the small molecular sizes of GLY and AMPA [54]. That is also the main disadvantage of NF and RO membranes, which is the high pressure required for operation. The pressure would be scaled up with energy consumption (0.2–0.4 kW.h/m^3 for NF, 0.4–1.7 kW.h/m^3 for RO [159, 160]) and operational cost [130, 166]. Additionally, pre-treatment [167, 168] and further concentrate treatment to eliminate micropollutants are required for membrane filtration [169].

In conclusion, adsorption by AC and membrane filtration provide efficient removal for GLY and AMPA, which will be investigated further in this dissertation.

Biological processes

Biological involves the degradation of GLY and AMPA by microorganisms, such as bacteria and fungi. Organisms break down GLY/AMPA into smaller-sized molecules (including AMPA formed during GLY degradation). In these enzymatic reactions, other by-products are produced [170]. GLY and AMPA decomposition can be carried out by fungi, bacteria, actinomycetes, and algae [170]. Borella *et al.* studied bacteria-microalgae for GLY removal, which can remove 54–79% GLY from 5–50 mg/L [171]. The degradation of different kinds of microorganisms could remove up to 90% of GLY [172]. However, these processes often take a long time, require energy for aeration, and produce sludge [173] (Figure 2.6). As the target is to treat surface water, biological treatment will not be studied in this dissertation.

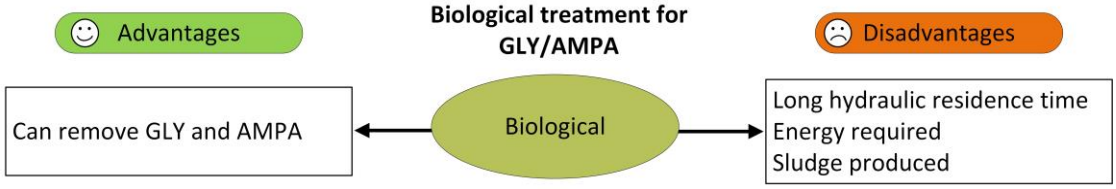

Figure 2.6. Biological treatment for GLY and AMPA in water

Advanced oxidation processes

Advanced oxidation processes (AOPs) are promising technologies with the potential for rapid, non-selective oxidation [174]. AOPs include ozonation, Fenton oxidation, electrochemical oxidation, and photochemical oxidation (Figure 2.7).

Ozonation and ultrasonication were applied to remove 45–80% GLY from water at an initial concentration of > 30 mg/L [175, 176]. Fenton reaction, such as photo-Fenton [177-179] and electro-Fenton [180, 181], could degrade 40–80% GLY from the initial concentration of 5–10 mg/L. Ti/PbO_2 anode was used to remove > 90% GLY from an initial concentration of 16.9 mg/L using electrochemical degradation [182]. However, ozonation can produce hazardous by-products, such as non-biodegradable bromates [191], while Fenton oxidation requires pre- and post-treatment, and electrochemical oxidation requires high energy and electrode maintenance

[173]. Furthermore, the stability of reactive oxygen species (ROS) precursors can also limit the performance of AOPs in GLY/AMPA degradation [183, 184].

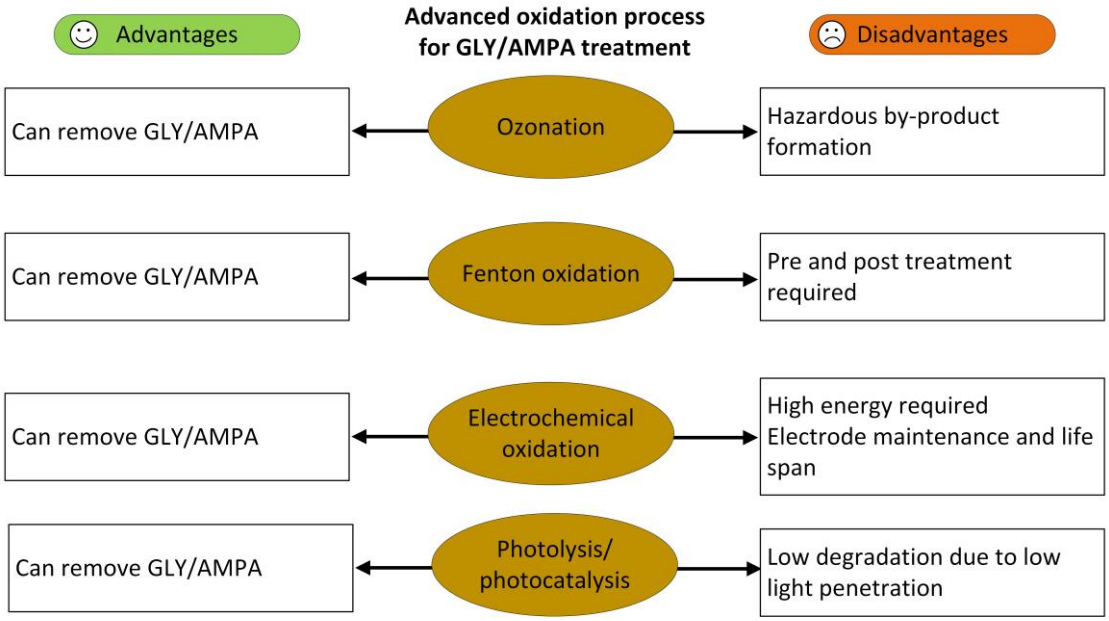

Figure 2.7. Advanced oxidation processes for GLY and AMPA treatment in water

Within AOP processes, heterogeneous photocatalysis using light-activated semiconductors introduces effective persistent micropollutants degradation, reducing the use of chemicals [185]. Due to the photocatalytic activity and physical and chemical stability, titanium dioxide (TiO_2) has been used for photocatalytic degradation [186-188]. GLY and AMPA can be effectively degraded by TiO_2-mediated photocatalysis [175]. A commercial Aeroxide© TiO_2-P25 can degrade >90% GLY from the initial concentration of 25 mg/L [189]. TiO_2-coated materials, such as magnetic NiFe2O4 [199] and graphene [200], can enhance photocatalytic degradation from 65% to >90%. However, photocatalytic degradation can be inhibited due to low light penetration in the media [190, 191].

Photocatalytic degradation shows potential for GLY/AMPA removal, which will be further studied in this dissertation.

Hybrid process

The hybrid process is the combination of different technologies (membranes, adsorption, or catalysts) in a multiple-function system [192]. In this concept, different points are connected (Figure 2.8).

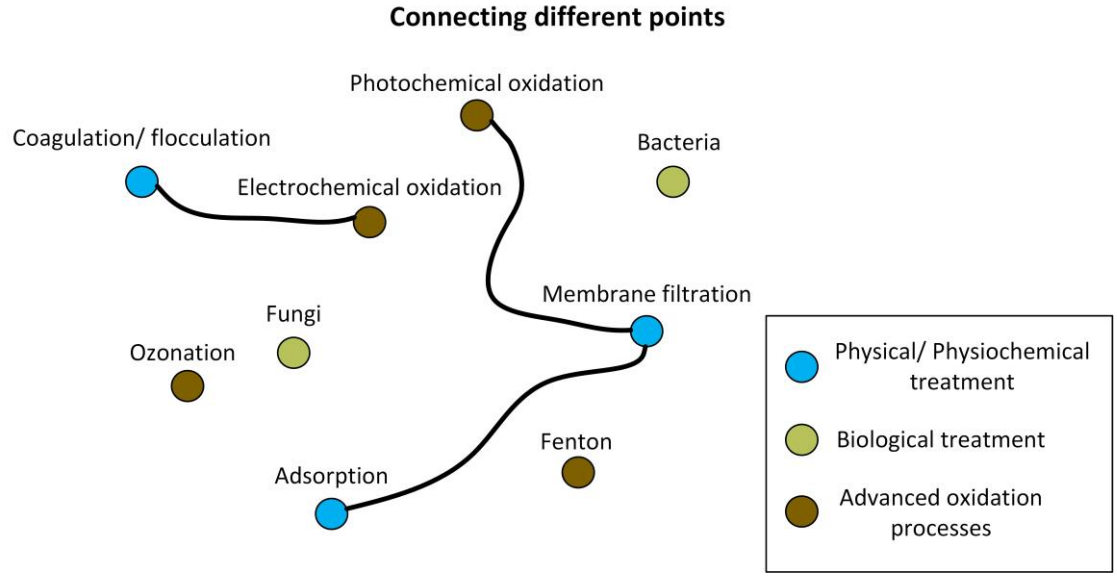

Figure 2.8. "Connecting" different water treatment technologies for GLY and AMPA removal in water

This process combines the advantages of different water treatment technologies to enhance performance while maintaining a low footprint (Figure 2.9) [193]. For example, adsorption with powdered activated carbon (PAC), which can adsorb micropollutants, was combined with UF, which retains PAC and also organic matter, bacteria, viruses, and particulates [204], or a biological method with a membrane or catalyst to degrade pollutants and then reject them from water [194]. Coagulation was combined with electrochemistry to enhance the removal [134]. However, the decision on which technologies should be chosen can be random, resulting in low performance of the hybrid system or causing additional issues (competition, unnecessary use of chemicals).

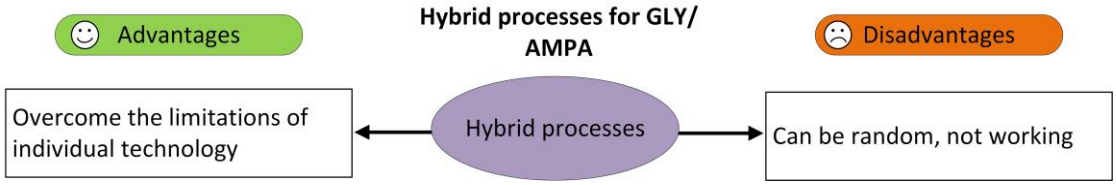

Figure 2.9. Hybrid processes for GLY and AMPA removal in water

Most reported studies on GLY/AMPA removal were carried out at high feed concentrations (in mg/L) [200, 206], which exhibited different reaction kinetics and transport [195]. In addition, achieving the water guideline (100 ng/L) remains a challenge that requires significant advancement in materials and technology processes.

2.5 GLY/AMPA adsorption by activated carbon

One of the commonly used technologies in the water treatment plant for micropollutant removal is adsorption by AC. Therefore, the first technology chosen for GLY and AMPA removal is

adsorption. First, it is important to understand the adsorption mechanisms of GLY and AMPA on AC.

GLY/AMPA adsorption mechanism on AC

The mass transfer mechanism of GLY and AMPA can be characterized in four steps (Figure 2.10) [196].

1) Bulk transfer: transport of GLY/AMPA from the bulk to the film (boundary) layer.
2) Film diffusion: transport of GLY/AMPA through the boundary layer to the AC surface.
3) Surface and intra-particle diffusion: Transport of GLY/AMPA on the surface and into the AC pore.
4) Adsorption: energetic interaction between GLY/AMPA and AC adsorption sites on both external and internal surfaces.

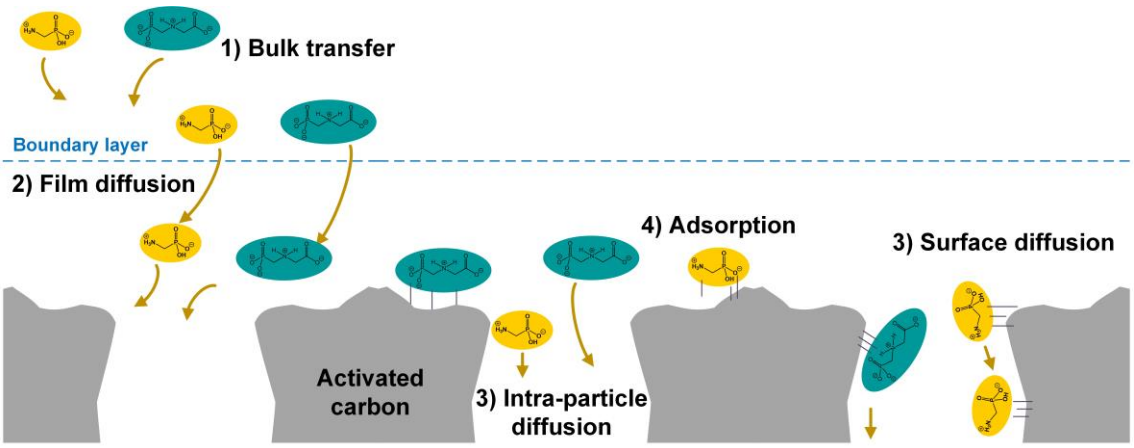

Figure 2.10. Schematic of GLY and AMPA mass transfer mechanisms by AC

While bulk transfer is considered fast, film diffusion, surface diffusion, and intra-particle diffusion are much slower, which defines the adsorption kinetics.

Energetic interactions between GLY/AMPA and AC include (1) hydrogen bonding, (2) van der Waals interaction, (3) XH–π interaction, and (4) cation–π interaction (Figure 2.11) [197, 198]. Hydrogen bonding occurs between the phosphonate or carboxylate groups of GLY/ AMPA and the functional groups on the AC surface [199]. Van der Waals interactions are applied to all GLY/AMPA molecules and AC under any conditions. Van der Waals interactions are stronger for larger molecules due to greater molecular polarizability; hence, GLY is expected to interact more strongly with AC than AMPA [200-202]. XH–π interaction, which can be considered as a type of hydrogen bonding, takes place between the electron-deficient hydrogen atom in the N–H and O–H bond and an electron-rich π-ring on AC (if applicable) [203]. Cation–π interaction is the interaction between amine groups of GLY and AMPA and the π-ring on AC (if applicable) [204]. However, the nearby carboxylate and phosphonate groups may hinder this interaction. All interactions occur when GLY/AMPA are close to the AC surface (within 0.5−1 nm) [203-205].

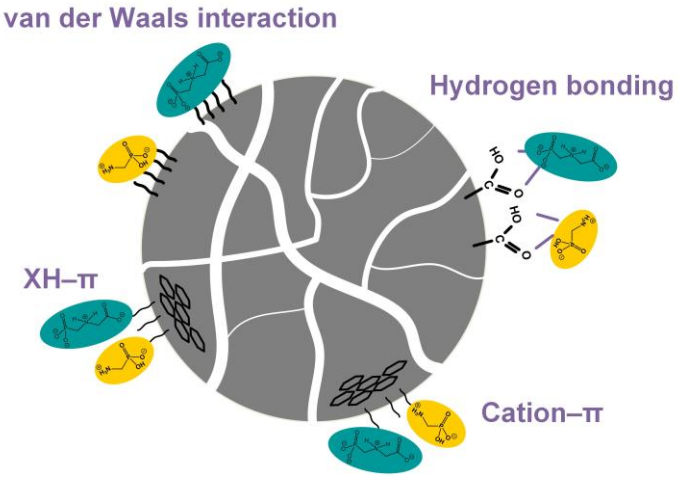

Figure 2.11. Schematic of energetic interactions between GLY/AMPA and AC

Challenges of adsorption

The important factors limiting adsorption include HRT and the availability of adsorption sites (surface area, pore volume, and loading). To achieve good adsorption performance, AC must have appropriate characteristics to overcome these limitations, which requires further investigation into adsorbent advancement. Polymer-based spherical activated carbon (PBSAC) can be a promising alternative adsorbent for micropollutant removal [206].

Polymer-based spherical activated carbon (PBSAC)

PBSAC is a commercial AC from Blücher, Germany. PBSAC has a specific surface area of 1600 – 2100 m^2/g, which is higher than GAC (500 – 1200 m^2/g) and similar to PAC (800–1700 m^2/g) [207-209]. The synthesis of PBSAC involves carbonization and activation of a well–defined, high–purity polymeric precursor [210]. PBSAC is uniform in shape and in its characteristics (size, porosity, and surface composition). Although PBSAC has a neutral net charge, Raman spectroscopy identified carboxylic groups on the PBSAC surface, with an oxygen content of 5% (the majority is carbon) [206]. Oxygen-containing groups on the PBSAC surface offer higher adsorption affinity for hydrophilic compounds such as GLY and AMPA. PBSAC has a pore volume of 0.6–1.3 cm^3/g, with a maximum of 3.5 cm^3/g [210], greater than PAC (0.2–1 cm^3/g) [209]. Compared to conventional AC, the increased surface area and pore volume may enable a larger adsorption capacity.

In previous studies, PBSAC could remove >90% of hydrophobic micropollutants, such as steroid hormones (17β-Estradiol), which have a higher molecular weight (272 g/mol) than GLY and AMPA [206]. The adsorption of steroid hormone was significantly faster with the smallest PBSAC size (diameter of 78 µm) than GAC (diameter of 0.4–1.1 mm) [206, 211, 212]. The EU guidelines for steroid hormones were achieved by adsorption on PBSAC [207]. With the proven high adsorption for micropollutants, PBSAC will be selected to remove GLY and AMPA from water in this dissertation, with the expectation of overcoming the complex physicochemical properties of GLY/AMPA.

While most lab-scale adsorption experiments are in batch mode, the hybrid adsorption-membrane system can operate in dynamic mode, taking advantage of both processes.

2.6 Membrane-adsorption hybrid processes

As mentioned in the previous section, this process combines the advantages of different water treatment technologies to enhance performance while maintaining a low footprint (Figure 2.9) [193].

Hybrid membrane process designs

Three main designs for hybrid systems include: (1) feed-side adsorption (adsorption before filtration), (2) integrated adsorption–filtration (adsorbents and membranes are in the same module), and (3) permeate-side adsorption (filtration before adsorption) (Figure 2.12) [193].

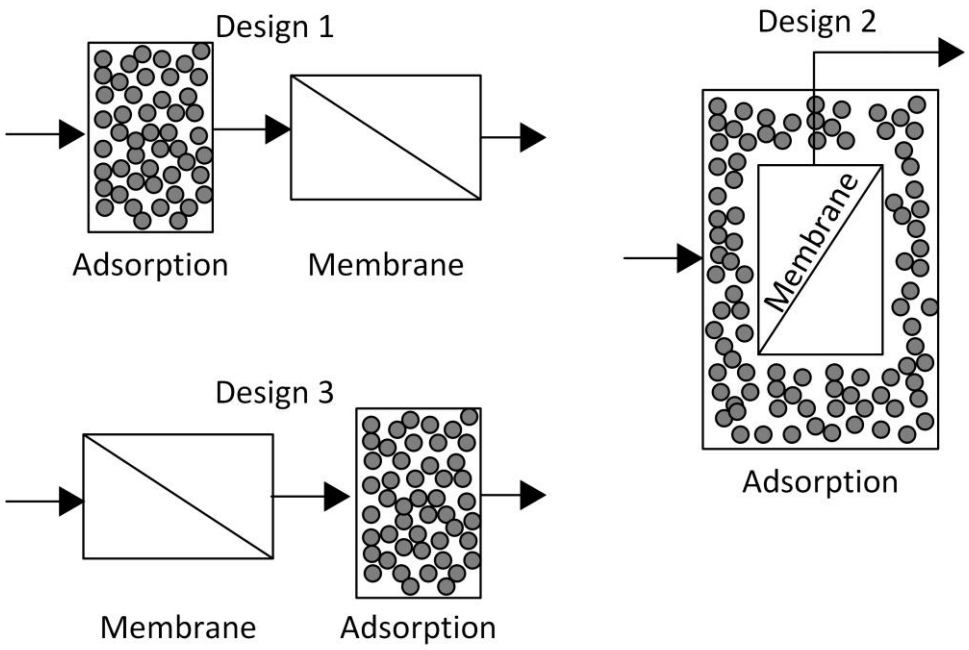

Figure 2.12. Three hybrid membrane process designs: feed-side adsorption (Design 1), integrated adsorption-filtration (Design 2), and permeate-side adsorption (Design 3). Adapted from [193].

Design (1) feed-side adsorption and design (2) integrated adsorption–filtration could remove 60–90% of micropollutants such as steroid hormones and pharmaceuticals from water [135, 192]. The addition of AC adsorption before membrane filtration can effectively reduce fouling in membrane processes [213, 214]. The drawback of these systems was direct contact between the adsorbents and all feed water components (such as organic matter, bacteria, and viruses) [137, 215], which could compete for adsorption sites and interfere with micropollutant adsorption [216-219]. On the other hand, permeate-side adsorption is more attractive, as micropollutants are removed by adsorption from polished water [232, 233], which means the membrane acts as a barrier to retain organic matter and bacteria, thereby enhancing adsorption perfor-

mance. The combination of adsorption, which can remove GLY/AMPA, and a membrane, which can retain AC particles and other water components (organic matter, bacteria, viruses, and particulates), is promising [193].

Hybrid membrane process and adsorptive composite membrane

The hybrid system can be mistaken for a composite membrane. The concept of adsorptive composite membrane is the immobilization of adsorbents in/on the membrane [48, 153]. The adsorptive composite membrane designs include mixed-matrix membranes [220], feed-side incorporation in MF/UF membranes [220], and permeate-side incorporation in MF/UF membranes [221]. While the hybrid system is often applied to AC (PAC, GAC), an adsorptive composite membrane is used for sub-micrometer to nanometer-sized adsorbents (i.e., nanoparticles or superfine PAC). UF membrane was integrated with carbon nanotubes in its ultrathin sub-millimeter support layer, which could remove 85% steroid hormones [221]. However, the use of carbon nanotubes raises toxicological concerns, as their release into water and the environment can be challenging to assess [222]. Moreover, due to the limit on adsorbent loading in adsorptive composite membranes, the hybrid membrane–adsorption system is more preferred for applications.

Ultrafiltration membrane with permeate side PBSAC (UF–PBSAC)

While NF membranes can remove GLY and AMPA, the main disadvantage remains in the high applied pressure. UF membranes with higher permeability cannot remove GLY and AMPA due to their large pore size, as discussed in the previous section, but require less energy for operation [161]. However, micropollutant removal can still be achieved by integrating membrane and adsorption in an in-situ or flow-through mode. In this case, UF membrane can be a barrier to retain organic matter and bacteria, subsequently enhancing the adsorption performance [223]. Based on this concept, Tagliavini *et al.* combined ultrafiltration with a millimetric permeate-side layer of polymer-based spherical activated carbon (UF–PBSAC) to remove steroid hormones. UF–PBSAC could remove > 96% steroid hormones from an initial concentration of 100 ng/L [207]. Steroid hormone adsorption was limited by mass transfer, as adsorption occurred only on the external surface of PBSAC at short HRT (< 20s) [207]. When adsorbents are incorporated into membranes for ‘dynamic’ adsorption, GLY and AMPA removal is expected to be poorer due to the short HRTs in the adsorbent layer, which can limit GLY/AMPA diffusion to the adsorption sites [139, 224]. Therefore, GLY/AMPA needs to overcome the mass transfer limitation to reach the adsorbent surface within a short HRT in a dynamic adsorption−filtration process.

In conclusion, UF–PBSAC can be studied for GLY/AMPA removal, in which PBSAC adsorbs GLY/AMPA while the membrane rejects organic matter and bacteria, which can interfere with adsorption performance. The limiting factor can be the HRT, in which GLY/AMPA has less time to interact with PBSAC in dynamic mode.

2.7 GLY/AMPA rejection by NF membrane

NF membrane can remove GLY and AMPA, as sub-nanometer pores reject target molecules [225-227]. In pressure-driven processes, pressure was applied to the membrane, pushing water and GLY/AMPA molecules toward the membrane surface. The rejection mechanisms of micropollutants by NF/RO membranes include (1) size exclusion, (2) Donnan exclusion, and (3) dielectric exclusion [228, 229].

Size exclusion

Membrane removes GLY/AMPA based on relative membrane pore size and molecular size (Figure 2.13) [230-232]. Molecules with a diameter smaller than the membrane pore diameter can pass through the membrane, and molecules with a diameter bigger than the membrane pore are retained in the concentrate. Rejection by size exclusion depends on NF membrane pores and the molecular characteristics of GLY/AMPA [233]. However, the membrane pores are not uniform in size [234, 235], and the GLY/AMPA molecules are diverse in shape and orientation [236], leading to the molecules subsequently passing through the membrane.

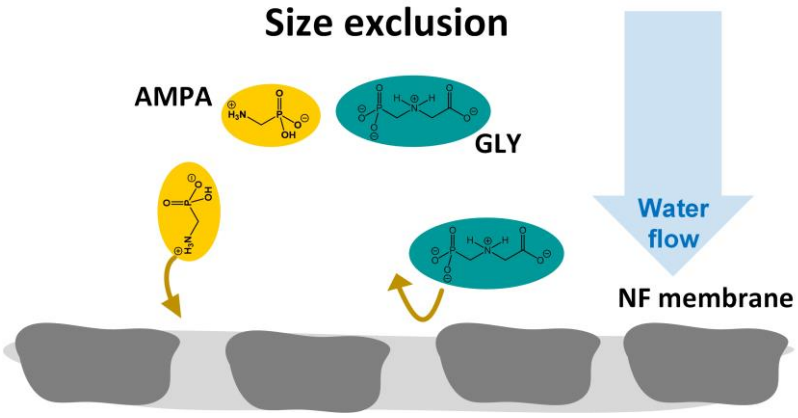

Figure 2.13. GLY/AMPA rejection by NF membrane via size exclusion

Donnan (charge) exclusion

GLY/AMPA can be retained by the membrane due to charge interactions (electrostatic repulsion/ attraction) between the charged GLY/AMPA molecules and the charged surface of the membrane [237-239]. Electrostatic repulsion occurs between GLY/AMPA and the membrane with the same charge, while electrostatic attraction occurs between ions/molecules and the membrane with a different charge.

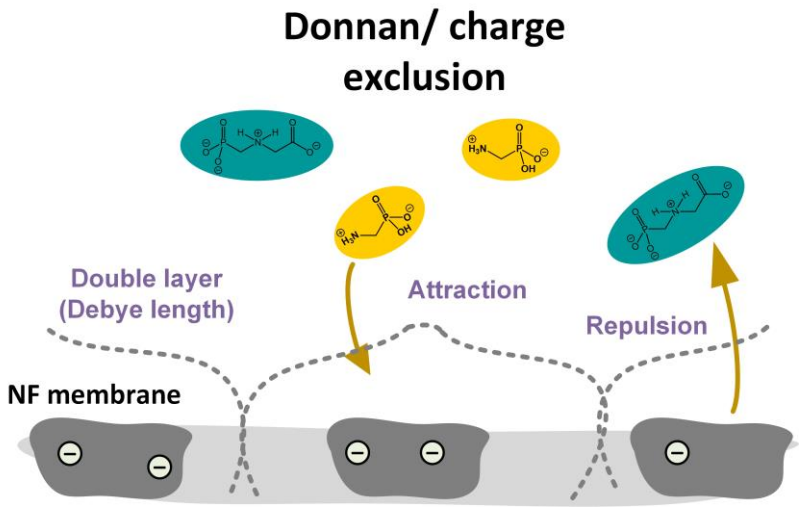

Figure 2.14. GLY/AMPA rejection by NF membrane via Donnan exclusion

The charge exclusion is defined by the double layer of the membrane, a structure containing ions formed on the interface between the membrane and the surrounding water environment [240-242]. The double layer on the membrane surface is characterized by the zeta potential ζ [240] and the double layer thickness of charge solutes on the membrane surface (Debye length, κ^{-1}) [241, 242]. While ζ quantifies the charge of the membrane, κ^{-1} defines the change in the interaction between the molecules and the pore. Zeta potential ζ is the electrical potential at the slipping plane at which distance from the membrane surface the electrolyte ions become mobile [240]. The more negative the zeta potential ζ is, the more negative the membrane surface charge is. The commercial NF membrane surface is usually negatively charged at operational pH [243, 244]. As GLY and AMPA are negatively charged at neutral pH 8, electrostatic repulsion between GLY/AMPA and the NF membrane.

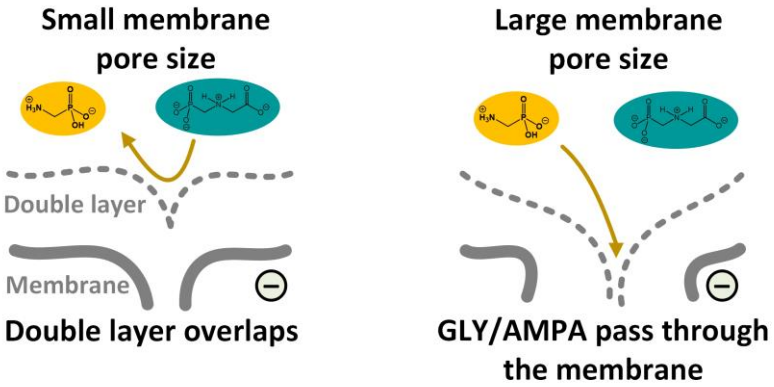

Figure 2.15. Debye length at different membrane pore sizes

The Debye length describes the thickness of the double layer, in which the transport of GLY and AMPA molecules smaller than the membrane pore size can be controlled by charge exclusion (Figure 2.15) [241, 242, 245]. If the Debye length is greater than the pore radius, charged species can interact with charged pore walls. Hence, depending on the charge of the pore wall,

the molecules might encounter the electrostatic resistance [246]. If the Debye length is smaller than the pore radius, molecules will be able to pass through the pores without electrostatic interaction with the pore wall. Naturally, pores are tortuous, which complicates the transport of GLY and AMPA molecules.

Dielectric exclusions

Dielectric exclusion is the phenomenon in which GLY and AMPA transport from the bulk solution to membrane pores is hindered by the difference in dielectric constant [237, 247]. In the bulk solution, a molecule is surrounded by water molecules, forming the hydration layer (Figure 2.16) [200]. When a GLY/AMPA molecule enters a membrane pore from the water solution, it needs to be dehydrated [248] and move from an environment with a higher dielectric constant to one with a lower dielectric constant [249, 250], which requires energy [237, 251, 252]. Therefore, dielectric exclusion is related to (1) the combined size of the molecule and the hydration layer being larger than the pore [247, 253], and (2) the resistance of the molecule entering the membrane pores due to the energy barrier caused by the hydration shell [254]. Dielectric exclusion is independent of the net charges of the GLY/AMPA and the membrane; hence, it always occurs in membrane filtration and plays an important role in micropollutant rejection [249]. Studies on ion rejection by NF membranes showed that dielectric exclusion contributed 50–70% to ion rejection [255]. It is potentially an important mechanism in NF pore transport that has been examined for ions [238, 256] but not yet for charged organic compounds.

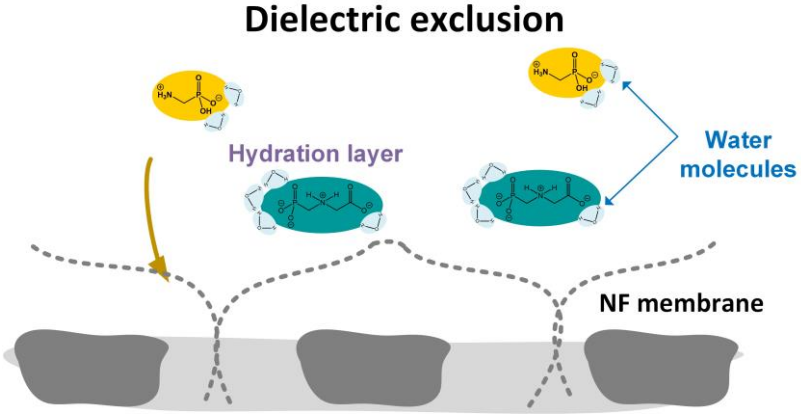

Figure 2.16. GLY/AMPA rejection by NF membrane via dielectric exclusion

Sorption–diffusion

GLY and AMPA can be adsorbed on membrane surface materials (such as polyamide) *via* H-bonding [130] and van der Waals interaction [130, 257]. Then, the molecules can partially transport through the membrane pores due to a combination of desorption, diffusion, and convection (Figure 2.17) [228, 229]. GLY/AMPA, as charged and hydrophilic micropollutants, have weaker interactions with polyamide than uncharged and hydrophobic micropollutants [258]. Therefore, the adsorption on membrane material is lower [130] and less GLY/AMPA is transported through NF membrane pores by sorption–diffusion than uncharged and hydrophobic micropollutants.

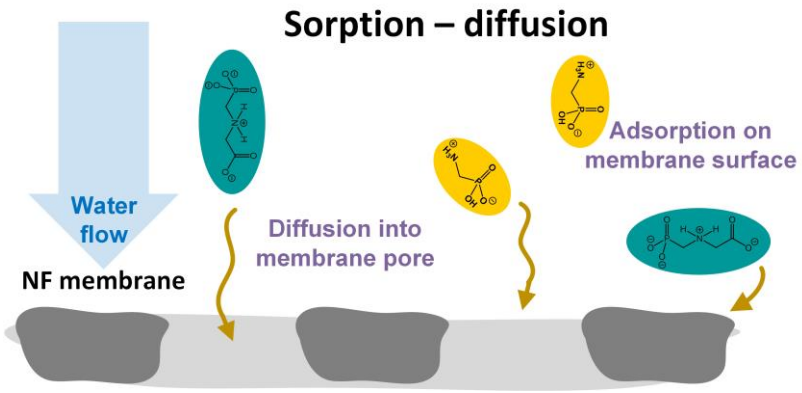

Figure 2.17. GLY/AMPA transport in NF membrane via sorption–diffusion

While adsorption is commonly used in water treatment, NF membranes can effectively reject micropollutants such as GLY and AMPA. As previous studies mainly focused on high concentrations of GLY/AMPA, herbicide removal at environmentally relevant concentrations is needed. From the transport mechanism, the removal of GLY and AMPA can be strongly dependent on the membrane choice (pore size, charge) and the charge of GLY and AMPA. In addition, flux can also be a limiting factor.

2.8 GLY/AMPA removal by photocatalytic degradation

Heterogeneous photocatalysis using TiO_2 can degrade 65% to >90% of GLY at an initial concentration of 25 mg/L in previous work [189]. In fact, TiO_2 has been extensively researched for photocatalytic degradation owing to its physical and chemical stability, and photocatalytic activity [186-188].

Mechanisms of GLY and AMPA photocatalysis degradation by TiO_2

TiO_2 absorbs photons, leading to the excitation of electrons from the valence band to the conduction band (e_{CB}^-) and generates electron holes in the valence band (h_{VB}^+) [259, 260]. The charge carriers e_{CB}^- and h_{VB}^+ can directly degrade GLY/AMPA adsorbed on the TiO_2 surface. These charge carriers can also react with oxygen and water in redox reactions, generating ROS. h_{VB}^+ can oxidize water molecules (H_2O) or hydroxide ions (OH^-), generating hydroxyl radicals (•OH), a ROS with strong reactivity [261, 262]. Meanwhile, e_{CB}^- can reduce oxygen to create superoxide radicals ($•O_2^-$) [263]. The photodetachment of electrons from $•O_2^-$ forms the singlet oxygen ($^1O_2$) [264, 265]. These ROS subsequently degrade GLY and AMPA [266].

GLY and AMPA can be oxidized by ROS, following two main pathways: (1) C–N bond cleavage, forming AMPA and glyoxylic acid, and (2) C–P bond cleavage, generating sarcosine, which is then degraded to glycine [267]. Pathway (2) is preferred due to the formation of safer intermediate products [267-269]. However, the C–P bond in GLY and AMPA, which has a high bond energy, is thermally stable and chemically resistant [270]. Therefore, AMPA is the main product of GLY degradation [175]. In synthetic and real water matrices, the presence of ROS

scavengers (*i.e.*, CO_3^{2-}, HCO_3^-) can compete with GLY and AMPA for ROS reactions, leading to incomplete degradation [271, 272].

Photocatalytic membrane reactors

Photo-catalyst recovery, mass transfer of reactants/ROS, and reduced illumination due to agglomeration and turbidity of photocatalyst nanoparticles are problems in conventional suspension photocatalysis systems [273, 274]. In batch, Chen *et al.* found that TiO_2 loading was a limiting factor for GLY degradation, as more ROS were produced [191]. However, further increase in TiO_2 loading could prevent light penetration and might cause catalyst agglomeration [190, 191]. The need for photocatalyst recovery and the potential for catalyst agglomeration in suspended systems can be reduced by using a photocatalytic membrane reactor, a hybrid technique that combines membrane filtration with photocatalysis in a single unit [275-277]. Another drawback of both batch and photocatalytic membrane reactors is mass transfer [277], which can be reduced by operating in turbulent flow [278] *via* diffusion in the membrane at low flux. The disadvantages of batch systems may be overcome by membrane photocatalysis, which offers a high surface-to-volume ratio, thereby improving pollutant-catalyst contact [279, 280]. TiO_2 has been integrated into polyether sulfone (PES) and poly(vinylidene fluoride) (PVDF) membranes to enhance the removal of micropollutants, such as steroid hormones [292] and pharmaceuticals [293, 294], with removal exceeding 90%. With such degradation efficiency, the TiO_2-based photocatalytic membrane is expected to degrade GLY and AMPA in water effectively.

The photocatalytic membrane must be stable under extended exposure to 1) ultraviolet light/sunlight, 2) reaction with ROS, and 3) applied pressure. PVDF membrane has shown the least total organic carbon (TOC) release under continuous UVA (350–400 nm, 2 mW/cm2) irradiation and negligible change in membrane resistance to UV light (estimated by flux) [281]. In a previous study on stability, the PVDF-TiO_2 membrane maintained its structural integrity and photocatalytic activity after 250 hours of accelerated ageing under intense UV-violet illumination (2223 W/m^2 of combined 365 nm and 405 nm light). The photodegradation of micropollutants remained stable under prolonged UV exposure, and the TiO_2 photocatalyst remained embedded within the polymer matrix, preventing leaching and maintaining photocatalytic activity [282]. Therefore, PVDF-TiO_2 membrane can be chosen for GLY/AMPA degradation evaluation.

2.9 Comparison between water treatment technologies

A comparison between different removal technologies for GLY and AMPA is important. However, a meaningful comparison is challenging due to the differences between each technique. As the target is to meet EU guidelines for herbicides, the concentration would be a criterion which will be compared with the guidelines (100 ng/L of each herbicide and 500 ng/L of total herbicides) [13]. Performance parameters, including removal of GLY/AMPA and permeability (flux), are fundamental for the direct comparison [135, 192]. The removal quantifies the amount of GLY/AMPA removed after treatment, while pure water permeability is a membrane property

that indicates HRT. In this dissertation, the filtration experiment will proceed at synthetic water (10 mM NaCl and 1 mM $NaHCO_3$), where no fouling is expected; hence, flux is expected to be stable before and after the experiment. The specific energy consumption (SEC) is the energy demand (kWh) per volume (m^3) of permeate and is a figure of merit for comparing different technologies of similar scale [283, 284]. However, this parameter does not consider the removal as a performance evaluation [285]. Moreover, comparing systems at different scales is impossible, as smaller systems will consume more energy to treat the same amount of water as larger systems [286, 287].

In this dissertation, theoretical energy consumption based on hydraulic energy (for the membrane system) and light energy (for the photocatalytic system) will be used to compare different systems at a lab scale. In the hybrid membrane–adsorption system and the nanofiltration membrane system, the energy was used for hydraulic energy ($E_{hydraulic}$, J) as follows.

$$E_{hydraulic} = \Delta P \cdot \mathrm{V} \tag{2.4}$$

where ΔP is the transmembrane pressure (Pa), and V is the permeate volume (L), assuming 100% pump efficiency and that motor losses, friction in tubing, and energy to maintain temperature and stirring were not considered.

In the photocatalytic membrane system, the required theoretical energy was from the pump, which is defined by hydraulic energy ($E_{hydraulic}$, J), and from the light source. The energy used for the light source (E_{light}) in the photocatalytic system is calculated by the following equation.

$$E_{light} = \mathrm{I} \cdot \mathrm{A} \cdot \mathrm{t} \tag{2.5}$$

where I is the irradiance at the membrane (W/m^2), A is the membrane surface area (m^2), and t is the illumination time (s), with the assumption that no light was lost and all light would reach the membrane surface during the experiment.

The total theoretical energy (E_{total}, J) of the photocatalytic membrane is the sum of hydraulic energy and light source energy.

$$E_{total} = E_{hydraulic} + E_{light} \tag{2.6}$$

To normalize energy consumption, the total energy was divided by the volume of treated water, and the removal of GLY and AMPA [288]. It is noted that theoretical considerations are used as the foundation, but this cannot be directly translated to larger-scale conditions, where membrane fouling, cleaning, and maintenance need to be considered. The theoretical energy will be presented in comparison in Chapter 8.

2.10 Summaries of the key interests

In this chapter, the properties, fate, and occurrence of GLY and AMPA in the water environment have been reviewed, indicating the need for further study of GLY and AMPA. The analytical methods and removal technologies of GLY and AMPA have been evaluated. The analysis

has not been optimized for environmentally relevant concentrations of GLY and AMPA, nor for water samples from removal experiments. Therefore, in Chapter 3, the analytical method development will be conducted to achieve a low LOD with a low sample volume and without sample pretreatment.

The removal of GLY and AMPA was incomplete due to the complex properties of the herbicides. To achieve the goal of reducing GLY and AMPA concentration to meet the EU guideline value for herbicides, investigations on four different technologies, including membrane filtration (nanofiltration membrane, NF), adsorption (polymer-based spherical activated carbon, PBSAC), adsorption–membrane hybrid system (ultrafiltration membrane with permeate-side polymer-based spherical activated carbon, UF–PBSAC), and photocatalytic membrane (TiO_2-coated poly(vinylidene fluoride) membrane, PVDF-TiO_2), will be conducted (Figure 2.18).

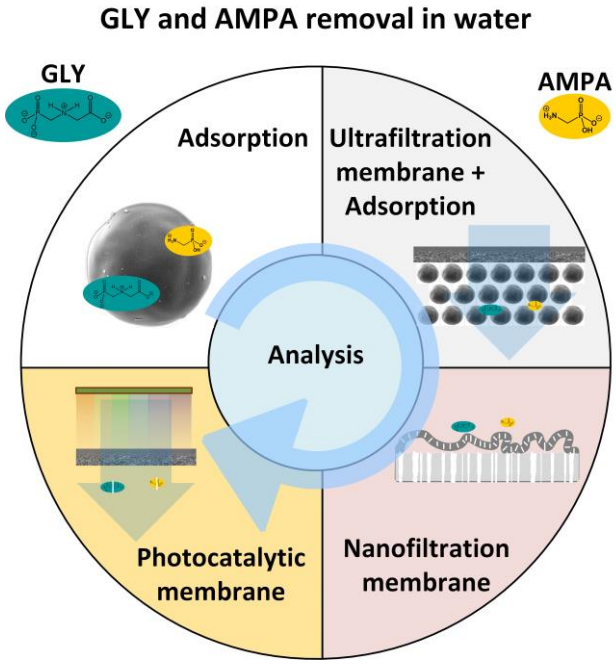

Figure 2.18: GLY/AMPA removal technologies of interest

Different water treatment technologies have their own advantages and disadvantages, as well as different micropollutant removal efficiencies.

- At the lab scale, adsorption could be limited by available adsorption sites (surface area, pore volume, loading) and by HRT.
- UF–PBSAC adsorption could be limited by HRT, where GLY/AMPA has less time to interact with PBSAC in a dynamic mode.
- NF membrane filtration could be strongly dependent on the membrane choice (pore size, charge), the charge of GLY and AMPA, and flux (HRT).
- PVDF-TiO_2 membrane could be dependent on the flux (HRT), the irradiance, and the ROS reaction.

Therefore, for each technology, the removal capacity, limiting factors, and optimization based on the studied limiting factors will be investigated. The different water treatment technologies will be compared based on permeate concentration, removal, permeability (HRT), and theoretical energy consumption.

3 Analytical method development

This chapter is adapted from a submitted manuscript to ChemSusChem (October 2025) entitled "Determination of glyphosate (GLY) and aminomethylphosphonic acid (AMPA) in water by direct injection liquid chromatography tandem mass spectrometry (LC-MS/MS)" by Phuong B. Trinh, Derek J. Mattern, and Andrea I. Schäfer [289].

The contribution of authors:

Phuong B. Trinh: conceptualization; performing sample analysis; trouble shooting; data analysis and interpretation; methodology; validation; visualization; writing – original draft

Derek J. Mattern: trouble shooting; methodology; resources; writing – review & editing

Andrea I. Schäfer: funding acquisition; project administration; resources; supervision; writing – review & editing

The chapter systematically describes the analytical method development for GLY and AMPA in water, starting from the problem identification of the analysis. The method optimization is subsequently presented following sample preparation, sample injection, and liquid chromatography. After finalizing the optimized analytical method, a comprehensive problem-solving strategy will be reviewed for GLY and AMPA analysis, and the method will be applied to water treatment technologies.

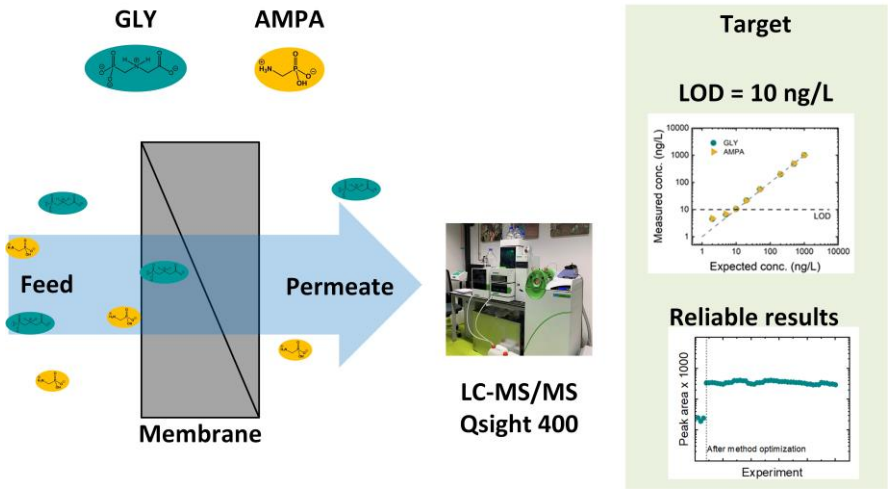

3.1 Chemicals and solution chemistry

GLY (Sigma-Aldrich, 98%) and AMPA (Sigma-Aldrich, 99%) powders were dissolved in Milli-Q water (Reference A+, Merck Millipore, USA) to prepare a mixture stock at a concentration of 100 mg/L for each compound (Stock 1). Stock 2 with GLY/AMPA 1 mg/L was prepared by diluting Stock 1 in Milli-Q water. Feed solutions of GLY and AMPA (0.1−500 µg/L) were prepared by diluting Stock 2 in Milli-Q water and background electrolyte solutions (1 mM $NaHCO_3$ and 10 mM NaCl). The feed with an elevated concentration of 1 mg/L was prepared by directly diluting Stock 1 in Milli-Q water and the stock background electrolyte solutions. All experiments proceeded in a GLY and AMPA mixture at 1000 ng/L for each compound, except for experiments with variable feed concentration.

The background electrolyte was a mixture of 1 mM $NaHCO_3$ and 10 mM NaCl, with a conductivity of 1400 µS/cm and a pH of 8.1 ± 0.1. For the experiment at varying pH, the pH was adjusted by 1 M HCl (diluted from 37% HCl, Roth, Germany) and 1 M NaOH (dissolved from pellets, Merck, 99%).

Analytical standards (analytical-grade, 100 mg/L in Milli-Q water) of GLY and AMPA were from Dr. Ehrenstorfer (Germany). The internal standard was ^{13}C GLY (analytical grade, 98%, Sigma-Aldrich (USA)), and the buffer was ammonium formate powder (analytical grade, 99%, VWR (Germany)).

3.2 Analytical method

GLY and AMPA analysis mostly focused on the higher concentrations at high LOD, higher than environmentally relevant concentrations (from ng/L to µg/L). In addition, sample preparation for analysis often requires a high extraction volume, which is not realistic for water samples from lab-scale water treatment experiments, where the sample volume ranges from 2–10 mL.

Each water treatment technology poses different challenges in analysis. Adsorption (PBSAC, UF–PBSAC) often has samples at low concentration, which is expected to be lower than 50 ng/L. Therefore, a low LOD is required. For NF membrane filtration, in addition to low-concentration samples, sample salinity was the main challenge, with permeate samples at low salinity and retentate samples at high salinity. Moreover, salinity can vary with different NF membranes. For the PVDF-TiO_2 membrane, degradation products can create new peaks and can co-elute with GLY and AMPA, leading to the over- or underestimation in analysis [100] and increasing ion suppression [101]. With the requirement for analysis at environmentally relevant low concentrations (in the range of ng/L to µg/L) and low sample volumes, studies on analytical method development are needed to support further investigation of treatment technologies.

As GLY and AMPA are “tricky” to analyze, the analytical method was developed by P.T. and Dr. Mattern (Perkin Elmer) and then modified by P.T. to adapt to the water conditions in the filtration system at IAMT. The main goal is to analyze GLY and AMPA in water (with background water containing 1 mM $NaHCO_3$ and 10 mM NaCl) using a low sample volume and a

low limit of detection (LOD) without a derivatization step. The target LOD was 10 ng/L, and the sample volume was < 2 mL.

GLY and AMPA were analyzed by liquid chromatography with tandem mass spectrometry (LC-MS/MS). The system had an LX50 ultra-high performance liquid chromatographic system coupled to a QSight 420 triple-quadrupole mass spectrometer (PerkinElmer, USA) [197] (Figure 3.1). The used column was a hydrophilic interaction liquid chromatography (HILIC) column, Obelisc N 2.1·150 mm, 5 µm (SIELC Technologies, USA). The main drawback of this column was the rapid degradation, leading to a short column lifetime [290].

Figure 3.1: Photo of liquid chromatography with mass spectrometry (LC-MS/MS)

3.3 The first approach: problem identification

The first analytical protocol involves direct injection of samples into LC-MS/MS without additional steps. GLY and AMPA samples were prepared in the background electrolyte solution and did not need a pre-filter. The chosen mobile phase was Milli-Q water with 0.05% ammonium formate (CH_2O_2) and acetonitrile (ACN) with 0.05% CH_2O_2, in an isocratic mobile phase of 85/15 v/v (H_2O:ACN + 0.05% CH_2O_2) at a flow rate of 0.6 mL/min. Electrospray ionization (ESI) was applied in negative mode at a source temperature of 450 °C and a surface-induced desolvation temperature of 320 °C. The injection volume was 100 µL, and the elution time was 6 minutes.

To evaluate the performance of the analytical method, 100 samples containing 1000 ng/L of GLY and AMPA were prepared in background electrolyte solutions (BG, 10 mM NaCl and 1 mM $NaHCO_3$) and analyzed on different days (Figure 3.2).

In the first method, the peak area of GLY and AMPA was not reproducible (Figure 3.2). The peak area of GLY and AMPA changed from 1000 to 75000 for GLY, and from 500 to 40000 for AMPA. In LC-MS/MS using an electrospray ionization source (ESI), after exiting the LC column, GLY/AMPA enter the ESI source at high voltage to form charged droplets [291]. The high electric field at the tip of the source sprays liquid into a fine mist of deprotonated droplets. The droplets shrink by solvent evaporation until the solvated ions can be expelled from the

droplet, which is then drawn into the MS [292]. With this principle, if the ionization is hindered, the analysis is not correct. Therefore, factors that can affect ionization can be the problem which include background solution and contamination.

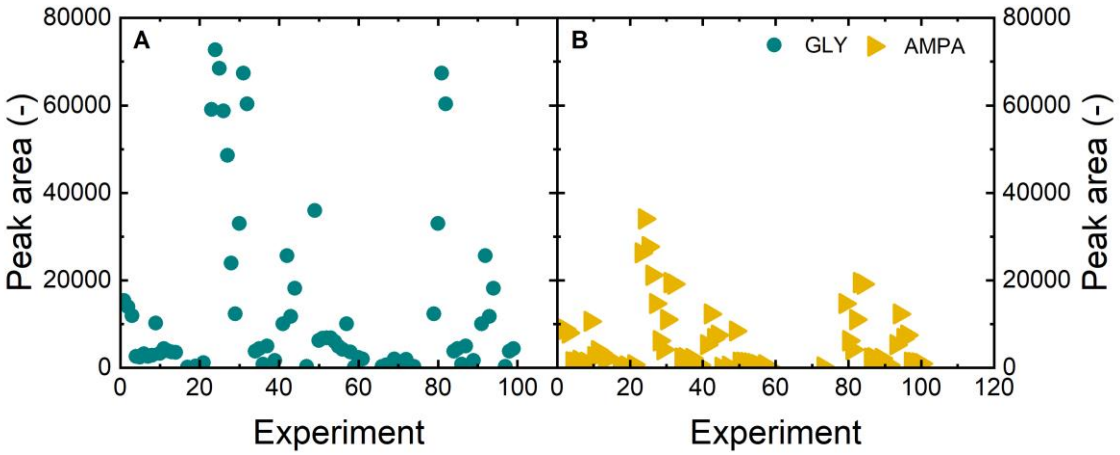

Figure 3.2. Peak area of GLY and AMPA 1000 ng/L in background electrolyte solution with 100 independent runs (commercial purchased analytical standard, flow rate 0.6 mL/min, ACN 15 %, injection volume 100 µL, independent runs). Adapted from [289].

To understand why the signal for GLY and AMPA varied significantly, GLY/AMPA at 1000 ng/L were measured in different solutions (Milli-Q and background electrolyte solution) (Figure 3.3).

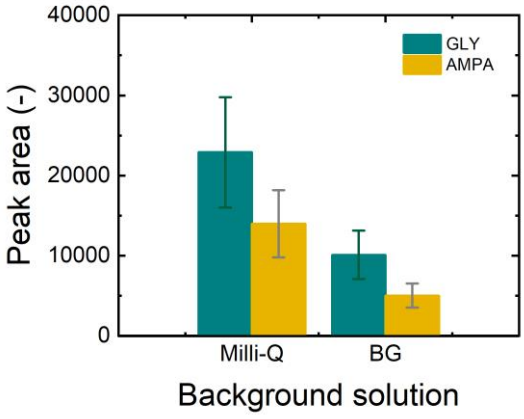

Figure 3.3. Peak area of GLY and AMPA 1000 ng/L prepared in Milli-Q and background electrolyte (BG) solution; (commercial purchased analytical standard, flow rate 0.6 mL/min, ACN 15 %, injection volume 100 µL, independent runs). Adapted from [289].

The peak area of GLY was 23000 ± 220, and the peak area of AMPA was 14000 ± 120 when the samples were diluted in Milli-Q water. However, the peak area declined significantly to 10000 ± 100 for GLY and 5020 ± 45 for AMPA when prepared in background electrolyte solutions. This phenomenon demonstrates that background salt could reduce the LC-MS/MS

signal intensity. Indeed, salt has been identified to cause ion suppression on the analysis of polar compounds by LC-MS/MS [293, 294]. Therefore, the analytical method needed to be optimized to be suitable for water samples in background electrolyte solutions.

Contamination can also interfere with the analysis by LC-MS/MS, especially the contamination from the phosphate compounds. Hellmanex is a common lab-cleaning detergent, an alkaline cleaning concentrate containing the main component tripotassium orthophosphate (K_3PO_4) [295]. In the lab, Hellmanex appears in glassware and in the system, which could affect the analysis of GLY and AMPA due to the phosphate group in Hellmanex molecules. Therefore, Hellmanex will be investigated for the contamination in the analysis (Figure 3.4). Glassware in the lab is usually cleaned with Hellmanex 2% [215], which is ~2000 mg/L K_3PO_4. Therefore, to evaluate the effect of Hellmanex on GLY/AMPA analysis, GLY and AMPA at 1000 ng/L in background electrolyte solution were prepared with Hellmanex concentrations of 0, 1, 2, 3, and 15% corresponding to K_3PO_4 concentrations of 0, 1, 2, 3, and 15 g/L.

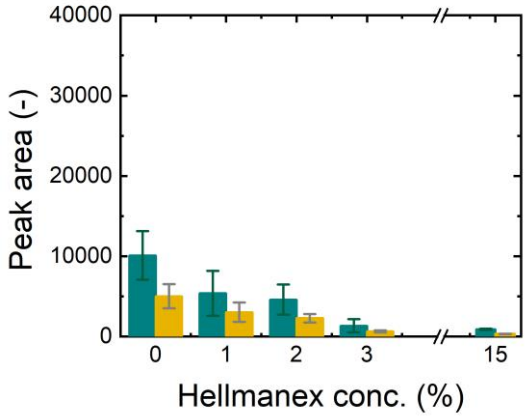

Figure 3.4. Peak area of GLY and AMPA 1000 ng/L with contamination of Hellmanex at concentration 0–15% (commercial purchased analytical standard, flow rate 0.6 mL/min, ACN 15 %, injection volume 100 µL, independent runs). Adapted from [289].

Obviously, Hellmanex interfered with the analysis by decreasing the peak area of GLY and AMPA. The peak area of GLY decreased from 10000 ± 100 to 890 ± 98, while the peak area of AMPA decreased from 5020 ± 45 to 339 ± 55 with the increase of Hellmanex concentration. The phosphate group in Hellmanex can exhibit similar chromatographic behavior to that of GLY/AMPA [296]. Subsequently, it can compete with the LC column interaction and cause ion suppression. Ion suppression can further reduce sensitivity, leading to depletion of the analyte signal [297]. As a result, Hellmanex (and other phosphate interferants) must be avoided in a laboratory where GLY and AMPA analysis is conducted. All glassware needs to be cleaned following the cleaning protocols using 2 M HCl and 2 M NaOH, then separated from other labware used for other purposes.

The two main issues with the LC-MS/MS system are inconsistency and low peak area, leading to unreliable results and a low LOD. Both can be affected by sample preparation, injection, column performance, or mass spectrometry. In fact, the core reason behind all these issues is ion

suppression, which is a major analytical problem in LC-MS/MS [129]. It can change the efficiency of droplet formation and droplet evaporation; hence, affecting the amount of charged ions in the ionization of MS [127]. It results from endogenous substances (NaCl and $NaHCO_3$ in background electrolyte solutions) and exogenous substances (Hellmanex) [127, 128]. These include all the mentioned factors (sample preparation, injection, column performance, and mass spectrometry). Ion suppression can be strong for the analysis of polar hydrophilic organic compounds in saline water [294, 298].

After identifying some major error sources, the next step is to optimize the analytical method for GLY and AMPA.

3.4 Analytical method optimization

To optimize the analytical method, the sample preparation procedure was determined by adding 10 µL of 200 mM NH_4COOH buffer and 10 µL of internal standard (^{13}C GLY, 100 µg/L) to 1000 µL of the sample. The final solution contained 2 mM NH_4COOH buffer and 1000 ng/L internal standard ^{13}C GLY. In addition, the mobile phase NH_4COOH 20 mM with 0.05% CH_2O_2 and ACN with 0.05% CH_2O_2 were prepared with the flow rate remaining at 0.6 mL/min. The role of a buffer is to stabilize the pH of the samples and the mobile phase, while an internal standard acts as a correction factor to normalize results, compensating for matrix effects, sample loss, injection volume, and ionization efficiency [299]. The same MS configuration was applied in negative mode ESI at a source temperature of 450 °C and a surface-induced desolvation temperature of 320 °C.

Method optimization: sample preparation

The comparison of calibration curves of GLY and AMPA (at concentrations of 0, 2, 5, 10, 20, 50, 100, 500, and 1000 ng/L for each compound) is shown in Figure 3.5.

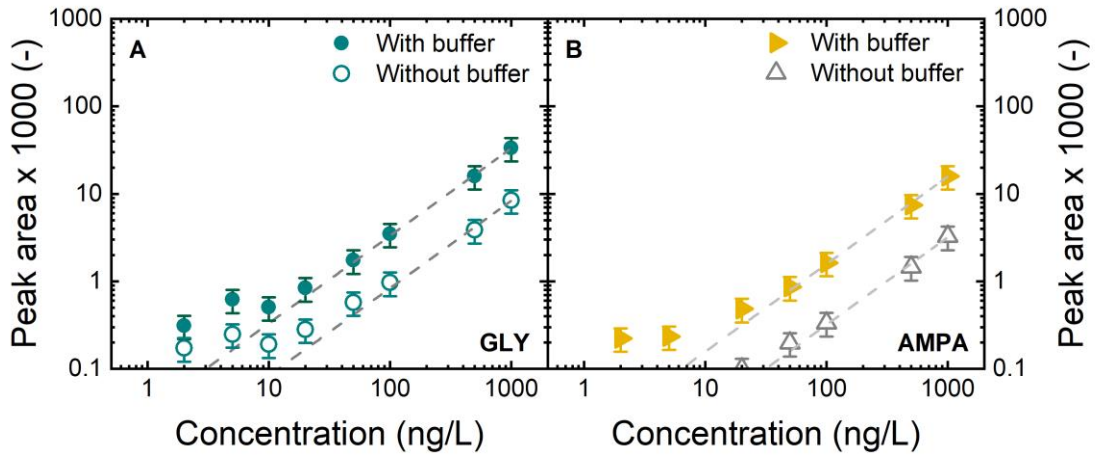

Figure 3.5: GLY and AMPA calibration curve with and without NH_4COOH buffer (commercial purchased analytical standard, flow rate 0.6 mL/min, ACN 15 %, injection volume 100 µL, n=3, 2 independent runs). Adapted from [289].

The peak area of GLY at 1000 ng/L increased from 8478 ± 700 to 33500 ± 302 after adding buffer. The peak area of AMPA increased from 3254 ± 356 to 16000 ± 650 (Figure 3.5). The Obelisc N column used in this work is a hydrophilic interaction column with a suitable pH range of 2.5–4.5 [300]. NH_4COOH is a common buffer for the analysis of polar compounds by HPLC [302, 303] to stabilize the pH at 3.5–4. The pH of the samples and the mobile phase was 3.5–4 after adding NH_4COOH buffer. The higher peak area is more suitable for analysis, with the target LOD of 10 ng/L. Therefore, the mobile phase is now NH_4COOH 20 mM with 0.05% HCOOH and ACN with 0.05% HCOOH.

Method optimization: mobile phase

Numerous studies have shown that mobile phase composition and injection volume had a significant impact on LC-MS/MS analysis [301, 302]. To optimize the interaction of GLY/AMPA with the LC column, the ratio of NH_4COOH:ACN was changed with ACN composition of 5, 10, 15, 20, 30, 40, 50% (Figure 3.6).

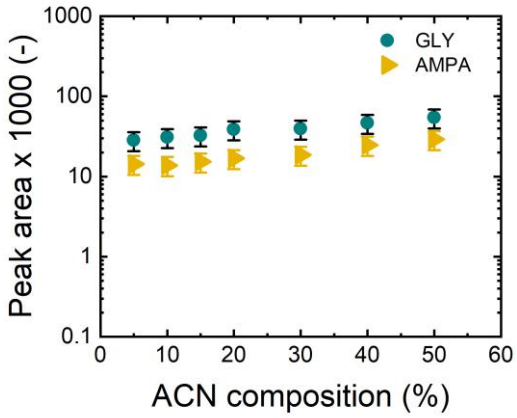

Figure 3.6: GLY and AMPA peak area by ACN composition (GLY/AMPA 1000 ng/L, injection volume 100 µL). Adapted from [289].

GLY peak area was stable at 29000–36000 ± 3100 with the increase of ACN composition from 5 to 30%, then increased to 54150 ± 5236 at the ACN composition of 50%. AMPA peak area was stable at 14200–16820 ± 1654 with ACN composition at 5–30%, and increased to 29000 ± 2563 with 50% ACN in the mobile phase. Even though the highest peak area was obtained at 50% ACN, a lower ACN composition will be chosen to ensure higher ionization efficiency [306] and stable ionization sprays for polar GLY/AMPA molecules [303]. Therefore, the composition NH_4COOH:ACN at 85:15% was chosen.

Method optimization: injection volume

Injection volume is important, as the target LOD is 10 ng/L and the sample volume is 2–10 mL with direct injection. The injection volume was determined at 10, 20, 50, 80, 100, and 150 µL, with the mobile phase composition NH_4COOH:ACN at 85:15% and the presence of NH_4COOH buffer (Figure 3.7).

The analyte retention did not change with changes in injection volume. For GLY, the peak area increased from 1135 ± 95 to 35472 ± 2965 with increasing injection volume from 10 to 80 µL, then remained the same at higher injection volumes. AMPA peak area increased from 184 ± 19 to 13648 ± 1208 when the injection volume increased from 10 to 100 µL, and remained stable at injection volumes 100–150 µL. The high injection volumes can cause extra-column band broadening, subsequently affecting the peak resolution [304]. Therefore, the injection volume of 100 µL was chosen to achieve high sensitivity without affecting the peak resolution.

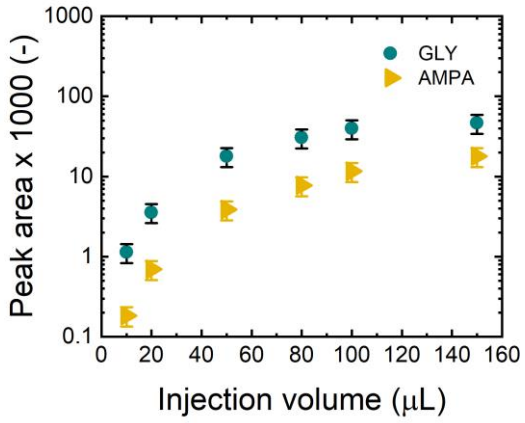

Figure 3.7: GLY and AMPA peak area by ACN composition (GLY/AMPA 1000 ng/L, injection volume 100 µL). Adapted from [289].

3.5 GLY/AMPA analysis under water matrix effect

Interference of salinity on GLY/AMPA analysis

Salinity can decrease the analysis response of electrospray ionization mass spectrometry [305, 306]. With the target of analyzing filtration samples which may contain high salt concentration, GLY and AMPA (1000 ng/L) were analyzed under different water conditions: different NaCl concentrations (1, 2, 5, 8, 10, 20 mM), different $NaHCO_3$ concentrations (0.1, 0.2, 0.5, 0.8, 1, 2 mM) (Figure 3.8).

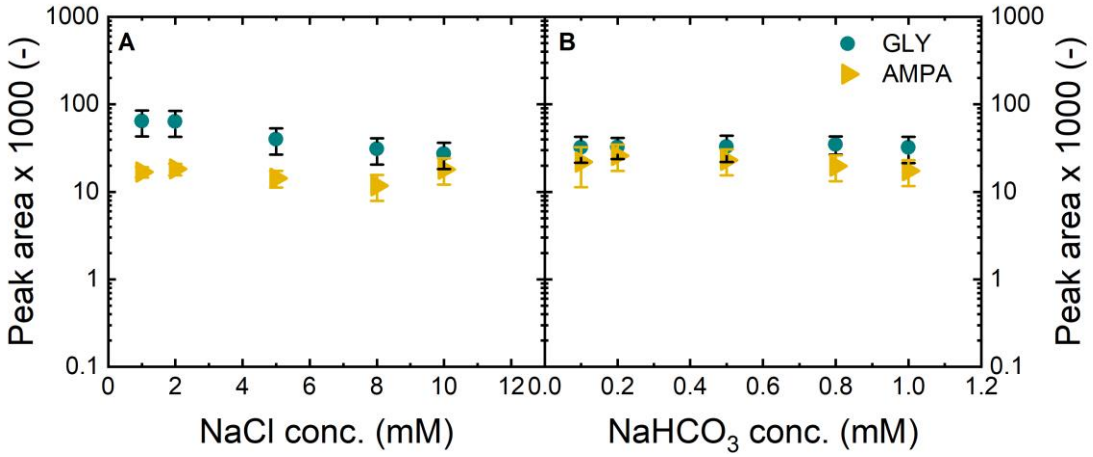

Figure 3.8: GLY and AMPA (1000 ng/L) peak area at different NaCl and $NaHCO_3$ concentrations (commercial purchased analytical standard, flow rate 0.6 mL/min, ACN 15 %, injection volume 100 µL, n=3, 6 independent runs). Adapted from [289].

The peak area of GLY and AMPA decreased with the increase of NaCl concentration (Figure 3.8 A). The peak area of GLY decreased from 64272 ± 2500 to 4936 ± 125 when the NaCl concentration increased from 1 to 20 mM. With the same NaCl concentration range, AMPA peak area declined from 18255 ± 990 to 7477 ± 156. However, the concentration of $NaHCO_3$ did not cause a significant change in the signal of GLY and AMPA. With the increase of $NaHCO_3$ concentration from 0.1 to 2 mM, the peak area of GLY and AMPA remained at 30000–35000 and 13000–15000, respectively (Figure 3.8 B). The low effect of $NaHCO_3$ was due to the lower concentration of $NaHCO_3$ compared to NaCl. In the standard background solution, the concentration of $NaHCO_3$ (1 mM) was 10 times lower than the concentration of NaCl (10 mM). Salts play a crucial role in LC separation and ionization in MS [307]. Moreover, salts can crystallize during electrospray ionization, making it hard to analyze and maintain the analytical instrument [308]. In this chapter, the NaCl concentration was 10 mM, whereas the GLY and AMPA concentrations in the feed solution were 1000 ng/L (equivalent to $6 \cdot 10^{-6}$ mM), which is a much lower concentration. Therefore, salts had a critical role in the analysis of GLY and AMPA by LC-MS/MS. Sample dilutions are required for high-salinity samples; the samples are diluted to a conductivity of 1400 µS/cm (similar to the background electrolyte solution).

Interference of pH on GLY/AMPA analysis

GLY has four ionization constants (pKa) of 0.8, 2.6, 5.8, 10.8, and AMPA has three pKa of 1.8, 5.4, 10.0 [44, 125]. With multiple pKa values, the charges of GLY and AMPA are significantly influenced by pH [119, 126]. Hence, the analysis of GLY and AMPA would be strongly affected by pH. To evaluate the analysis of samples at different pH, GLY and AMPA were analyzed at pH 2, 4, 6, 10, 11, and 12. Figure 3.9 compares the analysis of GLY/AMPA at 1000 ng/L at different pH before and after neutralization and buffer addition.

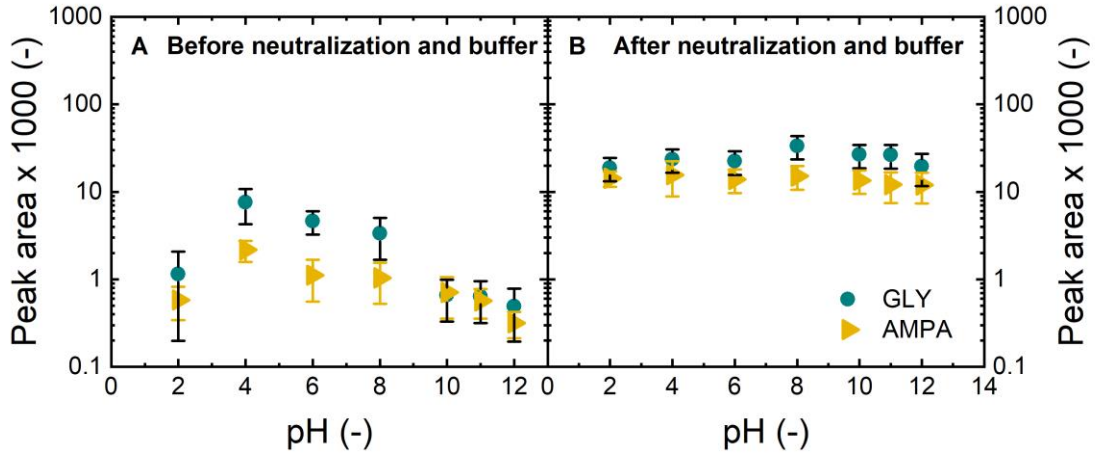

Figure 3.9: GLY and AMPA (1000 ng/L) peak area at different pH (commercial purchased analytical standard, flow rate 0.6 mL/min, ACN 15 %, injection volume 100 µL, n=3, 6 independent runs). Adapted from [289].

The impact of pH on analysis was reduced by neutralization and by the addition of NH_4COOH buffer (Figure 3.9). Before adding buffer, the peak area was not consistent. The peak area at pH 4–8 of GLY was 3400–7500 ± 2000, while the peak area of AMPA was 1115–2040 ± 560. This pH is more suitable for the HILIC Obelisc N column [300]. The peak area of the sample at extreme pH was < 1000 for both GLY and AMPA. After neutralization and adding buffer, the peak area of GLY and AMPA at 1000 ng/L was more stable at 30000–35000 ± 1520 and 13000–15000 ± 1015, respectively. For samples at extreme pH (2, 10–12), the pH can also be stabilized by adding buffer, but the required buffer volume can reach 600 µL for a 1000 µL sample, which will contribute to high dilution. Therefore, neutralization for extreme pH samples is recommended.

In conclusion, all samples need to be neutralized to pH 8, then added to a 200 mM NH_4COOH buffer to stabilize at pH 3.5 before analysis by LC-MS/MS.

Repeatability of analysis

To validate the repeatability of LC-MS/MS performance, 50 independent samples of GLY and AMPA at 1000 ng/L were measured (Figure 3.10).

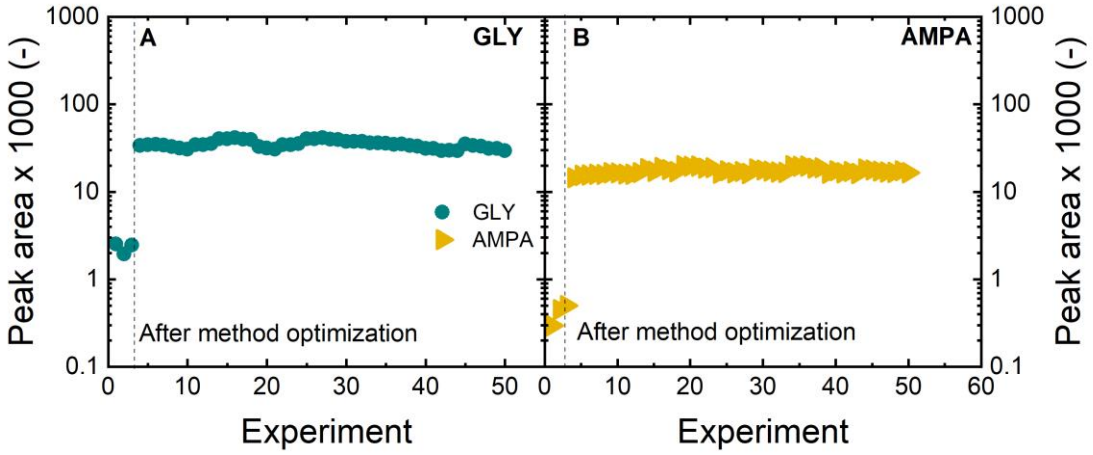

Figure 3.10: GLY and AMPA at 1000 ng/L after optimization from the commercial purchased analytical standard (Flow rate 0.6 mL/min, ACN 15 %, injection volume 100 µL, 50 independent runs). Adapted from [289].

After method optimization, GLY and AMPA peak area increased and remained stable at 30000–35000 ± 1520 and 13000–15000 ± 1015, respectively. Therefore, the analytical method for GLY and AMPA has been successfully established and optimized with reproducible results.

In conclusion, the method is now optimized and can be summarized as follows.

Final analytical method for GLY and AMPA by LC-MS/MS

1000 µL of sample is added with 10 µL of internal standard (^{13}C GLY 100 µg/l) and 10 µL of ammonium formate (NH_4COOH 200 mM) buffer so that the concentration of internal standard and buffer in each sample remains at 1000 ng/L and 2 mM, respectively, to stabilize sample pH at 3.5. Samples with pH < 4 or> 10 are neutralized to pH 8 with 1 M HCl and 1 M NaOH.

The hydrophilic interaction liquid chromatography column (HILIC) Obelisc N 2.1·150 mm, 5 µm (SIELC Technologies, USA) is used. Mobile phase is isocratic 85/15 v/v (NH_4COOH 20 mM: acetonitrile + 0.05% CH_2O_2) at the flow rate of 0.6 mL/min.

The system is cleaned and conditioned daily before measurement. Before measurement, the background is measured, and the system is conditioned with an isocratic mobile phase of 85/15 v/v (NH_4COOH 20 mM: acetonitrile + 0.05% CH_2O_2) for 1 hour. The background baseline is measured every day before each measurement. The highest noise recorded from the MS is the noise test data. If the noise is higher than 100, the analysis needs to be stopped, and the problems need to be identified. An example of high background noise is shown in Figure 3.11.

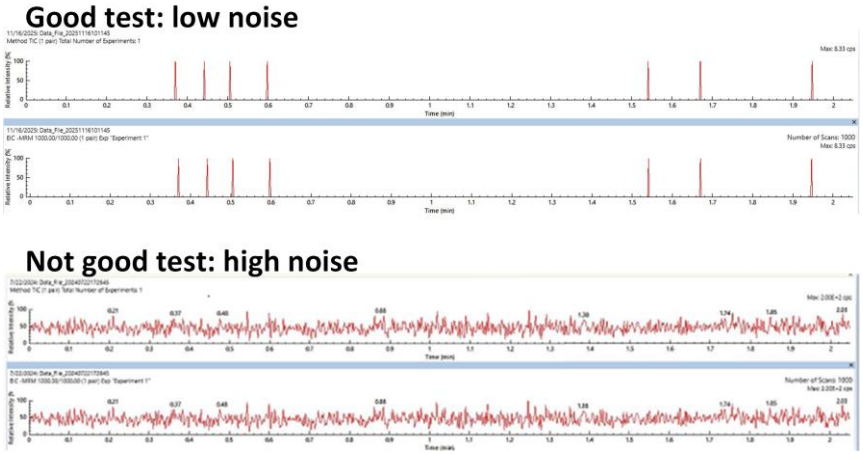

Figure 3.11: Background noise test example

It is noted that each problem can have different results in the noise test. The experience in problem identification and solution was built over years of working and problem-solving with LC-MS/MS by the authors.

After measurement, a cleaning solution consisting of 85% Milli-Q and 15% acetonitrile is used to clean the system with column by-pass.

The injection volume was 100 µL with the column temperature of 40 °C. Electrospray ionization: in negative mode at the source temperature of 450 °C and the surface-induced desolvation temperature at 320 °C. The elution time was 6 minutes.

Electrospray ionization (ESI) is employed in negative mode with a source temperature of 450 °C and an HSID temperature of 320 °C. Further details regarding optimized parameters are shown in Table 3.1.

Table 3.1: Mass spectrometer parameters for GLY and AMPA

Compound	**Precursor ion (*m/z*)**	**Quantification ion, *m/z***	**Quantification ion, *m/z***
GLY	168	63	81 / 79
GLY ^{13}C ITSD	169	63	63
AMPA	110	63	79

Limit of detection

The GLY and AMPA concentrations were calculated based on the calibration solutions of GLY and AMPA at concentrations of 0, 2, 5, 10, 20, 50, 100, 500, and 1000 ng/L for each compound (Figure 3.12). Data analysis was carried out using the Simplicity 3Q^{TM} software platform.

To construct the calibration curve, the integrated peak areas of standard solutions (0, 2, 5, 10, 20, 50, 100, 500, and 1000 ng/L) were plotted against concentration. Based on calibration curves, the peak area can be converted to the concentration.

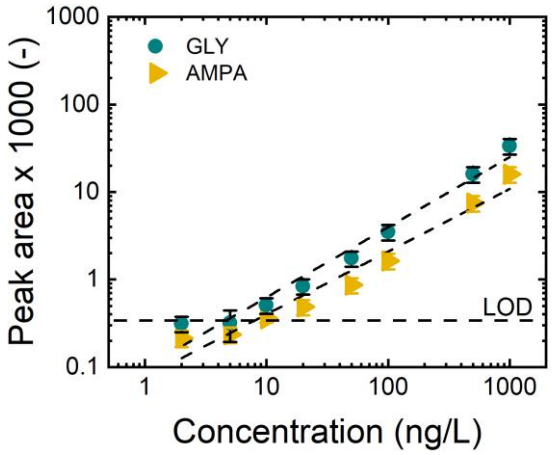

Figure 3.12: Calibration of GLY and AMPA by LC-MS/MS (Milli-Q water, buffer NH_4COOH 2 mM, internal standard ^{13}C GLY 1000 ng/L, pH 8.1 ± 0.1). Adapted from [289].

The linearity of both GLY and AMPA is acceptable with $R^2 > 0.995$ in the concentration range 10–1000 ng/L.

The LOD was determined following a method suggested by the US Environmental Protection Agency [309] as shown below:

$$LOD = \frac{s_{blank} + 3\,\sigma_{blank}}{b} \qquad (3.1) \qquad\qquad LOQ = \frac{s_{blank} + 10\,\sigma_{blank}}{b} \qquad (3.2)$$

where s_{blank} is the measured signal of the blank, σ is the standard deviation of the blank, and b is the slope of the calibration. In the calibration curve, the point at a concentration lower than LOD would be excluded from the sample data analysis.

The LOD of GLY and AMPA was measured and summarized in Table 3.2.

Table 3.2: Parameters obtained from calibration curves of GLY and AMPA

	Blank sample signal (s_{blank})	Standard deviation of the blank (σ_{blank})	Slope of calibration (b)	LOD (ng/L)	LOQ (ng/L)
GLY	292	12	33	10	12
AMPA	116	13	15	10	15

The limit of detection of the method was determined at 10 ng/L for both GLY and AMPA. For sample analysis, the calibration curve will be in the concentration range of 10–1000 ng/L. Samples with higher concentrations will be diluted to fit within this range: 10 – 1000 ng/L.

To validate the results obtained with the LC-MS/MS method, all 6 steps described in Table 3.3 are required. The purpose of all checks is to evaluate reproducibility, stability, and the acceptable range for data analysis with LC-MS/MS.

Table 3.3. Validation steps for LC-MS/MS analysis

Validation steps	Description and purpose
Before measurement	
Baseline in LC-MS/MS	The background baseline is measured every day before each measurement. The highest noise recorded from the MS is the noise test data. If the noise is higher than 100, the analysis needs to be stopped, and the problems need to be identified.
Calibration	The calibration is performed with a concentration of 0–1000 ng/L.
After measurement	
Reproducibility and stability	The reproducibility of calibration (peak area, residence time, peak shape) is checked. The residence time for GLY and AMPA in LC-MS/MS is 1 minute and 0.9 minutes, respectively.
Peak area	All peak area, peak shape, retention time, and MS parameters of all data from photocatalytic membrane filtration are checked after the measurement.
Variation between 3 repeats	As each sample was measured in triplicate, the peak area from the 3 repeats for each measurement is compared. Before measuring the samples, the calibration is analyzed. The measurement was done in the following sequence: 0 ng/L – permeate samples – feed samples – 1000 ng/L. Each sequence is done 3 times.
Feed values and sequences P1 – P15	All the feed values are collected. The data need to show the correct trends for membrane filtration processes (feed, permeate, and retentate).

3.6 Quantitation of GLY and AMPA in real water samples

To evaluate the performance of LC-MS/MS for water samples, different real water samples were measured by LC-MS/MS in KIT (without derivatization) and compared to the results from LC-MS/MS in Technologiezentrum Wasser (TZW) (with derivatization, DIN ISO 16308 [310]) (Figure 3.13). Real water samples were sourced from research projects involving surface waters from Gambia and Namibia, and from water treatment effluent in France, which had been analysed by LC-MS/MS at TZW. The results of the research, with detailed information about the nature of the samples, were reported in other publications for Gambia [311] and Namibia [288]. In addition, a surface water sample from Canada, which did not contain GLY/AMPA, was spiked with 1000 ng/L GLY and AMPA and measured by LC-MS/MS in KIT for recovery validation. Before measurement, all real water samples were filtered by a 0.45 µm polyethersulfone syringe filter.

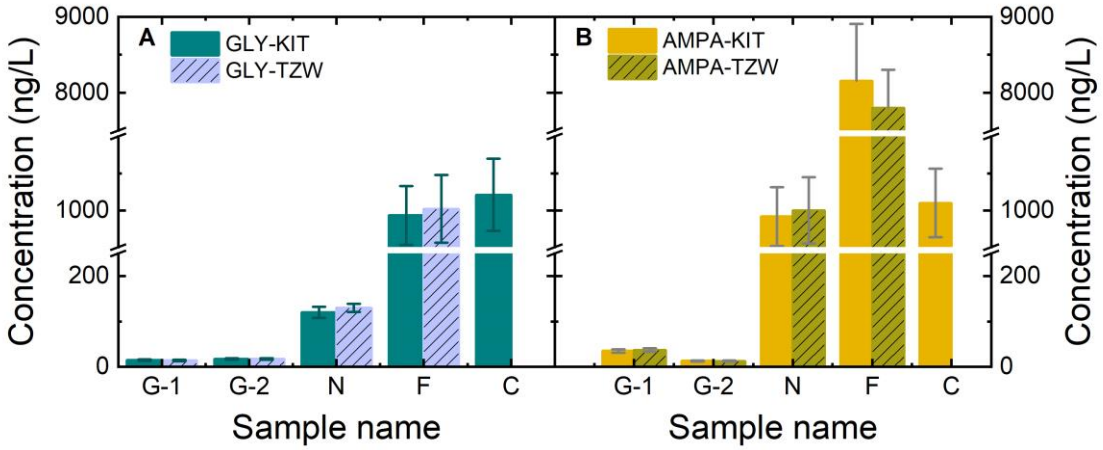

Figure 3.13: GLY and AMPA concentration in real water (sample measurement carried out at both KIT and TZW). Adapted from [289].

The results indicate that the values for GLY and AMPA obtained using the established method in KIT and the standard method analyzed at TZW were comparable.

Recovery of the analysis measures the efficiency of the analytical method in detecting GLY and AMPA. The recovery of Gambia, Namibia, and France samples, which were measured and compared with the analysis at TZW, was calculated using equation (3.3).

$$Recovery\ (\%) = \frac{c_{measured}}{c_{known}} \times 100 \quad (3.3) \qquad Recovery\ (\%) = \frac{c_{measured} - c_{unspiked}}{c_{spiked}} \quad (3.4)$$

where $c_{measured}$ is the GLY/AMPA concentration measured from LC-MS/MS at KIT, c_{known} is the GLY/AMPA concentration measured from LC-MS/MS at TZW.

The spiked samples recovery (Canada sample) was calculated following equation (3.4), where $c_{measured}$ is the GLY/AMPA concentration measured from LC-MS/MS at KIT, $c_{unspiked}$ is the GLY/AMPA concentration in the sample before spiking, c_{spiked} is the concentration of GLY/AMPA spiked into the samples. In this chapter, the unspiked water sample from Canada did not contain GLY and AMPA; hence, $c_{unspiked}$ is 0 ng/L.

From the obtained results, the difference between the two methods was around 3–7%, and the recovery was in the 93–97% range. For spiked samples, the concentrations of GLY and AMPA were 1000 ng/L, as expected. The measurements from GLY/AMPA removal experiments were repeatable and are shown in each chapter.

Now that validation has confirmed the accuracy of the analytical method, the next step is to investigate removal technologies for GLY and AMPA from water.

3.7 Error analysis

The error propagation, estimated by considering uncertainties from solution preparation, the analytical instrument, and the photocatalytic filtration system [316], is summarized, with the most significant contribution from analytical error.

Error source identification

Error sources for filtration experiments are listed in Table 3.4.

Table 3.4: Error type and sources considered in the error analysis

Step	Sources considered
Sample preparation	Sensor/instrument (balance, volumetric flask), materials (membranes) Error from the operator (calculations, pipetting, weighing)
Experimental operation	Sensor/instrument (temperature variation, pressure variation, balance) Uncontrolled parameters (room temperature and humidity)
Analytical error	Error from LC-MS/MS analysis Feed preparation by the operator Interference from the water matrix

Feed preparation: from analytical balance (± 0.1 mg, Adventurer ProAV 2102, Ohaus, Germany), volumetric flask (VWR borosilicate glass, 1000 ± 0.3 mL), measuring cylinder (VWR borosilicate glass, 250 ± 1 mL).

Error from feed preparation: human error (eye inspection of meniscus, pipetting, and dilution is < 0.1%). Errors from the operator were minimized in the experiments.

Filtration operation: pressure was adjusted by hand; flux variation was influenced by membrane permeability. The flux variation between membrane coupons was 10%. Temperature was adjusted and measured with a thermocouple (±0.5 °C, TJ2-CPSS-M60U-250-SB, Omega Engineering, Germany).

Error from filtration experiment: Temperature was controlled to ±0.3 °C, and pressure was adjusted to within 3%.

Analytical operation: errors were calculated corresponding to > 50 measurements. The main error source was the feed solution; the equal error source was membrane variability (resulting in flux and permeate concentration variations).

Other factors: sample degradation (samples were capped and put in the fridge at 4 °C), ion suppression (conductivity and pH were controlled), and water contamination (separated labware to minimize contamination).

The analysis error was calculated as the standard deviation from calibration based on >50 measurements. The error is summarized in Table 3.5.

Table 3.5: Error from analysis corresponding to GLY/AMPA concentration.

Concentration (c, ng/L)	Error from analysis (Δc_{anal}, ng/L)
1000	60
500	45
200	30
100	20
10	12

Therefore, the most contributed error is from analytical error.

Error calculation and propagation

Filtration was performed in a dead-end filtration system where permeate mass, temperature, and pressure were monitored during filtration. Pressure was adjusted by hand while temperature was controlled and measured by thermocouple (± 0.5 °C, TJ2-CPSS-M60U-250-SB, Omega Engineering, Germany) (assume that although the water viscosity, diffusivity of GLY/AMPA, and adsorption kinetics and thermodynamics change, the small temperature variation (0.5 °C) did not significantly affect adsorption). The variation of these parameters during filtration experiments was recorded and summarized in Table 3.6.

Table 3.6: Error sources, parameters, and quantified errors on permeability variation

Error source	Variable parameter	Quantified error with the max-min method
Temperature lab variation (ΔT)	Temperature during filtration	20 ± 0.5 °C (5 % viscosity variation)
Pressure setting by the operator (ΔP)	Pressure during filtration	Average variation of ± 0.1 bar (3% error)

The absolute error in flux ΔJ was calculated based on the relative error in mass change with time.

$$\Delta J = \sqrt{\Delta P^2 + \Delta T^2} \tag{3.5}$$

where ΔP was the error in pressure calculated by max–min variation during filtration, ΔT was the error in temperature control calculated by max–min variation during filtration.

Error propagation of GLY/AMPA concentration

Error for GLY/AMPA concentration was calculated using the error propagation method, where the analytical error from LC-MS/MS analysis, the error from feed preparation by the operator, and the error from the water flux variation for the different experiments were considered. Error from LC-MS/MS analysis was obtained from the variability of 50 calibration curves, which was the main error source. Error for feed preparation included the use of the analytical balance (± 0.1 mg, Adventurer ProAV 2102, Ohaus, Germany), the volumetric flask (VWR borosilicate glass, 1000 ± 0.3 mL), the measuring cylinder (VWR borosilicate glass, 250 ± 1 mL), and human error (eye inspection of meniscus).

Other factors: sample degradation (when the samples were mixed with buffer and internal standard, then kept for > 1 month, avoid by preparing samples fresh before measurement), ion suppression (hence, conductivity was controlled), and water contamination (samples were capped and put in fridge at 4 °C to avoid contamination).

The error in feed concentration included both analytical and sample preparation errors. The absolute error in feed concentration was propagated from analytical error and feed volume error, which was calculated as follows:

$$\Delta c_f = \sqrt{{\Delta c_a}^2 + {\Delta c_{pr}}^2} \approx \Delta c_a \tag{3.6}$$

where Δc_a is the error contributed by the analysis, which was the main and biggest error source; $\Delta c_{pr} = c_f \left(\frac{\Delta V_f}{V_f}\right)$ is the error from the feed solution preparation, which was negligible. Therefore, with c_f = 1000 ng/L, $\Delta c_f \approx \Delta c_a$ = 60 ng /L.

The absolute error in permeate sample concentration was propagated from analytical error, solution preparation error, and filtration error (error in flux, J), which was calculated as follows:

$$\Delta c_p = \sqrt{{\Delta c_{anal.}}^2 + {\Delta c_{prep.}}^2 + {\Delta c_{fil.}}^2} = \sqrt{{\Delta c_{anal.}}^2 + {c_p}^2 \left(\frac{\Delta V_p}{V_p}\right)^2 + {c_p}^2 \left(\frac{\Delta J}{J}\right)^2} \tag{3.7}$$

where $\Delta c_{pr} = c_P \left(\frac{\Delta V_P}{V_P}\right)$ is the error from the permeate solution preparation; $\Delta c_{fil.} = c_p \left(\frac{\Delta J}{J}\right)$ is the error contributed from the filtration process. The error from preparation was neglected.

Error from analysis (Δc_a) contributed the most, indicating that low permeate concentration c_P would have high error, with the highest error at the permeate concentration close to the LOD of the analysis. The error for GLY/AMPA concentration was summarized in Table 3.7.

Table 3.7: Error sources, parameters, and quantified errors on concentration variation

Error source	Variable parameter	Quantified error with the propagation method
Analytical error from LC-MS/MS (Δc_a)	Peak area	1000 ± 60 ng/L, 500 ± 38 ng/L, 100 ± 19 ng/L, 10 ± 3 ng/L
Water flux variation (ΔJ)	Flux	100 ± 5 L/m^2.h
Reported error for GLY/AMPA concentration (Δc_f, Δc_p)	Feed concentration Permeate concentration	1000 ± 60 ng/L 500 ± 45 ng/L, 100 ± 20 ng/L, 10 ± 3 ng/L

Error propagation for GLY/AMPA removal

Removal was calculated using equation (3.8), indicating that the removal error was attributed to errors in feed and permeate concentrations.

$$R = \left(1 - \frac{c_p}{c_f}\right) \cdot 100 \tag{3.8}$$

The absolute error in removal ΔR (in %) was determined from equation (3.9) with the propagation of error from feed and permeate samples.

$$\Delta R = (100 - R)\sqrt{\left(\frac{\Delta c_f}{c_f}\right)^2 + \left(\frac{\Delta c_p}{c_p}\right)^2} \tag{3.9}$$

where Δc_f and Δc_p are the absolute errors of the feed and permeate sample concentrations, respectively. Because ΔR is a fraction of $100 - R$, the removal error is higher when removal is lower and vice versa (Table 3.8).

Table 3.8: Error sources, parameters, and quantified errors on removal variation

Error source	Variable parameter	Quantified error with the propagation method
Feed concentration (Δc_f)	Concentration	1000 ± 60 ng/L,
Permeate concentration (Δc_p)	Concentration	500 ± 38 ng/L, 100 ± 19 ng/L, 10 ± 3 ng/L
Reported error for GLY/AMPA removal (ΔR)	Removal	50 ± 4.8%, 90 ± 1.9%, 99 ± 0.3%

Error propagation for GLY/AMPA specific adsorbed mass

Absolute mass adsorbed error of each feed and permeate sample (Δq_{ads}) in ng/g were calculated from the respective volume and concentration errors as calculated in equation (3.10).

$$\Delta q_{ads,i} = q_i \sqrt{\left(\frac{\Delta V_i}{V_i}\right)^2 + \left(\frac{\Delta c_i}{c_i}\right)^2} \tag{3.10}$$

The absolute mass adsorbed error Δq_{ads} (in ng) in the adsorption was determined by propagation of the absolute mass error of the feed and adsorption samples.

$$\Delta q_{ads} = \sqrt{{\Delta q_{ads,f}}^2 + \sum_{i=1}^{n} {\Delta q_{ads,i}}^2} \tag{3.11}$$

The absolute error of GLY/AMPA mass adsorbed was summarized in Table 3.9.

Table 3.9: Absolute error on the mass adsorbed calculated for different experimental parameters

Parameter varied	GLY mass adsorbed and absolute error (ng/g)	AMPA mass adsorbed and absolute error (ng/g)
PBSAC	41–158 ± 16	24–118 ± 21
UF–PBSAC	100–129 ± 15	42–88 ± 20

4 GLY and AMPA adsorption by PBSAC

This chapter is adapted from a publication in Journal of Hazardous Materials (2023): P.B. Trinh, A.I. Schäfer, Adsorption of glyphosate and metabolite aminomethylphosphonic acid (AMPA) from water by polymer-based spherical activated carbon (PBSAC), Journal of Hazardous Materials, (2023) 131211 [197].

The contribution of authors:

Phuong B. Trinh: performing experiments; samples analysis; data analysis and interpretation; validation; methodology; visualization; writing – original draft

Andrea I. Schäfer: conceptualization; methodology; funding acquisition; project administration; resources; supervision; validation; writing – review & editing

Other contribution: Dr. Eduard Madirov, Dr. Andrey Turshatov (Institute of Micro-structure Technology (IMT-KIT)): adsorbent characterization.

The thermodynamic parameters have been corrected in: P.B. Trinh, A.I. Schäfer, Corrigendum to "Adsorption of glyphosate and metabolite aminomethylphosphonic acid (AMPA) from water by polymer-based spherical activated carbon (PBSAC)", Journal of Hazardous Materials, 470 (2024) 134136 [312] due to the wrong calculation of thermodynamic parameters.

This chapter aims to investigate the adsorption performance of polymer-based spherical activated carbon (PBSAC) for GLY and AMPA removal. The adsorption performance is determined by the surface properties (such as surface area, adsorption site, and chemistry). Varied experimental parameters include PBSAC characteristics (dose, size, activation level, oxygen content), GLY/AMPA concentrations, pH, and water temperature. Finally, the adsorption mechanisms and limiting factors are evaluated for a better understanding of the integration with the membrane in the next step.

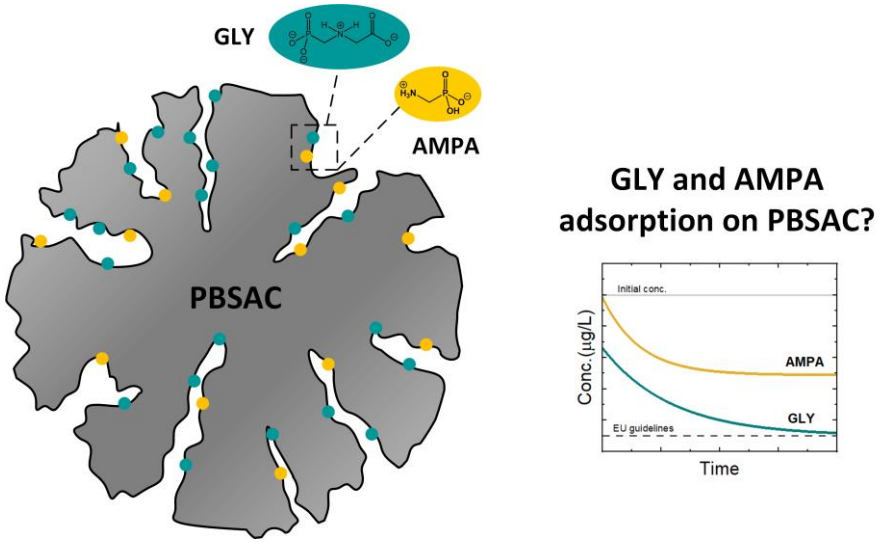

4.1 Introduction

Adsorption is a common water treatment technology [40]. This technique has been reported as a simple and chemical-free method for GLY and AMPA removal [313], with the compensation being the need for adsorbent regeneration and treatment of the residual waste stream [314]. However, research on adsorption mainly focused on high concentrations of GLY and AMPA (due to the lack of analytical techniques) [315, 316]. Those concentrations are not realistic in real water conditions. Moreover, effective removal of GLY and AMPA to reach EU guidelines remains a challenge. Therefore, a more advanced adsorbent needs to be investigated.

Tagliavini *et al.* investigated polymer-based spherical activated carbon (PBSAC), which showed good adsorption for steroid hormones (estrone, 17β-estradiol (E2), testosterone, and progesterone), with removals of >90% from an initial concentration of 100 ng/L [206]. The adsorption of steroid hormone was significantly faster with the smallest PBSAC size (diameter of 78 μm) than GAC (diameter of 0.4–1.1 mm) [206, 211, 212]. The EU guidelines for steroid hormones were achieved by adsorption onto PBSAC [207]. Due to its strong adsorption of micropollutants, PBSAC will be selected for the evaluation of GLY and AMPA removal. Compared to steroid hormones, GLY and AMPA are smaller, highly charged, and polar [44, 45]. The adsorption of GLY/AMPA can be lower and slower than that of steroid hormones.

This chapter focuses on the adsorption of GLY and AMPA by PBSAC. The particle characteristics and water conditions will be evaluated. The following specific research questions are addressed:

- Can PBSAC adsorb the charged, small herbicides GLY and AMPA to meet EU herbicide guidelines?
- How are the adsorption kinetics and maximum mass adsorbed of GLY and AMPA on PBSAC?
- Which PBSAC properties (size, porosity, and surface composition) contribute most, and how do water conditions (water temperature and pH) influence adsorption?

4.2 Adsorbents

PBSAC is a commercial AC from Blücher, Germany, with uniform size, high surface area (1600 – 2100 m^2/g), and high pore volume of PBSAC (0.6–1.3 cm^3/g), with a maximum up to 3.5 cm^3/g [210]. Adsorbent properties (particle diameter, surface oxygen, activation level (indicator of porosity), tap density, and surface area) are summarized in Table 4.1.

Table 4.1. PBSAC properties (particle diameter, surface oxygen, activation level, tap density, and surface area) provided by the manufacturer (Blücher) [206, 207, 210, 211].

Sample code	Diameter (µm)	Surface oxygen (%)	Activation level	Tap density (g/mL)	Surface area (m^2/g)
PB 78	78	5	~ 4	0.62	1420
PB 200 (O2)	200	5	~ 4	0.60	1440
PB 380	380	5	~ 4	0.54	1450
PB 450	450	5	~ 4	0.40	1920
PB 475	475	5	~ 4	0.57	1450
PB 580	580	5	~ 4	0.54	1510
PB 620	620	5	~ 4	0.60	1380
PB AL1	200	5	1	0.79	810
PB AL2	200	5	2	0.74	1020
PB AL3	200	5	3	0.69	1167
PB AL4	200	5	4	0.63	1365
PB AL5	200	5	5	0.49	1766
PB AL6	200	5	6	0.36	2045
PB 200 O1	200	1.5	~ 4	0.60	1436
PB 200 O3	200	10	~ 4	0.59	1436

In a previous study, PBSAC has a zero surface charge over a broad pH range [206]. However, the oxygen content of 1.5–10% on the PBSAC surface was reported by the manufacturer. As the adsorption mechanisms of PBSAC depend on the surface chemistry (elemental composition and functional groups), the oxygen-containing groups need to be characterized. The surface functional groups of PBSAC were analyzed using Fourier Transform Infrared Spectroscopy (FTIR, Vertex 70, Bruker, USA) equipped with a platinum attenuated total reflectance (ATR) accessory at room temperature by Dr. Eduard Madirov (Institute of Microstructure Technology (IMT)). The ATR-FTIR spectrum was recorded in the wavelength region of 400–4400 cm^{-1} (Figure 4.1).

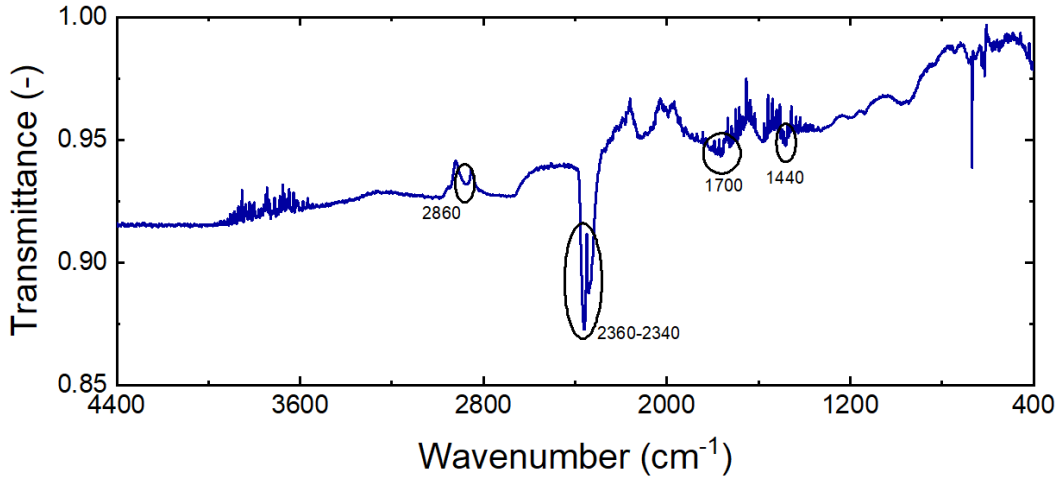

Figure 4.1: FTIR spectra of PBSAC 200 µm at room temperature. Adapted from [197].

A strong peak at 2360−2340 cm^{-1} was recorded, which could imply the presence of C=O stretching in carboxylate groups [317], but this peak could also correspond to O=C=O stretching in carbon dioxide that can be adsorbed on various types of surfaces [318]. Some noise was observed in the 3600–3800 and 1200–2000 cm^{-1} regions. Some peaks of carboxylate groups would be present in the 1200–2000 cm^{-1} region, including C=O stretching (at 1700 cm^{-1}), and O–H stretching at 1440 cm^{-1} [319]. As the reported surface oxygen was ~ 5%, the small peaks of carboxylate groups were not significant [207].

4.3 Static adsorption

The static adsorption experiments were performed in an incubator shaker (Figure 4.2, Innova 43R, New Brunswick Scientific, USA) following the experimental protocol established in previous work [206]. The shaking speed was 260 rpm while the temperature could be controlled in the range of 5–80 °C. All experiments were conducted at 20.0 ± 0.5 °C, except the experiment with varying temperature.

Figure 4.2: The incubator shaker used for static adsorption of GLY/AMPA onto PBSAC.

In the experiment, the GLY/AMPA mixture was prepared in a conical flask. PBSAC was weighed using an analytical balance (Ohaus Explorer Semi Microbalance, USA), then transferred to the GLY/AMPA mixture. The experiment lasted for 26 h. 2.5 mL of water samples (PBSAC-free) were collected at defined time intervals (5, 15, 30, 45 min, and 1, 3, 5, 7, 9, 24, and 26h) using a 5 mL pipette (Eppendorf, Germany). PBSAC settled rapidly; therefore, no filter was needed. The samples were stored in 20 mL glass vials and kept at 4 °C in the fridge.

4.4 Data analysis

Mass balance in static adsorption

Removal of GLY and AMPA (R, %) is determined in equation (4.1).

$$R = \left(1 - \frac{c_i}{c_f}\right) \cdot 100 \tag{4.1}$$

where c_i and c_f are the concentrations in the adsorption water sample and feed (initial), respectively.

The mass balance is important for determining the amounts of GLY and AMPA adsorbed, deposited, or degraded. Specific formulas for determining the mass balance for each type of static adsorption experiment are given below.

The adsorbed mass Δm_{ads} at time t can be determined from the liquid-phase concentrations with the equation (4.2).

$$m_{ads,n} = V_0 c_0 - V_i \sum_{i=1}^{n-1} c_i - (V_0 - (n-1)V_i)c_n \tag{4.2}$$

where $m_{ads,n}$ is the adsorbed mass after n extractions, c_0 and c_i are the concentrations in the solution at time 0 and t_i, respectively. V_0 = 250 mL is the initial total volume and V_i = 2.5 mL is the extracted volume. All the mass losses before the n extraction are summed $V_i \sum_{i=1}^{n-1} c_i$, and the volume of solution before the n extraction is $V_0 - (n-1)V_i$.

The specific adsorbed mass, or specific mass loss, is equal to the adsorbed mass or mass loss divided by the mass of adsorbent, as given in (4.3).

$$q_{ads,S,t} = \frac{m_{ads,t}}{m_{adsorbent}} \tag{4.3}$$

where $m_{adsorbent}$ (g) is the adsorbent mass.

Kinetic and isotherm models

To understand the kinetics and evaluate the maximum adsorbed mass of GLY/AMPA adsorption on PBSAC, three kinetic and two isotherm models have been applied to characterize the evolution of the adsorbed mass of GLY and AMPA per mass of adsorbent over time using the 'Non-linear curve fitting' option in OriginPro 2017/2020 (OriginLab, USA). The parameters used to characterize the adsorption process are shown in Table 4.2.

First-order, second-order kinetics, and the intra-particle diffusion model [325] were applied to fit the data using non-linear curve fitting in OriginPro software (OriginLab Corporation, USA). The first-order and second-order kinetic models define that the rate of adsorption is relevant to the concentrations of GLY and AMPA. The movement of GLY/AMPA from the liquid phase to the sorbed phase (i.e., the mass-action process) could be the rate-limiting factor [320]. These models are empirical, which do not show the limiting mechanism. The first-order model fits better when the quantity of adsorption sites (PBSAC) is low [321, 322]. Meanwhile, the second-order one fits better when the quantity of accessible adsorption sites (PBSAC) is high relative to the quantity of adsorbates (GLY/AMPA) [321, 322]. In the intra-particle diffusion model developed by Weber and Morris [323], intra-particle diffusion is the limiting factor of the adsorption.

Table 4.2: Parameters in adsorption of GLY and AMPA [324-329].

Model name	Assumptions	Formula	Equation
Kinetic models			
First-order kinetic model	Adsorption at the surface is a rate-determining mechanism.	$q_{ads} = q_e(1 - e_1^{-k_1 t})$	(4.4)
Second-order kinetic model	Adsorption at the surface is a rate-determining mechanism, rate is proportion to the liquid-phase concentration of GLY and AMPA.	$\frac{1}{q_{ads}} = \frac{1}{k_2 {q_e}^2 t} + \frac{1}{q_e}$	(4.5)
Intra-particle diffusion model	Diffusion into the inner pores is a rate-determining mechanism rate is proportion to the square of liquid-phase concentration of GLY and AMPA.	$q_{ads} = k_d\, t^{0.5}$	(4.6)
Isotherm models			
Langmuir	Monolayer coverage only, for adsorption on the homogeneous surface with identical adsorption sites	$q_e = q^0 \frac{b\, c_e}{1 + b\, c_e}$	(4.7)
Freundlich	Multi-layer coverage of adsorbates, applicable for adsorption on a heterogeneous surface	$q_e = k_F (c_e)^n$	(4.8)

t is experimental time (h)
q_e (µg/g) and c_e (µg/L) are the adsorbed mass and supernatant (liquid–phase) concentration at equilibrium
c_f (µg/L) is the initial (feed) GLY and AMPA concentration
$m_{adsorbent}$ (g) mass of PBSAC
q^0 is maximum adsorbed mass (µg/g)
k_1 (1/h), k_2 (g/µg.h), k_d (µg/g.h$^{0.5}$) are kinetic rate constants
k_F (ngn^{-1}.g/Ln), k_H (L/g) are isotherm coefficients

The Langmuir isotherm model assumes that GLY and AMPA adsorb on PBSAC monolayer surfaces, with homogeneous adsorption and identical adsorption sites [326, 328]. The empirical Freundlich model assumes multilayer adsorbate coverage and is applicable to adsorption on heterogeneous surfaces [326, 329].

Thermodynamic parameters

Thermodynamic parameters provide information on the inherent energetic changes, which are important for evaluating adsorption. The changes in Gibbs free energy (ΔG^0), enthalpy (ΔH^0), and entropy (ΔS^0) are widely used as basic thermodynamic characteristics of adsorption (Table 4.3).

The Gibbs free energy change (ΔG^0) indicates the degree of spontaneity of the adsorption process, in which a negative value indicates energetically favorable and hence spontaneous adsorption [330]. The enthalpy change (ΔH^0) is a measure of adsorption heat which is related to the strength of the interaction between adsorbate and adsorbent, ΔH^0 presents the temperature changes of the adsorbent during adsorption (exothermic) and desorption (endothermic) [331]. The entropy change (ΔS^0) relates to the disorder of molecules [332].

Table 4.3: Thermodynamic parameters in adsorption of GLY and AMPA [324-329, 331, 332].

Thermodynamic equations				
Parameter	Symbol	Unit	Formula	
Gibbs energy	ΔG^0	J/mol	$\Delta G^0 = -RT\ln(K)$	(4.9)
Thermodynamic dynamic constant	K	-	$\ln K = \frac{\Delta S^0}{R} - \frac{\Delta H^0}{RT}$	(4.10)
ΔH^0 (J/mol) and ΔS^0 (J/mol.K) are the enthalpy change and entropy change, respectively R_G is the thermodynamic gas constant (8.314 J/mol.K) T is the absolute temperature (K)				

In the main text of the paper, the calculation of the thermodynamic parameters was incorrect. The errors in ΔH^0 calculation was identified because the original ΔG^0 values for GLY were unusually too low (highly negative). After recalculation, the author found out that the signs of the enthalpy change (ΔH^0) of GLY and AMPA were wrong. The correct values should be +67 kJ/mol for GLY (instead of −67 kJ/mol) and +28 kJ/mol for AMPA (instead of −28 kJ/mol). The overall adsorption process (including both adsorption and diffusion) was thus endothermic, not exothermic.

There are changes in the entropy change (ΔS^0) after recalculation, which is +310 J/mol.K for GLY instead of +247 J/mol.K, and +157 J/mol.K for AMPA instead of +95 J/mol.K. The Gibbs free energy change ΔG^0 should vary between –19 and −42 kJ/mol for GLY, instead of −135 and −154 kJ/mol, and between −15 and −27 kJ/mol for AMPA, instead of −54 and −61 kJ/mol. However, the correction of ΔG^0 does not affect the conclusion that adsorption of GLY/AMPA was spontaneous and GLY has more affinity for the PBSAC surface than AMPA. In the results and discussion on thermodynamic parameters in this dissertation, the correct results are shown.

The adsorption of GLY and AMPA by PBSAC was investigated for general feasibility. Then the adsorption kinetics and adsorbed mass were evaluated. Parameters of interest were PBSAC properties (PBSAC dose, size, activation level, and surface oxygen content) and water conditions (water pH, GLY/AMPA concentration, and temperature).

4.5 Adsorption of GLY and AMPA by PBSAC

Static adsorption was carried out with an environmentally relevant concentration of 1 µg/L [98] to evaluate whether PBSAC can adsorb GLY and AMPA (0.1 µg/L) (Figure 4.3). The PBSAC dose was 0.5 g/L, which was also an adsorbent dose investigated in other studies [135, 136, 146, 206]. This PBSAC dose is higher than the usual industrial concentrations of PAC (up to 50 mg/L) [122, 123].

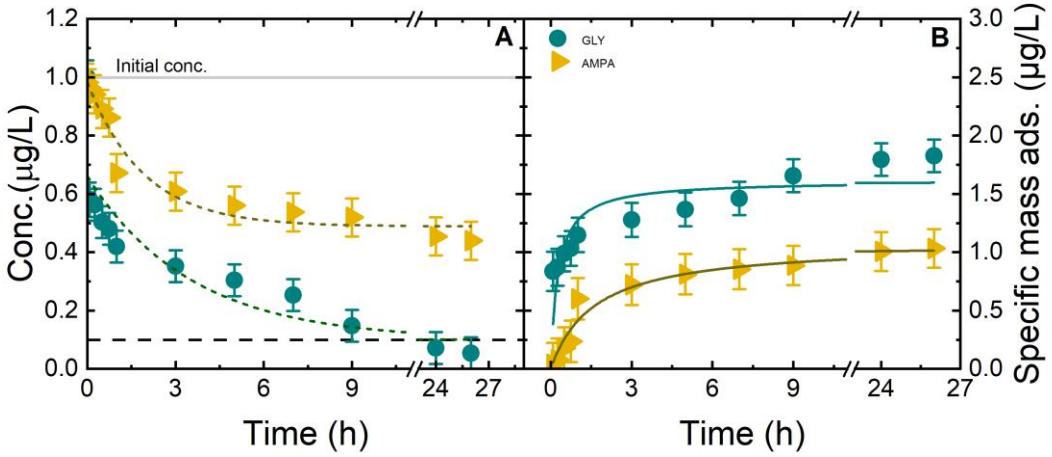

Figure 4.3. GLY/AMPA concentration (A) and specific mass adsorbed (B) by PBSAC with PBSAC size 200 µm, activation level ~ 4, oxygen content 5%, PBSAC dose 0.5 g/L, GLY/AMPA 1 µg/L each in mixture, 1mM $NaHCO_3$, 10 mM NaCl, 20 °C, 260 rpm, pH 8.1 ± 0.1. Solid curves in B are the best fits with the second-order kinetic model. Adapted from [197].

Figure 4.3 A shows that GLY and AMPA could be adsorbed on PBSAC, with the adsorption equilibrium being reached after 6 h (Figure 4.3 A). However, the EU guideline for individual herbicides (0.1 µg/L) was only reached for GLY [12, 13]. The mass adsorbed was 2 ± 0.2 µg/g for GLY and 1 ± 0.1 µg/g for AMPA. The adsorption kinetic models were applied for adsorption characterization [332], with the rate-controlling mechanism defined as mass transport between the liquid and solid phases (first- and second-order kinetic models) or diffusion into internal pores (intraparticle diffusion model) [333] (Table 4.4).

The second-order kinetic model fits best according to the R^2 values. The second-order model fit implies that adsorption sites (PBSAC) are abundant compared with the adsorbates (GLY/AMPA) [321, 322], which seems to be the case for GLY and AMPA adsorption by PBSAC. The theoretical mass adsorbed was 348 and 228 mg (Table 4.4), which were much higher than the mass adsorbed from static adsorption. Therefore, the adsorption site on PBSAC was not yet used up.

Table 4.4: First- and second-order kinetics and intra-particle diffusion constants and R^2 values of GLY adsorption by PBSAC. k_1: first order, k_2: second order, k_d: diffusion

		GLY	AMPA
Pseudo first order	k_1 (1/h)	2 ± 0.6	0.5 ± 0.1
	R^2	0.5	0.9
Pseudo second order	k_2 (g/µg.h)	2.1 ± 0.8	0.6 ± 0.1
	R^2	0.7	0.9
Intra-particle diffusion	k_d (µg/g.$h^{0.5}$)	0.20 ± 0.01	0.2 ± 0.03
	R^2	0.9	0.7
Theoretical mass adsorption monolayer (mg)		348	228

At this stage, PBSAC has been proven to be able to adsorb GLY and AMPA. A significant enhancement in AMPA removal requires modification of material and process properties. Next, the adsorption optimization will be determined with limiting factors (adsorbents, water chemistry) (Figure 4.4). Even though in excess, the PBSAC dose is expected to enhance GLY and AMPA removal, which will be investigated next.

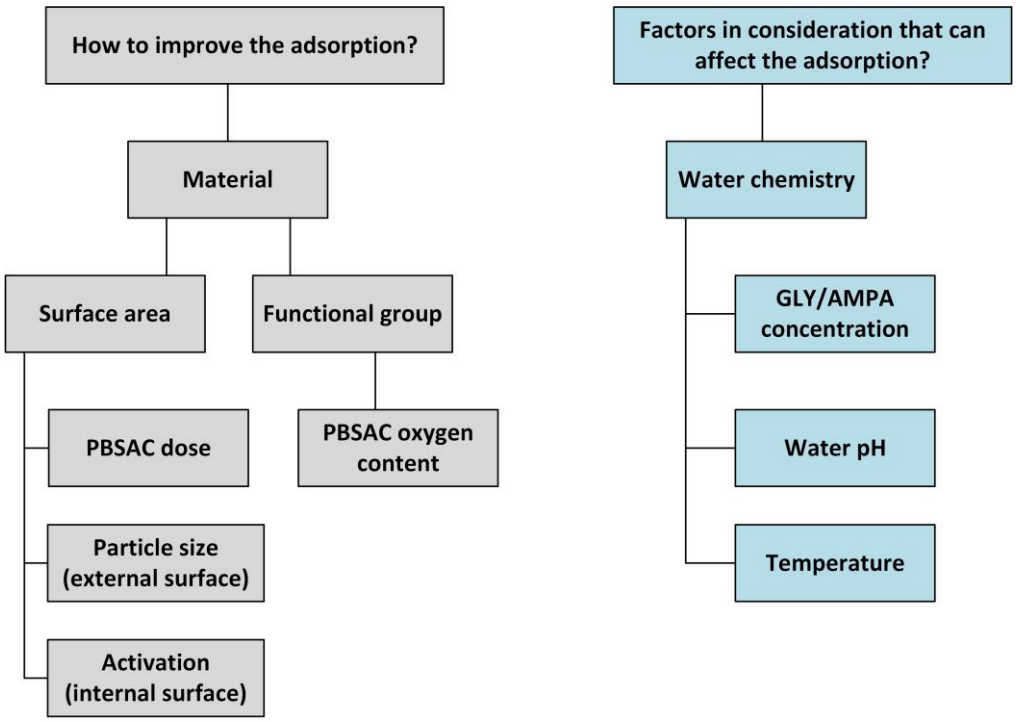

Figure 4.4. Factors in consideration to improve the adsorption of GLY/AMPA on PBSAC

4.6 Operational parameter: PBSAC dose

An increase in the PBSAC dose will enhance the removal if the surface area is the adsorption limitation. As the PBSAC surface is in excess (Table 4.4), both decreases and increases in the PBSAC dose (between 0.1 and 10 g/L) will be examined. Figure 4.5 shows the concentration and removal of GLY and AMPA by PBSAC at different doses (0.01–10 g/L).

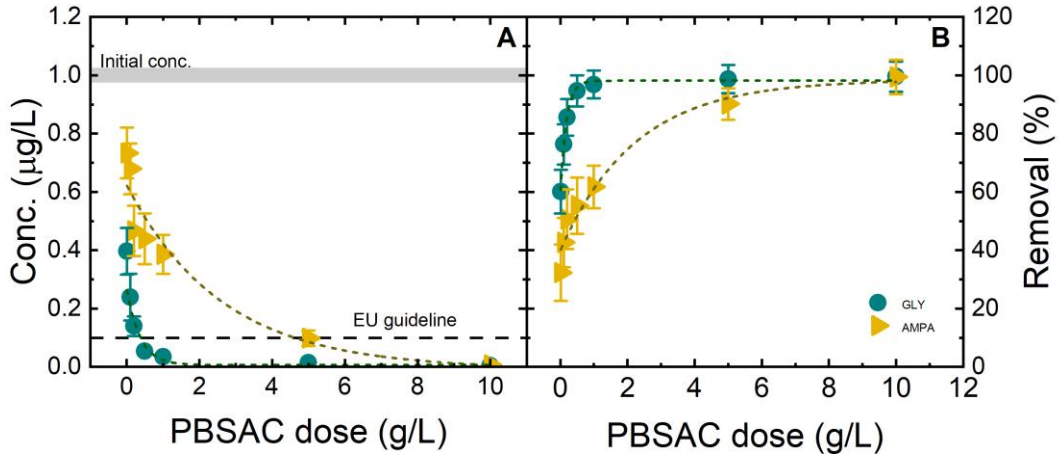

Figure 4.5. GLY/AMPA concentration (A) and removal (B) as functions of PBSAC dose at 26 h, with PBSAC size 200 µm, activation level ~ 4, oxygen content 5%, GLY/AMPA 1 µg/L each in mixture, 1 mM $NaHCO_3$, 10 mM NaCl, 20 °C, 260 rpm, pH 8.1 ± 0.1. Adapted from [197].

The GLY and AMPA concentrations rapidly decreased as the PBSAC dose increased, despite the excess at the surface (Figure 4.5 A). The PBSAC dose required to meet the EU guideline for herbicides (of 0.1 µg/L) is 0.1 g/L. Higher PBSAC dose offers more active sites on the PBSAC surface. The increase in GLY and AMPA removal with increasing dose (Figure 4.5 B) indicates that (1) the PBSAC surface is a limiting factor or (2) the adsorption of GLY and AMPA is slow. The second hypothesis is supported as the adsorption equilibrium was not reached even after 26 h at low PBSAC doses (Figure 9.1). GLY removal increased up to a PBSAC dose of 0.5 g/L; above that, no further removal was achieved due to the GLY removal. On the other hand, AMPA removal increased from 32 ± 8% to 99 ± 5% with the increase of PBSAC dose from 0.1 to 10 g/L. The specific mass adsorbed and the second-order kinetics constant are shown in Figure 4.6.

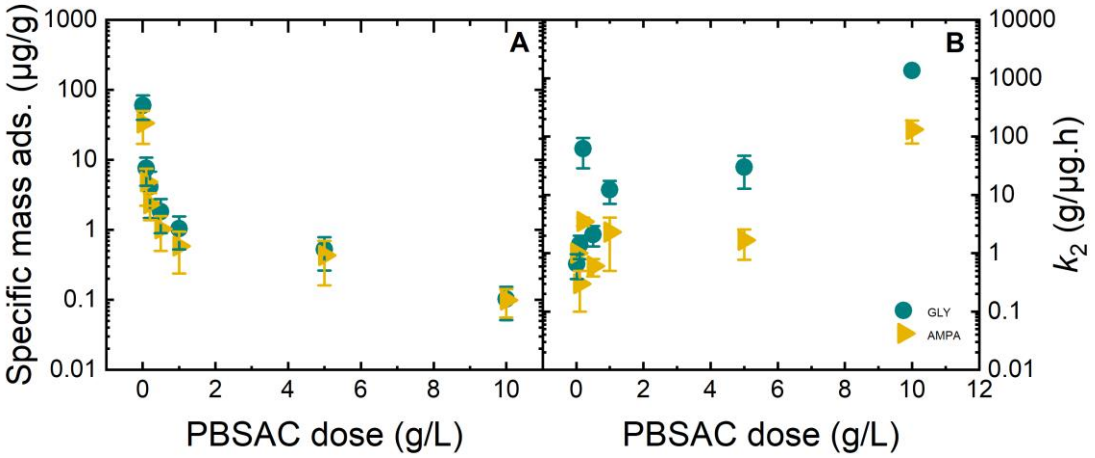

Figure 4.6: GLY/AMPA specific mass adsorbed (A) and reaction rate (second-order kinetics) $\boldsymbol{k_2}$ (B) as functions of PBSAC dose at 26 h with PBSAC size 200 µm, activation level ~ 4, oxygen content 5%, GLY/AMPA 1 µg/L each in mixture, 1 mM $NaHCO_3$, 10 mM NaCl, 20 °C, 260 rpm, pH 8.1 ± 0.1. Adapted from [197].

The specific adsorbed mass (q_{ads}) decreased from 60 ± 6 to 0.1 ± 0.05 µg/g for both GLY and AMPA with an increasing PBSAC dose (Figure 4.6 A). Adsorption kinetics were characterized using the first- and second-order kinetics models as well as intra-particle diffusion models (fitting parameters and R^2 displayed in Table 9.1 and Table 9.2). In general, GLY adsorption was fast, reaching equilibrium concentration in 6 h, whereas AMPA adsorption took longer, reaching equilibrium in 9 h. The kinetics can be fitted by first- and second-order models, suggesting that the adsorption-controlling mechanism may involve mass transport between the solid and liquid phases. On the other hand, even at the lowest dose, the intra-particle diffusion model did not fit the adsorption, indicating that internal pore diffusion is not the only controlling mechanism. Although intra-particle diffusion is not clearly demonstrated by kinetic experiments, this mechanism cannot be ruled out due to the PBSAC porous structure. This finding contradicts the previous research on steroid hormone adsorption by PBSAC. Steroid hormone adsorption fitted well with intra-particle diffusion at low PBSAC doses (< 0.01 g/L) [206]. In fact, the adsorption site on the external surface for GLY and AMPA is potentially more available than steroid hormones, because their molecular sizes (0.62 nm for GLY and 0.49 nm for AMPA [334]) are smaller than those of steroid hormones (0.82 nm [228]). Therefore, GLY and AMPA were expected to have higher maximum mass adsorbed on the external surface of PBSAC.

As the PBSAC dose increased, the adsorption kinetic constant from the second-order model increased from 1 to 1361 for GLY and from 0.3 to 132 for AMPA (Figure 4.6 B). Faster adsorption is possible because more active sites are available on the PBSAC. Even though GLY and AMPA can be removed with low PBSAC doses, higher doses are required to achieve high adsorption rates. Since mass transfer governs adsorption, the characteristics of the PBSAC material will be examined next to determine whether they can improve surface accessibility.

4.7 Material properties: particle size and external surface

Particle size determines adsorption to the external surface of PBSAC. An increase in PBSAC particle size from 78 to 625 µm corresponds to a decrease in external surface area from 64 to 8 m^2/g. Meanwhile, no significant change in the total surface area was observed [207] (Table 4.1). To determine whether the external surface can improve the adsorption, experiments were performed with the various PBSAC particle sizes (78–625 µm) (Figure 4.7).

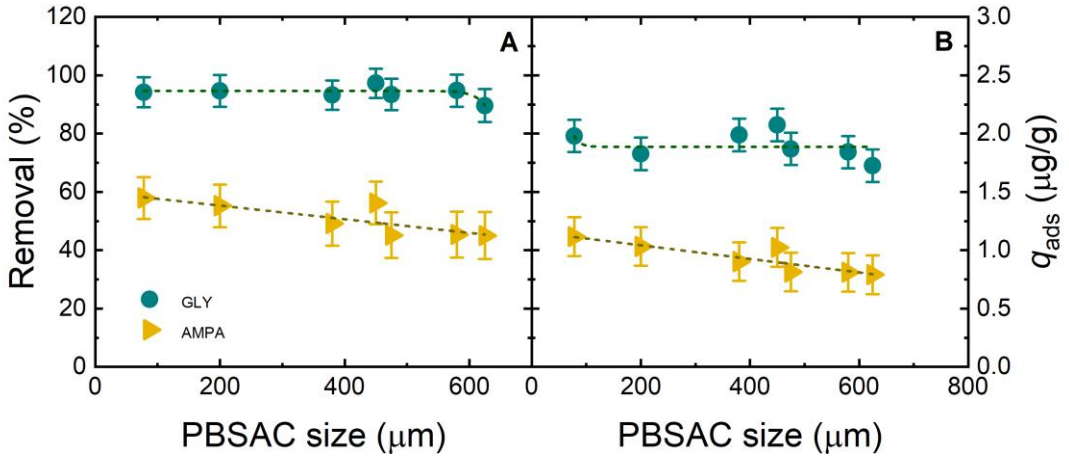

Figure 4.7. GLY/AMPA removal (A) and specific mass adsorbed (B) with varied PBSAC sizes at 26 h (activation level ~ 4, oxygen content 5%, PBSAC dose 0.5 g/L, GLY/AMPA 1 µg/L each in mixture, 1mM $NaHCO_3$, 10 mM NaCl, 20 °C, 260 rpm, pH 8.1 ± 0.1). Adapted from [197].

Higher adsorption was expected with a higher external surface area (smaller PBSAC size). However, the adsorption experiment results contradicted the expectation. In Figure 4.7 A and Figure 4.7 B, 90−95% of GLY was removed. The decreasing trend was more clearly observed in AMPA removal, where removal decreased from 60% to 45%. The specific mass adsorbed also did not show a significant trend with increasing PBSAC diameter, ranging from 2.0 to 1.8 µg/g for GLY and from 1.1 to 0.8 µg/g for AMPA (Figure 4.7 B). The slight decrease in specific mass adsorbed in AMPA adsorption indicates that the external surface area was a limiting factor for AMPA adsorption. In fact, static adsorption allows very long HRT, which can compromise the mass transfer conditions. Therefore, the GLY/AMPA molecules can diffuse into the internal surface of PBSAC, resulting in uniform adsorbed masses at equilibrium regardless of the amount of external surface.

The kinetic rate constant (Table 9.3) of PBSAC 78 µm was high at 52 ± 29 g/µg.h for GLY and 20 ± 10 g/µg.h for AMPA. The adsorption equilibrium of the PBSAC at the smallest size was achieved in less than 10 min. With higher PBSAC size, the kinetic rate constant is lower, showing insignificant change (0.7−2.5 g/µg.h for GLY and 0.1−0.6 g/µg.h for AMPA). With PBSAC 78 µm, more highly accessible adsorption sites are available [207], leading to faster adsorption. Because GLY/AMPA needs less time to diffuse to the external surface than the internal surface, the faster adsorption with the 78 µm particles can be attributed to the larger external surface than the 200−650 µm particles.

The porosity and, subsequently, the internal pore surface area of PBSAC will be affected by the activation level. Next, we'll look into how this variation affects GLY/AMPA adsorption.

4.8 Material properties: PBSAC activation level and internal surface

As PBSAC was produced by carbonization and activation of a polymeric precursor [210], the degree of activation corresponds to how much carbon has been "opened up" or the level of pore volume [211]. A higher activation level provides a larger PBSAC surface area and pore volume [211]. The surface area and pore volume increased from 1103 m^2/g and 0.331 cm^3/g (activation level 1) to 1867 m^2/g and 1.040 cm^3/g (activation level 6) [207]. Except for activation level variation experiments, other experiments were done with PBSAC at activation level 4, with a surface area of 1365 m^2/g. It was assumed that all activation level particles of PBSAC had the same diameter; a higher activation level is directly related to a larger internal surface area and more pore volume [207]. To investigate the roles of pore volume and internal surface area in GLY/AMPA adsorption, experiments with the GLY/AMPA mixture at six different PBSAC activation levels were performed.

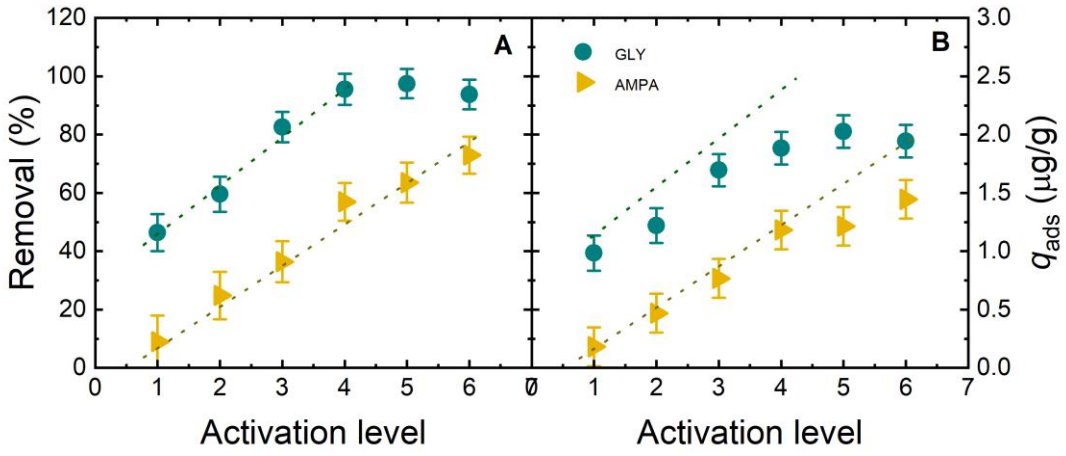

Figure 4.8. GLY/AMPA removal (A) and specific mass adsorbed (B) with varied PBSAC activation levels at 26 h (200 µm, oxygen content 5%, PBSAC dose 0.5 g/L, GLY/AMPA 1 µg/L each in mixture, 1 mM $NaHCO_3$, 10 mM NaCl, 20 °C, 260 rpm, pH 8.1 ± 0.1). Adapted from [197].

If the internal surface of PBSAC limits the adsorption, GLY/AMPA removal is expected to increase with increasing activation level [335]. The static adsorption results showed that adsorption was clearly dependent on PBSAC pores. In Figure 4.8 A, the removal of GLY was > 90%, making it reach the guideline for herbicides in water. However, AMPA could not meet the EU guidelines at all activation levels, even at the highest surface area (activation level 6), with the removal being highest at 72%.

The adsorbed mass increased from 1 to 2 µg/g for GLY, and from 0.2 to 1.5 µg/g for AMPA with higher activation levels (Figure 4.8 C), implying the significant role of internal surface area and pore volume in the adsorption of GLY and AMPA. The kinetic constant rate (k_2) increased with higher activation level (Table 9.4, Table 9.5). The results indicate that adsorption on the external surface was slower at a higher internal surface area. Interestingly, from activation level 4, the intra-particle diffusion model also fits the adsorption kinetics, and the rate constants

increase with increasing activation level (Table 9.4, Table 9.5), suggesting a decreasing contribution of the outer surface and an increasing contribution of the internal surface of PBSAC.

Conclusions on GLY/AMPA transport in/on PBSAC

From experiments with different particle sizes (external surface) and activation levels (internal surface), it is confirmed that GLY and AMPA can be adsorbed on the external and internal surfaces of PBSAC. Although the external surface of PBSAC was abundant, the diffusion of GLY/AMPA into pores was also a limiting factor. GLY and AMPA can transport to PBSAC via boundary-layer (film) diffusion, surface diffusion, and intra-pore diffusion (Figure 4.9) [196].

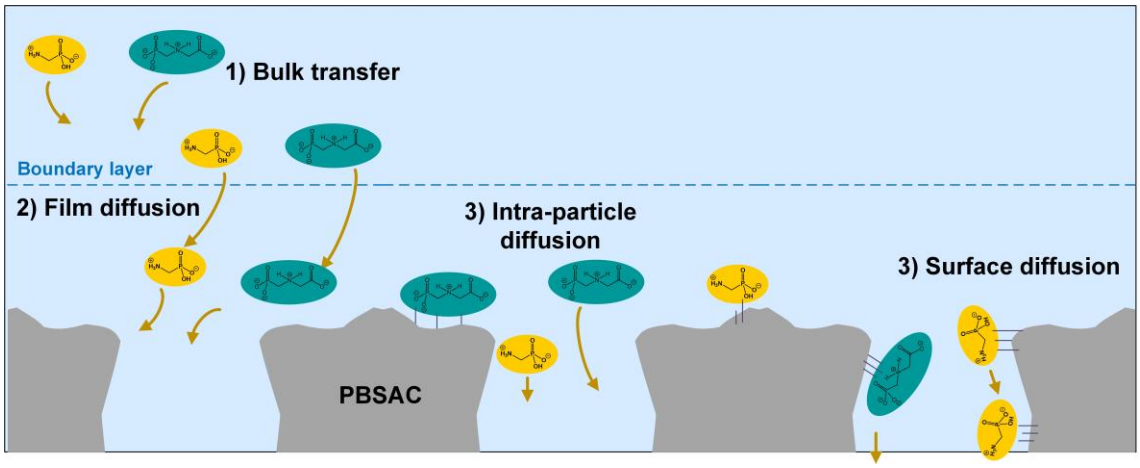

Figure 4.9. Transport of GLY and AMPA on PBSAC. Adapted from [197].

This finding differed from steroid hormone adsorption on PBSAC, where surface interaction was found to play a dominant role [206]. In fact, GLY and AMPA are more mobile in water than steroid hormones. At 20 °C, the diffusion coefficients are $6.9 \cdot 10^{-10}$ m^2/s for GLY and $8.7 \cdot 10^{-10}$ m^2/s for AMPA, which are higher than that of steroid hormone (17-β estradiol) of $5.4 \cdot 10^{-10}$ m^2/s [336]. Therefore, GLY and AMPA can penetrate into PBSAC pores within a shorter time than steroid hormones. This explains the contribution of intra-pore diffusion to GLY/AMPA adsorption, whereas steroid hormone adsorption is dominated by external surface adsorption. Other reasons might be the lower affinity of GLY and AMPA for PBSAC compared to that of steroid hormones, which might differ in the chemistry between GLY/AMPA and PBSAC. This needs investigation of the PBSAC surface oxygen content and water pH.

These factors contributed to the lower affinity of the PBSAC surface for GLY/AMPA compared to steroid hormones, although GLY and AMPA have higher mobility in water (at 20 °C, the diffusion coefficients are $6.9 \cdot 10^{-10}$ m^2/s for GLY and $8.7 \cdot 10^{-10}$ m^2/s for AMPA, which are higher than that of steroid hormone (17-β estradiol) of $5.4 \cdot 10^{-10}$ m^2/s [336]),

4.9 Material properties: PBSAC surface oxygen content

The surface oxygen content can affect adsorption on PBSAC by providing more hydrogen bond acceptors. GLY and AMPA are hydrophilic and negatively charged at pH 8 [49]. Oxygen-containing groups can enhance the interaction of PBSAC with water and reduce interactions with organic compounds [211, 337]. GLY and AMPA adsorption by PBSAC is shown in Figure 4.10.

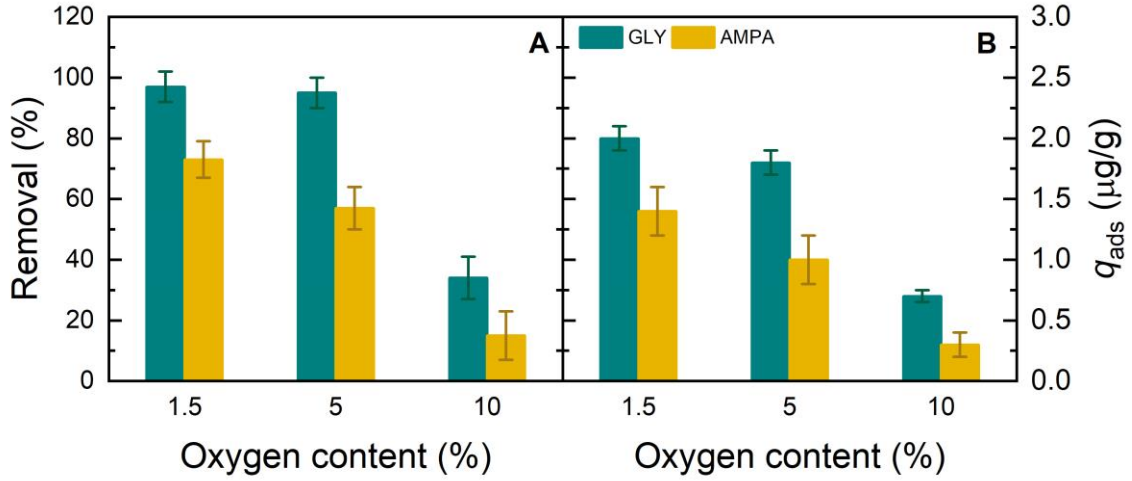

Figure 4.10: GLY/AMPA removal (A) and specific mass adsorbed (B) with varied PBSAC oxygen content at 26 h (200 µm, activation level ~ 4, PBSAC concentration 0.5 g/L, initial GLY/AMPA concentration 1 µg/L, 1 mM $NaHCO_3$, 10 mM NaCl, 20 °C, 260 rpm, pH 8.1 ± 0.1).

At higher surface O content of PBSAC, the removal of GLY/AMPA was lower, indicating the reduced interaction with organic molecules. The removal of GLY was 97% and 95% at oxygen content of 1.5% and 5%, respectively, achieving the EU guidelines. The removal then decreased to 34% for GLY and 16% for AMPA at the highest oxygen content (10%). The same trend was observed for mass adsorbed (q_{ads}) when q_{ads} decreased with the increase of oxygen content on the PBSAC surface. The carboxylic acid and hydroxyl group were detected on the PBSAC surface using Raman and X-ray photoelectron spectroscopies by Tagliavini *et al.*, which might account for the oxygen-containing group [206, 207]. Hydrogen bonds can form between water molecules and the oxygen-containing groups on the PBSAC surface, hindering the adsorption of GLY/AMPA on PBSAC [337].

4.10 Water quality: solution pH

GLY has four pKa (0.8, 2.6, 5.8, 10.8) and AMPA has three pKa (1.8, 5.4, 10.2) values. In consequence, the charge of GLY ranges from +0 to −3, and AMPA ranges from +0 to −2 at pH from 2 to 12 (Chapter 2.1. GLY and AMPA properties) [44]. pH is expected to play a critical role in adsorption. To determine the role of GLY and AMPA charge, adsorption by PBSAC was performed with different water pH from 2 to 12 (Figure 4.11).

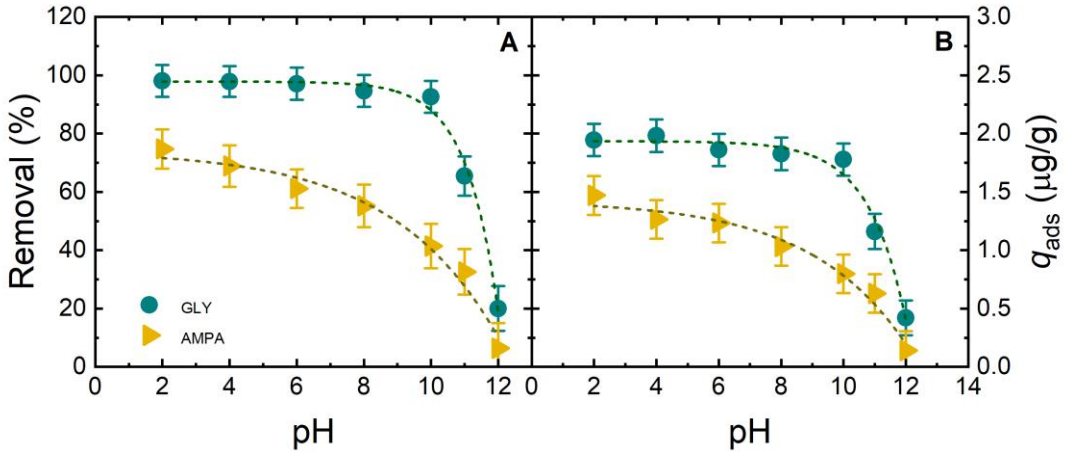

Figure 4.11. GLY/AMPA removal (A) and specific mass adsorbed (B) with different pH at 26 h (PBSAC 200 µm, activation level ~ 4, oxygen content 5%, dose 0.5 g/L, GLY/AMPA 1 µg/L each in mixture, 1mM $NaHCO_3$, 10 mM NaCl, 20 °C, 260 rpm). Adapted from [197].

Removal of both GLY and AMPA decreases significantly with increasing pH (Figure 4.11 A and B). Clearly, a low or neutral pH is required for the best GLY and AMPA adsorption. From Figure 4.11 C, the adsorbed mass was higher at acidic and neutral pH.

GLY is neutral charged at pH < 3, while AMPA is neutral at pH < 5. With further increases in pH, GLY and AMPA are negatively charged [199, 338]. Meanwhile, PBSAC has neutral charge in all pH [206]. The functional groups of GLY and AMPA can interact with the functional groups on PBSAC surface via hydrogen bonding and van der Waals interaction [199, 339].

The energetic interactions (hydrogen bonding and van der Waals interaction) occur within nanoseconds when the adsorbates are close (in the order of 1 nm) to the PBSAC surface (Figure 4.12) [340].

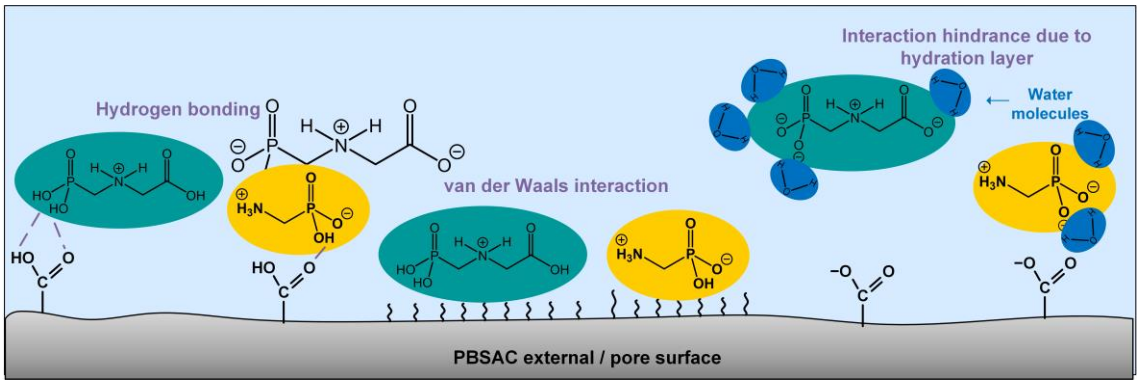

Figure 4.12. Adsorption mechanisms of GLY and AMPA on PBSAC, including hydrogen bonding and van der Waals interaction. The interaction/adsorption hindrance caused by the hydration shells around negative charges, especially at high pH, is highlighted. Adapted from [197].

The functional groups on the PBSAC surface can form hydrogen bonds with those of GLY and AMPA [199, 206, 339]. Besides, van der Waals interactions can be formed between GLY or AMPA and PBSAC [199]. Additionally, the hydration layer could become stronger as the

negative charges of GLY and AMPA increase [347], thereby hindering their adsorption to the PBSAC surface.

Comparing to hydrophobic compounds (steroid hormones), the less adsorption of GLY and AMPA can be due to 1) strong hydration of GLY/AMPA than neutral hormone molecules making it harder to reach PBSAC surface [341, 342], 2) weak van der Waals interaction with the PBSAC [343], and 3) absence of high affinity π-rings which plays a dominant role in steroid hormone adsorption [344].

4.11 Water quality: GLY and AMPA concentration

With the target of removing GLY and AMPA to meet EU guidelines, achievable water quality depends on contaminant concentrations in raw water; consequently, adsorption was investigated over a range of 0.1–1000 µg/L for GLY and AMPA [345] (Figure 4.13).

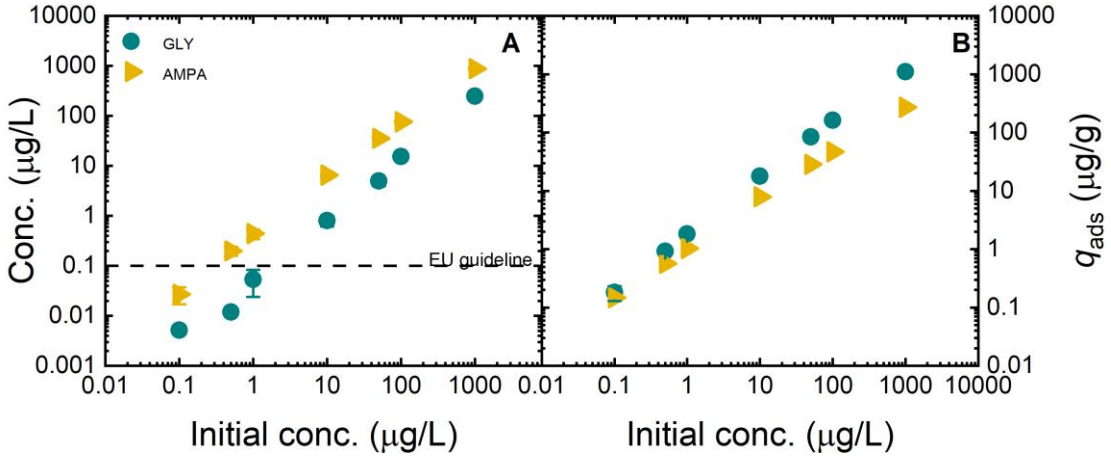

Figure 4.13. GLY/AMPA concentration (A) and specific mass adsorbed (B) with GLY and AMPA concentration at 26 h (PBSAC 200 µm, activation level ~ 4, oxygen content 5%, PBSAC dose 0.5 g/L, 1 mM $NaHCO_3$, 10 mM NaCl, 20 °C, 260 rpm, pH 8.1 ± 0.1). Adapted from [197].

In Figure 4.13 A, the EU guideline was met for GLY adsorption by PBSAC with initial concentrations ≤ 1 µg/L. Meanwhile, AMPA concentration was higher than 0.5 µg/L, leading to incomplete removal.

Concentration decreased from 10 to 1000 µg/L for GLY and 0.5 to 1000 µg/L for AMPA with increasing herbicide concentrations. The maximum adsorbed mass was not determined within the concentration range of 0.1–1000 µg/L. PBSAC exhibited a linear relationship between GLY/AMPA mass adsorbed and concentration up to a concentration of 1000 µg/L (Figure 4.13 B). The high initial GLY and AMPA concentrations were used for static adsorption to determine the maximum adsorbed mass of PBSAC. Figure 4.14 shows the adsorption isotherms of GLY and AMPA displayed by PBSAC.

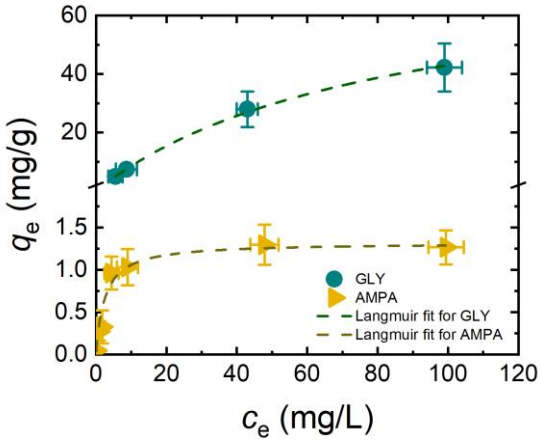

Figure 4.14: Adsorption isotherm displayed by PBSAC. The Langmuir model is applied (PBSAC 200 µm, PBSAC concentration 0.5 g/L, 1 mM $NaHCO_3$, 10 mM NaCl, 20 °C, 260 rpm, pH 8.1 ± 0.1). Adapted from [197].

The Langmuir isotherm fit the adsorption, which was relevant to the GLY and AMPA monolayer adsorption due to the low concentration of the herbicides [326]. The Freundlich and Henry isotherms [329, 346] did not fit the adsorption. The maximum specific adsorbed masses were determined to be 78 and 1.3 mg/g, respectively, using the Langmuir isotherm model.

4.12 Operational parameter: water temperature

To evaluate the impact of temperature on the adsorption of GLY and AMPA, experiments were conducted at temperatures of 5–80 °C, where lower temperatures are relevant in water treatment [347]. GLY/AMPA adsorption at different temperatures is shown in Figure 4.15.

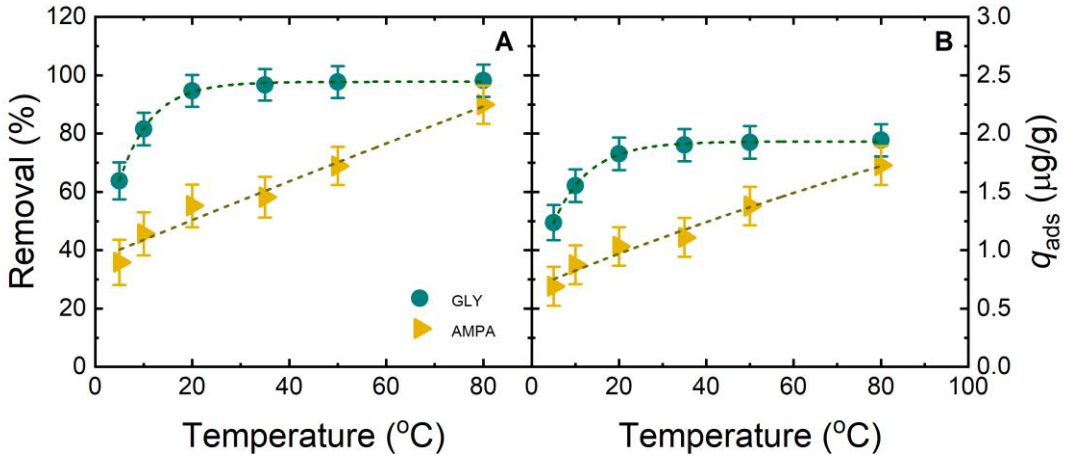

Figure 4.15. GLY/AMPA removal (A) and specific mass adsorbed (B) with different temperatures at 26 h (PBSAC 200 µm, activation level ~ 4, oxygen content 5%, PBSAC dose 0.5 g/L, initial GLY/AMPA concentration 1 µg/L, 1mM $NaHCO_3$, 10 mM NaCl, 260 rpm, pH 8.1 ± 0.1). Adapted from [197].

GLY removal increased when the temperature increased from 5 to 20 °C. However, the removal remained more than 90% at temperatures higher than 20 °C. Meanwhile, the removal of AMPA increased from 30% to 90% with the increase of temperature. At 80 °C, the removal was 90%, and the AMPA concentration met the EU guideline, although this temperature is unrealistic for water treatment. The mass adsorbed of GLY increased from 1.2 µg/g at 5 °C to 2 µg/g at 80 °C. The adsorbed mass of AMPA increased from 0.7 µg/g at 5 °C to 1.7 µg/g at 80 °C (Figure 4.15 B).

Thermodynamic parameters (the Gibbs free energy (ΔG^0, kJ/mol), enthalpy (ΔH^0, kJ/mol), and entropy (ΔS^0, J/mol.K) changes) of GLY and AMPA adsorption are shown in Table 4.5.

Table 4.5. The Gibbs energy (ΔG^0, kJ/mol), enthalpy (ΔH^0, kJ/mol), and entropy (ΔS^0, J/mol.K) changes of the adsorption of GLY and AMPA (PBSAC 200 µm, activation level ~ 4, oxygen content 5%, PBSAC dose 0.5 g/L, initial GLY/AMPA concentration 1 µg/L, 1 mM $NaHCO_3$, 10 mM NaCl, 260 rpm, pH 8.1 ± 0.1). Adapted from [197].

	GLY	AMPA
ΔH^0 (kJ/mol)	67 ± 11	28 ± 4
ΔS^0 (J/mol.K)	310 ± 62	157 ± 31
ΔG^0 (kJ/mol) at 5 °C	−19 ± 3	−15 ± 3
ΔG^0 (kJ/mol) at 20 °C	−24 ± 4	−18 ± 3
ΔG^0 (kJ/mol) at 80 °C	−42 ± 6	−27 ± 4

Enthalpy change (ΔH^0) of GLY and AMPA were +67 kJ/mol and +28 kJ/mol, respectively. The positive enthalpy changes mean the adsorption process was endothermic. As ΔH^0 < 80 kJ/mol, the adsorption mechanism was typically physical adsorption, which is realistic as PBSAC only has 5% of oxygen-containing groups [348, 349].

As the process involves both adsorption and diffusion, the entropy change is attributed to both processes rather than only adsorption. The entropy change (ΔS^0) were +310 J/mol.K for GLY and +157 J/mol.K for AMPA, indicating an increase in disorder at the solid−liquid interface during the adsorption. In this process, the adsorption of GLY/AMPA to PBSAC results in a loss of freedom (rotation and translation), leading to a decrease in entropy (S^0). At the same time, intra-particle diffusion of GLY and AMPA into the PBSAC pores proceeds, which is more favorable at high temperature [350], resulting in a positive entropy change ΔS^0. The desorption also happens during this time which increase the disorder. Therefore, the positive ΔS^0 is the sum of all these phenomenon [351].

The Gibbs energy change (ΔG^0) was negative at all temperatures, meaning the spontaneous adsorption process [332]. The ΔG^0 value decreased from –19 kJ/mol to–42 kJ/mol for GLY, and from –15 kJ/mol to –27 kJ/mol for AMPA with the increase of temperature, suggesting the higher adsorption at higher temperature, which was also observed in the static adsorption. Overall, the adsorption process is endothermic, likely physical, spontaneous, and more favorable at high temperatures.

4.13 Conclusions

In this chapter, the adsorption of GLY and AMPA was evaluated in static adsorption, with HRT ranging from 5 min to 26 h. The investigation of adsorption optimization proceeded from two different approaches: material characteristics and operational parameters. In addition, the interference on the adsorption of GLY and AMPA on PBSAC by water chemistry was also studied. The following points are obtained from this investigation.

- The adsorption of GLY and AMPA at environmentally relevant concentrations from water by PBSAC was achieved, with 95% removal of GLY and 57% removal of AMPA.
- Both the external and internal surfaces contribute to GLY and AMPA adsorption, although only a proportion of the surfaces has a high affinity for the charged herbicides.
- The process was influenced by hydrogen bonding and van der Waals interaction between charged GLY/AMPA and the PBSAC surface groups, and hindered by the hydration layer of GLY and AMPA.

In summary, adsorption, which is the current standard technology in water treatment plants in Germany for micropollutant removal, can remove GLY and AMPA at environmentally relevant concentrations. The static adsorption by PBSAC exhibited a good adsorption in which GLY was removed to below the EU guideline concentration of 0.1 µg/L. Meanwhile, AMPA could not be removed to the same level. As water always contains organic matter, bacteria, viruses, and particulates, adsorption will always be interfered with by these water components. To overcome this challenge, membrane filtration will be integrated with adsorption for GLY/AMPA removal in the next step.

5 Dynamic adsorption of GLY and AMPA by UF–PBSAC

This chapter is adapted from a publication in Water Research (2024) entitled: P.B. Trinh, A.I. Schäfer, Removal of glyphosate (GLY) and aminomethylphosphonic acid (AMPA) by ultrafiltration with permeate-side polymer-based spherical activated carbon (UF–PBSAC), Water Research, 250 (2024) 121021 [352].

The contribution of authors:

Phuong B. Trinh: performing experiments; samples analysis; data analysis and interpretation; validation; methodology; visualization; writing – original draft

Andrea I. Schäfer: conceptualization; methodology; funding acquisition; project administration; resources; supervision; validation; writing – review & editing

This chapter aims to investigate the GLY and AMPA adsorption performance of ultrafiltration membrane with permeate-side polymer-based spherical activated carbon (UF–PBSAC). The adsorption performance is determined by the adsorbent properties and the filtration operation conditions. Varied experimental parameters include PBSAC characteristics (size, PBSAC layer thickness), operation conditions (flux), and water conditions (GLY/AMPA concentrations, pH, and water temperature). Finally, the adsorption mechanisms and the limiting factors of dynamic adsorption are evaluated to optimize UF–PBSAC adsorption filtration.

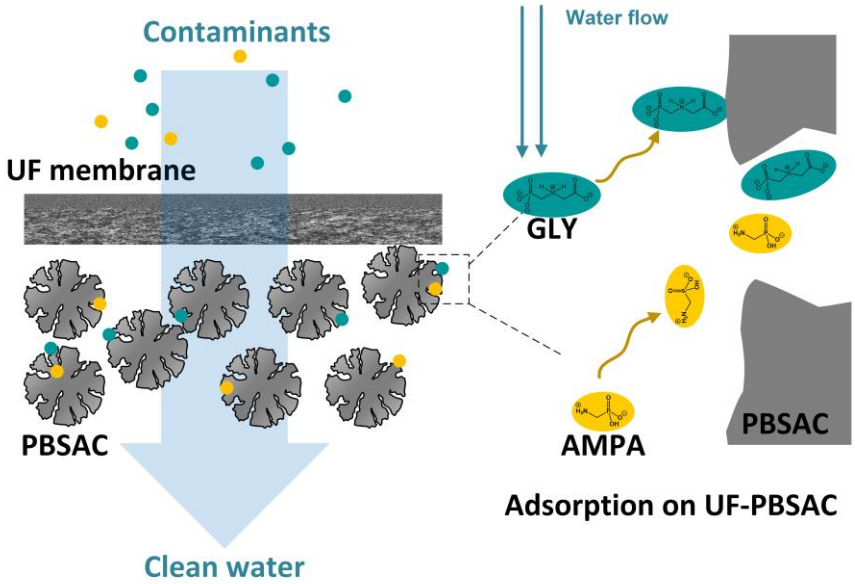

5.1 Introduction

The membrane–adsorption hybrid system takes advantage of both filtration and adsorption to overcome the limitations of each technology [192]. Tagliavini *et al.* have successfully combined ultrafiltration with a permeate-side polymer-based spherical activated carbon (UF–PBSAC) to remove steroid hormones with a removal of >96% from 100 ng/L in the feed solution [207]. With this vision, UF–PBSAC is expected to remove GLY and AMPA in water. In this process, PBSAC is in charge of adsorbing GLY and AMPA while UF acts as a barrier to remove organic matter, bacteria, viruses, and particulates, which can interfere with adsorption.

In Chapter 4, PBSAC was previously investigated for GLY/AMPA removal. Compared to steroid hormones, GLY and AMPA are smaller and more hydrophilic [61]. The hydrodynamic diameter of 17β-Estradiol is 0.79−0.86 nm, while the hydrodynamic diameter of GLY and AMPA are 0.62 nm and 0.49 nm, respectively [61]; hence, the van der Waals interaction is weaker [343]. Moreover, GLY and AMPA interaction with PBSAC does not involve π−π stacking like steroid hormones, and the strong hydration shell of GLY/AMPA can hinder adsorption. Therefore, the limitation of GLY and AMPA adsorption on UF–PBSAC can be the lower adsorption than steroid hormones, which need to be investigated based on material characteristics (surface area), operational parameters (flux, and PBSAC layer thickness, which are related to HRT), and water chemistry.

On the other hand, the higher mobility of GLY/AMPA than steroid hormones can help herbicides to penetrate into PBSAC pores within a shorter time, which might be beneficial compared to steroid hormones.

Based on the hypothesis, UF–PBSAC will be applied for GLY and AMPA removal, with the following specific research questions addressed.

- Can UF–PBSAC efficiently remove GLY/AMPA within short HRT in dynamic filtration?
- Which factors (external surface of PBSAC, HRT, material capacity, water pH, and water temperature) limit GLY/AMPA adsorption by UF–PBSAC?
- Can the EU regulation requirements be achieved when the limiting factors are minimized?

5.2 Filtration system and protocol

The dynamic filtration of UF–PBSAC was performed in a dead-end stainless steel system as described in the work of Tagliavini *et al.* [207] (Figure 5.1). The filtration protocol was adapted from previous work [195, 353-355] and is shown in Table 9.9. There are three parts in the cell: the base, the membrane cell, and the top. The stirrer is not used in this work for the UF membrane. The internal diameter of the membrane cell is 7 cm^2 with an effective filtration area of 38.5 cm^2 and an internal volume of 990 mL. To place PBSAC at the bottom of the cell, stainless steel porous ‘rings’ with a thickness of 1 or 2 mm were stacked on the porous support (SIKA-

5AX, GKN Powder Metallurgy, Germany, average pore diameter 10 μm, porosity 31%) to form a well that can accommodate a 1−6 mm layer of PBSAC. This porous layer also prevents the release of PBSAC into permeate. The PBSAC layer thickness can be adjusted by changing the bottom part of the stirred cell and adding more stainless-steel porous 'rings'.

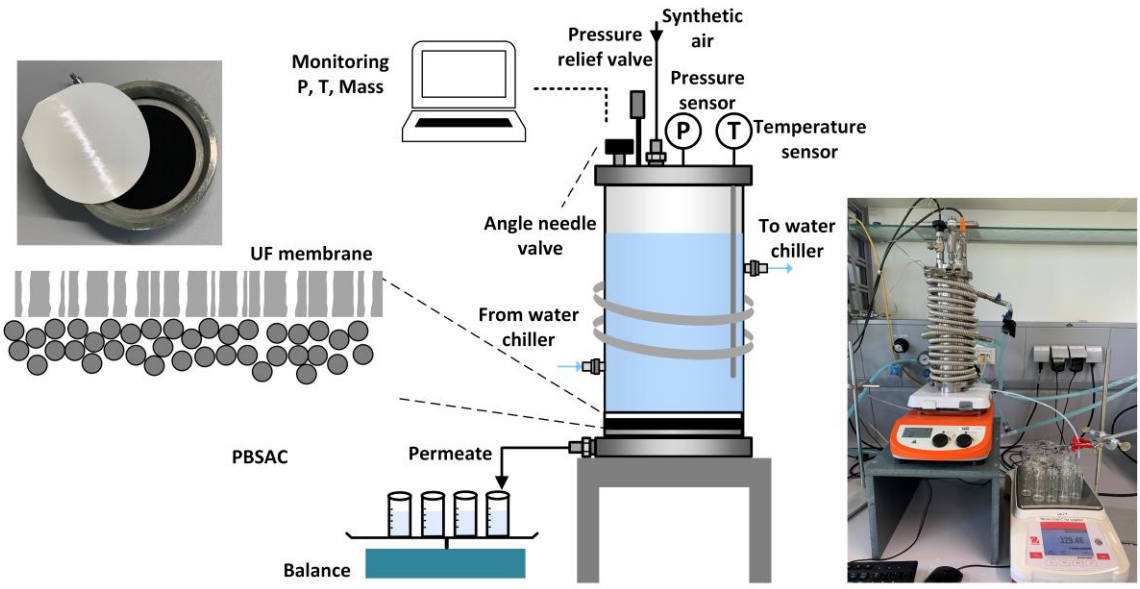

Figure 5.1: Schematic of UF–PBSAC filtration system with a modified bottom that allows variable depth of PBSAC.

The cell was connected to a synthetic air tank (Alpha Gas, Air Liquid, Germany), which contained 20% oxygen and 80% nitrogen. Pressure was measured by a pressure transducer (PX219–30V85G5V, Omega Engineering, Germany), and temperature was measured by a thermocouple (TJ2-CPSS-M60U-250-SB, Omega Engineering, Germany). Both sensors were assembled on the top part of the cell. The temperature of the stirred cell was controlled by a thermostatic circulator system composed of a chiller (LKB 2219 MultiTemp II, Bromma, Germany) and a stainless-steel, flexible serpentine (Water Way Engineering GmbH, Germany) wrapping around the stainless-steel stirred cell. The permeate mass was measured with an electronic balance (Adventurer ProAV 2102, Ohaus, Germany). All data were collected with a tailored LabView 2014 program (National Instruments, Germany).

Before the filtration experiments, the membrane was soaked in Milli-Q water for 1 hour to wet and remove storage chemicals. Then, a PBSAC layer with a 2 mm thickness was placed on the porous plate, and a UF membrane was placed on top of the PBSAC layer. UF–PBSAC was mounted in the membrane cell, which was subsequently compacted with Milli-Q water at 1.4 bar for 1 hour. The pure water permeability of the membrane was measured after compaction at a pressure of 1.4 bar. For the main filtration experiment, the cell was filled with 700 mL of feed solution (GLY/AMPA 1000 ng/L) and pressurized by synthetic air. 100 mL of permeate was collected at a defined permeate volume (100, 200, 300, 400, 500, 600 mL).

After the experiment, the pure water permeability of the membrane was measured again at a pressure of 1.4 bar. The membrane was then unmounted, the PBSAC removed, and the stirred

cell was disassembled and cleaned with 2 M HCl (pH 2), 2 M NaOH (pH 12), and Milli-Q water.

5.3 Ultrafiltration membrane choice

UF regenerated cellulose membrane (PLHGC 10 kDa, Merck Millipore, USA) with a nonwoven polypropylene support layer and a regenerated cellulose active layer was chosen for this work. The total thickness of the membrane was 230 µm with 0.5–1 µm active layer thickness. The membrane had negligible adsorption of micropollutants (interfered little with the adsorption by the bottom PBSAC layer). Moreover, PLHGC 10 kDa membranes can effectively remove humic substances [363, 364], which account for 85% of natural organic matter [356] and are typically treatable by 10 kDa membranes [357, 358]. In addition, ultrafiltration would be an effective barrier to pathogens that need to be retained in water treatment applications. The role of UF membrane in UF–PBSAC for micropollutant removal with the presence of humic acid was conducted in previous work [215]. Therefore, this chapter will only evaluate the adsorption performance of GLY and AMPA in synthetic water.

5.4 Adsorbents

Information on adsorbents was presented in Chapter 4 (Table 4.1). In this chapter, PBSAC at different sizes was used (78, 200, 380, 450, 475, 580, 625 µm).

5.5 Data analysis

Removal of GLY and AMPA, and the mass adsorbed, were calculated using the same equations in Chapter 4.

Flux and permeability of UF–PBSAC membrane filtration

Water flux J_v (L/m^2.h) is determined from the permeate mass using:

$$J_v = \frac{Q_p}{A} \tag{5.1}$$

where $Q_p = \frac{\Delta m_p}{\Delta t \rho_w}$ is the permeate flow rate (m^3/s); Δm_p is the change of mass in elapsed time Δt; ρ_w is the density of water (equal to 1000 ± 10 g/L at 20-22 °C [359]); A: active membrane area (m^2).

The water permeability L_p (L/m^2.h.bar) is determined from the water flux and transmembrane pressure ΔP (bar) in equation (5.2).

$$L_p = \frac{J}{\Delta P} \tag{5.2}$$

Hydraulic residence time of UF–PBSAC

In adsorption by UF–PBSAC, HRT can limit the access and diffusion of GLY and AMPA to the PBSAC surface and pores [353]. The HRT of GLY and AMPA in UF–PBSAC is calculated using equation (5.3). and reported in Figure 5.2

$$\bar{t} = \frac{V}{Q} = \frac{V_m \cdot \varepsilon}{Q} = \frac{A \cdot \delta \cdot \varepsilon}{Q} = \frac{\delta \cdot \varepsilon}{J} \tag{5.3}$$

where V is the volume of membrane occupied by feed solution (L), V_m is membrane volume (L), δ is membrane thickness (m), and ε is membrane porosity, assuming that PBSAC layer porosity was 0.4 and HRT in the UF membrane was neglected.

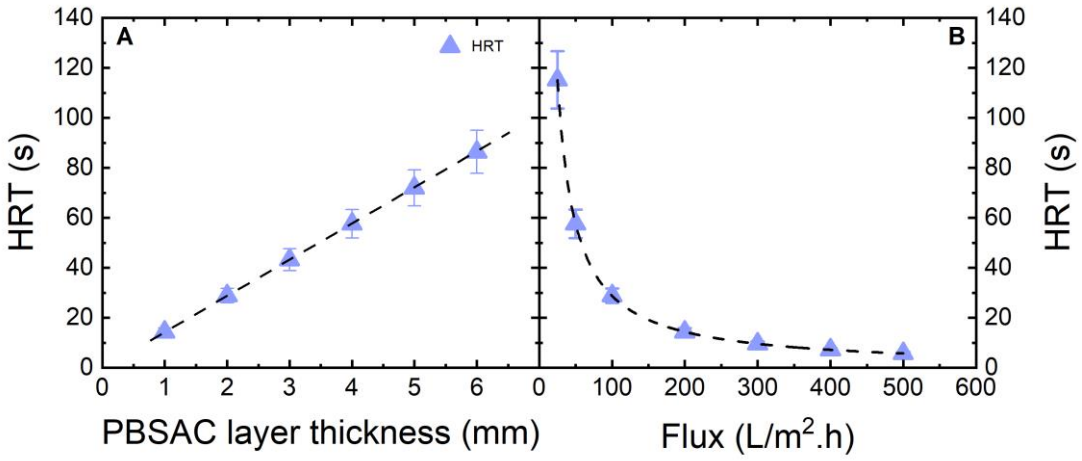

Figure 5.2: HRT of GLY/AMPA of UF–PBSAC. Adapted from [352].

For varying PBSAC layer thickness, the HRT increased from 14 s to 86 s as the PBSAC layer thickness increased from 1 to 6 mm. Meanwhile, the HRT decreased reciprocally from 115 s to 5 s with the increase of flux from 25 to 500 L/m^2.h. In this short HRT, the investigation into whether GLY and AMPA can be removed will be performed.

To evaluate dynamic adsorption performance, UF–PBSAC was first examined for GLY/AMPA removal at an environmentally relevant feed concentration (1000 ng/L of each herbicide). Then, the limiting factors of adsorption were investigated to determine the optimized conditions for process optimization.

5.6 GLY/AMPA removal by UF–PBSAC

To determine whether GLY and AMPA can be adsorbed on UF–PBSAC in a short HRT, the filtration of UF membrane and UF–PBSAC membrane was conducted with a feed concentration of 1000 ng/L (environmentally relevant concentration in Germany [98]). The PBSAC layer thickness was 2 mm, the same thickness used by Tagliavini et al. to achieve 96% removal of

steroid hormones [207]. The breakthrough of GLY and AMPA from the filtration of UF and UF–PBSAC membranes is shown in Figure 5.3.

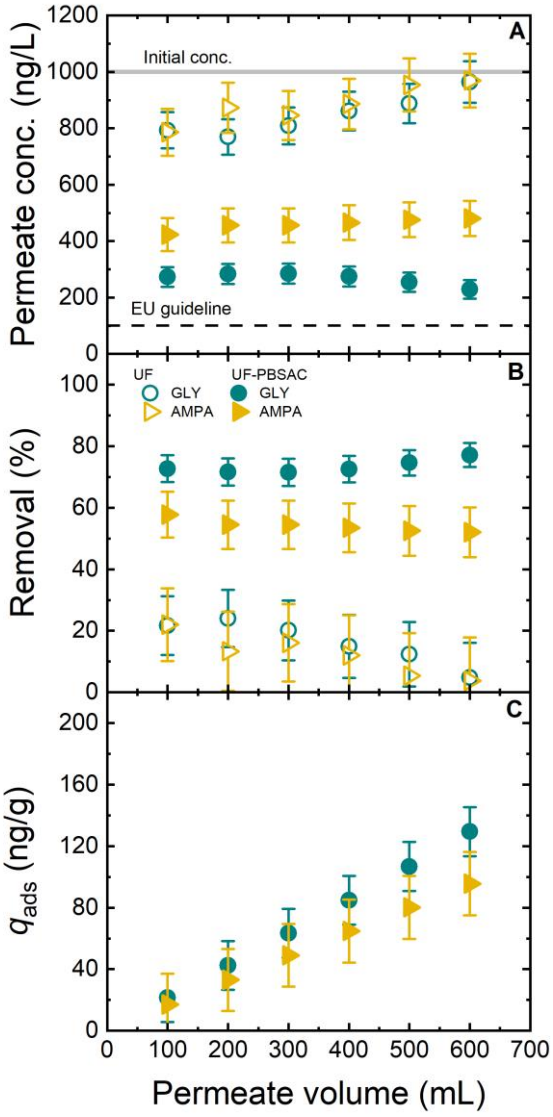

Figure 5.3. GLY/AMPA permeate concentration (A), removal (B), and specific adsorbed mass (C) (200 µm PBSAC diameter, 2 mm layer thickness, 100 L/m^2.h flux, 1000 ng/L GLY/AMPA, 1mM $NaHCO_3$, 10 mM NaCl, 20 ± 0.5 °C, pH 8.1 ± 0.1). Adapted from [352].

UF membrane (without PBSAC) can adsorb GLY and AMPA in the first 300 mL, then the removal gradually reduced to < 5%, indicating a near adsorption saturation (Figure 5.3 A). This removal was due to the adsorption, but retention as GLY and AMPA are much smaller than the membrane pores. The molecular diameters of GLY and AMPA are 0.62 nm and 0.49 nm, respectively, [197] which are smaller than the PLHGC 10 kDa membrane pore diameter at ~5.4 nm [221, 334]. The regenerated cellulose, which contained hydroxyl groups [369] in the active layer of the UF membrane, could interact with the functional groups of GLY and AMPA (phosphonate and carboxylate groups), allowing adsorption to occur [360].

UF–PBSAC can remove GLY and AMPA with a thin PBSAC layer *via* dynamic adsorption. The removal was 77 ± 4% for GLY and 52 ± 5% for AMPA (Figure 5.3 B). The GLY and AMPA permeate concentrations with UF–PBSAC were stable at around 228 ± 12 ng/L and 480 ± 32 ng/L (Figure 5.3 A), respectively, during the filtration experiment. The permeate concentrations did not meet the EU regulation for individual herbicides (100 ng/L) [13].

The stable permeate concentration during filtration (Figure 5.3 A), while specific adsorbed mass keeps increasing linearly (Figure 5.3 C), indicates the steady-state adsorption. This was due to the abundance of the external surface of PBSAC in the layer, which was also the case in the adsorption of steroid hormones by UF–PBSAC [207]. Compared to the theoretical mass adsorbed of GLY and AMPA on PBSAC (Table 9.6), the observed mass adsorbed was much lower at 129 ± 11 ng/g for GLY and 95 ± 8 ng/g for AMPA.

Compared to static adsorption (Chapter 4), the mass adsorbed of GLY and AMPA by UF–PBSAC were lower (1800 ng/g for GLY and 1000 ng/g for AMPA [197]). In dynamic adsorption, GLY and AMPA did not reach both the external and internal surfaces of PBSAC as much as in static adsorption. This has proven the concern on HRT for adsorption in UF–PBSAC as mentioned previously.

At this stage, UF–PBSAC has shown an adequate performance in adsorbing GLY and AMPA. Next, the optimization of adsorption will be determined with parameters in consideration for limiting factors (adsorbents, water chemistry) (Figure 5.7).

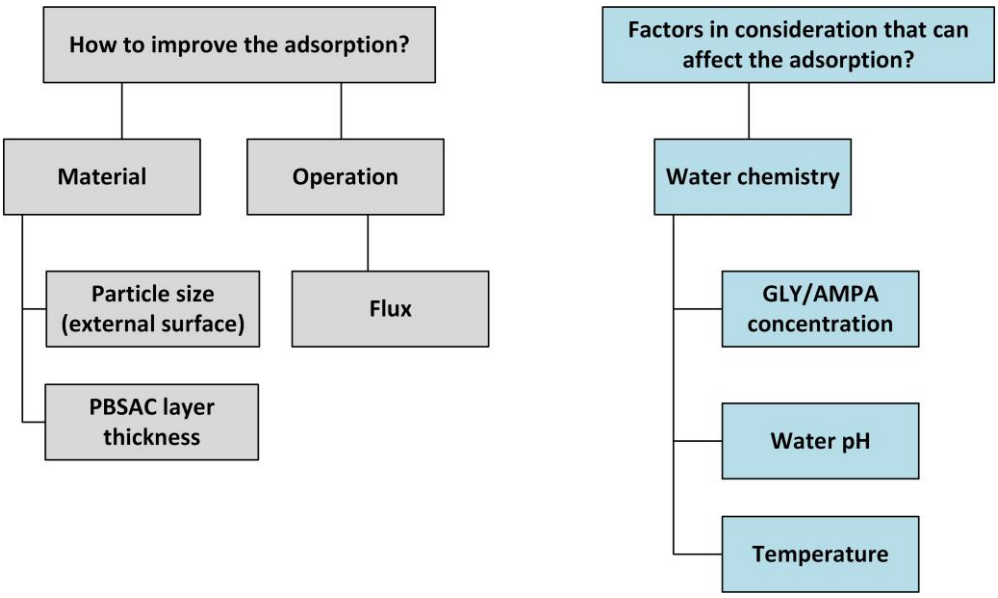

Figure 5.4. Factors in consideration to improve the adsorption of GLY/AMPA on PBSAC

In the UF–PBSAC process, within 29 s, GLY and AMPA needed to pass the PBSAC boundary layer, reach the PBSAC surface, before the molecules could diffuse into the PBSAC pores, which was independent of HRT (Figure 5.5). The diffusion of GLY and AMPA is driven by concentration, which will be determined in the next section.

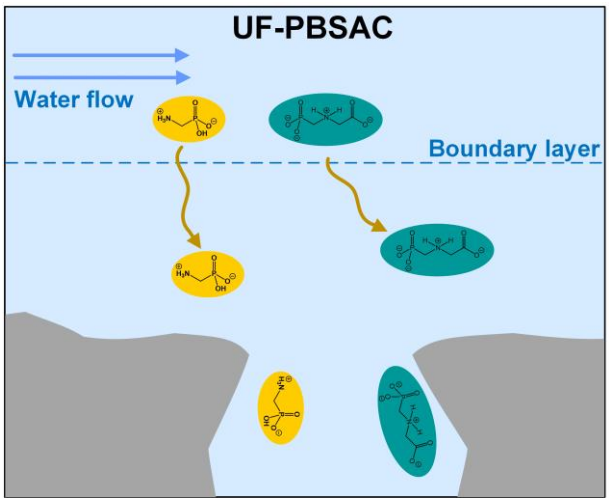

Figure 5.5. The GLY/AMPA adsorption on UF–PBSAC. Adapted from [352].

5.7 Adsorption with varying GLY and AMPA concentrations

To investigate the extent to which the adsorption of GLY and AMPA is limited by the initial concentrations, adsorption was performed at feed concentrations varying from 100 ng/L to 1000 µg/L (a relevant range in groundwater and surface water [345], Figure 5.6).

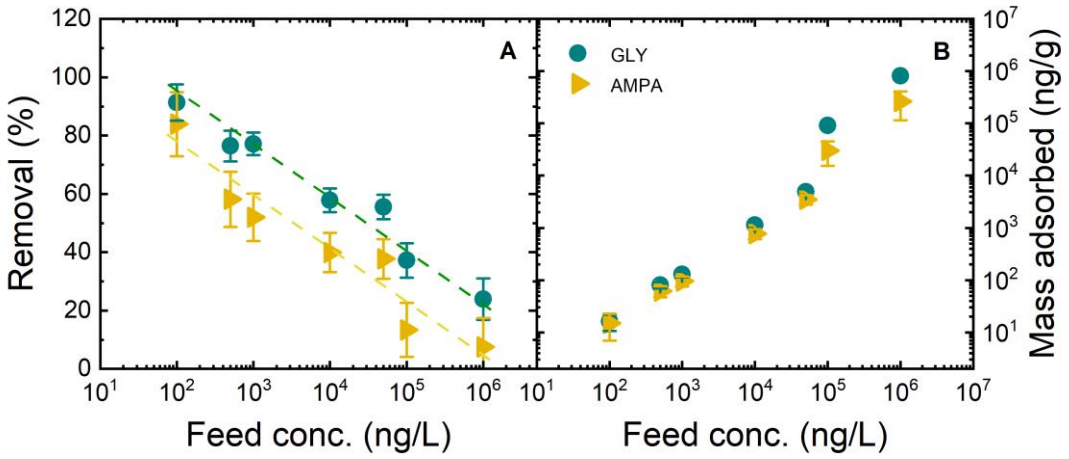

Figure 5.6. GLY/AMPA permeate removal (A) and specific adsorbed mass (B) as a function of feed concentration (reported values at permeate volume 600 mL, 200 µm PBSAC diameter, 2 mm layer thickness, 100 L/m^2.h flux, 1mM $NaHCO_3$, 10 mM NaCl, 20 ± 0.5 °C, pH 8.1 ± 0.1. Adapted from [352].

In all feed concentrations, it was found that AMPA removal was 10 to 20% lower than GLY removal. This might be due to the higher affinity of GLY towards PBSAC than AMPA. The higher affinity of GLY was proven in static adsorption (Chapter 4). In static adsorption, the maximum mass adsorbed of GLY was higher than that of AMPA [197]. Because AMPA is smaller, the van der Waals interactions with the PBSAC surface are weaker, leading to lower

affinity towards PBSAC [343]. Moreover, AMPA does not have carboxylate groups compared with GLY, resulting in weaker hydrogen bonding with functional groups on PBSAC [343]. Consequently, AMPA and PBSAC interaction is less strong than GLY [197].

In Figure 5.6 A and B, the removal decreased significantly from 91 to 23% for GLY and from 83 to 7% for AMPA when the feed concentration increased. At higher feed concentrations, the mass adsorbed increased from 16 ng/g to 82 µg/g for GLY and from 7 ng/g to 15 µg/g for AMPA (Figure 5.6 C). AMPA removal at the initial concentration of 1000 µg/L was low, indicating the maximum adsorbed mass at ~ 15 µg/L. Meanwhile, the maximum adsorbed mass of GLY was close to 82 µg/g, which was much lower than in static adsorption (Chapter 4). In static adsorption, the maximum adsorbed mass of GLY and AMPA was 78 and 1.3 mg/g, respectively. The decrease in removal with increasing feed concentration implied that the accessible surface (within a short HRT of 29 s) was a limiting factor to adsorption.

The decrease in GLY/AMPA removal was different from steroid hormones at the same concentration range (100 ng/L to 100 µg/L). The removal of steroid hormones only decreased by 5% [353]. This difference was attributed to the high affinity of PBSAC towards steroid hormones, in which the hydrophobic interaction was more favorable. As a result, adsorption sites for GLY/AMPA adsorption expired more quickly, even though GLY and AMPA have smaller molecular diameters and can access the PBSAC pore more easily, as discussed in the introduction of Chapter 5. Next, the limitation of the external surface to the GLY/AMPA will be examined.

5.8 Material property: PBSAC external surface

In the adsorption on PBSAC, GLY and AMPA are adsorbed to the external surface (boundary layer) and/or diffuse into the pores [196]. In dynamic adsorption, such as UF–PBSAC, external surface adsorption was shown to be the limiting factor, and diffusion into pores was not significant [207]. This is also expected for GLY and AMPA, which have lower surface affinity for PBSAC than steroid hormones. Therefore, varying PBSAC size will be chosen for the filtration of UF–PBSAC to evaluate the role of the external surface in GLY/AMPA dynamic adsorption (Figure 5.7). With the increase of PBSAC size, the external surface area decreased from 64 to 8 m^2/g (corresponding to a total external surface area range from 217 to 27 m^2 in UF−PBSAC, considering the mass of PBSAC of 3.4–3.9 g, Table 9.6) [207].

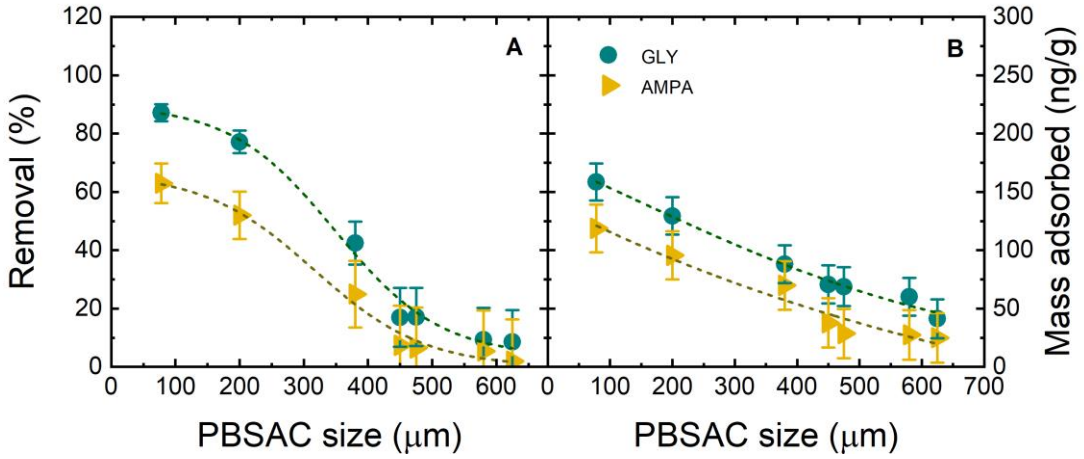

Figure 5.7. GLY/AMPA removal (A) and specific adsorbed mass (B) as a function of PBSAC size (reported values at permeate volume 600 mL, 2 mm layer thickness, 1000 ng/L GLY/AMPA, 100 L/m^2.h flux, 1mM $NaHCO_3$, 10 mM NaCl, 20 ± 0.5 °C, pH 8.1 ± 0.1). Adapted from [352].

The adsorption of GLY and AMPA on UF–PBSAC decreased with the increase of PBSAC size, corresponding to the decrease in the PBSAC external surface (Figure 5.7 B). With the highest external surface (PBSAC size 78 μm), the permeate concentration was 128 ± 7 ng/L for GLY and 370 ± 23 ng/L for AMPA (Figure 5.7 A). Although these concentrations were still higher than the EU regulation for individual herbicides (100 ng/L [13]), this increase in adsorption indicates that the external surface area needs to be considered for optimizing the filtration system.

The GLY removal decreased from 87 ± 4 to 8 ± 1%, and the removal of AMPA decreased from 62 ± 5 to 5 ± 1% with the increase in PBSAC size from 78 to 625 μm (Figure 5.7 B). The mass adsorbed also declined from 158 ± 14 to 41 ± 3 ng/g and from 118 ± 16 to 25 ± 3 ng/g for GLY and AMPA, respectively (Figure 5.7 C). The decrease of GLY and AMPA adsorption indicated that the external surface area for adsorption was a limiting factor. In fact, the total external surface of UF–PBSAC was abundant compared to the observed GLY/AMPA mass adsorbed. Theoretically, GLY/AMPA occupied only about 0.008% of the total external surface area of 88.4 m^2 in the PBSAC filtration system. After reaching the external surface of PBSAC, GLY and AMPA could diffuse into the pores, where adsorption would be slower than at the external surface.

The influence of external surface on GLY/AMPA adsorption by UF–PBSAC was contrary to that in static adsorption with PBSAC (Chapter 4) [197]. In static adsorption (HRT 26 h), while GLY adsorption was unchanged with the mass adsorbed 1800–2000 ng/g, AMPA mass adsorbed only slightly decreased from 1100 to 800 ng/g with the decrease of external surface. With longer HRT, GLY and AMPA could gradually diffuse into PBSAC pores and adsorb to the internal surface. This finding indicated that the external surface was the limiting factor for adsorption in short HRT (< 1 min), but not for adsorption in long HRT (hours).

Next, GLY/AMPA adsorption would be examined, with both the external surface area and HRT varied by varying the PBSAC layer thickness, to verify the roles of HRT and the PBSAC external surface.

5.9 Operational parameter: PBSAC layer thickness

When increasing the PBSAC layer thickness, the HRT and total surface area of PBSAC both increase. The HRT increased from 14 s to 86 s with an increase in the PBSAC layer from 1 to 6 mm. Meanwhile, the external surface of PBSAC with a size of 200 µm increases from 30 to 267 m^2 (Table 9.7). The permeate volume, removal, and mass adsorbed of filtration at varying PBSAC layer thickness are shown in Figure 5.8.

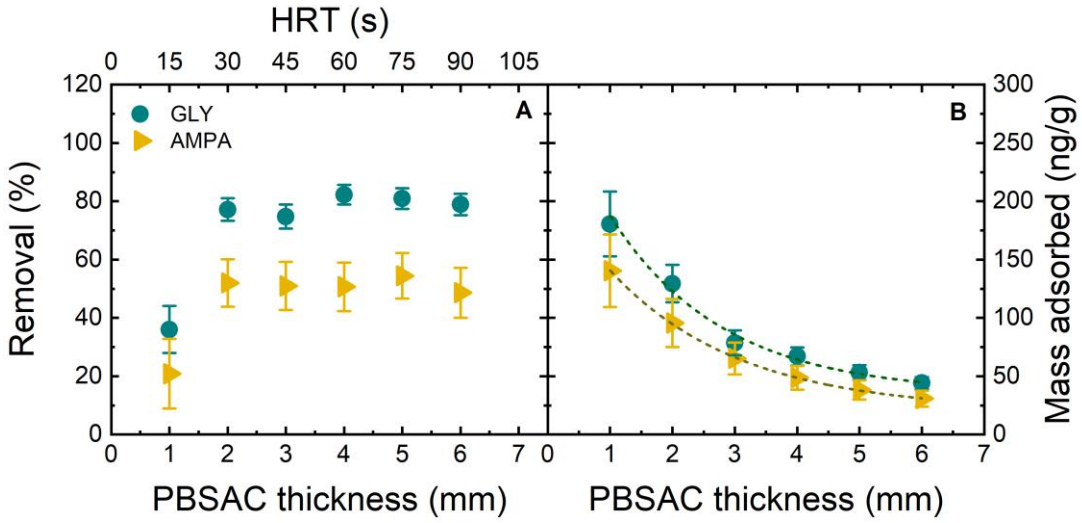

Figure 5.8. GLY/AMPA removal (A) and specific adsorbed mass (B) as a function of PBSAC layer thickness (reported values at permeate volume 600 mL, 200 µm PBSAC diameter, 1000 ng/L GLY/AMPA, 100 $L/m^2.h$ flux, 1mM $NaHCO_3$, 10 mM NaCl, 20 ± 0.5 °C, pH 8.1 ± 0.1). Adapted from [352].

It is expected that adsorption is enhanced with the increase in PBSAC layer thickness. However, the adsorption results contradicted the expectation. Indeed, the removal did increase with the increase from the lowest PBSAC layer thickness (1 mm) to the 2 mm layer. At the thinnest PBSAC layer (1 mm), the removal was 35 ± 2% and 20 ± 2% for GLY and AMPA, respectively. Although the total surface area was abundant at 1680 m^2 (with the theoretical mass adsorbed on the external surface being 28 mg), the adsorption could not proceed due to (1) limited HRT at 14 s, and (2) insufficient contact with the PBSAC at such a thin layer. A lower steroid hormone removal with UF–PBSAC with 1 mm was also observed by Tagliavini and Schäfer, in which removal decreased from 92−97% to 90% [207]. In the following study, Tagliavini *et al.* explained that the lower removal was due to the limited dispersion of the hormone within submillimetric adsorbent layers [361].

The increase in layer thickness led to an increase in the number of adsorption sites for GLY/AMPA. However, UF–PBSAC with the layer thickness > 2 mm did not exhibit a change in removal. The removal remained at 77–78 ± 4% for GLY and 52–54 ± 5% for AMPA. Even though the HRT and the adsorption sites of PBSAC increased, the contact time of each GLY/AMPA molecule to each PBSAC particle did not increase. It means the time that the GLY/AMPA molecule passes through the boundary layer of PBSAC and diffuses into the pore was still the same for all PBSAC layer thicknesses. The higher layer thickness only increased

the possibility of the GLY/AMPA molecule in contact with PBSAC. Moreover, the adsorption rate decreased at the bottom part of the PBSAC layer due to lower GLY/AMPA concentrations reaching the bottom adsorbent layers [361, 362]. The same phenomenon was also observed for steroid hormone removal by UF–PBSAC mat, where the increase in PBSAC mat layer thickness from 6 to 12 nm did not improve the removal [353].

The static adsorption in Chapter 4 showed that GLY/AMPA adsorption on PBSAC was a slow process, which was controlled by both external adsorption and intra-pore diffusion [197]. The real factor that needs to be considered is the contact time between GLY/AMPA and PBSAC, which is defined by flux.

5.10 Operational parameter: flux / hydraulic residence time

The external surface area was still abundant; GLY and AMPA adsorption can be enhanced by longer HRT with lower flux, which allows the herbicide molecules to diffuse into the PBSAC surface and pores. To examine this hypothesis, flux was varied between 25 and 500 L/m^2.h, which was in the typical range of UF, corresponding to HRTs between 115 and 6 s (Figure 5.2). The PBSAC layer thickness was 2 mm; only HRT was varied (Figure 5.9).

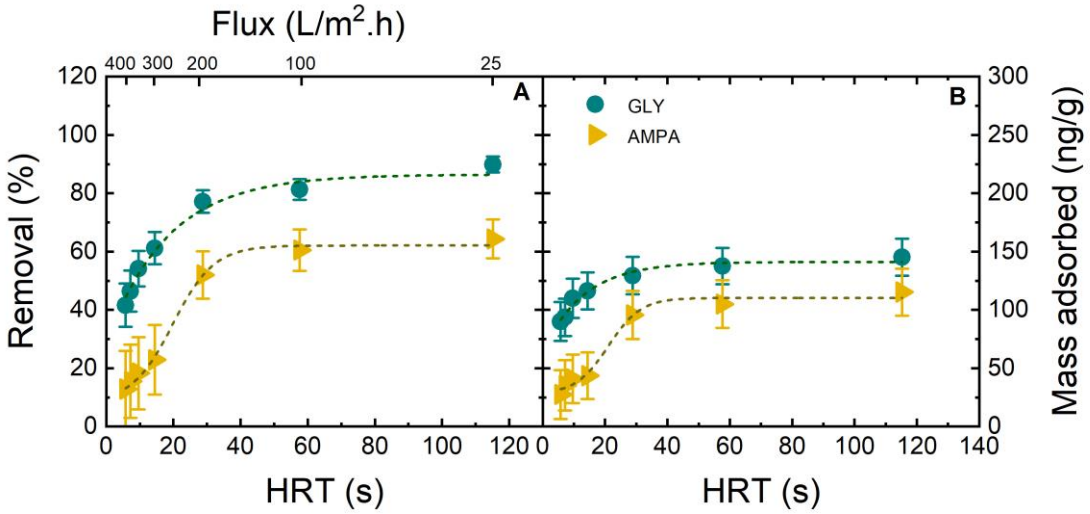

Figure 5.9. GLY/AMPA removal (A) and specific adsorbed mass (B) as a function of flux/ HRT (reported values at permeate volume 600 mL, 200 µm PBSAC diameter, 2 mm layer thickness, 1000 ng/L GLY/AMPA, 1mM $NaHCO_3$, 10 mM NaCl, 20 ± 0.5 °C, pH 8.1 ± 0.1). Adapted from [352].

The results in Figure 5.9 show that flux, thus HRT, played an important role in the adsorption of GLY/AMPA on UF–PBSAC, despite the excess of the external surface. At the lowest flux of 25 L/m^2.h (HRT 115 s), the removal was highest at 90 ± 8% for GLY and 65 ± 5% for AMPA. At this flow rate, the permeate concentration of GLY was below the EU guidelines for herbicides (<100 ng/L). This low flux, which was in the same flux range as the NF membrane, was obtained at a pressure of 0.2 bar. Compared to denser membranes, NF would need 4–20 bar to

achieve the flux of 36–325 L/m^2.h [363], while RO would need 6–80 bar to achieve the flux of 12–45 L/m^2.h, depending on salinity [364]. The lower required pressure is an advantage of using UF–PBSAC compared to the NF/RO membrane.

When increasing flux from 25 to 500 L/m^2.h, GLY and AMPA removal decreased from 90 ± 8 to 41 ± 3 % for GLY and from 65 ± 5 to 12 ± 1 % for AMPA, indicating the control of HRT on adsorption. At higher HRT, GLY and AMPA can diffuse into the pores and access the PBSAC internal surface (Figure 5.10). It can be important, as GLY/AMPA adsorption on PBSAC is a slow process, with intra-particle diffusion also a limiting factor.

The mass adsorbed decreased from 145 ± 13 to 100 ± 9 ng/g with the increase of flux from 25 to 500 L/m^2.h (Figure 5.9 B). For AMPA, the mass adsorbed decreased from 115 ± 13 ng/g to 43 ± 4 ng/g when flux increased from 25 to 200 L/m^2.h, then remained stable at 38–43 ng/g at flux > 200 L/m^2.h (HRT > 30 s). The adsorbed mass of AMPA remained constant with HRTs above 30 s, which was the same HRT where no increase in removal was observed with a higher PBSAC layer thickness. At this high HRT, GLY/AMPA had sufficient time to diffuse into the pores, and HRT was not a limiting factor.

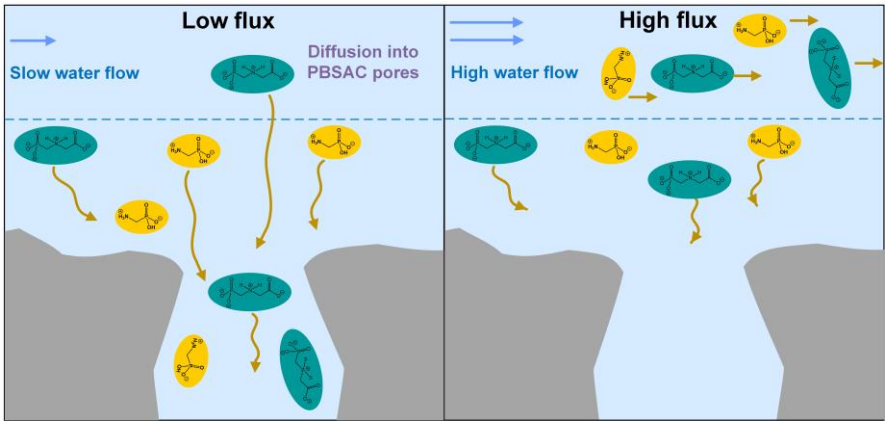

Figure 5.10. The GLY/AMPA adsorption on UF–PBSAC at varying flux. Adapted from [352].

In static adsorption, water quality controls the adsorption of GLY and AMPA on PBSAC. Therefore, the water quality will be studied to find the optimized parameters for adsorption on UF–PBSAC.

5.11 Water quality: solution pH

With four pKa of GLY and three pKa of AMPA [44], adsorption of GLY and AMPA on PBS-AC was found to be strongly dependent on solution pH in static adsorption (Chapter 4) [352]. To access the adsorption ability of UF–PBSAC at GLY/AMPA charge, the filtration with UF–PBSAC was performed with varying water pH from 2 to 12 to investigate the role of GLY and AMPA charges on adsorption (Figure 5.11).

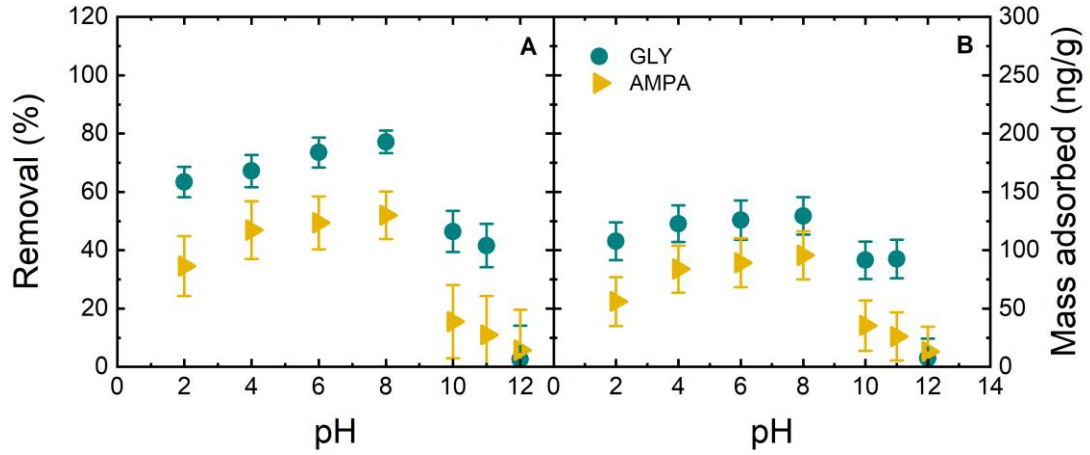

Figure 5.11. GLY/AMPA removal (A) and specific adsorbed mass (B) as a function of pH (reported values at permeate volume 600 mL, 200 µm PBSAC diameter, 2 mm layer thickness, 1000 ng/L GLY/AMPA, 100 L/m^2.h flux, 1mM $NaHCO_3$, 10 mM NaCl, 20 ± 0.5 °C). Adapted from [352].

At acidic and neutral pH, the removal of GLY and AMPA was 65–77 ± 4% and 38–52 ± 5% at pH 2–8. At this pH, the charges of GLY and AMPA were 0 and –1, respectively. From pH 10, the removal of GLY and AMPA decreased to <5%, where the charges of GLY and AMPA were –3 and –2, respectively. This phenomenon was also observed in the static adsorption of GLY/AMPA with PBSAC, where higher removal was observed at acidic and neutral pH [197].

The interaction between GLY/AMPA and PBSAC was discussed in Chapter 4. In summary, the energetic adsorption mechanisms for GLY and AMPA on PBSAC were van der Waals interactions and hydrogen bonding. At higher pH, the functional groups of GLY and AMPA (phosphonate and carboxylate) could not accept protons from the carboxylic groups or other positions on the PBSAC surface to form more hydrogen bonds [199, 339]. Moreover, by increasing the negative charge of GLY/AMPA (higher pH), GLY/AMPA removal and specific adsorbed mass were reduced. The reason can be the strong hydration layer surrounding GLY and AMPA at high pH, which may hinder the interaction of GLY/AMPA with the PBSAC surface and the diffusion of GLY/AMPA into the PBSAC pores (Figure 5.12) [57, 58, 365].

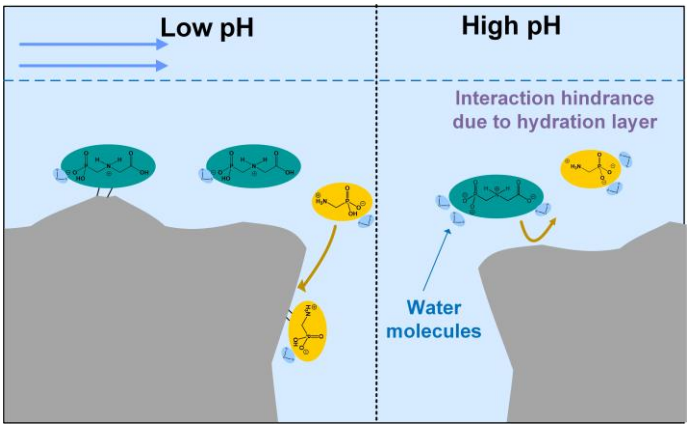

Figure 5.12. The GLY/AMPA adsorption on UF–PBSAC at low and high pH. Adapted from [352].

5.12 Operational parameter: feed temperatures

In static adsorption, the GLY and AMPA adsorption was enhanced at higher temperatures (Chapter 4). Therefore, to find the optimized condition for the dynamic adsorption, the filtration at varying temperatures was performed in the temperature range from 10 to 50 °C, which are relevant temperatures in water treatment (Figure 5.13) [366].

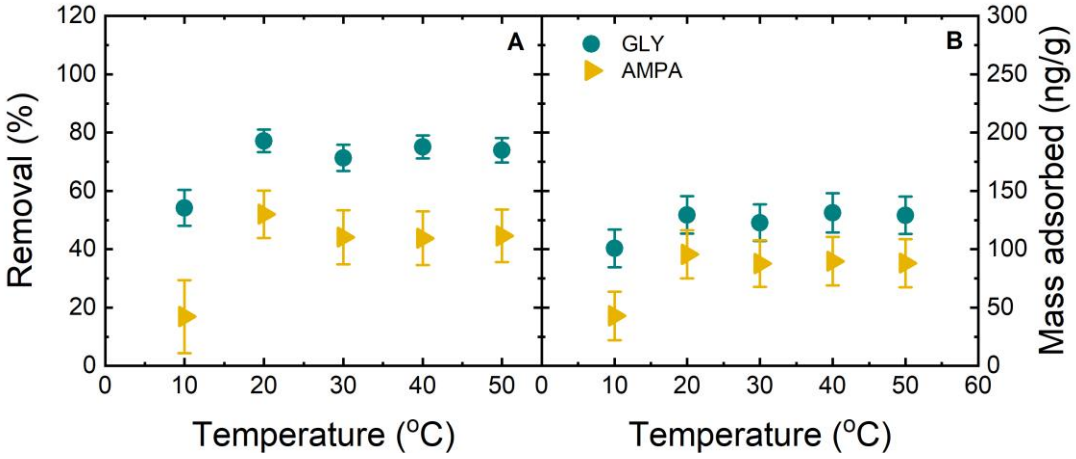

Figure 5.13. GLY/AMPA removal (A) and specific adsorbed mass (B) as a function of temperature (reported values at permeate volume 600 mL, 200 µm PBSAC, 2 mm layer thickness, 1000 ng/L GLY/AMPA, 100 L/m^2.h flux, 1mM $NaHCO_3$, 10 mM NaCl, pH 8.1 ± 0.1). Adapted from [352].

Except for the lowest temperatures (10 °C), no significant change was observed (Figure 5.13). The removal was lowest at 10 °C, with 30% GLY and < 10% AMPA being removed. The mass adsorbed was lowest at 100 ng/g and 42 ng/g for GLY and AMPA, respectively. The adsorbed mass was lower at low temperatures, implying that the dynamic adsorption by UF–PBSAC was controlled by kinetics rather than thermodynamics.

Even though the adsorption is an exothermic process that favors low temperatures (Figure 5.14) [197], the higher diffusivity was obtained at higher temperatures, allowing GLY/AMPA to diffuse into PBSAC pores. The diffusivity of GLY decreased from $1.5 \cdot 10^{-9}$ m^2/s (50 °C) to $5.1 \cdot 10^{-10}$ m^2/s (10 °C) and AMPA from $1.9 \cdot 10^{-9}$ m^2/s (50 °C) to $6.4 \cdot 10^{-10}$ m^2/s (10 °C) [196]. Therefore, at lower temperatures, GLY and AMPA diffused more slowly into PBSAC pores, affecting the adsorption at short HRT (Figure 5.14).

In the range of 20–50 °C, the removal remained at 75–80 % for GLY and 40–50 % for AMPA, while the adsorbed mass was 125–130 ng/g (GLY) and 88–95 ng/g (AMPA), which was different from static adsorption. In static adsorption, increasing temperature led to an increase in AMPA removal from 55 to 68%, while GLY removal remained 94–97% [197]. This insignificant change is attributed to increasing diffusivity, decreasing adsorption affinity, and more significant mass transfer limitation due to the short HRT.

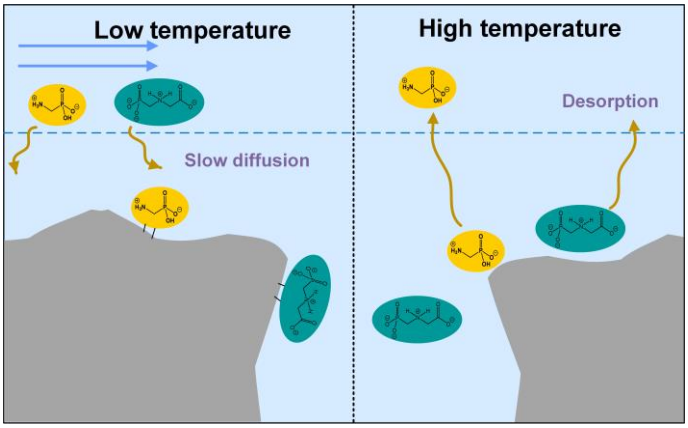

Figure 5.14. The GLY/AMPA adsorption/ desorption on UF–PBSAC at varying temperatures. Adapted from [352].

This result shows that temperature > 10 °C is not a limiting factor for adsorption by UF–PBSAC, and this parameter will not be considered in the optimized process, as the process was relatively robust towards temperature changes.

5.13 Optimization of UF–PBSAC adsorption for GLY/AMPA removal

The UF–PBSAC filtration is optimized by minimizing the limiting factors (external surface area and HRT). Experiments proceeded with UF–PBSAC at a PBSAC size of 78 µm, a flux of 25 L/m^2.h, and PBSAC layer thicknesses of 2 mm and 6 mm (Figure 5.15).

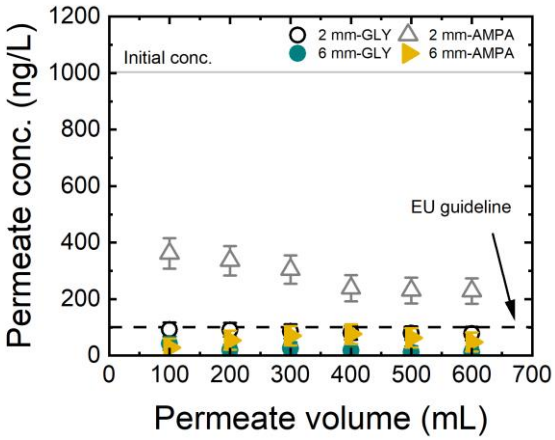

Figure 5.15. GLY/AMPA permeate concentration (780 µm PBSAC diameter, 2 mm and 6 mm layer thickness, 1000 ng/L GLY/AMPA, 25 L/m^2.h flux, 1mM $NaHCO_3$, 10 mM NaCl, 20 ± 0.5 °C, pH 8.1 ± 0.1). Adapted from [352].

With UF–PBSAC at 2 mm, 78 µm, and flux 25 L/m^2.h, the permeate concentrations for GLY and AMPA were 78 ng/L and 228 ng/L, respectively. The EU regulation requirement for herbicides (100 ng/L) was reached for GLY but not AMPA (Figure 5.15). However, the total concentration of 306 ng/L was lower than the regulation value for total herbicides (500 ng/L) [13].

UF–PBSAC with a PBSAC layer thickness of 6 mm, and EU regulation for herbicides (100 ng/L individual, 500 ng/L for total herbicides) were met for both GLY (11 ng/L) and AMPA (47 ng/L). Higher adsorption of GLY and AMPA was obtained with more adsorption sites and a longer HRT (120 s), which allowed GLY/AMPA to have more time to interact with the PBSAC surface.

5.14 Conclusions

This chapter evaluated the dynamic adsorption of GLY and AMPA on UF–PBSAC at HRTs ranging from 5 to 115 s. In this process, PBSAC is in charge of adsorbing GLY and AMPA while UF acts as a barrier to remove organic matter, bacteria, viruses, and particulates, which can interfere with the adsorption. The investigation of dynamic adsorption optimization considered the limiting factors and adsorption mechanisms. The following points are obtained from this investigation.

- With a 2 mm layer of PBSAC, UF–PBSAC could remove 77 % GLY and 52 % AMPA, which was lower than in static adsorption. This finding indicates that adsorption sites limit the adsorption.
- Both surface area and HRT play an important role in the adsorption. More surface area provides more adsorption sites, while HRT allows GLY and AMPA to diffuse into PBSAC pores.
- At optimized conditions, by decreasing PBSAC size to 78 µm, decreasing flux to 25 $L/m^2.h$, and increasing PBSAC layer thickness to 6 mm, EU guidelines for herbicides in water were achieved with 98% GLY and 95% AMPA removal.

Overall, adsorption of GLY and AMPA by UF–PBSAC was possible in dynamic filtration with relatively short HRTs. In the dynamic system, although the surface area of PBSAC was abundant, the mass transfer is still controlling the adsorption due to (1) less accessible surface, (2) short HRT. The hybrid adsorption– UF membrane filtration system at optimized conditions has proven to be effective for the removal of GLY and AMPA. However, a flux of 25 $L/m^2.h$ (115 s) was required to achieve reasonable performance, which is low for a filtration process, posing a challenge for further investigation on recovery enhancement.

As UF–PBSAC has proven its efficiency in removing GLY and AMPA. Can the NF membrane, which is a denser membrane, have better performance? This will be answered in the next chapter.

6 GLY and AMPA rejection by nanofiltration membrane

This chapter is adapted from a publication in Nature Communications entitled: P.B. Trinh, M.N. Nguyen, Z. Futera, B. Minofar, M. Personeni, P.B. Petersen, A.I. Schäfer, The role of hydration in the removal of glyphosate (GLY) and aminomethylphosphonic acid (AMPA) by nanofiltration membranes, Nature Communications, 17 (2026) 3741 [365].

The contribution of authors:

Phuong B. Trinh: conceptualization; performing experiments; samples analysis; data analysis and interpretation; methodology; validation; visualization; writing – original draft

Minh N. Nguyen: conceptualization; data analysis and interpretation; methodology; supervision; validation; visualization; writing – review & editing

Zdenek Futera: performing molecular dynamics simulation, data analysis and interpretation; funding acquisition; methodology; validation; visualization; writing – review & editing

Babak Minofar: performing molecular dynamics simulation, data interpretation; funding acquisition; methodology; validation; writing – review & editing

Marco Personeni: FTIR measurement and the hydration layer characterization; data analysis; formal analysis; investigation; methodology; validation; visualization; writing – review & editing

Poul Petersen: conceptualization; data interpretation; funding acquisition; methodology; supervision; validation; writing – review & editing

Andrea I. Schäfer: conceptualization, funding acquisition; project administration; resources; supervision; validation; writing – review & editing

This chapter aims to investigate the rejection of GLY and AMPA by nanofiltration membranes (six membrane types with increasing molecular weight cut-off (MWCO)). The herbicide rejection is determined by size exclusion, charge exclusion, and dielectric exclusion. The size exclusion is linked to the MWCO of the six membrane types. The charge and dielectric exclusion are investigated in a membrane with moderate and loose pore size at varied pH and flux.

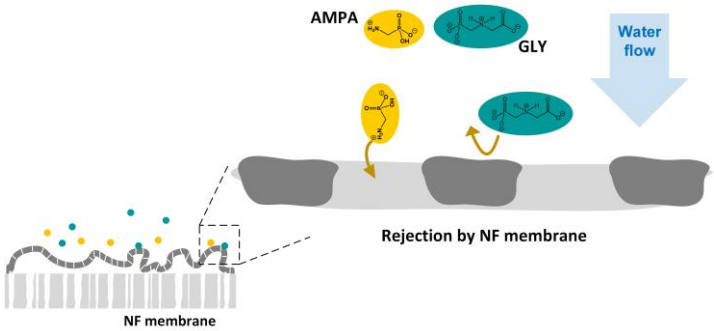

6.1 Introduction

PBSAC adsorption and UF–PBSAC dynamic adsorption have shown efficient removal of GLY and AMPA in Chapters 4 and 5. What will happen if the NF membrane replaces them? Can the GLY and AMPA still be removed effectively? This chapter will focus on NF membrane technology for GLY and AMPA removal.

In principle, NF membrane can remove GLY and AMPA, in which sub-nanometer pores reject target molecules [225-227]. In previous studies, GLY and AMPA rejection were investigated at concentrations higher than environmentally relevant concentrations. A study on environmentally relevant concentrations is still needed.

As pressure-driven processes, pressure was applied to the membrane, pushing water and GLY/AMPA molecules to the membrane surface. The rejection mechanisms of micropollutants by NF/RO membranes include (1) size exclusion, (2) Donnan exclusion, and (3) dielectric exclusion [228, 229]. The details on transport and removal mechanism of GLY and AMPA in NF membrane were discussed in Chapter 2. Based on the rejection mechanism, the parameters considered were determined for evaluating NF performance (Figure 6.1).

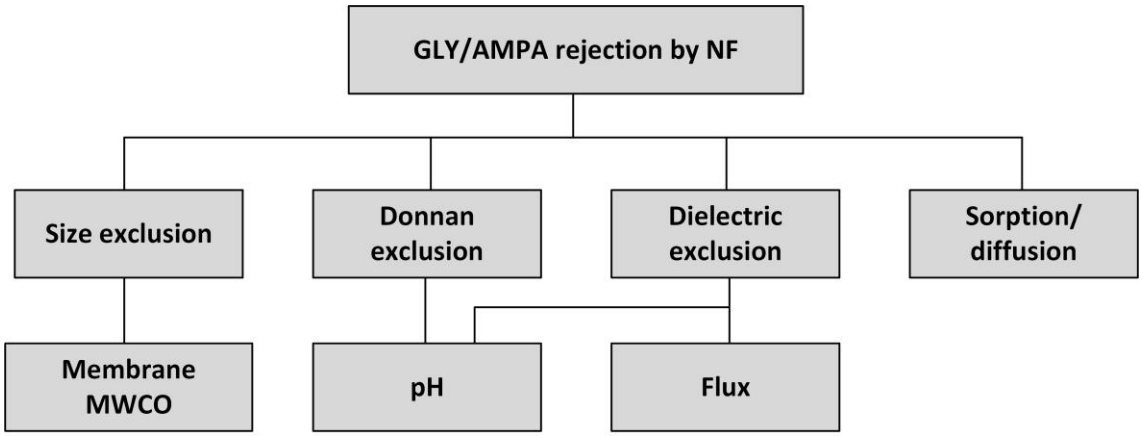

Figure 6.1: Parameters in consideration for GLY/AMPA rejection by NF

As the main target is GLY/AMPA, size exclusion is now related to MWCO. Meanwhile, the Donnan exclusion (defined by the charge and the Debye length [241, 242]) is related to the charge of the membrane and GLY/AMPA, which is affected by water pH [162]. The dielectric exclusion, which is strongly related to the hydration layer of solutes [247, 253], can be affected by water pH and flux of the filtration process [256, 367].

This chapter investigates the removal of GLY and AMPA by the NF membrane with the following research questions:

- How much GLY and AMPA can be removed by the NF membrane at environmentally relevant concentrations?
- Which membrane presents strong removal for GLY and AMPA?
- How does the rejection of the NF membrane vary with pH and flux?

6.2 Membrane filtration system and protocol

The NF filtration was performed in a dead-end stainless steel system produced at KIT [207] (Figure 6.2). The filtration system was described in Chapter 5. In summary, in this system, the membrane has an internal diameter of 7 cm, an effective filtration area of 38.5 cm^2, and an internal feed volume of 990 mL.

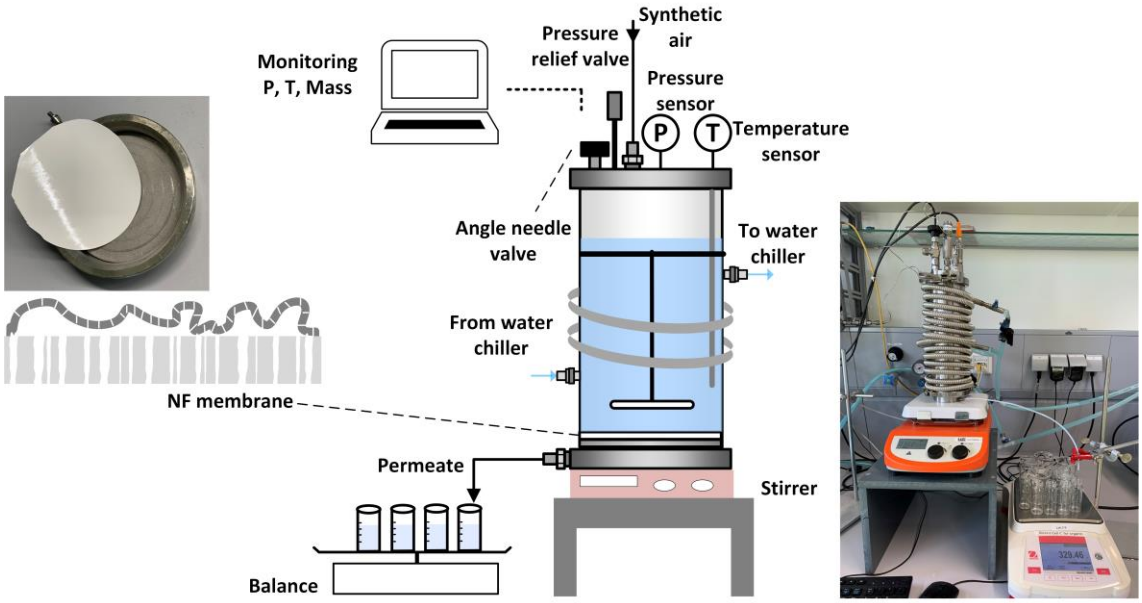

Figure 6.2: Schematic of the nanofiltration membrane system.

The filtration protocol described in previous research [354, 363] is summarized in Table 9.8. Before the filtration experiments, the membrane was soaked in NaCl 10 mM for 1 hour to enhance pore opening and swelling of the active layer (material of polyamide and sulfonated polyether sulfone) [368]. After being washed with Milli-Q water, the membrane was pre-compacted with Milli-Q water at 9.6 bar for 1 hour. Then, the membrane pure water flux (pre-experiment permeability) was measured with three different pressures (1, 5, and 9.6 bar). After the permeability test, the membrane was filtered with GLY/AMPA solution at the target pressure. After the filtration, the pure water flux of the membrane (post-experiment permeability) was measured again. The experimental conditions (flux, temperature, conductivity, and pressure) were monitored with a tailored LabView 2014 program.

Filtration experiments were conducted in different conditions. For each NF experiment, 600 mL of GLY/AMPA was filtered under different pH (2, 4, 6, 8, 10, 11, 12) or different flux (25, 35, 50, 60, 75, and 100 $L/m^2.h$ for NF 90, NF 270, and 25, 35, 50, 60, and 75 $L/m^2.h$ for HY 50). After each experiment, the system was cleaned.

6.3 Membrane

In this chapter, six types of NF membranes were used in this study, including BW 30, NF 90, NF 270, HY 70, HY 50, and HY 10. The NF membranes used in this project are listed in Table 6.1.

Table 6.1: NF membrane types and properties (MWCO, permeability, pore diameter, and isoelectric point (IEP) [244, 354, 369, 370]. NF 270 and NF 90 surfaces have a positive net charge at IEP < 4 and a negative net charge at pH > 4. The HY membrane surface has a negative net charge at all pH 2−12.

No	Membrane type	Company	MWCO (Da)	Permeability ($L/m^2.h.bar$)	Pore diameter (nm)[61]	Zeta potential pH 8	Active layer materials
1	BW 30	DuPont, USA	80−120 [a]	4 ± 1 [a]	0.41–0.51	-40 [e]	Polyamide
2	FilmTec NF 90		90−180 [b]	8 ± 2 [b]	0.44–0.63	-49 [b]	Fully aromatic polyamide
3	FilmTec NF 270		150−340 [b]	14 ± 2 [a]	0.57–0.89	-116 [b]	Semi-aromatic piperazine-based polyamide
4	HydraCoRe 70 (HY 70)	Nitto – Hydranautics, USA	600–700 [c]	3.1 ± 0.3 [d]	1.21–1.31	-33 [d]	Sulfonated polyether sulfone polymer
5	HydraCoRe 50 (HY 50)		1000–1500[c]	7.8 ± 0.5 [d]	1.58–1.96	-33 [d]	Sulfonated polyether sulfone polymer
6	HydraCoRe 10 (HY 10)		3000–3600 [c]	58 ± 8 [d]	2.83–3.12	-38 [d]	Sulfonated polyether sulfone polymer

[a] Cai et al. [369], [b] Imbrogno and Schäfer [354], [c] Nominal value provided by supplier (Nitto – Hydranautics), [d] Boussouga et al., [e] Idil Mouhoumed et al. [370], [f] not determined as IEP is below 2.

6.4 Data analysis

Removal of GLY and AMPA, flux, and permeability of the membrane were calculated by the same equation in Chapter 5.

Mass balance in filtration

Specific formulas to determine the mass balance for NF filtration are given as follows.

All filtration experiments were conducted in a dead-end (flow-through) configuration. Therefore, the mass adsorbed was calculated for dead-end filtration. In dead-end filtration, $m_{ads,t}$ is calculated with the following equation.

$$m_{ads,t} = (V_f - V_{r,t})c_f - \sum V_{p,t}c_{p,t} \tag{6.1}$$

where V_f and $V_{r,t}$ are the feed and residual volumes in the feed tank at time t; c_f and $c_{p,t}$ are the feed and permeate (filtrated) concentrations.

The specific adsorbed mass, or specific mass loss, is equal to the adsorbed mass or mass loss divided by the membrane area as follows.

$$q_{ads,A,t} = \frac{m_{ads,t}}{A} \tag{6.2}$$

where A (cm^2) is the effective membrane area, respectively.

Debye length calculation

To characterize the electrical double layer of the membrane (as detailed in Chapter 2), the Debye length will be calculated. The double layer, which is affected by electrolyte concentration, will then impact the effective size of membrane pores [241]. The membrane pore is assumed to have a cylindrical structure.

The thickness of the electrical double layer is characterized by the Debye length (κ^{-1}, m) and is calculated using equation (6.3) [371].

$$\kappa^{-1} = \sqrt{\frac{\varepsilon_0 \cdot \varepsilon_\tau \cdot R \cdot T}{F^2 \cdot \sum_i (z_i^2 \cdot C_i)}} \tag{6.3}$$

where ε_0: vacuum permittivity ($8.854 \cdot 10^{-12}$ C/V.m) [372]; ε_τ: feed solution relative permittivity; R: idea gas constant (8.3143 J/mol.K); T: feed temperature (K); F: Faraday constant (96487 C/mol); z_i: valence of ion (z_{Na}^{+}=z_{Cl}^{-}=1); C_i: ion molar concentration (mol/L).

Feed solution permittivity (ε_τ) (C/V.m) is calculated using the empirical formula [373].

$$\varepsilon_\tau = \varepsilon_W \left(1 - 0.17 \frac{C_{NaCl}}{\text{mol/L}}\right) \tag{6.4}$$

where ε_W: relative permittivity of water (78.3 C/V.m at 25 ºC) [374]; C_{NaCl}: molar concentration of NaCl in bulk solution (mol/L).

Dividing κ^{-1} by the pore radius (r_p, m) of the membrane, which is assumed to have a cylindrical structure, the Debye ratio (λ) was obtained, which is a key dimensionless parameter for indicating the electrostatic effects [375]. The lower the value of λ is, the less the electrical double layer overlaps in the pores; hence, the electrostatic interactions contribute less to the rejection [376]. The ratio λ is calculated using equation (6.5) [375].

$$\lambda = \frac{\kappa^{-1}}{r_p} \tag{6.5}$$

where the membrane pore radius (r_p, nm) (Table 6.1).

Calculation of pore radius

The membrane pore radius (r_p, nm) was calculated using the empirical formula [61], with the assumption that the membrane is a porous support of uniformly cylindrical pores. Solute-solute, solute-pore interactions, and hydration are not considered in this model. Due to the simplicity and the establishment of this model for NF characterization, this model was used for the estimation of pore radius.

$$r_p = 2.037 \cdot 10^{-11} \cdot \left(\frac{\mathrm{MWCO}}{\mathrm{g/mol}}\right)^{0.53} \tag{6.6}$$

Calculation of real removal by NF membrane

When GLY/AMPA is transported to the membrane surface, the molecules accumulate in the boundary layer of the membrane, forming a concentration polarization layer [377]. Consequently, the concentration of GLY/AMPA on the membrane surface is different compared to the bulk solution. The concentration polarization layer involves (1) the observed retention (R_{obs}) which is the experimental removal and calculated from feed and permeate concentration in equation (6.7); (2) the real removal (R_{real}) which is a theoretical removal calculated from the concentration of GLY/AMPA on the membrane surface (c_m) in equation (6.8).

The observed removal of GLY and AMPA (R_{obs}, %) is determined by the same equation of removal in previous chapters and mentioned again as follows.

$$R_{obs} = \left(1 - \frac{c_p}{c_f}\right) \cdot 100 \tag{6.7}$$

where c_p and c_f are the GLY or AMPA concentrations in the permeate and feed (initial), respectively.

The real removal of GLY and AMPA (R_{real}, %) is determined as follows [378].

$$R_{real} = \left(1 - \frac{c_p}{c_m}\right) \cdot 100 \tag{6.8}$$

where c_p and c_m are the GLY or AMPA concentrations in the permeate and on the membrane surface, respectively.

Calculation of GLY and AMPA concentration at the NF membrane surface

The concentration at the membrane surface (c_m, ng/L) is calculated as follows.

$$c_m = c_b \left((1 - R_{obs}) + R_{obs} \cdot e^{\frac{J_v}{k_m}}\right) \tag{6.9}$$

where k_m is the external mass transfer coefficient (m/s).

Calculation of external mass transfer coefficient

The GLY/ AMPA external mass transfer, which is characterized by the external mass transfer coefficient k_m, controls the transport of GLY and AMPA from the bulk solution to the membrane surface. It plays an important role in the concentration polarization and rejection of solute by NF membranes [377]. The external mass transfer coefficient k_m can be calculated from Sherwood number as represented in (6.10) [379, 380].

$$Sh = \frac{k_m \cdot D_h}{D} = a \cdot Re^b \cdot Sc^c \tag{6.10}$$

where D_h is hydraulic diameter (m), D is diffusion coefficient (m^2 /s), Re and Sc are the dimensionless Reynolds and Schmidt numbers ($Sc = \nu/D$), respectively; a, b, c are adjustable dimensionless parameters, which are dependent on system geometry and laminar or turbulent conditions [381].

For the stirred cell system in this study, Sh and Re are calculated using the following equation [382, 383].

If Re < 30000 (laminar) $$Sh = 0.285 \cdot Re^{0.567} \cdot Sc^{0.33} \tag{6.11}$$

If 32000 < Re > 82000 (turbulent) $$Sh = 0.044 \cdot Re^{0.75} \cdot Sc^{0.33} \tag{6.12}$$

$$Re = \frac{\omega \cdot r^2}{\nu} \tag{6.13}$$

Estimation of membrane porosity and hydraulic residence time (HRT)

GLY and AMPA can be adsorbed on the NF membrane active layer, which is dependent on membrane materials and HRT [130]. Consequently, the HRT of GLY and AMPA in the membrane active layer was calculated using equation (6.14).

$$\bar{t} = \frac{V}{Q} = \frac{V_m \cdot \varepsilon}{Q} = \frac{A \cdot \delta \cdot \varepsilon}{Q} = \frac{\delta \cdot \varepsilon}{J_v} \tag{6.14}$$

where ε is the membrane porosity, V is the volume of membrane occupied by feed solution (L), $V_m = A \cdot \delta$ is membrane active volume (L), A is membrane area (m^2), δ is membrane thickness (m), and ε is membrane porosity.

The NF membrane porosity (ε) is calculated according to the Hagen-Poiseuille Law that determines the water velocity of an incompressible and Newtonian fluid (such as water) through a cylindrical pipe in (6.15) [384].

$$\varepsilon = \frac{8 \cdot \mu \cdot \delta \cdot J}{{r_p}^2 \cdot \Delta P} = \frac{32 \cdot \mu \cdot \delta \cdot J}{{d_p}^2 \cdot \Delta P} \tag{6.15}$$

where μ is the dynamic viscosity of water (Pa.s), δ is the membrane thickness (m), r_p and d_p are the radius and diameter of the membrane pore, respectively. Table 6.2 shows the HRT and porosity of each NF membrane used in this Chapter.

Table 6.2: Hydraulic residence time of NF membranes

Membrane	Active layer thickness (nm)	Membrane porosity (%)	Flux (L/m^2.h)	Pressure (bar)	HRT (s)
BW 30	200–300 [385]	0.4–0.6	30	7.5	0.01–0.02
NF 90	218–250 [386, 387]	0.8–0.9	50	6.3	0.01–0.02
NF 270	21–40 [228, 386]	0.08–0.1	50	3.4	0.0001–0.0002
HY 70	~300 [388]	0.06	30	9.6	0.002
HY 50	~300 [388]	0.08	50	6.4	0.001
HY 10	~300 [388]	0.2	50	0.9	0.004

The HRT was in the range of 0.0001–0.02 s, depending on the membrane pore and active layer thickness.

6.5 Removal of GLY and AMPA by NF membranes

First of all, to evaluate the removal efficiency of GLY and AMPA by NF membranes, the filtration of dense NF membranes (BW 30, NF 90, NF 270) and loose NF membranes (HY 70, HY 50, HY 10) was performed with a feed concentration of 1000 ng/L that was relevant in German surface waters [98]. The permeate concentration is shown in Figure 6.3 (BW 30, NF 90, NF 270) and Figure 6.4 (HY 70, HY 50, HY 10) with the permeate volume.

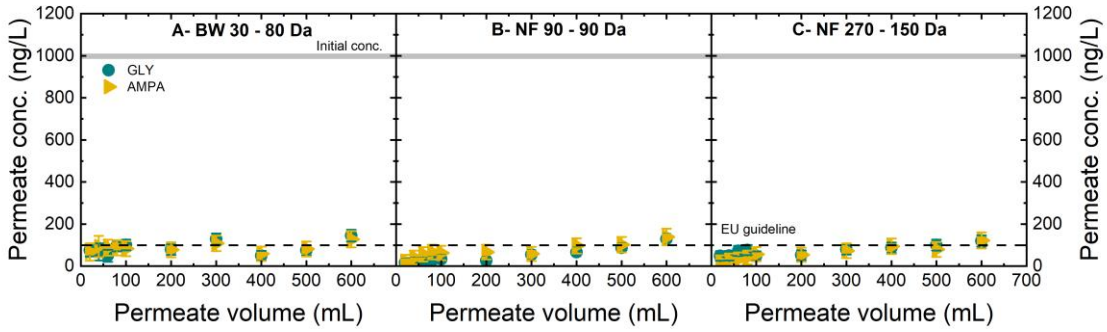

Figure 6.3. GLY/AMPA permeate concentration as a function of permeate volume with removal by BW 30 (A), NF 90 (B), NF 270 (C), (flux 50 L/m^2.h, initial GLY/AMPA concentration 1000 ng/L (each, mixed), 1mM NaHCO3, 10 mM NaCl, pH 8.1 ± 0.1, 20 ºC). Flux for BW 30 was 30 L/m^2.h instead of 50 L/m^2.h because the maximum pressure was reached. Adapted from [365].

For dense membranes (BW 30, NF 90, NF 270) with a MWCO of 80–340 Da, the permeate concentration increased slightly from 70 ± 10 ng/L at a permeate volume of 20 mL to 120 ± 20 ng/L at a permeate volume of 600 mL. The rejection of GLY and AMPA was due to both ad-

sorption and steric exclusion [389]. The permeate concentration was still higher than the EU guidelines for herbicides in water (100 ng/L) [12, 13].

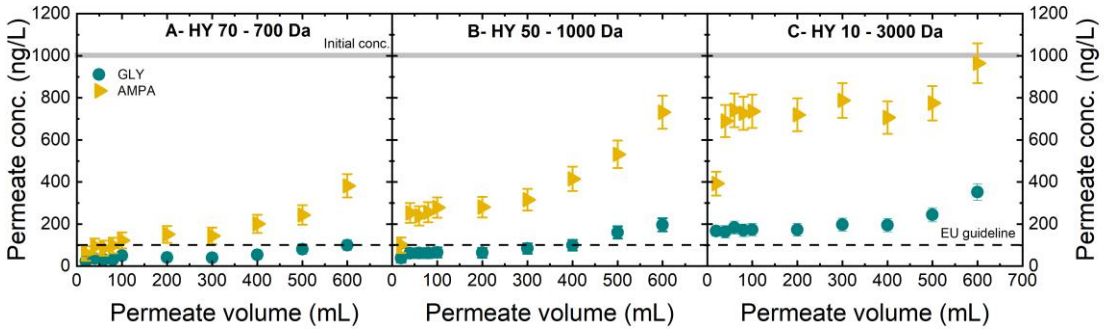

Figure 6.4. GLY/AMPA permeate concentration as a function of permeate volume with removal by HY 70 (A), HY 50 (B), and HY 10 (C) (flux 50 L/m^2.h, initial GLY/AMPA concentration 1000 ng/L (each, mixed), 1mM NaHCO3, 10 mM NaCl, pH 8.1 ± 0.1, 20 ºC). Flux for HY 70 was 30 L/m^2.h instead of 50 L/m^2.h because the maximum pressure was reached. Adapted from [365].

For loose membrane (HY 70, HY 50, HY 10), GLY permeate concentrations were low for HY 70 and HY 50 at the concentration of 100 ± 16 ng/L and 196 ± 25 ng/L, respectively (Figure 6.4 A, B). The permeate concentration of GLY was the highest with the most open membrane (HY 10), at 351 ± 33 ng/L, due to the large pore diameter (2.83 nm [61]). The permeate concentration of GLY was lower than that of AMPA, indicating better rejection, which may be due to the smaller diameter of GLY (0.62 nm [61]) than AMPA (0.49 nm [61]). The permeate concentration of AMPA was higher for loose membranes than for dense membranes. The increase in the concentration was also more significant in loose membranes. The permeate concentration of AMPA increased from 60 ± 25 to 382 ± 55 ng/L for HY 70, from 100 ± 26 to 731 ± 75 ng/L for HY 50, and from 392 ± 36 to 964 ± 94 ng/L for HY 10. The AMPA permeate concentration of HY 50 and HY 10 in the first 20 mL was low due to adsorption onto the membrane active layer (sulfonated polyether sulfone) [390].

Therefore, the removal of GLY/AMPA by the NF membrane was initially due to adsorption and size exclusion, then decreased as diffusion increased. Further investigation on the size exclusion and adsorption of GLY and AMPA will be carried out as a function of MWCO.

6.6 Retention and adsorption of GLY and AMPA by size exclusion

To determine the contribution of size exclusion and adsorption to GLY/AMPA rejection, filtration of GLY and AMPA at pH 8 was performed with six different membranes: BW 30, NF 90, and NF 270 (active layer material of polyamide), HY 70, HY 50, and HY 10 (active layer material of polyether sulfone). The removal and mass adsorbed are shown in Figure 6.5.

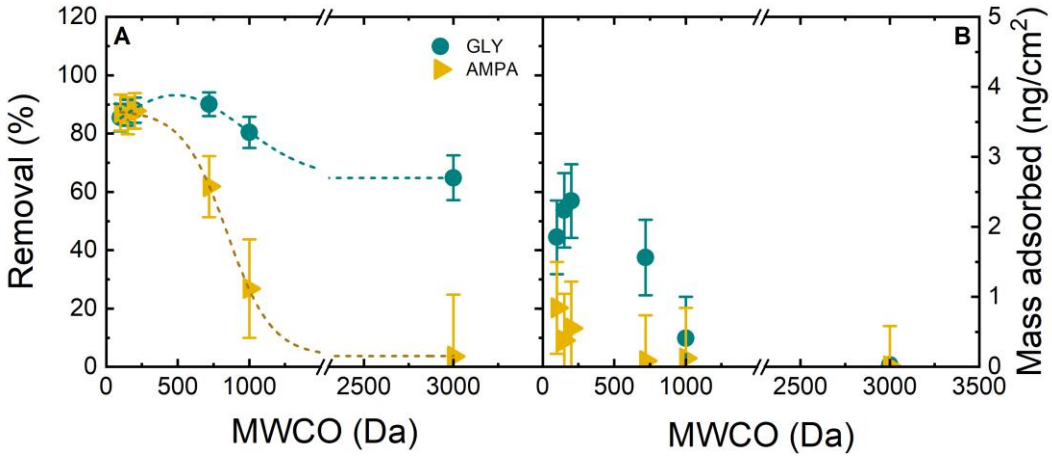

Figure 6.5. GLY/AMPA removal (A) and mass adsorbed (B) as a function of membrane MWCO (flux 50 L/m^2.h, initial GLY/AMPA concentration 1 µg/L, 1mM $NaHCO_3$, 10 mM NaCl, 20 ˚C, pH 8.1 ± 0.1). Flux for BW 30 and HY 70 was 30 L/m^2.h instead of 50 L/m^2.h because the maximum pressure was reached. Adapted from [365].

From the pore sizes of the membrane (Table 6.1), it was expected that the BW 30 and NF 90 membranes could completely remove GLY and NF 270 could partially remove GLY, as the membrane pore sizes are smaller or in the same range as the diameter of GLY (0.62 nm [61]). AMPA (0.49 nm [61]) was expected to be highly removed by the three dense membranes due to the small membrane pore size. The filtration experiments showed that the membrane with MWCO < 200 Da [354, 369], which are BW 30, NF 90, NF 270, could remove 85–88% GLY and AMPA (Figure 6.5 A). The removal of the dense membrane was due to the adsorption and size exclusion, as discussed in the breakthrough of NF (Figure 6.6). However, the incomplete removal was because of the non-uniform pore size distribution [234, 235].

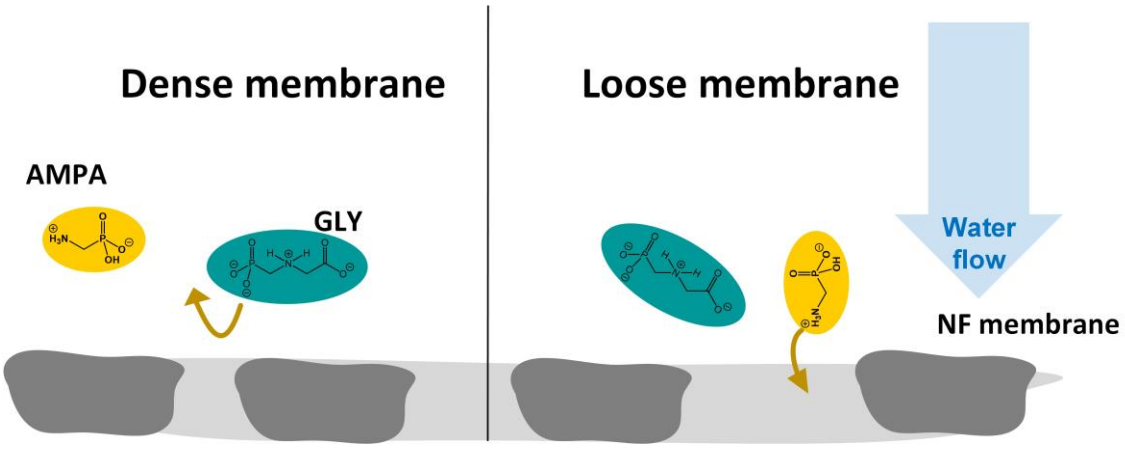

Figure 6.6. GLY/AMPA rejection by NF membrane via size exclusion.

Additionally, molecular shape and orientation affect transport through membrane pores [236]. Together with continuous adsorption-desorption and diffusion of GLY and AMPA into the membrane pores, this allowed the molecules to pass through the membrane [391]. The loose membranes with MWCO > 200 Da (HY 70, HY 50, and HY 10) were expected not to remove

GLY and AMPA due to size exclusion, as the pore diameters are large (0.67–2.83 nm [61]). In the filtration experiment, HY membranes can remove GLY and AMPA to a low extent. The removal decreased from 87 to 64% (GLY) and from 87 to 3% (AMPA) with the increase of MWCO. The partial removal of GLY and AMPA by HY membranes was due to another mechanism.

GLY mass adsorbed was 2–2.5 ± 1 ng/cm^2 while the AMPA mass adsorbed was 0.5–0.8 ± 0.2 ng/cm^2 on polyamide membrane (BW 30, NF 90, NF 270) (Figure 6.5 B). GLY and AMPA can be weakly adsorbed onto polyamide via hydrogen bonding, van der Waals interactions, and electrostatic interactions with membrane surface functional groups, such as amine groups [130, 387, 392]. These interactions can be desorbed during filtration, leading to the diffusion of GLY/AMPA into the permeate. On the other hand, sulfonated polyether sulfone (a hydrophobic material) has low adsorption affinity for hydrophilic compounds such as GLY and AMPA [387, 393]. This was proven by the mass adsorbed of GLY and AMPA by HY membrane, which were (< 0.4 ng/cm^2 for GLY, and < 0.1 ng/cm^2 for AMPA).

Next, the role of charge and dielectric exclusion will be evaluated; BW 30 (dominated by size exclusion) will be excluded.

6.7 Charge and dielectric exclusion of GLY and AMPA with NF membrane

The membrane double layer was studied by the Debye length and charge at the pore center. Debye length (κ^{-1}) and Debye ratio (λ) is reported as a function of MWCO of the membranes (Figure 6.7). If the diameter of GLY/AMPA is larger than the Debye length, Donnan exclusion can be a relevant mechanism, although the strength of electrostatic interactions will depend on the electrostatic potential in the pore space.

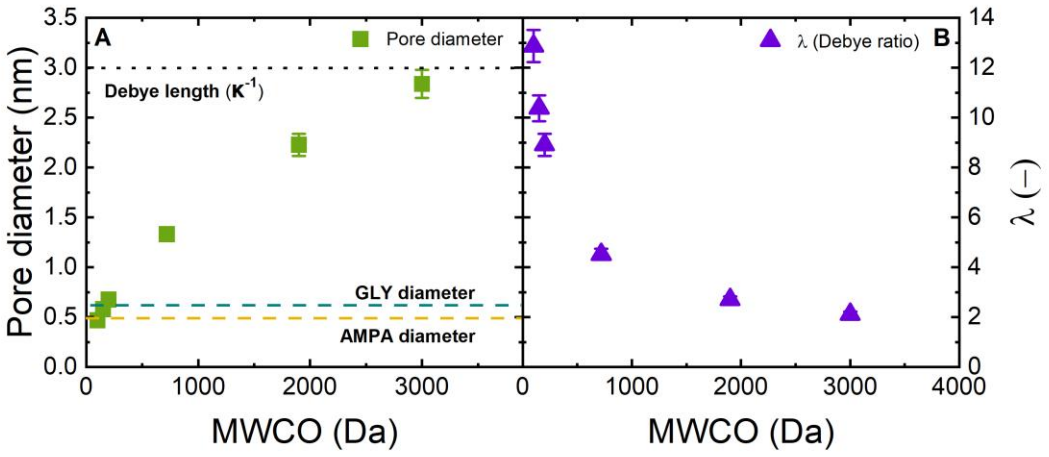

Figure 6.7. Membrane pore diameter (A) and Debye ratio (λ) (B) for NF membranes as a function of MWCO (κ^{-1} = 3 nm at C_{NaCl} = 10 mM and 20 °C). Adapted from [365].

The Debye length κ^{-1} was 3 nm, which is larger than the pore dimensions of all membranes (0.41–2.83 nm [61], Figure 6.7 A). The Debye ratio (λ) decreased from 12.8 to 2.1 with the increase of MWCO from 100 to 3000 Da (Figure 6.7 B). From the Debye length, it was expected that GLY and AMPA always have electrostatic interactions with all membranes at different pH (Figure 6.8). At the dense membrane (BW 30, NF 90, NF 270), the ratio between Debye length and pore radius is higher than that in the loose membrane (HY 70, HY 50, HY 10). Overall, the pore size is smaller than the Debye length, in which the GLY and AMPA molecules might encounter the electrostatic resistance in all membranes [246].

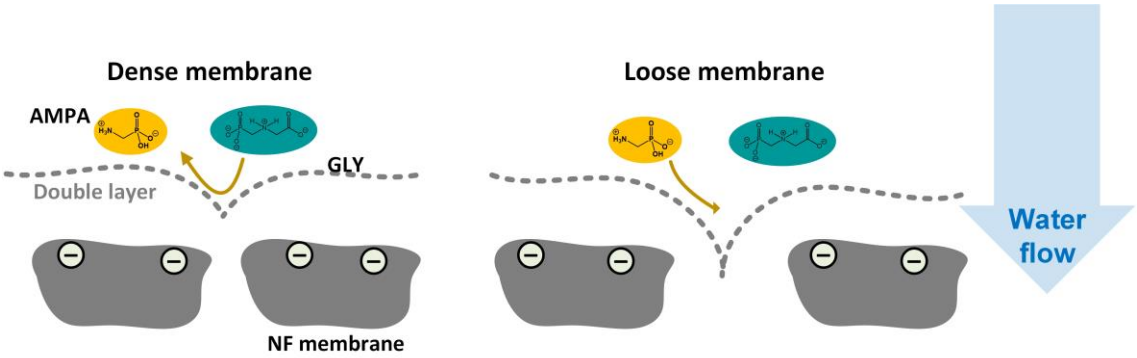

Figure 6.8. Debye length at different membrane pore sizes

The potential at the membrane surface and at the pore center was calculated based on the zeta potential of the NF membrane, the Debye length, and the average pore radius (Figure 6.9). The zeta potential of the NF membrane was provided by Y.B. in the study of Boussouga *et al.* [244].

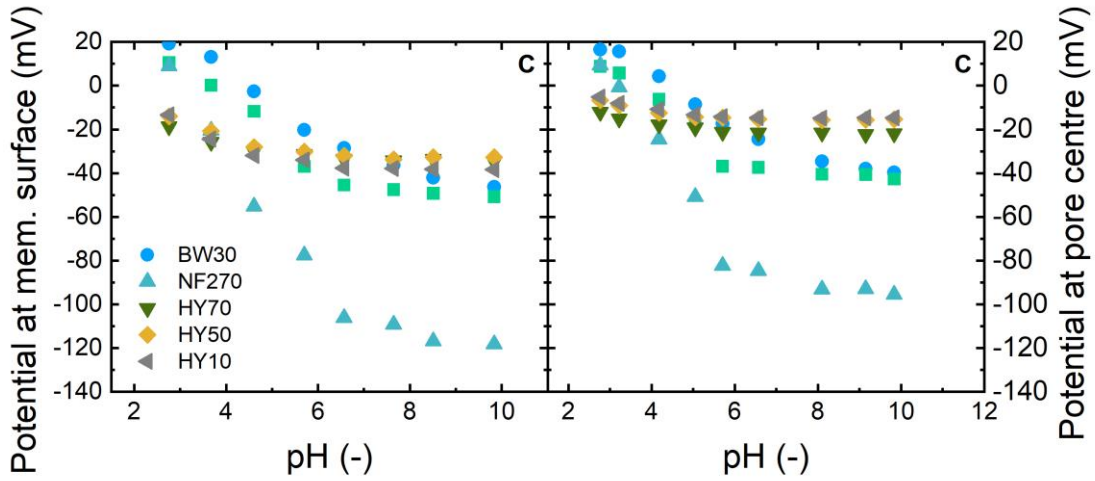

Figure 6.9: (A) Zeta potential at membrane surface, adapted from [244]; (B) Zeta potential at pore center of NF membranes at pH 8. Calculated by M.N. Adapted from [365].

The zeta potential of NF membranes was below 0 mV, −35 mV for BW30, –40 mV for NF 90, and −95 mV for NF 270, which represents the membrane functional groups (carboxyl and amine) [394]. BW 30, NF 90, and NF 270 are more negatively charged than the HY 70, HY 50,

and HY 10 membranes, indicating more charge interactions with the GLY/AMPA molecules (Figure 6.9). The zeta potential of HY membranes was higher than −20 mV. HY 70 and HY 10 membranes, which have characteristics similar to those of HY 50, will be omitted. NF90, NF270, and HY50 membranes were selected for evaluating charge and dielectric exclusion at different pH (Figure 6.10).

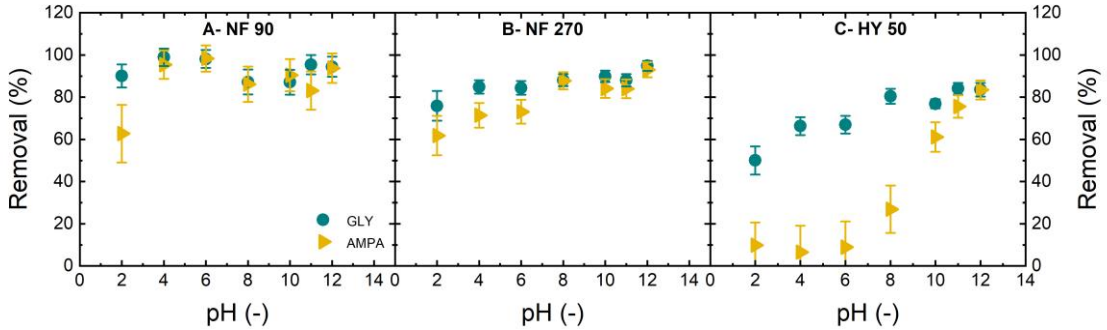

Figure 6.10. Removal as a function of pH with GLY/AMPA removal by NF 90, NF 270, and HY 50 (flux 50 L/m^2.h, initial GLY/AMPA concentration 1 µg/L, 1mM $NaHCO_3$, 10 mM NaCl, 20 °C). Adapted from [365].

The removal of GLY was 50–90 ± 5% while the removal of AMPA was 9–62 ± 12% at pH 2 (Figure 6.10). At this pH, the charges of GLY and AMPA are 0, and the zeta potential at the pore center of NF 90 and NF 270 are positive (8–9 mV), and the charge of HY 50 is negative (−15 mV). Due to the neutral charges of GLY and AMPA, less contribution of charge exclusion was expected. Therefore, the contribution of dielectric exclusion was observed in HY 50, where membrane pores are bigger than GLY/AMPA molecular diameters, and the adsorption was low.

At pH > 2, the removal of GLY and AMPA could be a combination of all removal mechanisms: size exclusion (in the case of NF 90), charge exclusion, and dielectric exclusion. GLY and AMPA removal by NF 90 remained at 90 ± 5 % at all pH. For NF 270, GLY removal increased from 84 ± 3 to 94 ± 5 %, and AMPA removal increased from 71 ± 6 to 92 ± 5 % with the increase of pH from 4 to 12. GLY removal of HY 50 increased from 84 ± 3 to 94 ± 5 %, and AMPA removal increased from 12 ± 5 to 83 ± 11 % with the increase of pH from 4 to 12. The significant improvement in GLY and AMPA removal by the HY 50 membrane could be due to stronger electrostatic repulsion and/or a denser hydration layer (Figure 6.11). In detail, the charge on GLY/AMPA and the membrane becomes more negative with increasing pH, indicating stronger electrostatic repulsion between GLY/AMPA and the membrane surface. The other reason might be the denser hydration layer at higher pH, which contributes to stronger dielectric exclusion of the membrane, as shown by FTIR hydration characterization and molecular dynamics simulation [365]. The diameter of GLY and AMPA hydration layer (including GLY/AMPA molecules) was estimated to be ~1.6 nm, depending on pH [365], indicating a strong contribution of the hydration layer to the transport of GLY and AMPA in NF membranes.

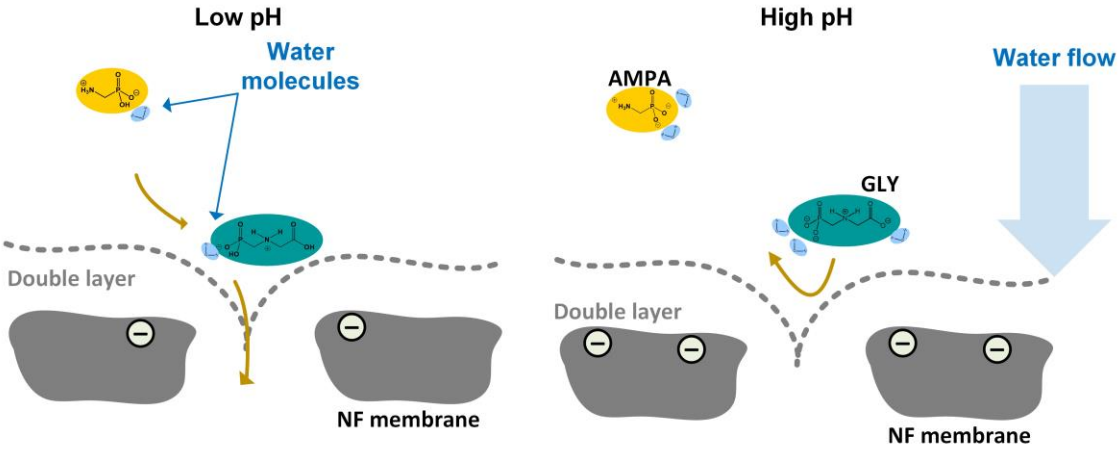

Figure 6.11. Membrane charge and hydration layer of GLY and AMPA change with different water pH

Removal of GLY was always higher than that of AMPA for all pH, which is due to the higher negative charge of GLY than AMPA at the same pH, enhancing charge exclusion. Moreover, the larger size and more negative charge of GLY also contribute to a stronger hydration layer with more functional groups and a more negative charge than AMPA [365].

6.8 Removal of GLY and AMPA at different flux

Following the discussion on the hydration layer in the previous section, to enter the membrane pores, GLY and AMPA must overcome an energy barrier and become dehydrated. In NF membranes, it was expected that the hydration layer would be shredded more at high pressures, leading to lower dielectric exclusion and lower removal of GLY and AMPA. To confirm this hypothesis, the filtration at varying flux with NF membranes was conducted (25, 35, 50, 60, 75, and 100 L/m^2.h for NF 90, NF 270, and 25, 35, 50, 60, and 75 L/m^2.h for HY 50 due to the maximum system pressure being reached), and the removal was shown in Figure 6.12.

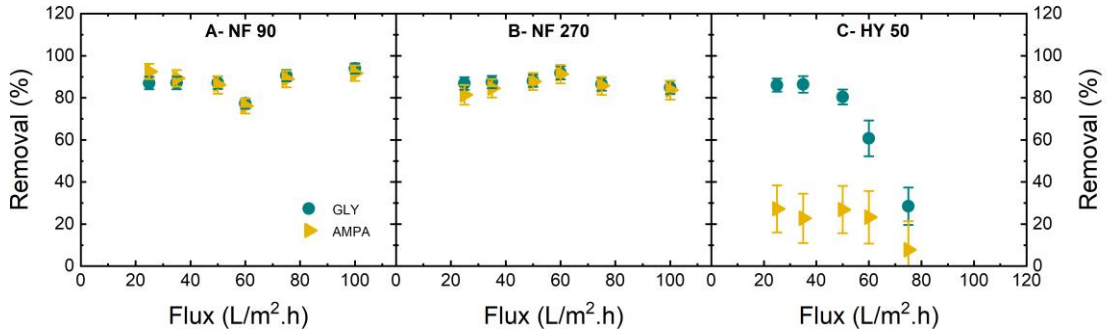

Figure 6.12. Removal as a function of flux with GLY/AMPA removal by NF 90 (A), NF 270 (B), HY50 (C) membrane (initial GLY/AMPA concentration 1 µg/L, 1mM $NaHCO_3$, 10 mM NaCl, pH 8, 20 °C). Adapted from [365].

The removal of GLY and AMPA by NF 90 and NF 270 remained at 80–90 % with increasing flux from 25 to 100 L/m^2.h. The constant removal was due to the strong charge and dielectric

exclusion of these two membranes (in the NF 90 case, size exclusion also contributed). Hence, no clear change in dielectric exclusion by flux could be observed. Meanwhile, a significant decrease in removal was observed in HY 50 with increasing flux. The removal decreased from 86 ± 3 to 28 ± 8% for GLY, and from 27 ± 11 to 7 ± 5 % for AMPA (Figure 6.12 C). The possible phenomena that can happen in this process include (1) concentration polarization on the membrane surface, and (2) dehydration of GLY and AMPA.

To evaluate the contribution of concentration polarization to the rejection of GLY and AMPA, the permeate concentration, the concentration of GLY/AMPA on the membrane surface, and the real removal of the membrane were evaluated on NF 90, NF 270, and HY 50 membranes (Figure 6.13).

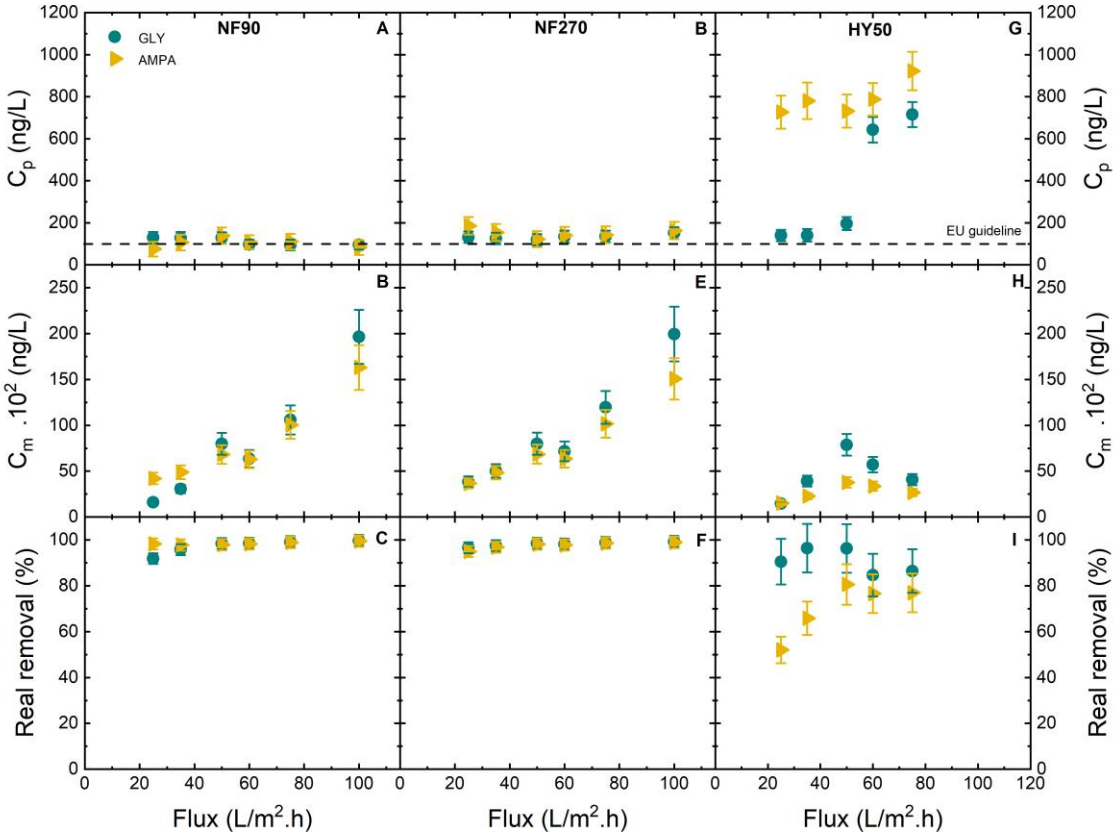

Figure 6.13: Concentration of permeate and on membrane surface, and real removal as a function of flux with GLY/AMPA removal by NF 90, NF 270, HY50 membrane (initial GLY/AMPA concentration 1 µg/L, 1mM $NaHCO_3$, 10 mM NaCl, pH 8, 20 °C).

At higher flux corresponding to lower HRT, c_m was higher for NF 90 and NF 270 than HY 50, indicating the more important role of concentration polarization on the dense membrane than the loose membrane.

In the dense membrane (NF 90, NF 270), the permeate concentration was low at 95–130 ± 10 ng/L for NF 90 and at 130–190 ± 15 ng/L for NF 270 (Figure 6.13). Meanwhile, concentration at the membrane surface increased from 1600 to 20000 ng/L for NF 90 and from 4000 to 20000 ng/L for NF 270 (Figure 6.13 D, E), with the real removal of the dense membrane at 92–98%

for dense membrane. This phenomenon indicates that the high removal of NF 90 and NF 270 was significantly contributed to by concentration polarization (besides Donnan exclusion) (Figure 6.14).

With the loose membrane (HY 50), the permeate concentration increased from 140 ± 12 ng/L to 715 ± 65 ng/L for GLY and from 727 ± 65 ng/L to 922 ± 90 ng/L for AMPA. The concentration at the membrane surface increased from 1470 ng/L to 7867 ng/L for GLY, and from 1515 ng/L to 3767 ng/L for AMPA when flux increased from 25 to 50 L/m^2.h. At higher flux, the concentration at the membrane surface decreased to 4088 ng/L and 2677 ng/L for GLY and AMPA, respectively. This result indicates that the increase in GLY and AMPA removal by HY 50 membrane at flux lower than 50 L/m^2.h was controlled by concentration polarization (in addition to Donnan exclusion). At low flux (25 L/m^2.h), less GLY and AMPA accumulate on the membrane surface, leading to a lower concentration of GLY/AMPA on the membrane surface. On the other hand, more GLY and AMPA accumulate on the membrane surface at higher flux (50 L/m^2.h), more GLY/AMPA pass through the membrane, leading to higher permeate concentration.

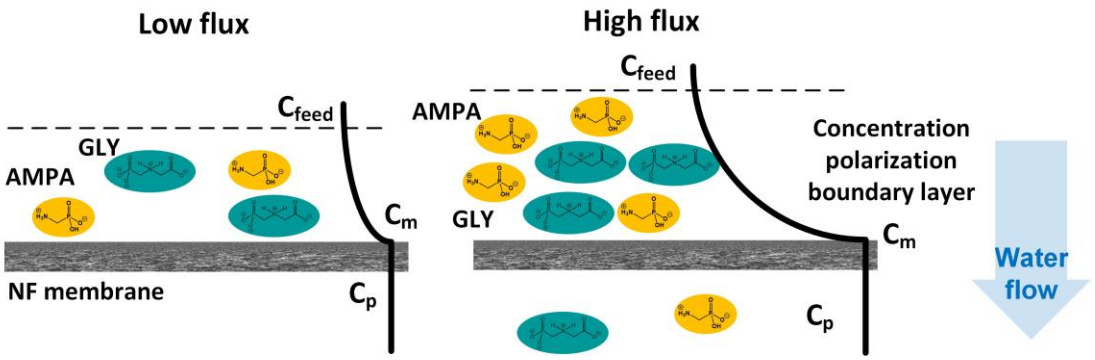

Figure 6.14. Concentration polarization boundary layer on NF membrane at low and high flux

However, at higher flux (> 50 L/m^2.h), the rejection is attributed to dielectric exclusion and the increased hydration shell shredding, where insignificant variation of GLY/AMPA concentration on the membrane surface was observed. In fact, the hypothesis on the shredding of the hydration layer could be reasonable. At higher flux, GLY and AMPA would receive more energy to shred the hydration layer and undergo dehydration to enter the membrane pores, resulting in lower removal. This is a confirmation of the hypothesis on the hydration layer and dielectric exclusion affected by flux/ pressure that was expected at first. Higher pressure (higher flux) applied to the membrane provides GLY/AMPA kinetic energy to overcome the energy barrier; hence, the hydration layer will be shredded [395-397]. The same phenomenon was also reported in computational [405, 408] and experimental studies on ions [396, 398]. The removal of GLY decreased more strongly than AMPA, which was due to the higher charge of GLY than AMPA. With the smaller size and lower negative charge, AMPA does not need higher energy to pass through membrane pores. Nevertheless, molecules with high charge density and bigger size, such as GLY, need more energy to shed the hydration shell [399, 400]. Previous studies on ion rejection also found that the rejection of strongly hydrated ions (F– and Cl–) became more selective than that of weakly hydrated ions (Br–) with changes in applied pressure [401].

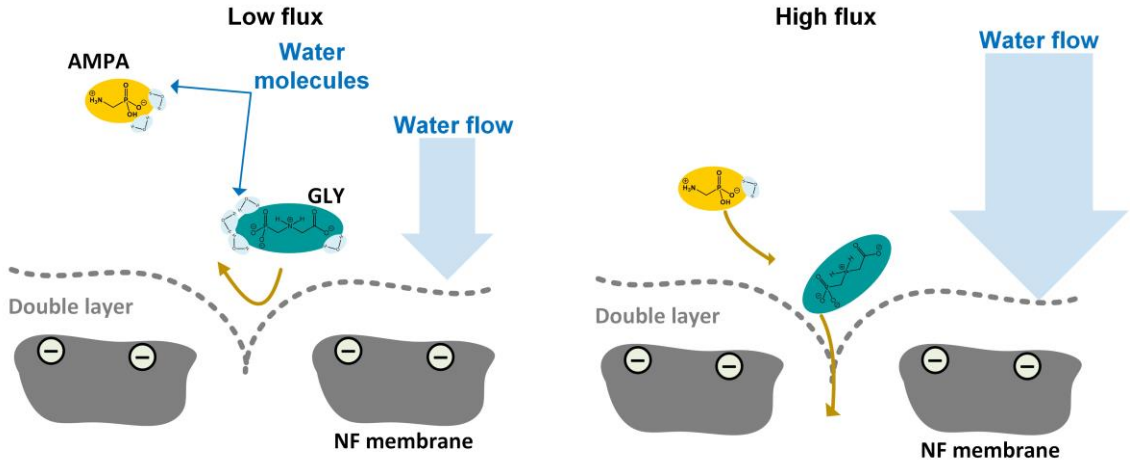

Figure 6.15. GLY/AMPA rejection by NF membrane via dielectric exclusion

During the transport of GLY and AMPA on and in the NF membrane, GLY and AMPA can be adsorbed on the NF membrane active layer, which is dependent on membrane materials and HRT [130]. To evaluate the adsorption of GLY and AMPA on the NF membrane, the mass adsorbed of GLY/AMPA on the membrane at different fluxes was evaluated in Figure 6.16.

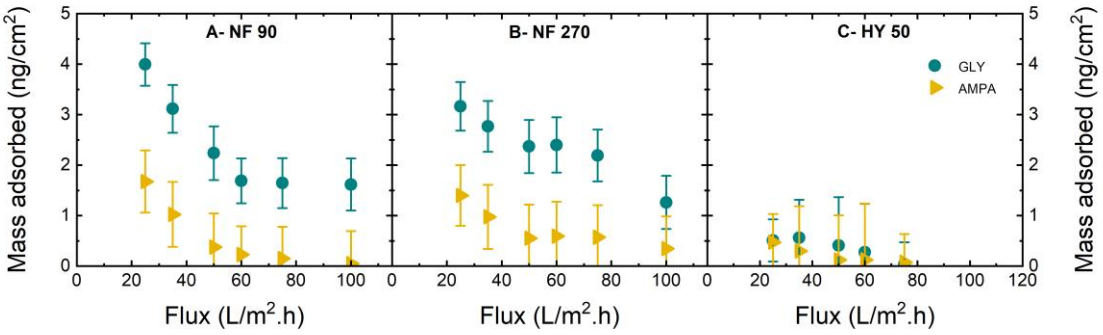

Figure 6.16: GLY/AMPA mass adsorbed on membrane as a function of flux with GLY/AMPA removal by NF 90, NF 270, HY50 membrane (initial GLY/AMPA concentration 1 µg/L, 1mM $NaHCO_3$, 10 mM NaCl, pH 8, 20 °C). Adapted from [365].

In the dense membrane, the mass adsorbed was significant at the lowest flux (25 L/m^2.h, HRT 0.03 s), where mass adsorbed on NF 90 was 4 ± 1 ng/cm^2 and 3.6 ± 1 ng/cm^2 for GLY and AMPA, respectively. The mass adsorbed then decreased to 1.6 ± 0.2 ng/cm^2 and 1.1 ± 0.2 ng/cm^2 for GLY and AMPA, respectively, at the highest flux 100 L/m^2.h (HRT 0.006 s). NF 270 could also adsorb 3 ± 1 ng/cm^2 and 1.4 ± 1 ng/cm^2 for GLY and AMPA, respectively, at the flux 25 L/m^2.h (HRT 0.00002 s). The mass adsorbed decreased by 70% with the increase of flux and reached 1.2 ± 0.2 ng/cm^2 and 0.3 ± 0.1 ng/cm^2 for GLY and AMPA, respectively, at the flux of 100 L/m^2.h ($6 \cdot 10^{-5}$ s), indicating the role of HRT in the adsorption of the membrane. At the lower pressure, GLY and AMPA were filtered through the membrane more slowly, creating more HRT for the adsorption onto the membrane surface materials. The major role of HRT on GLY/AMPA adsorption on the membrane was different from the previous paper, which concluded that HRT did not contribute significantly to the adsorption of 17β-Estradiol on NF 90 and NF 270 membranes [363]. The results showed that the concentration on the membrane

surface and HRT controlled the transport of GLY and AMPA in dense membranes with the active layer made of polyamide (NF 90, NF 270).

With the loose membrane (HY 50), the adsorbed mass of HY 50 was insignificant, decreasing from 0.4 ± 0.5 ng/cm^2 to ~ 0 ng/cm^2 with the increase of flux from 25 L/m^2.h (HRT 0.004 s) to 75 L/m^2.h (HRT 0.001 s) due to the low adsorption capability of HY 50 membrane material (sulfonated polyether sulfone polymer) [393]. The low adsorption on the membrane indicates that the adsorption was not governed by the HRT.

Overall, the transport of GLY and AMPA by membranes with the smaller pore size (NF 90, NF 270) was governed by the interplay of concentration polarization, while the hydration layer plays an important role in membranes with the bigger pore size (HY 50).

6.9 Conclusions

This chapter evaluated the removal of GLY and AMPA by the NF membrane. The rejection efficiency and transport of GLY and AMPA in NF membranes were evaluated using six membranes (BW 30, NF 90, NF 270, HY 70, HY 50, HY 10) covering a range of MWCOs from 80 Da to 3000 Da. The following points are obtained from this investigation.

- The rejection of GLY and AMPA was incomplete even at the membrane with the smallest MWCO, posing a challenge for removing GLY/AMPA.
- Size exclusion was dominant in the filtration of the membrane at low MWCO (< 150 Da), with 90% GLY/AMPA removed. Donnan exclusion and dielectric exclusion are more dominant for membranes with MWCO > 200 Da. The Debye length and pore radius of the membrane showed that Donnan exclusion would always happen with all membrane pore sizes.
- Concentration polarization strongly contributes to the rejection of GLY/AMPA at the membrane with the low MWCO. Meanwhile, more flux applied on the membrane with the bigger pore size can give more energy for dehydration, letting GLY and AMPA pass through the membrane pore.

NF membrane can partially remove GLY and AMPA; however, the removal was incomplete, making the final permeate concentration higher than the EU guidelines for herbicides. Additionally, this system requires concentrate treatment and high pressure for operation, implying higher energy (which will be discussed in Chapter 8).

At this point, the chosen technologies include adsorption by PBSAC, hybrid membrane–adsorption system UF–PBSAC, and NF membrane filtration. While PBSAC is in static adsorption, UF–PBSAC can effectively remove GLY and AMPA, but at low flux, and NF can partially remove these herbicides. Another option for removing micropollutants is the photodegradation membrane, which will be investigated in the next chapter.

7 Photodegradation of GLY and AMPA using PVDF-TiO_2 membrane

This chapter is adapted from a publication in Advanced Functional Materials entitled: P.B. Trinh, S. Liu, N.F. Himma, B. Fiser, A.I. Schäfer, Continuous-flow photocatalytic degradation of glyphosate and aminomethylphosphonic acid under simulated sunlight with TiO2-coated poly(vinylidene fluoride) membrane, Advanced Functional Materials, 36, no. 21 (2026) e11431 [402].

The contribution of authors:

Phuong B. Trinh: conceptualization; performing experiments; samples analysis; data analysis and interpretation; methodology; validation; visualization; writing – original draft

Siqi Liu: conceptualization; data interpretation; methodology; supervision; validation; visualization; writing – review & editing

Nurul F. Himma: performing experiments; sample preparation; data analysis; visualization

Béla Fiser: data curation; formal analysis; funding acquisition; investigation; methodology; validation; visualization; writing – review & editing

Andrea I. Schäfer: conceptualization, funding acquisition; project administration; resources; supervision; validation; writing – review & editing

This chapter aims to investigate the GLY and AMPA removal by photocatalysis on MF membrane. The limiting factors to the degradation are evaluated to optimize the filtration system. The varied parameters include flux, light intensity, water quality (GLY and AMPA concentration, pH). The predominant reactive oxygen content and the degradation pathway was investigated.

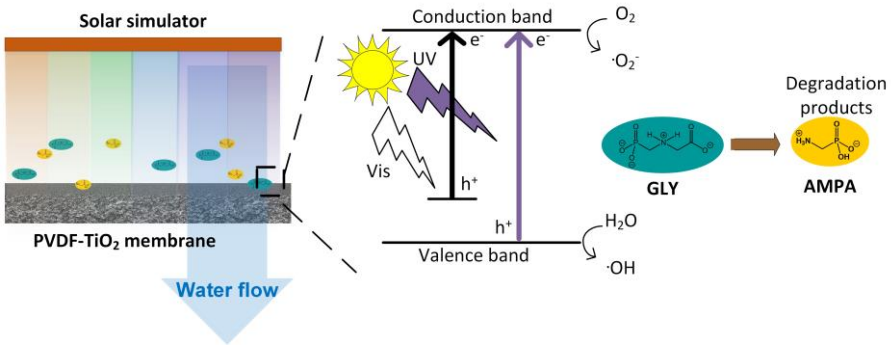

7.1 Introduction

In previous work, photocatalysis using TiO_2 in batch can degrade 65% to >90% of GLY at an initial concentration of 25 mg/L [189]. However, catalyst recovery, mass transfer of reactants/ROS, and reduced illumination due to agglomeration and turbidity of photocatalyst nanoparticles are problems in conventional suspension photocatalysis systems [273, 274]. The need for photocatalyst recovery and the potential for catalyst agglomeration in suspended systems can be reduced by using a photocatalytic membrane reactor, a hybrid technique that combines membrane filtration with photocatalysis in a single unit [275-277]. Moreover, the membrane offers a high surface-to-volume ratio and a long contact time for the degradation of GLY and AMPA [279, 280]. TiO_2 has been integrated into a poly(vinylidene fluoride) (PVDF) membrane to enhance the removal of steroid hormones [355] with the removal > 90%. With this vision, the PVDF-TiO_2 membrane is expected to degrade GLY and AMPA in water effectively.

Studies on TiO_2-based photocatalysis for GLY degradation are frequently conducted under UVA irradiation [190, 191, 403], which has the maximum absorption wavelength λ_{max} around 400 nm [404]. This is because TiO_2 has a wide band gap (3.0–3.2 eV [405]) and a rapid charge recombination of the electron-hole pairs, which reduces photocatalytic efficiency under visible light [406, 407]. However, there has been a lot of study on developing photocatalysis technologies that are powered by abundant solar energy due to the increasing need to minimize carbon emissions from fossil fuel-based electricity generation [408, 409]. Even though the UV spectrum accounts for just 5% of the solar radiation that reaches the Earth's surface [420, 421], TiO2 photocatalysis is nevertheless effective in the presence of sunlight and can break down contaminants in water [410, 411]. Carbon-doped TiO_2/ clinoptilolite nanocomposite was investigated for GLY photodegradation under visible light in batch [412]. The results showed that 84% of GLY could be degraded from an initial concentration of 30 mg/L, and AMPA was identified as a degradation product [412]. Therefore, GLY and AMPA photodegradation by TiO_2 could be investigated under solar light at environmentally relevant conditions.

This study investigates the removal of GLY and AMPA from water at environmentally relevant concentrations using a photocatalytic membrane in a flow-through configuration. The following research questions were addressed.

- How much GLY and AMPA are photodegraded by PVDF-TiO_2 membrane under simulated sunlight compared to UV light?
- What are the limiting factors in the continuous photocatalytic degradation under simulated sunlight?
- What is the degradation mechanism and optimization performance of the PVDF-TiO_2 membrane?

7.2 Photocatalytic membrane filtration system and filtration protocol

The membrane photocatalysis experiments were conducted using a custom-built micro cross-flow system (Figure 7.1). Further details of this setup and its comprehensive hydrodynamic characterization have been reported in previous work [354, 413].

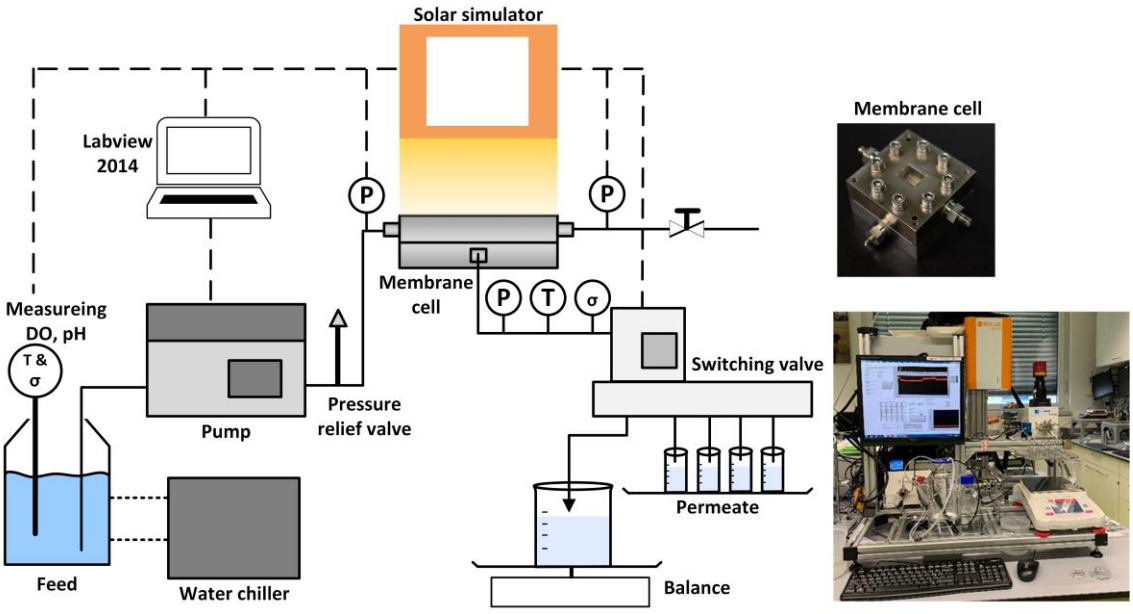

Figure 7.1: Schematic illustration of the membrane photocatalysis set-up and the photograph (inset) of photocatalytic membrane cell with dead-end configuration (retentate valve closed). The system is equipped with pressure P, temperature T, conductivity σ, pH, and dissolved oxygen O_2 sensors.

The membrane cell consists of a stainless steel module (or microreactor) with an active membrane area of 2 cm^2, a channel height of 0.7 mm, and a quartz window (active illumination area: 2 cm2; Zell Quarzglas, Germany). A high-pressure pump (Pump 80P, pump head 500 mL SST, KNAUER Wissenschaftliche Geräte GmbH, Germany) was used. A UV LED (M365LP1, peak wavelength: 365 nm, Thorlabs, USA) with an LED driver (DC2200, Thorlabs) served as the UV light source, as described in a previous study [413]. A solar simulator (SINUS-70, wavelength range: 350—1150 nm, WAVELABS Solar Metrology Systems GmbH, Germany) provided a broad range of light wavelengths (Figure 7.2). The system was equipped with the feed pressure sensors (WIKA S-10, 0–1 bar; WIKA A-10, 0–40 bar, Germany), a permeate pressure sensor (WIKA S-10, 0–1 bar, Germany), and a permeate in-line conductivity sensor (ET131, eDAQ, Australia). A water chiller (Minichiller 300 OLÉ, Peter Huber Kältemaschinenbau, Germany) was used to control and maintain the feed temperature, while a 16-port switching valve (Azura V2.1S, Knauer) was used to automatically collect multiple samples. The system was connected to a computer running LabVIEW software (Version 14.0.1, National Instruments, Germany) for automated control of the switching valve, feed flow rate, time, and light intensity for the UV LED. The solar simulator was controlled by SinusGUI v2.5 (Wavelabs, USA). Experimental

parameters, including pressure, temperature, conductivity, and permeate mass, were monitored via a data acquisition card (USB-6000, National Instruments, USA).

The filtration protocol is summarized in Table 9.10. In short, the membrane was placed on the bottom of the membrane cell. After pre-condition and pure water flux, the solar simulator was prepared and calibrated (Figure 7.2). Then, the filtration starts in the dark phase for the first 100 mL to achieve the adsorption equilibrium. After the dark phase, the light (UV, solar simulator) was turned on for the photodegradation at the same flow rate. After the filtration experiment, the pure water flux was measured again.

The solar simulator can generate a spectrum that is almost identical to the spectrum of sunlight (Figure 7.2) (Installation and Operating Manual, SINUS-70, WAVELABS Solar Metrology Systems GmbH, Germany). 21 LED channels in the light engine cover specific wavelength ranges (from a peak wavelength of 372 nm to 1200 nm). The global standard solar spectrum (air mass 1.5 global, AM1.5g [414]) is used with the spectral range from 350 nm to 1150 nm.

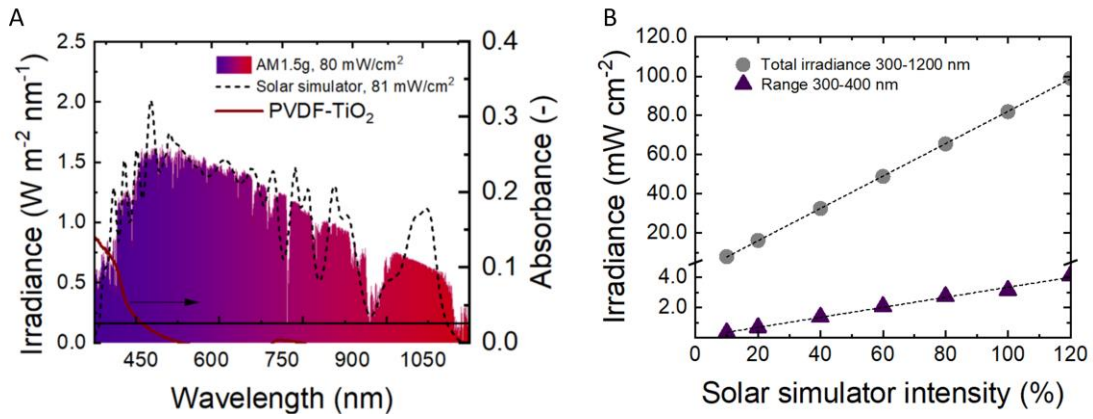

Figure 7.2: (A) The spectrum generated by the solar simulator (SINUS-70, WAVELABS) at an intensity of 100% compared to the standard solar spectrum (AM1.5g [414]), and the absorbance spectrum of PVDF-TiO_2 membrane, showing at what wavelength range the solar light could be absorbed. (B) Total irradiance and UV fraction (300–400 nm) irradiance at different intensities of solar simulator. Adapted from Lyubimenko *et al.* [415].

Figure 7.2 shows the comparison between the standard solar spectrum, the spectrum generated by the solar simulator, and the absorbance spectrum of the membrane used. By integrating the solar irradiance in the wavelength range < 400 nm, UV irradiance accounts for 4.2% of the simulated solar irradiance. Hence, the solar irradiance at 50 mW/cm^2 is equivalent to UV irradiance at 2.1 mW/cm^2, and values were chosen accordingly for experiments.

The calibration of the UV-LED lamp is shown in Figure 7.3.

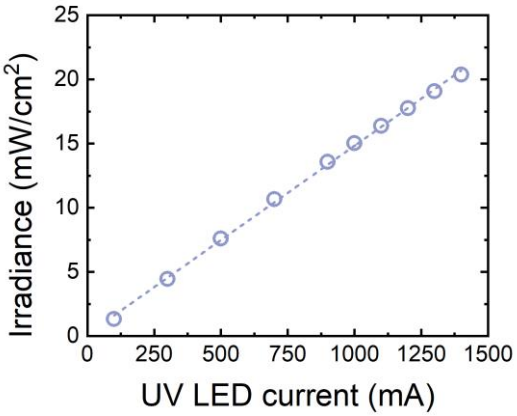

Figure 7.3. Calibration of the UV-LED lamp

A UV LED (M365LP1, peak wavelength: 365 nm, Thorlabs, USA) with an LED driver (DC2200, Thorlabs) served as the UV light source, as described in the previous study [413].

7.3 Photocatalytic membrane

The photocatalytic membrane was a PVDF-TiO_2 membrane prepared and supplied by the Institute of Surface Engineering (IOM), Leipzig; the preparation method and membrane characteristics were previously described by Fischer *et al.* [413, 416]. In brief, the TiO_2 nanoparticle (NPs) suspension was prepared by mixing 4 mL of titanium (IV) isopropoxide (TTIP) with 80 mL of 0.1 M HCl and stirring for 15 minutes at room temperature. The mixture solution was then heated in a pressure vessel at 210 °C for 20 hours, cooled, and subsequently dispersed using an ultrasonic probe for 90 seconds at 40 W (Sonoplus, HD2200 Generator, KE76 probe, BANDELIN electronic GmbH & Co. KG, Berlin, Germany). A standard PVDF membrane (0.22 μm, Millipore, USA) (90 mm × 90 mm) was then placed (with the active layer facing downwards) into the suspension and shaken for 5 min. The membrane was subsequently washed with Milli-Q water and dried at 100 °C for 30 min. The PVDF-TiO_2 membrane contained 5.2 ± 0.2 % TiO_2 on the membrane surface with the pore size of 0.22 μm [413] with the membrane thickness of $1.25 \cdot 10^{-4}$ m, porosity of 0.6 [417].

7.4 Data analysis

Removal of GLY and AMPA, flux, and permeability of the membrane were calculated by the same equation in Chapter 5.

Rate of disappearance

The rate of disappearance ($-r_i''$, mol/m^2.s) in the photocatalytic membrane system is determined in equation (7.1).

$$-r_i'' = -\frac{1}{A}\frac{dN_i}{dt} = \frac{1}{A}\frac{Q}{3600}\frac{(c_{i,f} - c_{i,p})}{10^6 \cdot M_i} \tag{7.1}$$

where N_i is moles GLY and AMPA reacted and M_i is the molecular weight of GLY or AMPA (169.07 g/mol for GLY and 111.04 g/mol for AMPA).

Hydraulic residence time

The degradation of GLY and AMPA is dependent on HRT. HRT and molar flux were calculated at different fluxes (Figure 7.4) and were calculated with the following equation.

$$t_R = \frac{V_p}{Q_f} = \frac{h_m \varepsilon}{J_w} \tag{7.2}$$

where pore volume $V_p = A h_m \varepsilon$ (L), Q_f is the feed flow rate (L/h), J_w is the water flux ($m^3/m^2.h$), A is effective membrane area ($2 \cdot 10^{-4}$ m^2), h_m is the membrane thickness ($1.25 \cdot 10^{-4}$ m), ε is membrane porosity (60%) [417].

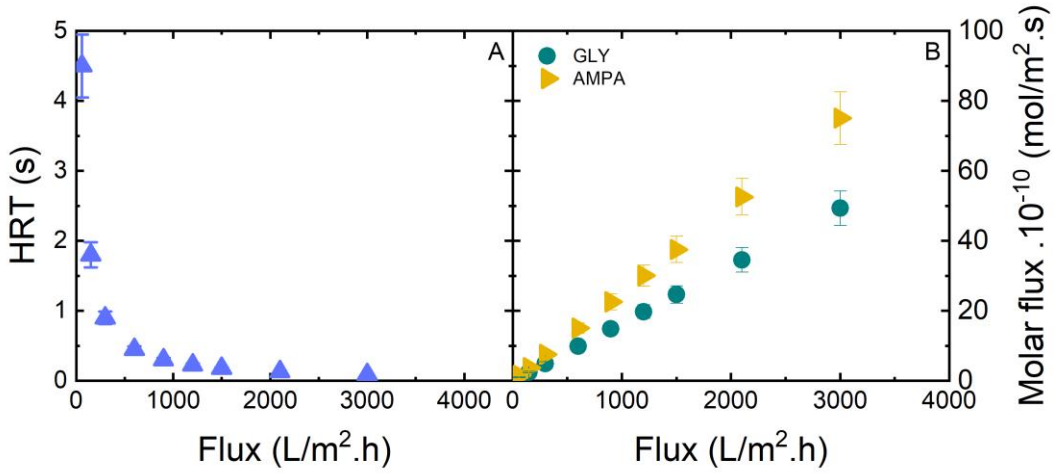

Figure 7.4: Hydraulic residence time (s) (A) and molar flux of GLY/AMPA (B) on PVDF-TiO_2 membrane. Adapted from [402].

The hydraulic residence time decreased from 4.5 to 0.09 s when the flux increased from 60 to 3000 L/m^2.h. The molar flux increased from 10^{10} to $49 \cdot 10^{10}$ mol/m^2.s for GLY and from 10^{10} to $75 \cdot 10^{10}$ mol/m^2.s for AMPA.

7.5 Reactive oxygen species identification

Different scavengers, including iso-propanol (IPA, > 99.8%, HPLC grade, VWR, Germany), p-benzoquinone (p-BQ, > 98%, Thermo Scientific Chemicals, Germany), furfruyl alcohol (FFA, 98%, Thermo Scientific Chemicals, Germany), and sodium oxalate (SO, 99%, Thermo Scientific Chemicals, Germany) were selected to identify the contributions of •OH, $•O_2^-$, $^1O_2$, and h_{VB}^+, respectively. The used scavengers were: isopropanol (IPA, > 99.8%, HPLC grade, VWR,

Germany) – for hydroxyl radical (•OH); p-Benzoquinone (p-BQ, > 98%) – for superoxide radicals ($\bullet O_2^-$); furfuryl alcohol (FFA, 98%) – for singlet oxygen ($^1O_2$); sodium oxalate (SO, 99%) for valence band holes (h_{VB}^+), all from Thermo Scientific Chemicals, Germany (Table 7.1).

Table 7.1: Kinetic rate between scavenger and target radicals in water.

Scavenger	Target radicals	References
Ethanol (EtOH)	•OH / $\bullet SO_4^-$	[418]
Methanol (MeOH)	•OH / $\bullet SO_4^-$	[418]
Iso-propanol (IPA)	•OH / $\bullet O_2^-$ / $\bullet SO_4^-$	[419, 420]
HCO_3^-	e_{CB}^- / •OH / $\bullet SO_4^-$	[418, 421, 422]
p-benzoquinone (BQ)	$\bullet O_2^-$ / •OH	[423, 424]
Furfruyl alcohol (FFA)	$^1O_2$ / •OH	[418, 425]
Sodium oxalate (SO)	h_{VB}^+	[426]

To evaluate the photocatalytic degradation performance, the removal of GLY and AMPA was examined under both UV and solar light. The limiting factors affecting photodegradation were then systematically investigated. The photodegradation pathway was analyzed using the G3MP2B3 composite computational chemistry method, which was employed to determine all unique BDE values (by Bela Fiser at the University of Lodz). Finally, an optimized experiment was conducted where limiting factors were reduced to determine whether GLY and AMPA removal is able to meet EU regulatory requirements in principle. The standard experimental conditions are shown in Table S3, and the operating parameters are presented in Figures S9 to S20.

Both UV and solar light were used to study the photodegradation of GLY and AMPA. Then, a thorough investigation into the limiting factors influencing photodegradation was conducted. The G3MP2B3 composite computational chemistry approach was used to analyze the photodegradation pathway and identify each unique BDE value. To determine whether the removal of GLY and AMPA meets EU herbicide guidelines, an experiment was conducted at optimized conditions, reducing limiting variables.

7.6 Photocatalytic degradation with simulated solar light and UV light

To evaluate the removal of GLY and AMPA by PVDF-TiO_2 membrane, the photolysis and photocatalysis were investigated under simulated solar light (350—1150 nm, 50 mW/cm^2) and UV light (365 nm, 2.1 mW/cm^2) (Figure 7.5). The irradiance was adjusted to reflect the UV light in the simulated solar light. UV irradiance accounts for 4.2% of the simulated solar irradiance (Figure 7.2). Therefore, the solar irradiance at 50 mW/cm^2 is equivalent to UV irradiance at 2.1 mW/cm^2.

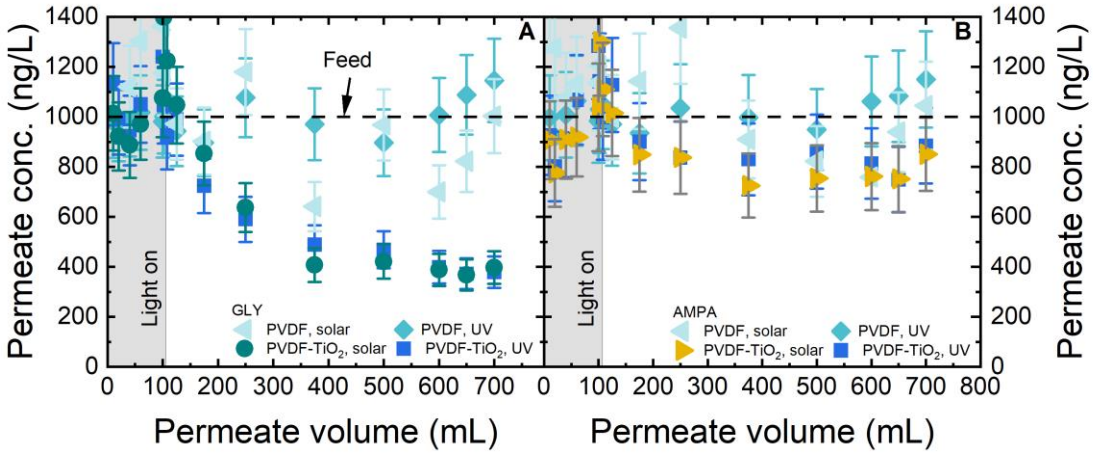

Figure 7.5. GLY (A) and AMPA (B) permeate concentration vs. cumulated permeate volume under solar simulator and UV light (PVDF and PVDF-TiO_2, c_f (GLY/AMPA) = 1 µg/L, J_w= 600 L/m^2.h, I (AM1.5g 350–1150 nm) = 50 mW/cm^2, I (365 nm) = 2.1 mW/cm^2, pH 8.1 ± 0.1, 23 ± 1°C). Adapted from [402].

In photolysis, no significant degradation of GLY or AMPA was observed under either UV or simulated solar light, with permeate concentrations of GLY and AMPA at 0.9–1 ± 0.1 µg/L (Figure 7.5). Therefore, no measurable photolysis occurred. In the previous study of Papagiannaki *et al.*, photolysis can remove 90% GLY under UV light (wavelength 254 nm, irradiance ~23 J/cm^2) in batch experiments [427]. However, in this study, photolysis was not observed in dynamic filtration, possibly due to the high flux or the low HRT (0.45 s). At this HRT, the reaction time was not enough for photolysis.

To verify the adsorption of GLY and AMPA, filtration by PVDF-TiO_2 membrane was conducted in the full dark phase (Figure 7.6).

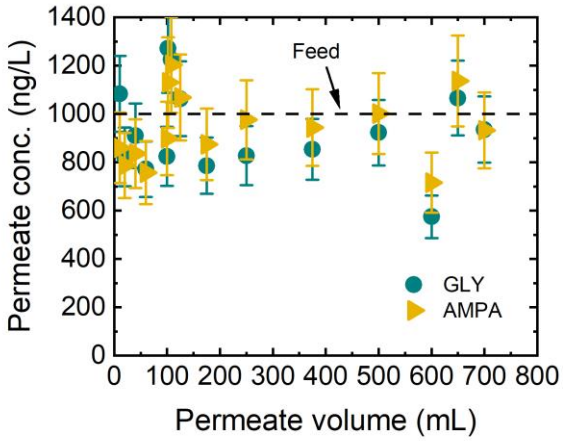

Figure 7.6: Normalized GLY and AMPA concentration in permeate (c_p/c_f) vs. cumulated permeate concentration without light (PVDF-TiO_2, c_f (GLY/AMPA) = 1 µg/L, J_w= 600 L/m^2.h, pH 8.1 ± 0.1, 23 ± 1°C). Adapted from [402].

A similar phenomenon that was observed in Figure 7.5 was observed in the dark-phase experiment, where the permeate concentrations were 1 ± 0.1 µg/L, indicating that the adsorption of GLY or AMPA onto the PVDF-TiO_2 membrane has reached equilibrium (Figure 7.6).

Since photolysis and membrane adsorption did not contribute to GLY and AMPA removal, photocatalytic degradation by the PVDF-TiO_2 membrane can be investigated under UV and simulated solar light. Under UV light ($I_{365\,nm}$ = 2.1 mW/cm^2), the permeate concentration decreased from 1000 ± 100 ng/L (feed solution) to 400 ± 60 ng/L for GLY and 800 ± 80 ng/L for AMPA. Other research on GLY degradation also found that GLY could be degraded under UV irradiation [190, 191, 403]. Under simulated solar light, the permeate concentration decreased from 1000 ± 100 ng/L to 400 ± 60 ng/L for GLY and 800 ± 80 ng/L for AMPA. The comparable permeate concentrations between UV and solar light indicate that non-UV solar spectra did not contribute to the degradation of GLY and AMPA. This was further supported by filtration experiments conducted at different wavelengths (Figure 7.7).

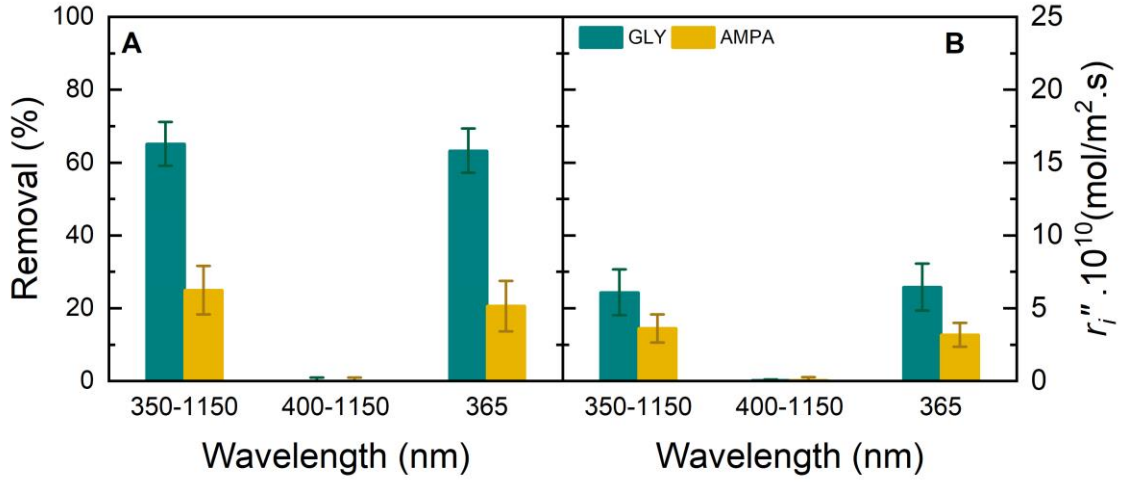

Figure 7.7: Removal (A) and rate of disappearance (B) of GLY and AMPA under different wavelength ranges (PVDF-TiO_2, c_f (GLY/AMPA) = 1 µg/L, J_w= 600 L/m^2.h, I (AM1.5g 350–1150 nm) = 50 mW/cm^2, I (400–1150 nm) = 48 mW/cm^2, I (365 nm) = 2.1 mW/cm^2, pH 8.1 ± 0.1, 23 ± 1°C). Adapted from [402].

The filtration at different wavelengths (UV, non-UV, and solar) shows that the removal and rate of disappearance (r_i'') for GLY and AMPA under 350–1150 nm were comparable to those observed under 365 nm. GLY removal was 65 ± 6% under 50—1150 nm and 63 ± 6% under 365 nm, while AMPA removal was 25 ± 6% and 20 ± 7 %, respectively. The corresponding r_i'' values were (6–7) ± 1 · 10^{10} mol/m^2.s for GLY and 3 ± 0.5 · 10^{10} mol/m^2.s for AMPA. Meanwhile, at wavelengths of 400–1150 nm (non-UV range), both removal and r_i'' were negligible, confirming that non-UV wavelengths did not contribute to GLY and AMPA degradation. Moreover, the removal and rate of disappearance of GLY were higher than those of AMPA. The reason for this result could be (1) AMPA is more stable than GLY during the photodegradation [56]; (2) AMPA was formed as a by-product of GLY photodegradation. This hypothesis needs confirmation by the filtration of individual compounds.

7.7 Individual GLY and AMPA degradation

To investigate whether AMPA was generated in the GLY degradation, the photocatalytic degradation of GLY and AMPA was examined individually under simulated solar light (AM1.5G, 350–1150 nm, irradiance = 50 mW/cm^2) (Figure 7.8).

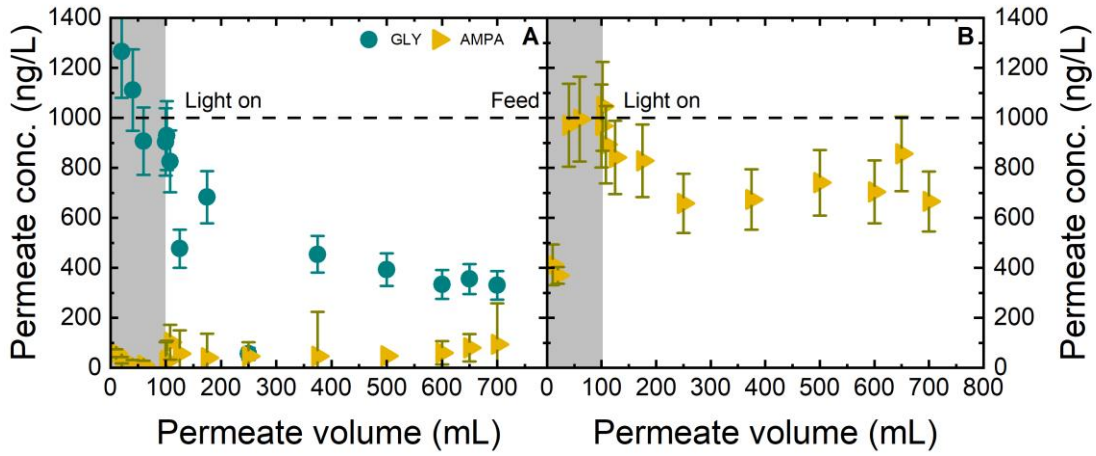

Figure 7.8. Permeate concentration (c_p) vs. cumulated permeate volume with individual GLY (A) and individual AMPA (B) (PVDF-TiO_2, c_f (GLY/AMPA) = 1 µg/L, J_w= 600 L/m^2.h, I (AM1.5g 350–1150 nm) = 50 mW/cm^2, pH 8.1 ± 0.1, and 23 ± 1°C). Adapted from [402].

GLY permeate concentration was lower than AMPA concentration during the filtration experiment. Hence, GLY was degraded better than AMPA by the PVDF-TiO_2 membrane under solar light. The permeate concentration of AMPA was 720 ng/L; less AMPA was degraded, as AMPA is more persistent than GLY [428]. Therefore, AMPA would be degraded more slowly and to a lower extent than GLY. Moreover, the degradation of GLY and AMPA by TiO_2 could be influenced by the adsorption–diffusion steps in the heterogeneous reaction between ROS and micropollutants [429]. GLY and AMPA, and their photodegradation products, can adsorb onto TiO_2 and membrane surface *via* hydrogen bonding, van der Waals interactions, and surface complexation with the functional groups [429, 430]. As GLY has stronger functional group interactions [430] and a higher molecular weight [200], GLY has a higher affinity for TiO_2 than AMPA. Subsequently, more GLY can be in contact with the reaction space of TiO_2 than AMPA, and more GLY could be degraded.

In the individual photodegradation of GLY (Figure 7.8A), there was no significant difference in GLY permeate concentration between the mixture (400 ± 45 ng/L, Figure 7.5A) and the individual experiment (300 ± 33 µg/L, Figure 7.8A). The same phenomenon was obtained from AMPA. AMPA permeate concentration was 700 ± 70 ng/L and 800 ± 80 ng/L for the individual and mixture experiment, respectively. Therefore, the reaction competition between GLY and AMPA for degradation sites [431], or the formation of AMPA during GLY degradation [432], could thus not be determined.

In Figure 7.8 A, AMPA was detected in the permeate at a concentration of 100 ± 11 ng/L during GLY degradation. In the study of GLY photodegradation by TiO_2 in batch experiments, AMPA was also found as a reaction intermediate [189]. The degradation of GLY to AMPA pathway is also kinetically preferred [433], increasing the possibility of AMPA formation even though no clear evidence is identifiable in these low HRT experiments.

To gain deeper insight into the mechanisms of GLY and AMPA degradation by the PVDF-TiO_2 membrane under simulated solar light, and to optimize the process, the limiting factors were investigated under varying operating conditions, including irradiance, flux, and water quality (initial herbicide concentration and pH).

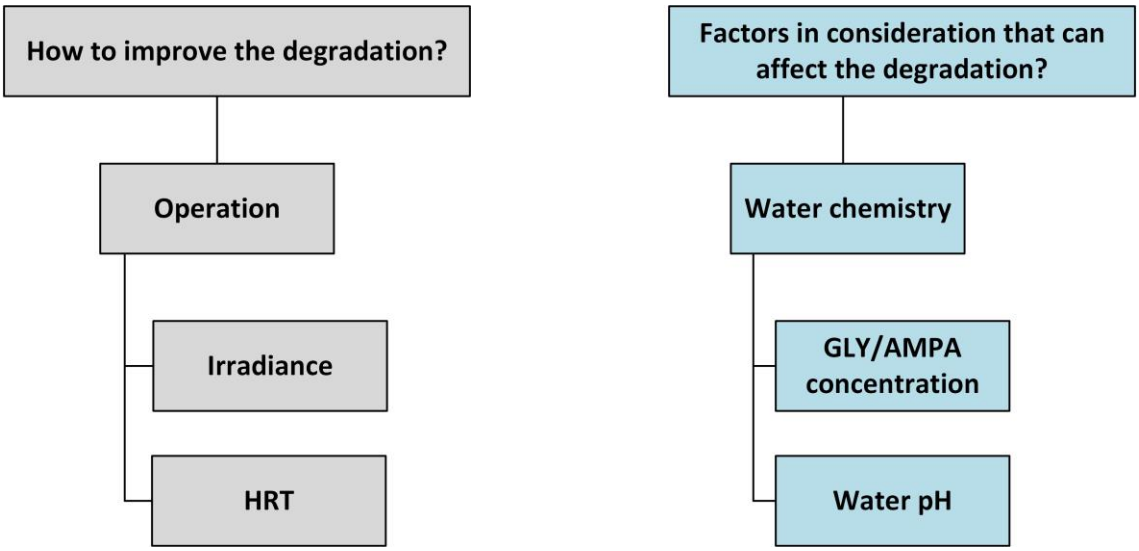

Figure 7.9: Factors in consideration to optimize photodegradation of GLY and AMPA by PVDF-TiO_2 membrane

7.8 Photocatalytic degradation of GLY/AMPA enhancement by irradiance

Light intensity determines the number of photons available at the photocatalyst surface, which affects ROS generation. To evaluate photon availability as a limiting factor for GLY and AMPA degradation, photocatalytic experiments were conducted under varying irradiance intensity for UV (0.4–4.1 mW/cm^2) and simulated solar light (10–98 mW/cm^2) (Figure 7.10).

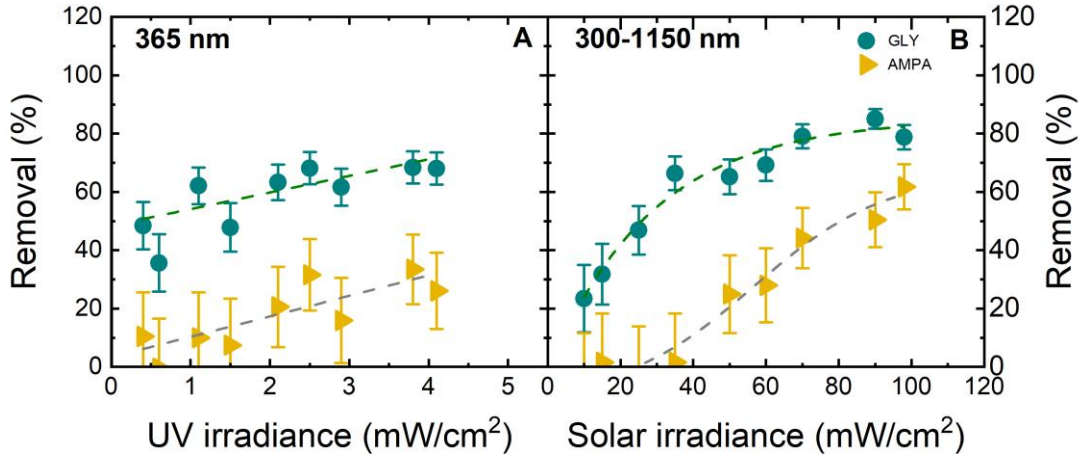

Figure 7.10. Removal of GLY and AMPA at varied irradiance of UV light (A) and solar simulator (B) (PVDF-TiO_2, c_f (GLY/AMPA) = 1 µg/L, J_w = 600 L/m^2.h, pH 8.1 ± 0.1, and 23 ± 1°C). Intensity of light in the UV wavelengths induced by the solar irradiator (B) is equivalent to the intensity of UV light induced by the LED (A). Adapted from [402].

Under UV light, GLY removal increased slightly from 48 ± 8% to 68 ± 6% as UV irradiance increased from 0.4 to 4.1 mW/cm^2 (Figure 7.10 A). Meanwhile, AMPA removal increased from 10 ± 8% to 26 ± 13%. Under solar light, GLY removal increased significantly from 23 ± 11% to 79 ± 4% as solar irradiance increased from 10 to 70 mW/cm^2, then remained at 79–85% for irradiance > 70 mW/cm^2 (Figure 7.10 B). AMPA removal increased from 25 ± 13% to 62 ± 8% with the increase of irradiance from 50 to 98 mW/cm^2.

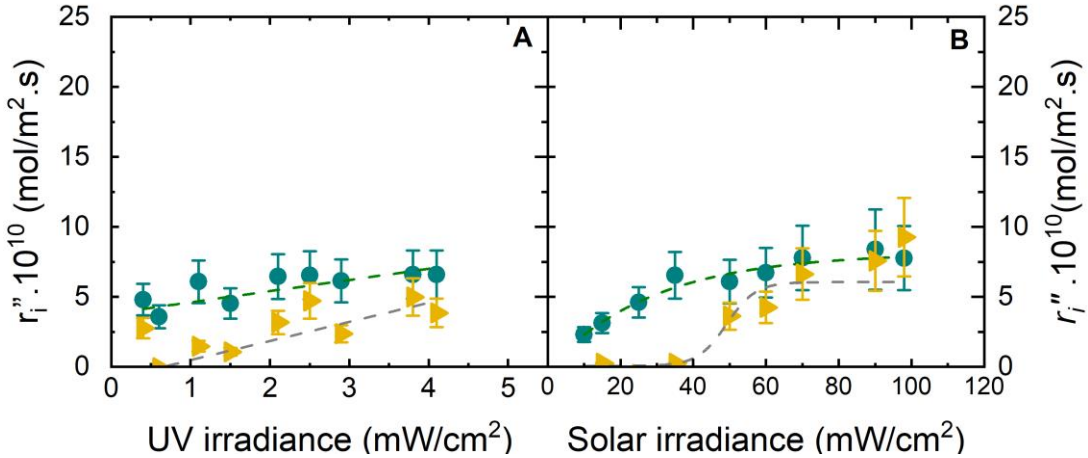

Figure 7.11. Rate of disappearance (r_i'') of GLY and AMPA at varied irradiance of UV light (A) and solar simulator (B) (PVDF-TiO_2, c_f (GLY/AMPA) = 1 µg/L, J_w = 600 L/m^2.h, pH 8.1 ± 0.1, and 23 ± 1°C). Intensity of light in the UV wavelengths induced by the solar irradiator (B) is equivalent to the intensity of UV light induced by the LED (A). Adapted from [402].

Under UV light, the rate of disappearance (r_i'') increased from 5 ± 1 to 7 ± 1 · 10^{10} mol/m^2.s for GLY and from 1 ± 1 to 4 ± 1 · 10^{10} mol/m^2.s for AMPA (Figure 7.10 A). The slight increase in GLY and AMPA degradation rates (r_i'') with increasing UV irradiance indicates the light inten-

sity as a limiting factor for photodegradation. This is in contradiction to the previous study on steroid hormone degradation by the same PVDF-TiO_2 membrane, where steroid hormone removal increased significantly from 10 to 74 ± 7 % when increasing the UV irradiance from 0.5 to 5 mW/cm^2 [413]. Under solar light, the r_i'' of GLY increased from 2 ± 0.3 · 10^{10} mol/m^2.s to 8 ± 2 · 10^{10} mol/m^2.s for the irradiance range from 10 to 70 mW/cm^2, stabilizing at 8 ± 2 · 10^{10} mol/m^2.s for irradiance > 70 mW/cm^2 (Figure 7.10 B). The increase in the rate of disappearance indicates an increase in the electron-hole formation rate. Consequently, ROS production was increased, and the removal of GLY could be increased [434]. Therefore, ROS generation is limited by photon availability. However, at higher irradiance (> 70 mW/cm^2), r_i'' was stable at 8 ± 2 · 10^{10} mol/m^2.s, which was attributed to electron-hole recombination, which makes r_i'' independent of light irradiance [434]. For AMPA, eelow 35 mW/cm^2, no degradation was observed, with r_i'' of AMPA remaining < 1 · 10^{10} mol/m^2.s. This was due to the insufficient ROS generation and the lower photodegradability of AMPA compared to GLY. Since mass transfer is likely to be a limiting factor in the photodegradation of GLY and AMPA by the PVDF-TiO_2 membrane, due to the low GLY/AMPA concentrations, flux and initial concentration were further investigated.

The small difference between UV and solar degradation was evaluated by filtration experiments using PVDF-TiO_2 membrane under the UV channel of a solar simulator at a comparable irradiance to that of the solar simulator (Figure 7.12). For easier follow-up, the removal under the UV channel of the solar simulator is presented in the corresponding solar irradiance.

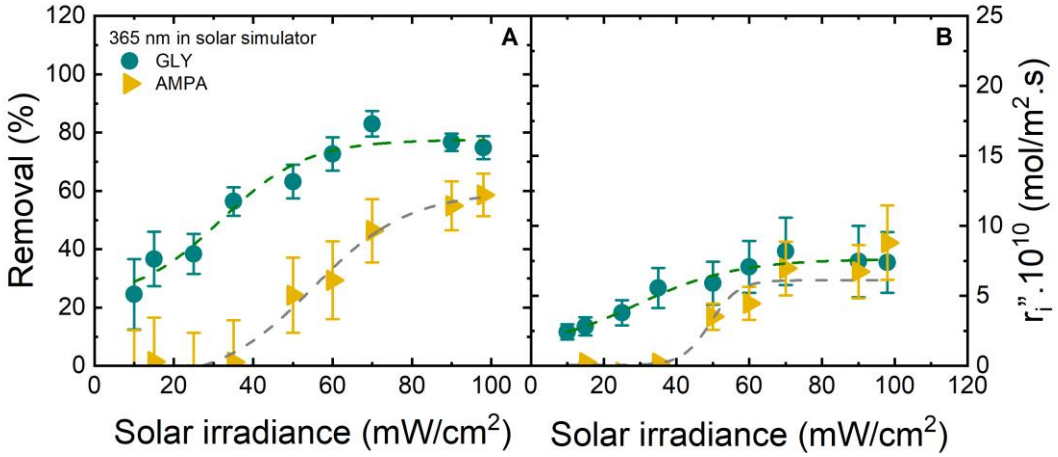

Figure 7.12. Removal (A) and rate of disappearance (r_i'') (B) of GLY/ AMPA under UV channel of the solar simulator at varied irradiance (PVDF-TiO_2, c_f (GLY/AMPA) = 1 µg/L, J_w = 600 L/m^2.h, pH 8.1 ± 0.1, and 23 ± 1°C). Adapted from [402].

The slight difference in the removal and rate of disappearance of GLY and AMPA between UV and solar was contributed by the difference in light characteristics between the UV lamp and solar simulator.

7.9 Mass transfer and hydraulic residence time

Water flux controlled the HRT and the molar flux of GLY and AMPA**.** To identify the threshold for a contact-time-independent region in GLY/AMPA removal, filtration experiments were conducted across a flux range of 60–3000 L/m^2.h (Figure 7.13). This flux range corresponds to HRT decrease from 4.5 to 0.09 seconds and a molar flux increase (that indicates the amount of herbicide brought to the membrane) from 10^{10} to 49 · 10^{10} mol/m^2.s for GLY and 10^{10} to 75 · 10^{10} mol/m^2.s for AMPA (Figure 7.4).

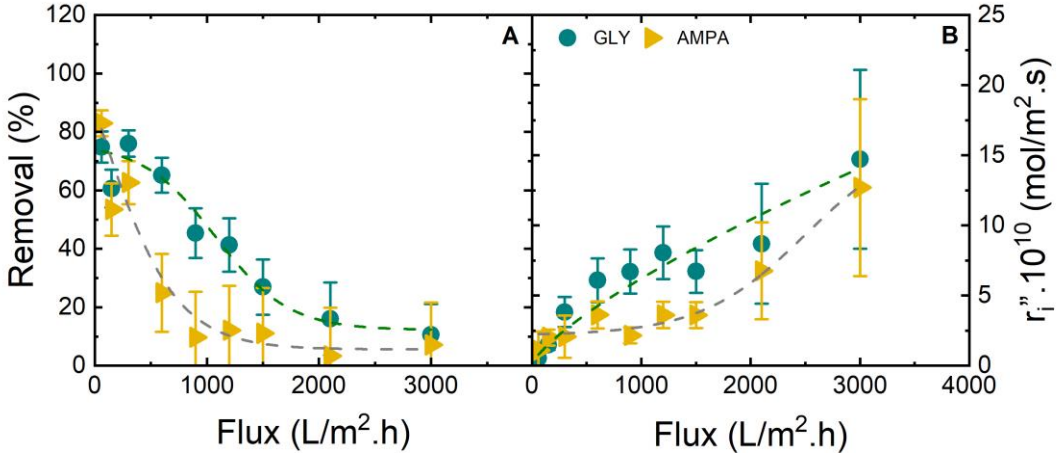

Figure 7.13. Removal (A) and rate of disappearance (r_i'') (B) of GLY/ AMPA under solar simulator at varied water flux (PVDF-TiO_2, c_f (GLY/AMPA) = 1 µg/L, I (AM1.5g 350–1150 nm) = 50 mW/cm^2, pH 8.1 ± 0.1, and 23 ± 1°C). Adapted from [402].

Both GLY and AMPA removal decreased as flux increased from 60 to 1500 L/m^2.h, then stabilized at flux levels above 2000 L/m^2.h (Figure 7.13 A), which was associated with a reduction in hydraulic residence time from 4.5 to 0.09 seconds. GLY removal decreased from 75 ± 5% to 10 ± 9% as flux increased from 60 to 1500 L/m^2.h (with hydraulic residence time decreased from 4.5 to 0.2 seconds). At flux levels below 2000 L/m^2.h, GLY r_i'' increased from 10^{10} to 10 ± 3 · 10^{10} mol/m^2.s, corresponding to an increase in molar flux from 10^{10} to 25 · 10^{10} mol/m^2.s for GLY (Figure 7.4).

Similarly, AMPA removal decreased from 82 ± 4% to 7 ± 6% as flux increased from 60 to 1500 L/m^2.h (with hydraulic residence time decreasing from 4.5 to 0.2 seconds). AMPA r_i'' increased from 10^{10} to 4 ± 1 · 10^{10} mol/m^2.s at flux below 1500 L/m^2.h, associated with a rise in molar flux from 10^{10} to 38 · 10^{10} mol/m^2.s for AMPA. The decrease in removal and the increase in the rate of disappearance r_i'' of GLY and AMPA suggested that photocatalytic reaction kinetics were not limited by the surface reaction rate but rather by mass transfer and molar flux to the membrane surface. The increase in r_i'' of GLY with flux was more pronounced compared to AMPA at flux below 1500 L/m^2.h, likely due to the higher diffusivity of AMPA (9 · 10^{-10} m^2/s at 23 °C) compared to GLY (7 · 10^{-10} m^2/s at 23 °C) [61], allowing more AMPA to pass through the membrane.

At flux levels above 2000 L/m^2.h (hydraulic residence time < 0.2 seconds), GLY and AMPA removal stabilized at 10–15 ± 9% and 5–7 ± 4 %, respectively. GLY r_i'' increased from 10^{10} to $10 \pm 3 \cdot 10^{10}$ mol/m^2.s, while AMPA r_i'' increased to $12 \pm 4 \cdot 10^{10}$ mol/m^2.s at a flux of 3000 L/m^2.h. At low hydraulic residence times (< 0.2 seconds), degradation was controlled by the surface reaction rate, a trend consistent with findings in other flow-through photocatalytic reactor studies [413, 435].

7.10 Water quality: GLY and AMPA concentration

To investigate the extent to which the removal and degradation rates of GLY and AMPA are limited by their initial concentrations, photocatalysis was performed across a wide range of concentrations (0.1—10000 µg/L), which are environmentally relevant (Figure 7.14). The HRT in these experiments is 0.5 seconds.

GLY and AMPA removal decreased (from 65 ± 6% to 5 ± 4% for GLY and from 82 ± 8% to 2 ± 2% for AMPA) as the feed concentration increased from 0.1 to 10000 µg/L (Figure 7.14). The rate of disappearance (r_i'') for both GLY and AMPA rose from $0.4 \pm 1 \cdot 10^{10}$ to $4671 \pm 597 \cdot 10^{10}$ mol/m^2.s for GLY and from $1.1 \pm 1 \cdot 10^{10}$ to $2703 \pm 373 \cdot 10^{10}$ mol/m^2.s for AMPA with an increase in feed concentration. This linear increase in r_i'' was attributed to the higher initial concentration, resulting in greater surface coverage of the photocatalyst. Therefore, the accessible surface (within the hydraulic residence time of 0.5 seconds) was a limiting factor for the photodegradation of GLY and AMPA by the PVDF-TiO$_2$ membrane.

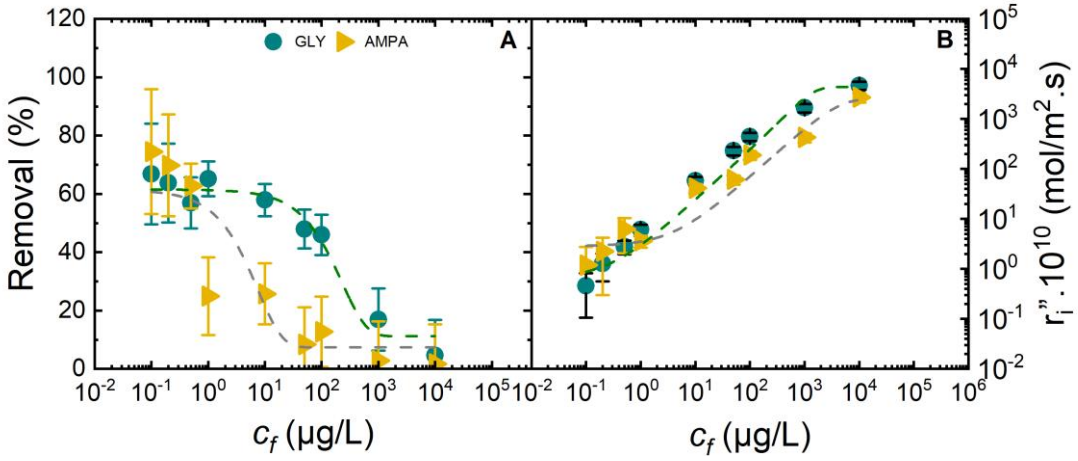

Figure 7.14. Removal (A) and rate of disappearance (r_i'') (B) of GLY/ AMPA under solar simulator at varied feed concentration (PVDF-TiO$_2$, J_w = 600 L/m^2.h, I (AM1.5g 350–1150 nm) = 50 mW/cm^2, pH 8.1 ± 0.1, and 23 ± 1°C). Adapted from [402].

At concentrations exceeding 1000 µg/L, the minimal removal of GLY and AMPA (2–5%) indicates that the PVDF-TiO$_2$ membrane had reached its maximum adsorption and photocatalytic capacity. However, r_i'' for both compounds continued to increase, reaching $4671 \pm 597 \cdot 10^{10}$ mol/m^2.s and $2703 \pm 373 \cdot 10^{10}$ mol/m^2.s, respectively, indicating that degradation was still

controlled by the feed concentration. This implies that the degradation rate was governed by the availability of micropollutant molecules in the photocatalytic membrane reactor, where mass transfer limitation was eliminated by the convection flow.

7.11 Water quality: pH of GLY/AMPA solution

The solution pH can influence the photocatalytic degradation of GLY and AMPA by altering the surface interaction between GLY/AMPA and catalysts and affecting the ROS concentration. To evaluate the extent to which the pH-dependent interaction contributes to GLY and AMPA degradation, filtration was investigated by performing photocatalysis at varied initial pH from 2 to 12 (Figure 7.15).

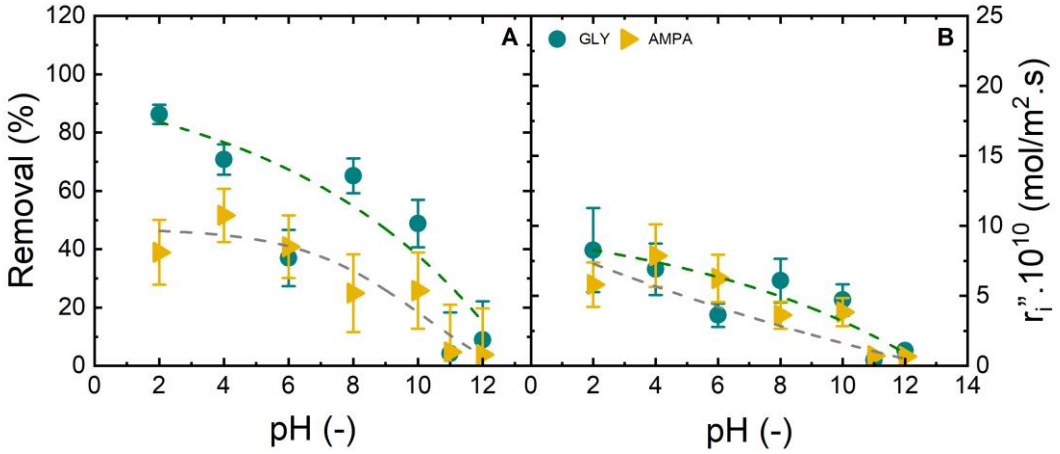

Figure 7.15. Removal (A) and rate of disappearance (r_i'') (B) of GLY/ AMPA under solar simulator at varied initial pH of feed solution (PVDF-TiO_2, c_f (GLY/AMPA) = 1 µg/L, J_w = 600 L/m^2.h, I (AM1.5g 350–1150 nm) = 50 mW/cm^2, and 23 ± 1°C). Adapted from [402].

The removal of GLY and AMPA decreased from 86 ± 3 to 4 ± 4 % for GLY and from 51 ± 9 to 3 ± 3 % for AMPA (Figure 7.15) with the increase of pH from 2 to 12 corresponding to the charge of GLY from +0 to –3 and charge of AMPA from +0 to –2 (Table S3). Meanwhile, r_i'' of GLY and AMPA decreased from 8 ± 2 · 10^{10} mol/m^2.s to 1 ± 0.2 · 10^{10} mol/m^2.s, and from 6 ± 2 · 10^{10} mol/m^2.s to 1 ± 0.2 · 10^{10} mol/m^2.s, respectively. The PVDF-TiO_2 membrane exhibited a pH_{IEP} at 3.3 [436], suggesting that it is negatively charged at pH > 3.3. Therefore, at low pH (acidic conditions), GLY and AMPA accumulate on the metal oxide surface (TiO_2 in this study) due to the electrostatic attraction [429, 437, 438]. At pH > 4, GLY and AMPA have the charge from –1 to –3 while TiO_2 has the negative charge, which induced electrostatic repulsion between GLY/AMPA and TiO_2. Moreover, the pH increase will enhance the competition of OH– with the complexation, where more OH– can form a covalent bond with TiO_2, resulting in the mononuclear monodentate between GLY/AMPA functional groups with metal (Ti) as the dominant complexation structure at high pH [429, 437]. Therefore, lower adsorption onto TiO_2 would result in lower photocatalytic degradation of GLY and AMPA by PVDF-TiO_2 membrane.

In addition, different pH would affect the formation of ROS by changing the ROS concentration. The decrease in removal at increasing pH was also observed in other research, where acidic pH was preferred for the photodegradation of GLY, favorable for the formation of •OOH, which is less reactive [191]. In batch, GLY degradation increased from 36 % to 67 % with the decrease of pH from neutral to acidic conditions, which was attributed to the more ROS formation (•OH and $•O_2^-$) [191]. At high pH, the concentration of scavenger radicals such as CO_3^{2-} and HCO_3^- may be enhanced, which leads to a decline in •OH concentration, limiting the efficiency of photo-degradation at higher pH [412].

Identifying the contribution of various ROS in the photocatalytic membrane reactor is critical for a deeper understanding of the GLY/AMPA degradation mechanism, which was then studied using different scavengers.

7.12 Identification of predominant reactive oxygen species in the degradation of GLY and AMPA

The role of key reactive species, including hydroxyl radical (•OH), superoxide radicals ($•O_2^-$), singlet oxygen ($^1O_2$), valence band holes (h_{VB}^+), was determined through scavenging experiments, in which the contribution of each species to GLY/AMPA degradation was examined based on the inhibitory effects of the scavengers (Figure 7.16).

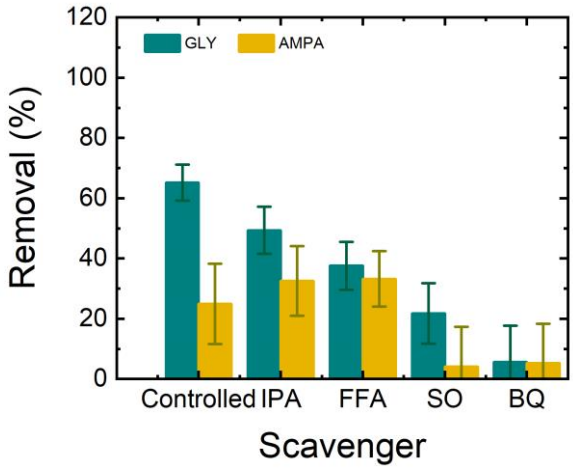

Figure 7.16. Removal of GLY/ AMPA under solar simulator with varied types of scavenger (PVDF-TiO_2, c_f (GLY/AMPA) = 1 µg/L, J_w = 600 L/m^2.h, I (AM1.5g 350–1150 nm) = 50 mW/cm^2, pH 8.1 ± 0.1, 23 ± 1°C). Adapted from [402].

The •OH scavenger, IPA, did not significantly impact the removal of GLY and AMPA, indicating that •OH did not contribute to the GLY/AMPA degradation, where the removal was 50 ± 8 % and 32 ± 10 %, respectively (Figure 7.16). This may be due to the scavenging effect of $NaHCO_3$ at a concentration (1 mM) that was 6 orders of magnitude higher than that of GLY/AMPA [439]; hence, inhibiting the photodegradation. FFA reduced the removal from 65 ± 6 to 38 ± 8 % for GLY and did not change the removal of AMPA. FFA can react with $^1O_2$

($k_{FFA,^1O_2} = 1.2 \cdot 10^8\ M^{-1}s^{-1}$) at high rates, and react with $\bullet O_2^-$ at a lower rate ($k_{FFA,\bullet O_2^-} = 3.5 \cdot 10^3\ M^{-1}s^{-1}$ [440]). The inhibited removal could be attributed to the scavenging of a small fraction of $\cdot O_2^-$ by FFA, making it difficult to clearly determine the role of $^1O_2$. In the presence of SO, the GLY/AMPA removal decreased from 65 ± 6 to 22 ± 10 % and from 25 ± 11 to 4 ± 4 %, respectively. This implied that a portion of adsorbed GLY/AMPA could be degraded directly by the h_{VB}^+ at the catalyst surface. The removal of GLY/AMPA was completely inhibited by BQ where the GLY removal was 6 ± 4 % and AMPA removal was 5 ± 4 %. Hence, $\bullet O_2^-$ appear to be the primary species contributing to the removal of GLY/AMPA.

After identifying the main reactive species, the degradation pathway of GLY and AMPA by PVDF-TiO_2 membrane would be determined.

7.13 Determination of bond dissociation enthalpy and degradation pathway

Since $\bullet O_2^-$ was identified as the dominant ROS for GLY/AMPA degradation (Figure 7.16), the final step in explaining the photodegradation was to determine potential radical attack points on GLY and AMPA molecules to understand their degradation pathways. To achieve this, the X–H (where X can be C, N, or O) and X–Y (where X and Y can be P, C, N, or O) homolytic bond dissociation enthalpies (BDEs) were calculated for each unique bond (Figure 7.17). The modelling was done by Bela Fiser at the University of Lodz. The 3D starting structures of GLY and AMPA were prepared using GaussView 6 software by Bela Fiser at the University of Lodz [441]. The protonation states were determined based on the experimental conditions (pH = 8), where the dominant species had charges of –2 for GLY and –1 for AMPA.

GLY and AMPA degradation involves the oxidation by reactive oxygen species (ROS), which can occur through two main pathways: (1) C–N bond cleavage to produce AMPA and glyoxylic acid, and (2) C–P bond cleavage to produce sarcosine, which is then degraded to glycine [267]. The latter pathway is more beneficial due to the formation of safer intermediate products [267-269]. However, the C–P bond in the phosphonic group is more thermally stable and chemically resistant [270]. The study on bond dissociation enthalpies (BDEs) showed that the weakest C–H bond in GLY is located between the amine and carboxyl group, and the corresponding BDE value is 419.2 kJ/mol. In AMPA, the weakest X–H bond is the only C–H bond in the structure with a BDE value of 431.7 kJ/mol, which is similar to the corresponding bond located in GLY [402]. The weakest X–Y bond in GLY is the C–N bond, which will produce AMPA, and an additional side product, which was also the result obtained from the photodegradation experiment (Figure 7.8).

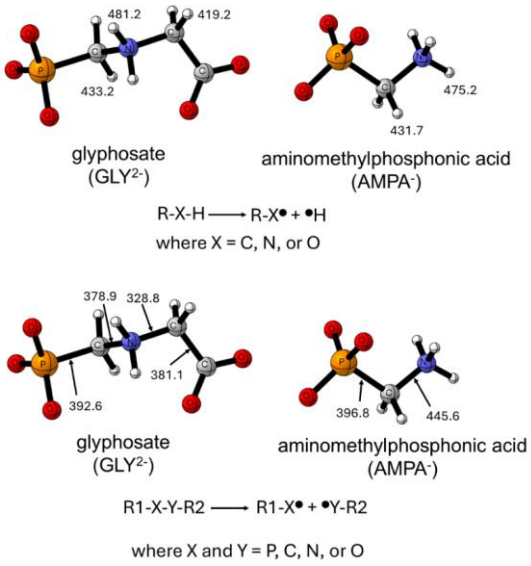

Figure 7.17. BDE (in kJ/mol) maps of GLY and AMPA at their most probable protonation state. Thermodynamic properties of the species and the corresponding radicals were determined by using the G3MP2B3 composite level of theory. BDE values (in kJ/mol) calculated by using the depicted equations for all unique bonds. The protonation states of the species were considered according to the experimental condition (pH = 8), and thus, the charge of GLY and AMPA is -2 and -1, respectively. Reprinted from [402].

Since $\bullet O_2^-$ was identified as the dominant ROS for GLY/AMPA degradation and from the BDE calculation, the degradation pathway of GLY and AMPA by PVDF-TiO_2 membrane is proposed in Figure 7.18, integrated with experimental data and insights from previous studies [433, 442].

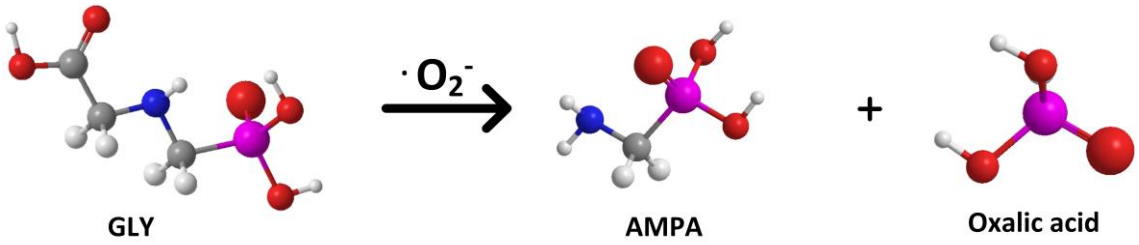

Figure 7.18. Probable glyphosate (GLY^{2-}) degradation pathway to $AMPA^-$ and oxalic acid.

Overall, GLY was degraded by PVDF-TiO_2 membrane with $\bullet O_2^-$ as the dominant ROS. AMPA was formed during the degradation, which was also found in the experiment. From the studied limiting factors, the optimization of the PVDF-TiO_2 membrane will be conducted next.

7.14 Enhanced photocatalytic degradation at optimized conditions

To evaluate whether the use of the solar simulator to activate PVDF-TiO_2 can achieve the guideline of 0.1 µg/L GLY and 0.1 µg/L AMPA in water intended for human consumption,

photocatalysis will be performed at optimized conditions (flux 60 L/m².h, solar irradiance 98 mW/cm²) (Figure 7.19).

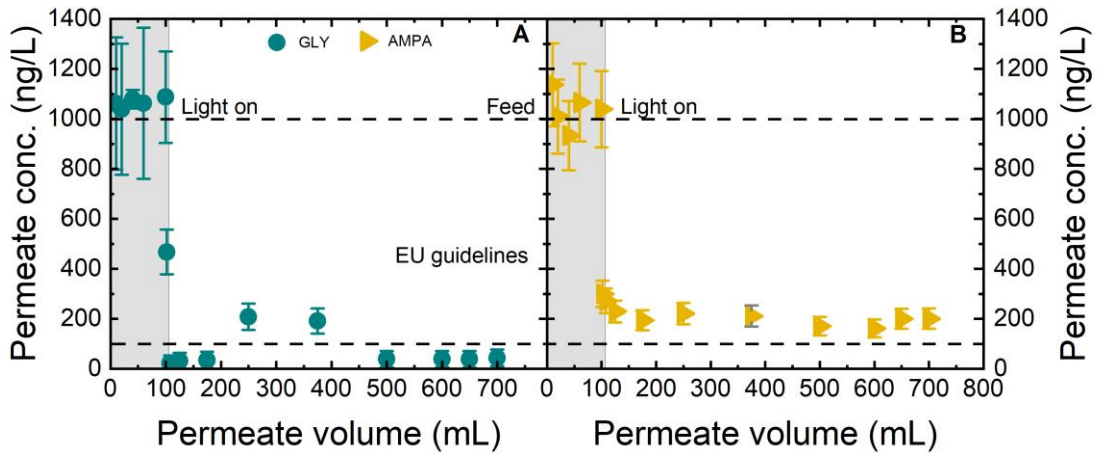

Figure 7.19. Permeate concentration of GLY (A) and AMPA (B) vs. cumulated permeate concentration at optimized conditions (PVDF-TiO₂, c_f (GLY/AMPA) = 1 µg/L, J_w = 60 L/m².h, I (AM1.5g 350–1150 nm) = 98 mW/cm², pH 8.1 ± 0.1, 23 ± 1°C). Adapted from [402].

The optimized conditions were at flux 60 L/m².h, which corresponded to the hydraulic residence time of 4.5 s and under the solar irradiance of 98 mW/cm². GLY permeate concentration was 40 ± 5 ng/L, which satisfied the EU guideline for individual herbicides (100 ng/L [13]). However, AMPA could not reach the EU guideline, with the permeate concentration of AMPA of 200 ± 23 ng/L (Figure 7.19). The total GLY and AMPA permeate concentration (300 ± 42 ng/L) was lower than EU guidelines for total herbicides (500 ng/L [13]). Therefore, photocatalytic degradation by PVDF-TiO₂ membrane in a flow-through configuration could effectively remove GLY and AMPA from water; further study on AMPA removal enhancement needs to be addressed.

7.15 Conclusions

In this chapter, GLY and AMPA were removed by photodegradation using PVDF-TiO₂ membrane under solar simulator (AM1.5g 350–1150 nm) in a flow-through configuration. The following points are obtained from this investigation.

- The photodegradation using PVDF-TiO₂ membrane under solar simulator was comparable to that under UV light, in which non-UV wavelength did not contribute to the degradation of GLY and AMPA.
- The GLY/AMPA degradation was limited by light intensity and HRT, with higher irradiance and lower HRT enhancing removal. •O_2^- was the dominant reactive oxygen species in the photodegradation of GLY and AMPA, with AMPA produced in the GLY degradation process.

- PVDF-TiO_2 membrane at optimized conditions (highest irradiance of 98 mW/cm^2, and lowest flux of 60 $L/m^2.h$) achieved 95% GLY and 80% AMPA removal.

Photocatalytic degradation using PVDF-TiO_2 membrane can degrade GLY and AMPA. However, the degradation was incomplete, where EU guidelines for herbicides were not achieved for AMPA. Moreover, degradation by-products were produced during this process, posing a challenge to further permeate treatment. Additionally, although the PVDF-TiO_2 membrane used less pump pressure, the energy for light might be excessive.

At last, four water treatment technologies will be compared for GLY and AMPA removal.

8 Conclusions and outlook

In this dissertation, after four chapters, four different water treatment technologies were evaluated, including adsorption on PBSAC, dynamic adsorption on UF–PBSAC, filtration by NF membrane, and photodegradation by PVDF-TIO_2 membrane.

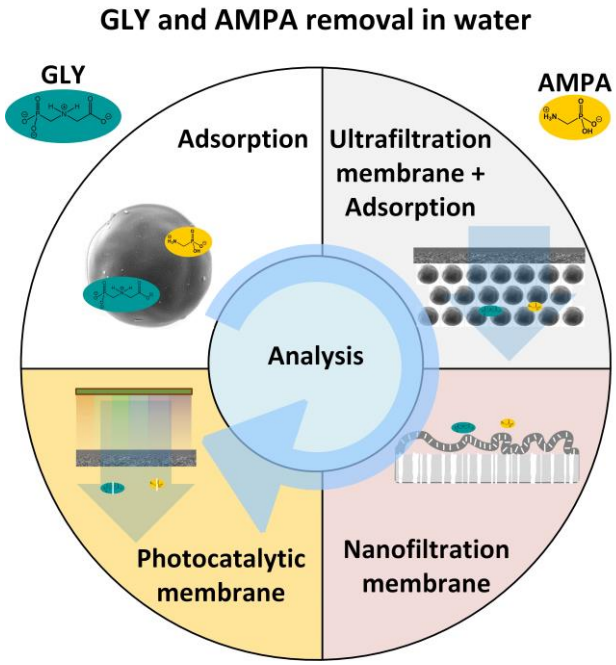

Figure 8.1: GLY/AMPA removal technologies of interest

The last target of this dissertation is to find a promising technology for GLY and AMPA removal with the following criteria in consideration.

- Evaluation of the "effectiveness": the removal efficiency of each technology and whether the EU guidelines for herbicides in water can be achieved at lab scale systems.
- Evaluation of the "sustainability": the estimated energy consumption of each technology at the optimized filtration conditions.

Next, the comparison between different technologies will be performed.

8.1 Comparison and discussions

To compare "effectiveness", permeate concentration and HRT were considered. Meanwhile, the theoretical energy consumption and the normalized theoretical energy per % removal will be evaluated for the "sustainability" with the standard experimental conditions and the optimized conditions of each technology. In detail, the list of comparison includes:

- PBSAC adsorption with PBSAC size 200 µm.
- UF–PBSAC at standard conditions: PBSAC size 78 µm, flux 100 L/m^2.h, PBSAC layer thickness of 2 mm.
- UF–PBSAC at optimized conditions: PBSAC size 78 µm, flux 25 L/m^2.h, PBSAC layer thickness of 6 mm.
- NF membrane: BW 30, NF 90, NF 270, HY 70, HY 50, HY 10.
- PVDF-TiO_2 membrane at standard conditions: highest irradiance of 50 mW/cm^2, and lowest flux of 600 L/m^2.h.
- PVDF-TiO_2 membrane at standard conditions: highest irradiance of 98 mW/cm^2, and lowest flux of 60 L/m^2.h.

All the calculations were discussed and mentioned in Chapter 2.

Firstly, to evaluate the effectiveness of each technology, the permeate concentration at the end of the experiments was compared (Figure 8.2).

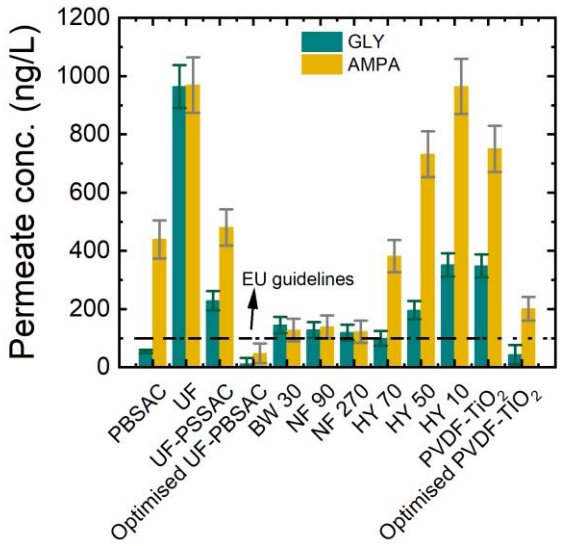

Figure 8.2. Permeate concentration at the end of the experiments, comparing the EU guidelines for herbicides (100 ng/L for each compound)

UF–PBSAC could remove GLY and AMPA effectively at optimized conditions due to the adsorption to PBSAC, when the UF membrane alone cannot remove the herbicides (Figure 8.2). The permeate concentration of filtration at optimized conditions of UF–PBSAC was lowest (12 ± 1 ng/L and 47 ± 2 ng/L for GLY and AMPA, respectively) and lower than EU guidelines for each herbicide (100 ng/L [13]). However, UF–PBSAC with less adsorbent and the higher flux cannot achieve this removal. The removal of GLY and AMPA by NF membranes was incomplete, even with the lowest MWCO membranes. The permeate concentration from the dense membrane (BW 30, NF 90, NF 270) was 110–140 ± 7 ng/L for GLY and 120–140 ± 7 ng/L for AMPA. Loose membrane (HY 70, HY 50, HY 10) could not remove GLY and AMPA effectively. The PVDF-TiO_2 membrane at optimized conditions could degrade GLY and AMPA to

the concentration of 43 ± 3 ng/L of GLY and 201 ng/L of AMPA, in which GLY concentration was lower than EU guidelines. To sum up, UF–PBSAC can remove most GLY and AMPA.

To evaluate the potential of filtration technologies in this dissertation, the pure water permeability and HRT of each membrane system were compared (Figure 8.3). PBSAC, which was in static adsorption, will not be considered.

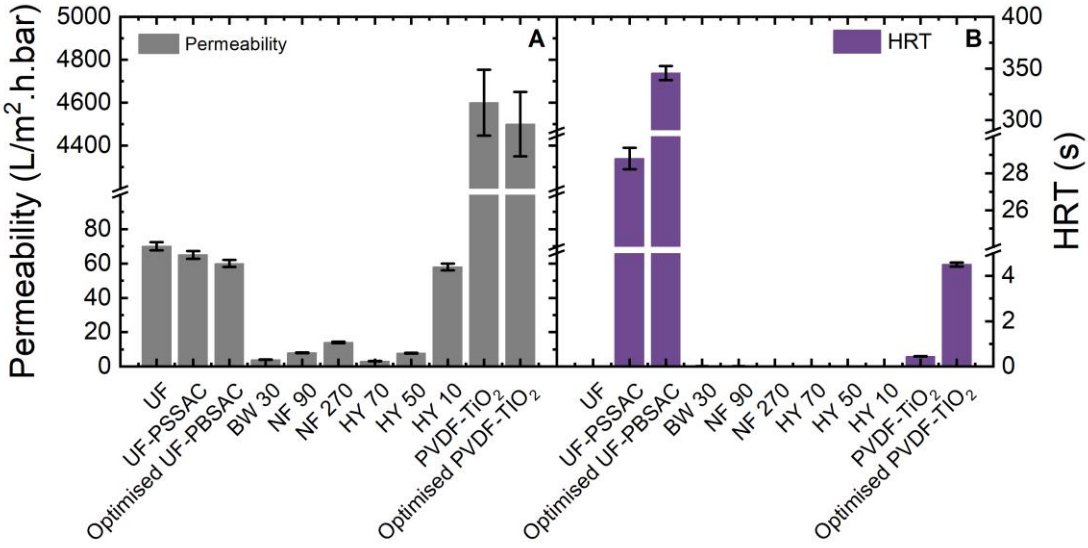

Figure 8.3. Pure water permeability (A) and HRT (B) of the filtration system

The HRT is related to the removal efficiency, which was discussed in Figure 8.2, while the permeability of the filtration membrane is related to the amount of permeate that can be produced. The permeability of the filtration membrane increased with membrane types from dense NF to loose NF, to UF and UF–PBSAC, to PVDF-TiO_2 membrane. With the permeability of 60–70 L/m^2.h, the highest HRT was in UF–PBSAC, where the HRT at the optimized conditions was 346 s, enhancing the adsorption of GLY and AMPA to PBSAC, making UF–PBSAC the most effective technique. For NF membranes, HRT, which is related to the adsorption of GLY/AMPA on the membrane, was low (< 0.01 s). This low HRT explains why the adsorption on the NF membrane was low in Chapter 6. It is noted that the main rejection mechanism of NF was size, charge, and dielectric exclusion. For the membrane with the highest permeability (4500–4600 L/m^2.h), the HRT was 0.5 s at the optimized conditions. At this HRT, the GLY and AMPA removal was incomplete, suggesting that the photocatalytic membrane requires significantly lower flux to achieve efficient removal.

Finally, to compare the energy needed for each technology, the theoretical energy and theoretical energy required for removal was evaluated in Figure 8.4. It is noted that theoretical considerations are used as the foundation, but this cannot be directly translated to larger-scale conditions, where membrane fouling, cleaning, and maintenance need to be considered.

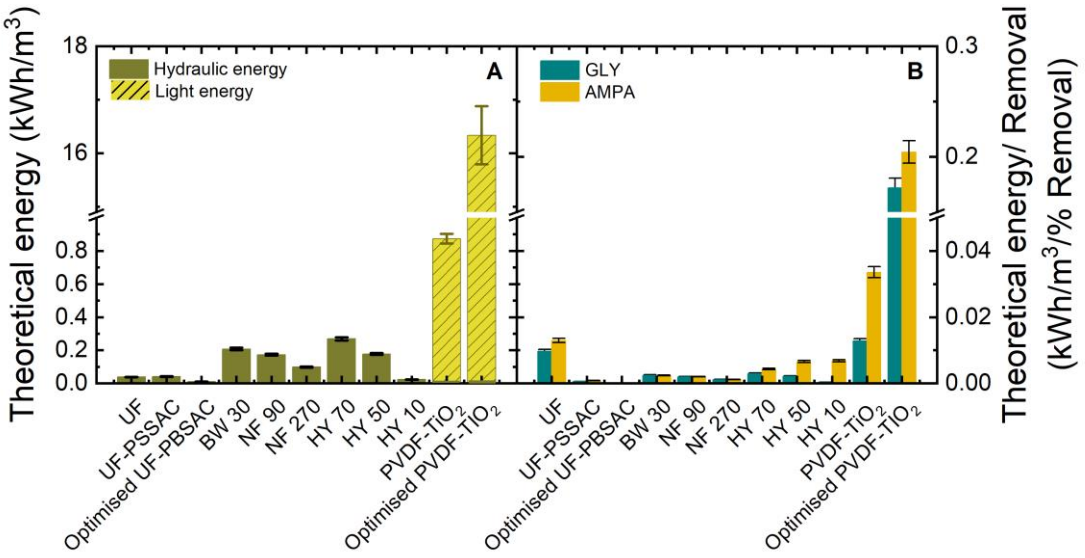

Figure 8.4. Permeate concentration at the end of the experiments, comparing the EU guidelines for herbicides (100 ng/L for each compound)

UF–PBSAC consumed the lowest theoretical energy among all technologies in this dissertation. The total theoretical energy consumption was 0.01–0.03 kWh/m^3, which was comparable to the reported energy for ozonation for micropollutant removal (depending on ozone dose) [284]. The optimized UF–PBSAC, which could remove most GLY/AMPA, needed 0.01 kWh/m^3 for operation. NF membranes required more energy, with the theoretical energy of 0.1–0.3 kWh/m^3 to remove 70–80% GLY and AMPA. In the PVDF-TiO_2 membrane, the hydraulic energy was low due to the high permeability of this membrane. However, the energy required for light was high, especially for optimized conditions (light intensity of optimized conditions at 98 mW/cm^2), which was 16.3 ± 0.5 kWh/m^3, making it the highest theoretical energy consumption. It is noted that these data are theoretical energy, which assumes full performance of the pump and light source (Chapter 2). When considering theoretical energy consumption and removal (Figure 8.4B), UF–PBSAC appears to be the most promising technology, removing 98% GLY and 95% AMPA (EU guidelines for herbicides achieved) at a low transmembrane pressure < 2 bar (low energy consumption).

8.2 Summary and conclusions

In this dissertation, herbicides GLY and AMPA were investigated for analysis and removal, which remain a challenge for water management. Therefore, the target is to evaluate the removal efficiency of different technologies for treating herbicides in water to meet EU guidelines (100 ng/L for individual herbicides and 500 ng/L for total herbicides) [12, 13].

Chapter 2 is a literature review on the properties and occurrence of GLY and AMPA in the water environment. Due to the extensive usage of GLY in agriculture and industry, GLY and its metabolite AMPA were found in surface and ground water at the level of 0.2–370 µg/L in groundwater and surface water [30, 92-94]. GLY can occur in some water bodies in much

higher concentrations *i.e.*, milligrams per liter [67]. This has raised the question of how to treat GLY and AMPA in water. Chapter 2 discussed the current water treatment technologies for micropollutants, GLY/AMPA removal. The four technologies were focused on: adsorption, hybrid adsorption–membrane, membrane filtration, and photocatalytic membrane. Each technology was reviewed with new research, advantages, and disadvantages. Additionally, the method to compare different water treatment technologies was reviewed for the final comparison.

To study GLY/AMPA removal, the analysis was required that enabled the studies on a lab scale for water treatment technologies. However, the analysis of GLY and AMPA was challenging due to the complex physicochemical properties of the herbicides and the low LOD, which is in the environmentally relevant concentration. Therefore, in **Chapter 3**, the first challenge is to analyze these two herbicides in water. The current analytical methods and the challenges in the measurement of GLY and AMPA were highlighted in Chapter 2. From these current analytical techniques, the first step was to develop the analytical method for GLY and AMPA in water using LC-MS/MS. The systematic problem identification and solving were conducted for method development. The target is to analyze GLY and AMPA in water at low concentration, requiring low injection volume and no derivatization step. After review, the developed analytical method had the LOD of 10 ng/L, needed injection volume of 100 µL, and required no derivatization step.

From chapter 4 to chapter 7, four different technologies were investigated for the removal efficiency of GLY and AMPA from the environmentally relevant concentration (1000 ng/L) in water (Figure 8.5).

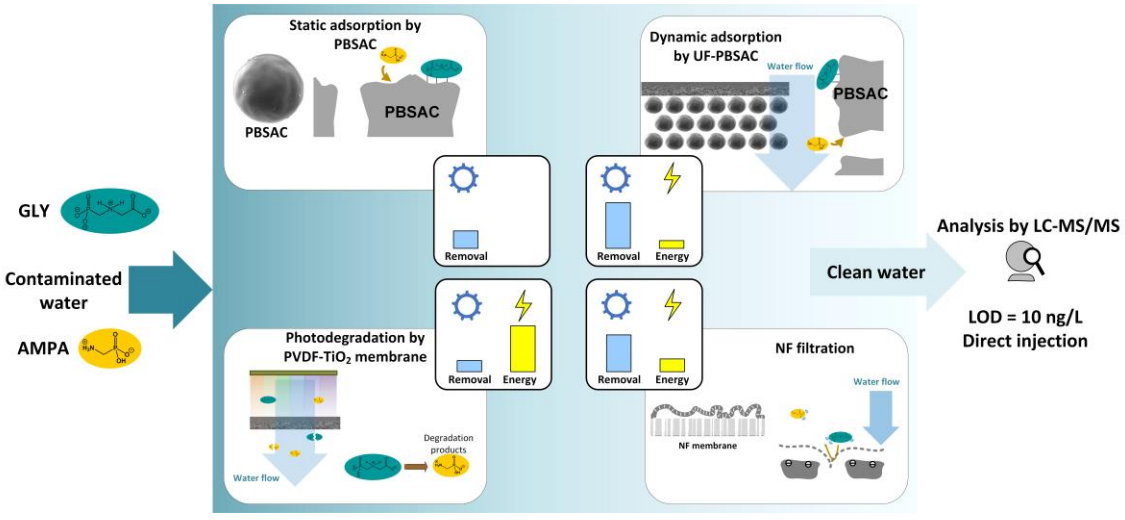

Figure 8.5: Schematic of water treatment technologies for GLY and AMPA removal with comparison of removal and energy

Chapter 4 investigated the removal of GLY and AMPA by PBSAC in static adsorption. The adsorption of GLY and AMPA at environmentally relevant concentrations from water by PBSAC was achievable, with 95% GLY and 57% AMPA removed at a PBSAC dose of 0.5 g/L from an initial concentration of 1000 ng/L. GLY was adsorbed more than AMPA due to the higher affinity towards PBSAC. The maximum adsorbed mass of PBSAC was 78 mg/g GLY and 1.3

mg/g AMPA. To understand the adsorption of GLY and AMPA on PBSAC, a systematic evaluation of material properties, operational factors, and water chemistry was performed. PBSAC size, activation level, and surface oxygen content were the PBSAC material properties under consideration. Both the external and internal surfaces contributed to GLY and AMPA adsorption, although only a part of the PBSAC surface is available for adsorption of the charged herbicides. When the external surface area increases by varying PBSAC size, GLY and AMPA adsorption only slightly enhanced. However, when the internal surface area increased by varying pore volume, a significant increase in adsorption was observed. The adsorption of GLY and AMPA was also controlled by water chemistry, where GLY and AMPA adsorbed on PBSAC via hydrogen bonding and van der Waals interaction, and was hindered by the hydration layer. In summary, adsorption by PBSAC could achieve the EU guideline concentration for GLY, but the AMPA concentration was still higher than the EU guideline.

In **Chapter 5**, PBSAC was integrated with the UF membrane for GLY and AMPA dynamic adsorption. GLY and AMPA can be effectively adsorbed by UF–PBSAC dynamically within a short HRT (5–115 s). In this system, PBSAC is in charge of adsorbing GLY and AMPA while UF acts as a barrier to remove organic matter, bacteria, viruses, and particulates, which can interfere with the adsorption. With a 2 mm layer of PBSAC, UF–PBSAC can remove 77% of GLY and 52% of AMPA, which was lower than in static adsorption. This finding indicates that adsorption sites limit the adsorption. Both surface area and HRT play an important role in the adsorption. More surface area provides more adsorption sites, leading to higher removal of GLY and AMPA. Meanwhile, HRT allows GLY and AMPA to diffuse into PBSAC pores. The limiting factors were minimized at the optimized conditions (small PBSAC size 78 µm, low flux 25 $L/m^2.h$, and high PBSAC layer thickness 6 mm). Under these conditions, 98% GLY and 95% AMPA were removed by UF–PBSAC, in which EU regulation was met. Moreover, this system can perform high removal at low pressure (energy) (in the comparison in Chapter 8). As UF–PBSAC has proven the efficiency in removing GLY and AMPA, NF can be an alternative option.

NF was applied for GLY and AMPA rejection in **Chapter 6**. The rejection efficiency and transport of GLY and AMPA in NF membranes were evaluated using six membranes (BW 30, NF 90, NF 270, HY 70, HY 50, HY 10) covering a range of MWCO from 80 Da to 3000 Da. NF membrane can partially remove GLY and AMPA due to size exclusion, Donnan exclusion, and dielectric exclusion. Size exclusion was dominant in the filtration of the membrane at low MWCO (< 150 Da), with 90% GLY/AMPA removed. In the membrane with MWCO > 200 Da, Donnan exclusion and dielectric exclusion were more dominant. The Debye length and pore radius of the membrane showed that Donnan exclusion would always happen with all membrane pore sizes in the range of 80 to 3000 Da. The removal was enhanced by the increase in pH under the effect of Donnan exclusion and dielectric exclusion. Donnan exclusion at low pH had a lower contribution to the rejection, as GLY and AMPA have a neutral charge. Meanwhile, at higher pH, membrane charge becomes more negative, and the charge of GLY and AMPA is also more negative, enhancing the charge repulsion between GLY/AMPA and the membrane. Moreover, the dielectric exclusion was also stronger at higher pH, leading to stronger rejection of GLY and AMPA. NF 90 and NF 270 membranes can remove ~ 90%, while HY 50 can remove 83% at higher pH. The rejection of GLY and AMPA was lower with higher flux. The

transport of GLY and AMPA through the membrane is contributed by concentration and dehydration. For NF 90 and NF 270, concentration polarization increased at higher flux, while the contribution of dehydration could not be quantified. For HY 50, higher flux provided more energy for dehydration, letting GLY and AMPA pass through the membrane.

Chapter 7 studied the photocatalytic degradation of GLY and AMPA using PVDF-TiO_2 membrane under simulated solar irradiation in a continuous flow-through configuration. The removal of GLY and AMPA under solar simulator (AM1.5G, 350–1150 nm) was comparable to that under UV light (365 nm), in which non-UV wavelength did not contribute to the degradation of GLY and AMPA. 65% GLY and 25% AMPA were removed from the feed concentration of 1000 ng/L. To determine the optimized conditions, the limiting factors were investigated, in which light intensity and HRT were found to control the photodegradation. GLY and AMPA removal increased significantly with the increase of solar irradiance, while lower HRT enhanced the removal. The scavenger revealed that $\bullet O_2^-$ and h_{VB}^+ were the dominant ROS in the photodegradation of GLY and AMPA. Moreover, AMPA was found in the experiment of individual GLY, implying the formation of AMPA during GLY photodegradation, which was later confirmed by BDE calculation.

At last, the comprehensive comparison between four water treatment technologies was conducted for GLY and AMPA removal. While NF can partially remove GLY and AMPA, but requiring high pressure, the highest energy requirement was from the PVDF-TiO_2 membrane. The removal of the PVDF-TiO_2 membrane was incomplete; moreover, higher energy was needed for light irradiation. When considering energy and removal, UF–PBSAC appeared to be the most promising technology that achieved the EU guidelines for herbicides with low transmembrane pressure. However, the low flux was the drawback of this technology.

8.3 Outlooks

In this dissertation, the investigation on the removal of GLY and AMPA in water is limited to the lab scale. With the target of effectively and sustainably removing these herbicides, additional work will be needed.

The studied technologies in this dissertation have their own advantages and disadvantages. More studies to minimize the disadvantages of each technique should be considered. For UF–PBSAC, although the removal was efficient, the flux was too low (25 $L/m^2.h$) for real application in water treatment. An adsorbent with a larger pore volume could be beneficial, as the adsorption of GLY and AMPA on PBSAC was also controlled by the internal surface area. Ion exchange can be an option, as GLY and AMPA are highly charged; the interaction between GLY/AMPA and ion exchange is expected to happen. Other technologies can also be considered, such as the electrocatalytic membrane that has less energy consumption than the photocatalytic membrane [288]. Additionally, the adsorbent regeneration and membrane cleaning should be considered in future studies.

This dissertation investigated the removal of GLY and AMPA in water under laboratory-controlled conditions. The next step is to investigate the removal efficiency in real water, where

water matrices are complex. The interaction of GLY and AMPA will be varied as those hydrophilic compounds are known to bind with colloids and metal ions (Ca^{2+}, Mg^{2+}, Fe^{3+}, and Al^{3+}), depending on pH [51, 443, 444], which adds further challenges to the removal process.

As the investigation was done in a lab-scale system, which was limited to under 1 L of filtration, upscaling the system is needed in the next work for long-term filtration. In this dissertation, UF–PBSAC has not reached the adsorption equilibrium, which makes the evaluation of adsorption incomplete. A continuous system for UF–PBSAC can be designed for GLY and AMPA removal.

A take-home message of the dissertation is shown in Figure 8.6.

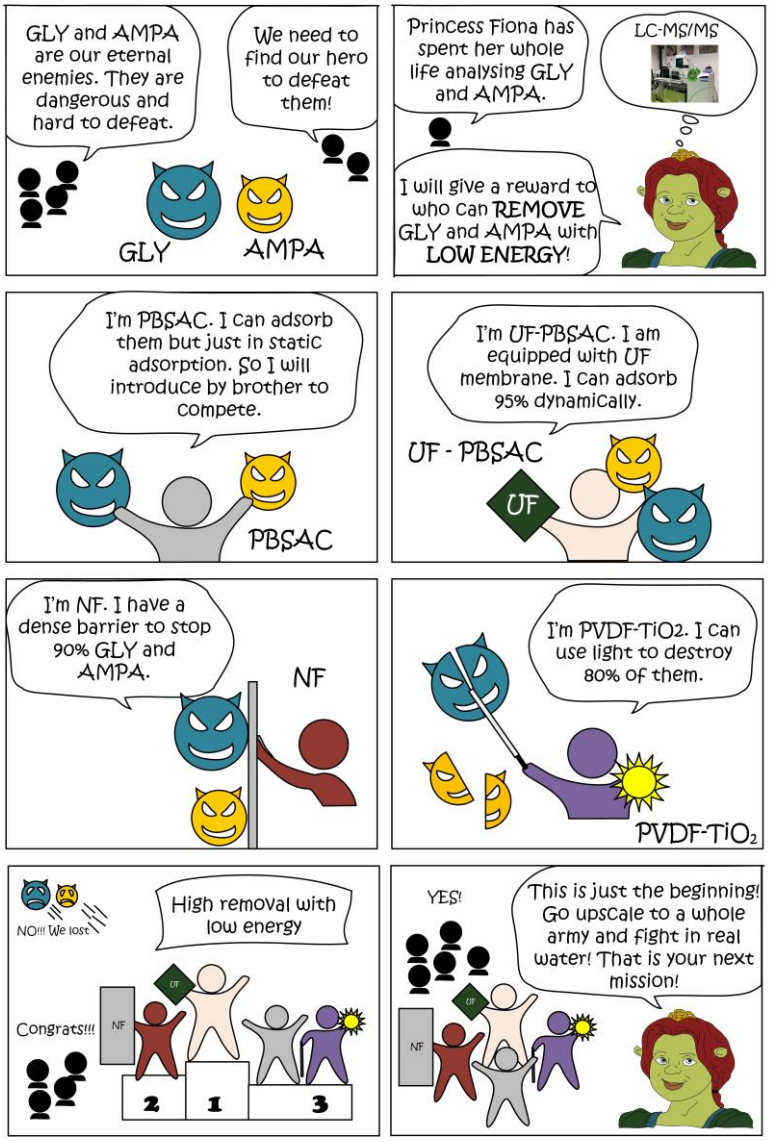

Figure 8.6. Summaries of the dissertation. Illustrated by P.T.

9 Appendices

9.1 Kinetics of GLY and AMPA adsorption by PBSAC

The PBSAC dose varied between 0.1 and 10 g/L with a constant GLY and AMPA concentration of 1 µg/L to evaluate the kinetics of GLY and AMPA adsorption.

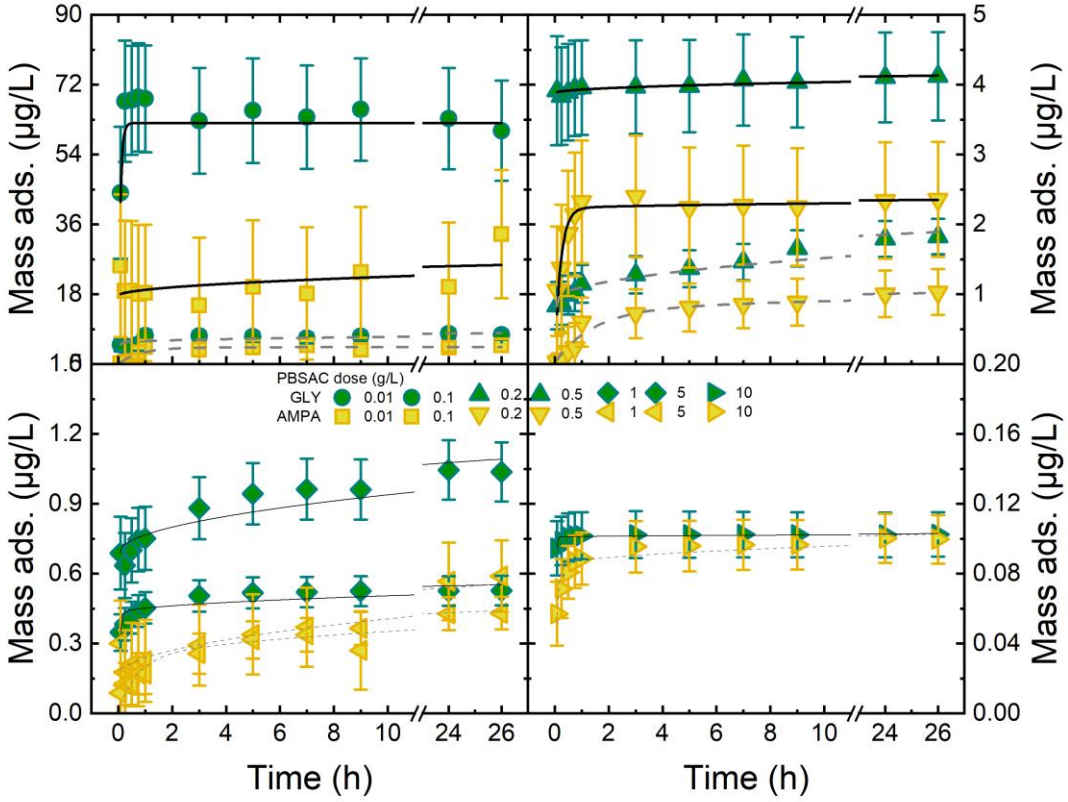

Figure 9.1: Specific adsorbed mass of GLY and AMPA as a function of time and PBSAC dose with pseudo-second-order kinetics model fit (PBSAC 200 µm, initial GLY/AMPA concentration 1 µg/L, 1mM $NaHCO_3$, 10 mM NaCl, 20 °C, 260 rpm, pH 8.1 ± 0.1)

The adsorption process was fast for GLY when the equilibrium concentration was reached in 6 h, while AMPA adsorption was slower to reach equilibrium at 9−24 h. The adsorption equilibrium is reached faster at a higher PBSAC concentration because of a more accessible surface. The second-order kinetics model was fit with the mass adsorbed of GLY and AMPA with the PBSAC dose. The first- and second-order kinetics and intra-particle diffusion constants, along with the respective R^2 values, are given in the following tables.

The first- and second-order models could fit the kinetics, while the intra-particle diffusion model did not fit the data. The fit of first- and second-order models indicates that adsorption is driven by the amount of contaminant taken up or disappearing from the bulk phase. Intra-particle diffusion does not fit, so it is not the exclusive transport mechanism.

Table 9.1: First- and second-order kinetics and intra-particle diffusion constants and R^2 values of GLY adsorption by PBSAC. k_1: first order, k_2: second order, k_d: diffusion.

PBSAC concentration (g/L)		0.01	0.1	0.2	0.5	1	5	10
Pseudo-first order	k_1 (1/h)	14 ± 2	4.3 ± 1	46 ± 15	2 ± 0.6	13 ± 7	11 ± 3	32 ± 2
	R^2	0.8	0.2	0.1	0.5	0.1	0.4	0.8
Pseudo-second order	k_2 (g/µg.h)	0.7 ± 0.3	1.4 ± 0.6	61 ± 32	2.1 ± 0.8	12 ± 5	30 ± 7	1361 ± 63
	R^2	0.4	0.5	0.3	0.7	0.6	0.8	0.9
Intra-particle diffusion	k_d (µg/g.h$^{0.5}$)	− 0.4 ± 1.0	0.5 ± 0.1	0.05	0.20 ± 0.01	0.08 ± 0.01	0.03 ± 0.01	7 ± 3
	R^2	0.01	0.5	0.8	0.9	0.8	0.7	0.3

Table 9.2: First- and second-order kinetics and intra-particle diffusion constants and R^2 values of AMPA adsorption by PBSAC. k_1: first order, k_2: second order, k_d: diffusion.

PBSAC concentration (g/L)		0.01	0.1	0.2	0.5	1	5	10
Pseudo-first order	k_1 (1/h)	Not fit	1.2 ± 0.4	4.3 ± 0.5	0.5 ± 0.1	1.1 ± 0.6	0.5 ± 0.1	7.6 ± 1.6
	R^2	Not fit	0.8	0.8	0.9	0.2	0.8	0.7
Pseudo-second order	k_2 (g/µg.h)	1	0.3 ± 0.1	3.5 ± 0.6	0.6 ± 0.1	2.3 ± 1.8	1.6 ± 0.4	132 ± 15
	R^2	0.5	0.8	0.9	0.9	0.3	0.9	0.9
Intra-particle diffusion	k_d (µg/g.h$^{0.5}$)	1.6 ± 0.8	0.7 ± 0.2	0.1 ± 0.06	0.2 ± 0.03	0.08 ± 0.01	0.07 ± 0.01	0.005 ± 0.001
	R^2	0.3	0.5	0.4	0.7	0.8	0.9	0.5

9.2 Fitting parameters of the adsorption models

Influence of PBSAC size on adsorption–kinetic parameters

The second-order kinetics constants and R^2 values of GLY and AMPA adsorption by PBSAC at different sizes are shown in Table 9.3 to determine the impact of activation on the kinetics of the adsorption.

Table 9.3: Second-order kinetics constants and R^2 values of GLY and AMPA adsorption by PBSAC at different activation levels.

PBSAC size (µm)		78	200	380	450	475	580	625
GLY	k_2 (g/µg.h)	52 ± 29	2.1 ± 0.9	2.5 ± 0.9	1.8 ± 0.6	2.1 ± 0.6	0.7 ± 0.2	0.7 ± 0.2
	R^2	0.1 *	0.69	0.7	0.7	0.8	0.9	0.9
AMPA	k_2 (g/µg.h)	20 ± 10	0.6 ± 0.1	0.3 ± 0.1	0.10 ± 0.06	0.10 ± 0.06	0.40 ± 0.08	0.6 ± 0.1
	R^2	0.2 *	0.95	0.9	0.8	0.8	0.9	0.9

* R^2 is low because the data points are on a horizontal line, as the adsorption equilibrium was reached in less than 5 min.

The kinetic rate constant (k_2) is high with PBSAC 78 µm as adsorption equilibrium was achieved in less than 10 min, and shows insignificant trend with PBSAC sizes of 200–625 µm (k_2 varied at around 0.5–3 g/µg.h for GLY and 0.05–0.7 g/µg.h for AMPA).

Influence of PBSAC activation level and internal surface on adsorption–kinetic parameters

The second-order kinetics constants and R^2 values of GLY and AMPA adsorption by PBSAC at different activation levels are shown in Table 9.4 to determine the impact of activation on the kinetics of the adsorption.

Table 9.4 Second-order kinetics constants and R^2 values of GLY and AMPA adsorption by PBSAC at different activation levels

Activation level		A1	A2	A3	A4	A5	A6
GLY	k_2 (g/µg.h)	-	4 ± 1	3.2 ± 1.9	0.5 ± 0.2	0.4 ± 0.1	0.3 ± 0.1
	R^2	-	0.8	0.4	0.8	0.9	0.9
AMPA	k_2 (g/µg.h)	152 ± 120	0.3 ± 0.1	1.7 ± 0.5	0.20 ± 0.04	0.2 ± 0.1	0.07 ± 0.02
	R^2	0.07 *	0.91	0.85	0.94	0.87	0.94

* R^2 is low because the data points are on a horizontal line, as the adsorption equilibrium was reached in less than 5 min.

It can be seen that k_2 decreased with the increase of activation levels, which means the adsorption was slower.

Table 9.5: Intra-particle diffusion kinetics constants and R^2 values of GLY and AMPA adsorption by PBSAC at different activation levels

Activation level		A1	A2	A3	A4	A5	A6
GLY	k_2 (g/µg.h)	0.003 ± 0.002	0.1 ± 0.02	0.2 ± 0.005	0.3 ± 0.02	0.3 ± 0.03	0.4 ± 0.02
	R^2	0.07 *	0.8	0.9	0.9	0.9	0.9
AMPA	k_2 (g/µg.h)	−0.01 ± 0.01	0.08 ± 0.005	0.1 ± 0.01	0.2 ± 0.01	0.2 ± 0.01	0.3 ± 0.01
	R^2	0.05 *	0.9	0.8	0.9	0.9	0.9

* R^2 is low because the data points are on a horizontal line, as adsorption equilibrium was reached in less than 5 min.

Meanwhile, the adsorption kinetics start to fit with intra-particle diffusion and rate constants, k_d, increase with the higher activation level (higher internal surface area).

9.3 Theoretical adsorption of UF–PBSAC

The theoretical maximum adsorbed mass of GLY and AMPA to different PBSAC sizes (78–625 µm) was calculated.

Table 9.6: Theoretical GLY and AMPA mass adsorption monolayer with different PBSAC sizes.

Particle size (µm)	78	200	380	475	580	625
Mass in 2 mm thick UF–PBSAC layer (g)	3.9	3.4	3.4	3.6	3.4	3.8
Total surface area (according to BET model for Ar adsorption) (m^2)	4831	4882	4913	4913	5131	1692
External surface (presuming particle porosity 0.4) in m^2 [207]	217	88	47	41	34	27
Internal surface in m^2	4614	4794	4866	4872	5097	4665
Theoretical GLY maximum adsorbed mass monolayer (mg)	4509	4557	4585	4585	4789	4379
Theoretical AMPA maximum adsorbed mass monolayer (mg)	4742	4792	4822	4822	5035	4603

The theoretical GLY and AMPA maximum adsorbed mass by UF–PBSAC was >4500 mg for all PBSAC sizes. Compared with the observed GLY and AMPA mass adsorbed in this study, the maximum adsorbed mass was lower than the theoretical maximum adsorbed mass. The theoretical maximum adsorbed mass of GLY and AMPA to different PBSAC layer thicknesses could be estimated in Table 9.7.

Table 9.7: Theoretical GLY and AMPA mass adsorption monolayer with different PBSAC layer thickness.

PBSAC layer thickness (g/L)	1	2	3	4	5	6
Total surface area (according to BET model for Ar adsorption) (m^2)	1680	4882	7381	9850	12292	14762
External surface (presuming particle porosity 0.4) in m^2 [207]	30	88	133	178	222	267
Internal surface in m^2	1650	4794	7248	9672	12070	14495
Theoretical GLY maximum adsorbed mass at the external surface (mg)	28	82	125	166	207	249
Theoretical GLY maximum adsorbed mass at the internal surface (mg)	1540	4475	6764	9029	11266	13530
Theoretical GLY mass adsorption monolayer (mg)	1568	4557	6889	9195	11473	13779
Theoretical AMPA maximum adsorbed mass at the external surface (mg)	30	87	131	175	218	262
Theoretical AMPA maximum adsorbed mass at the internal surface (mg)	1619	4705	7113	9494	11847	14227
Theoretical AMPA mass adsorption monolayer (mg)	1649	4792	7244	9669	12065	14489

The amount of GLY and AMPA in water (900 ng) was much lower than that which could be theoretically adsorbed by PBSAC (> 1500 mg). Therefore, the total PBSAC surface was not likely a limiting factor to GLY/AMPA adsorption.

9.4 Filtration protocol

The filtration protocol for three filtration system were summarized in Table 9.8, Table 9.9, and Table 9.10.

NF filtration protocol

Table 9.8: NF membrane filtration protocol

No.	Step	Conditions (duration, volume, pressure, flow…)	Justification
1	Membrane conditioning	Soaking the membrane coupon in NaCl 10 mM solution for 1 hour	Soaking in NaCl enhances opening of the pores and swelling of the active layer due to the interaction of electrolytes with the polyamide layer [368].
2	Mounting the membrane in the cell	Mount the membrane coupon at the bottom of the cell with the shiny side facing the inside of the cell	The shiny side is the active layer of the membrane and must be in contact with the feed solution within the membrane cell
3	Fixing the pressure	Open the pressure gauge and adjust the pressure at 9.6 bar. Close the pressure valve on the top of the cell and open the manual on-off valve to allow the synthetic air to flow within the cell	
4	Compaction	Filtration of MilliQ water for 1 hour at 9.6 bar	Membrane is fully wet by water and adjusted to operate at the maximum pressure of the experimental protocol (highest operative pressure of the stirred cell is 10 bar)
5	Pure Water Flux (before)	Filtration of MilliQ water for 20-30 minutes at the pressure 1, 5, and 9.6 bar	Measure membrane permeability.
7	Remove water from the bottom of the cell	Use a syringe to take out remaining water in the plastic tube of the permeate and bottom of the cell	The residual water in the bottom of the cell dilutes the hormone concentration in the initial permeate
6	Filtration of hormone solution	GLY/AMPA concentration in the permeate is measured at different flux values. Fixed stirrer speed: 400 Feed volume: 800 mL Sample: collect 5 permeate samples of 20 mL each (until 100 mL), then 5 permeate samples of 100 mL each Temperature: 22.1 (±0.5) °C Feed composition: 1000 ng/L GLY/AMPA in a background solution (10 mM NaCl, 1 mM $NaHCO_3$) Filtration time: after filtering 600 mL	Breakthrough curve phenomenon is observed in NF due to adsorption of GLY/AMPA on the membrane until saturation equilibrium is reached. This adsorption results in variable GLY/AMPA retention as diffusion through the membrane occurs after membrane saturation .
7	Remove the pressure within the cell and empty the cell	Close the on-off valve and open the pressure valve; and let the remaining synthetic air to flow out; when the pressure is zero in the pressure close all the valves and dismount the cell; take the retentate (about 100 mL) to measure conductivity and fill the cell with MilliQ water (about 400 mL)	
8	Pure Water Flux (after)	Filtration of MilliQ water for about 20-30 minutes at the same pressure used before the experiment	Compare permeability before and after the filtration experiments. In this protocol permeability does not change

UF–PBSAC filtration protocol

Table 9.9: UF–PBSAC membrane filtration protocol

No.	Step	Conditions (duration, volume, pressure, flow…)	Justification
1	Membrane conditioning	Soaking the membrane coupon in Milli-Q solution for 1 hour	
2	Prepare PBSAC layer	Put the stainless steel porous 'rings' with the suitable thickness in on the porous support in the bottom part of the stirred cell. Weight PBSAC and load on them on the porous support.	
2	Mounting the membrane in the cell	Mount the membrane coupon at the bottom of the cell with the shiny side facing the inside of the cell	The shiny side is the active layer of the membrane and must be in contact with the feed solution within the membrane cell
3	Fixing the pressure	Open the pressure gauge and adjust the pressure at 1.4 bar. Close the pressure valve on the top of the cell and open the manual on-off valve to allow the synthetic air to flow within the cell	
4	Compaction	Filtration of MilliQ water for 1 hour at 1.4 bar	Membrane is fully wet by water and adjusted to operate at the maximum pressure of the experimental protocol
5	Pure Water Flux (before)	Filtration of MilliQ water for 20-30 minutes at the pressure 1, 3, and 5 bar	Measure membrane permeability.
7	Remove water from the bottom of the cell	Use a syringe to take out remaining water in the plastic tube of the permeate and bottom of the cell	The residual water in the bottom of the cell dilutes the hormone concentration in the initial permeate
6	Filtration of hormone solution	GLY/AMPA concentration in the permeate is measured at different flux values. Feed volume: 700 mL Sample: 6 permeate samples of 100 mL each Temperature: 22.1 (±0.5) °C Feed composition: 1000 ng/L GLY/AMPA in a background solution (10 mM NaCl, 1 mM $NaHCO_3$) Filtration time: after filtering 600 mL	Breakthrough curve phenomenon is observed in NF due to adsorption of GLY/AMPA on the membrane until saturation equilibrium is reached. This adsorption results in variable GLY/AMPA retention as diffusion through the membrane occurs after membrane saturation [445-448].
7	Remove the pressure within the cell and empty the cell	Close the on-off valve and open the pressure valve; and let the remaining synthetic air to flow out; when the pressure is zero in the pressure close all the valves and dismount the cell; take the retentate (about 100 mL) to measure conductivity and fill the cell with MilliQ water (about 400 mL)	
8	Pure Water Flux (after)	Filtration of MilliQ water for about 20-30 minutes at the same pressure used before the experiment	Compare permeability before and after the filtration experiments. In this protocol permeability does not change

Photocatalytic filtration protocol

Table 9.10: Protocol for the photocatalytic filtration

No	Step	Conditions	Justification
1	Mounting of membrane sample	Put membrane (2.5 cm diameter) onto the bottom part of a stainless-steel membrane cell. Close the cell and tighten the screws using 2 N.m torque wrench.	
2	Purging/ flushing the pump	Run with Milli-Q water at 500 mL/min for 10 s with purge valve of the pump open and valve on the pump outlet (towards the membrane cell) closed.	Prevent pump clogging
3	Flushing	Run with Milli-Q water at 100 mL/min for 2 min with retentate valve open (cross-flow).	Remove air bubbles which can interfere with sensors.
4	Preconditioning membrane	Run with Milli-Q water at 10 mL/min for 10 min with retentate valve closed (dead-end)	Pre-compaction of the membrane at the highest operative flow rate to obtain stable flux during filtration.
5	Pure water flux	Run with Milli-Q water at different flow rate (5, 2, 1, 0.5, and 0.2 mL/min) for 5 min and collect the pressure data.	Permeability test
6	Prepare solar simulator*	Switch on the chiller, controller, and PC. Adjust the intensity of the selected spectrum in the WAVELABS software. Set the duration and activate the recipe.	Since the light engine performance decreases with time, intensity adjustment is done before every experiment.
7	Flush the pump with GLY-AMPA solution	Switch feed tank, run with GLY-AMPA solution at 100 mL/min for 30 sec with purge valve of the pump open and valve on the pump outlet closed.	Eliminate the remained water in the pump and change with GLY-AMPA solution.
8	Adsorption in dark phase	Run with light off for 100 mL (50 min at 2 mL/min standard condition), taking samples at points 10, 20, 40, 60, and 100 mL. Sample volume is 2 mL.	Filtration until the equilibrium is reached, as possible adsorption leads to unsteady trend at the early stages of filtration.
9	Degradation with light	Switch the light on (by starting the recipe) and run for 600 mL (300 min at 2 mL/min), taking samples at points 102, 108, 125, 175, 250, 375, 500, 600, 650, and 700 mL. Sample volume is 2 mL.	Shorter intervals are chosen in the beginning to record the rapid change of permeate concentration, while larger intervals are chosen in the more stable conditions.
10	Purging, flushing, and pure water flux	Repeat steps 2, 3, and 5 with Milli-Q water.	Pure water flux after filtration is to see if there is membrane fouling or modification.
11	System cleaning	Flushing the samples line with Milli-Q water at 10 mL/min for 2 min and then drying with air.	Remove the sample residues and eliminate remained water in tubes.
*For new spectrum (400–1150 nm), spectral calibration and manual calibration of the light intensity are performed after creating the spectrum and corresponding recipe. All these steps are performed before starting the experiment.			

List of figures

List of tables

List of abbreviations

AC Activated carbon

AMPA Aminomethylphosphonic acid

AOPs Advanced oxidation processes

BMBF Federal Ministry of Education and Research

DAAD German Academic Exchange Service

DFT Density functional theory

EU European Union

FTIR Fourier Transform Infrared Spectroscopy

GAC Granular activated carbon

GLY Glyphosate

HY HydraCore

HPLC High-performance liquid chromatography

HRT Hydraulic residence time

IAMT Institute for Advanced Membrane Technology

IFG Institute of Functional Interfaces

IMT Institut für Mikrostrukturtechnik

KOMS-BW Competence Center for Trace Substances – Baden-Württemberg

KIT Karlsruhe Institute of Technology

LC Liquid chromatography

LC-MS/MS: Liquid chromatography with tandem mass spectrometry

LOD Limit of detection

LOQ Limit of quantification

MF Microfiltration

MOF Metal organic frameworks

MW	Molecular weight
MWCO	Molecular weight cut-off
MS	Mass spectrometry
NF	Nanofiltration
PAC	Powder activated carbon
PBSAC	Polymer-based spherical activated carbon
PVDF	Polyvinylidene fluoride (membrane)
RO	Reverse osmosis
ROS	Reactive oxygen species
UF	Ultrafiltration
UV	Ultraviolet
WHO	World Health Organisation
WTP	Water treatment plant
WWTP	Wastewater treatment plant

List of symbols

q_{ads}	Specific mass adsorbed
$-r_i''$	Rate of disappearance
ζ	Zeta potential
$\bar{t}$	Hydraulic residence time
V	volume of membrane occupied by feed solution
V_m	membrane volume
δ	membrane thickness
ε	membrane porosity
Q	Flow rate
A	membrane area
J	water flux
κ^{-1}	Debye length
ε_0	vacuum permittivity
ε_τ	feed solution relative permittivity
R	idea gas constant
T	feed temperature
F	Faraday constant
z_i	valence of ion
C_i	ion molar concentration
ε_W	relative permittivity of water
k_m	external mass transfer coefficient
Sh	Sherwood number
ζ	Zeta potential
e_{CB}^-	Conduction band

h_{VB}^{+}	Valence band
$E_{hydraulic}$	Theoretical hydraulic energy
E_{light}	Theoretical light energy
E_{total}	Theoretical energy consumption
c_f	Concentration of feed
c_p	concentration of permeate
ΔG^0	Gibbs free energy
ΔS^0	Change of entropy
ΔH^0	Change of enthalpy

Bibliography

[1] United Nation, The sustainable development goals report, in, 2024.

[2] S. Omer, 2025, Global water crisis: Facts, FAQs, and how to help, World Vision, accessed on 30 October 2025, https://www.worldvision.org/clean-water-news-stories/global-water-crisis-facts.

[3] United Nation, Goal 6: Clean water and sanitation, in, The Sustainable Development Goals, 2015.

[4] UNESCO World Water Assessment Programme, The United Nations world water development report 2024: Water for prosperity and peace 2024, in, UNESCO.

[5] A. du Plessis, Persistent degradation: Global water quality challenges and required actions, One Earth, 5 (2022) 129-131.

[6] M. Clara, B. Strenn, O. Gans, E. Martinez, N. Kreuzinger, H. Kroiss, Removal of selected pharmaceuticals, fragrances and endocrine disrupting compounds in a membrane bioreactor and conventional wastewater treatment plants, Water Research, 39 (2005) 4797-4807.

[7] S. Finckh, E. Carmona, D. Borchardt, O. Büttner, M. Krauss, T. Schulze, S. Yang, W. Brack, Mapping chemical footprints of organic micropollutants in European streams, Environment International, 183 (2024) 108371.

[8] J.L. Wilkinson, A.B.A. Boxall, D.W. Kolpin, K.M.Y. Leung, R.W.S. Lai, C. Galbán-Malagón, A.D. Adell, J. Mondon, M. Metian, R.A. Marchant, A. Bouzas-Monroy, A. Cuni-Sanchez, A. Coors, P. Carriquiriborde, M. Rojo, C. Gordon, M. Cara, M. Moermond, T. Luarte, V. Petrosyan, Y. Perikhanyan, C.S. Mahon, C.J. McGurk, T. Hofmann, T. Kormoker, V. Iniguez, J. Guzman-Otazo, J.L. Tavares, F. Gildasio De Figueiredo, M.T.P. Razzolini, V. Dougnon, G. Gbaguidi, O. Traoré, J.M. Blais, L.E. Kimpe, M. Wong, D. Wong, R. Ntchantcho, J. Pizarro, G.G. Ying, C.E. Chen, M. Páez, J. Martínez-Lara, J.P. Otamonga, J. Poté, S.A. Ifo, P. Wilson, S. Echeverría-Sáenz, N. Udikovic-Kolic, M. Milakovic, D. Fatta-Kassinos, L. Ioannou-Ttofa, V. Belušová, J. Vymazal, M. Cárdenas-Bustamante, B.A. Kassa, J. Garric, A. Chaumot, P. Gibba, I. Kunchulia, S. Seidensticker, G. Lyberatos, H.P. Halldórsson, M. Melling, T. Shashidhar, M. Lamba, A. Nastiti, A. Supriatin, N. Pourang, A. Abedini, O. Abdullah, S.S. Gharbia, F. Pilla, B. Chefetz, T. Topaz, K.M. Yao, B. Aubakirova, R. Beisenova, L. Olaka, J.K. Mulu, P. Chatanga, V. Ntuli, N.T. Blama, S. Sherif, A.Z. Aris, L.J. Looi, M. Niang, S.T. Traore, R. Oldenkamp, O. Ogunbanwo, M. Ashfaq, M. Iqbal, Z. Abdeen, A. O'Dea, J.M. Morales-Saldaña, M. Custodio, H. de la Cruz, I. Navarrete, F. Carvalho, A.B. Gogra, B.M. Koroma, V. Cerkvenik-Flajs, M. Gombač, M. Thwala, K. Choi, H. Kang, J.L.C. Ladu, A. Rico, P. Amerasinghe, A. Sobek, G. Horlitz, A.K. Zenker, A.C. King, J.J. Jiang, R. Kariuki, M. Tumbo, U. Tezel, T.T. Onay, J.B. Lejju, Y. Vystavna, Y. Vergeles, H. Heinzen, A. Pérez-Parada, D.B. Sims, M. Figy, D. Good, C. Teta, Pharmaceutical pollution of the world's rivers, Proceedings of the National Academy of Sciences of the United States of America, 119 (2022).

[9] P. Fantke, R. Friedrich, O. Jolliet, Health impact and damage cost assessment of pesticides in Europe, Environment International, 49 (2012) 9-17.

[10] FAO Statistics, Pesticide use, in, http://www.fao.org/faostat/en/#data/RP/visualize, Accessed on 3 November, 2022.

[11] N. Markert, C. Schürings, C.K. Feld, Water Framework Directive micropollutant monitoring mirrors catchment land use: Importance of agricultural and urban sources revealed, Science of The Total Environment, 917 (2024) 170583.

[12] European Commission, Proposal for a Directive of the European Parliament and of the Council amending Directive 2000/60/EC establishing a framework for community action in the field of water policy, Directive 2006/118/EC on the protection of groundwater against pollution and deterioration and Directive 2008/105/EC on environmental quality standards in the field of water policy, in, 2022.

[13] The European Parliament and the Council of European Union, Directive (EU) 2020/2184 of the European parliament and of the council of 16 December 2020 on the quality of water intended for human consumption, in: Directive - 2020/2184, Official Journal of the European Union, 2020, pp. 37-38.

[14] S.O. Duke, The history and current status of glyphosate, Pest Management Science, 74 (2018) 1027-1034.

[15] C. Gillezeau, M. van Gerwen, R.M. Shaffer, I. Rana, L. Zhang, L. Sheppard, E. Taioli, The evidence of human exposure to glyphosate: A review, Environmental health, 18 (2019) 2-2.

[16] F. Maggi, D. la Cecilia, F.H.M. Tang, A. McBratney, The global environmental hazard of glyphosate use, Science of The Total Environment, 717 (2020) 137167.

[17] C. Antier, P. Kudsk, X. Reboud, L. Ulber, P.V. Baret, A. Messéan, Glyphosate use in the European agricultural sector and a framework for its further monitoring, Sustainability 12 (2020) 56-82.

[18] Agropages, 2025, Glyphosate prices rise, boosting industry leaders' performance, accessed accessed on September 2 2025, https://news.agropages.com/News/NewsDetail---54367.htm?utm_source=chatgpt.com.

[19] F. Maggi, F.H.M. Tang, F.N. Tubiello, Agricultural pesticide land budget and river discharge to oceans, Nature, 620 (2023) 1013-1017.

[20] L. Yang, X. He, S. Ru, Y. Zhang, Herbicide leakage into seawater impacts primary productivity and zooplankton globally, Nature Communications, 15 (2024) 1783.

[21] Q. Zhang, Y. Li, C. Kroeze, W. Xu, L. Gai, M. Vitsas, L. Ma, F. Zhang, M. Strokal, A global assessment of glyphosate and AMPA inputs into rivers: Over half of the pollutants are from corn and soybean production, Water Research, 261 (2024) 121986.

[22] A.C. Schomberg, S. Bringezu, A.W.H. Beusen, Water quality footprint of agricultural emissions of nitrogen, phosphorus and glyphosate associated with German bioeconomy, Communications Earth & Environment, 4 (2023) 404.

[23] V.J. Koller, M. Fürhacker, A. Nersesyan, M. Mišík, M. Eisenbauer, S. Knasmueller, Cytotoxic and DNA-damaging properties of glyphosate and Roundup in human-derived buccal epithelial cells, Archives of toxicology, 86 (2012) 805-813.

[24] K.Z. Guyton, D. Loomis, Y. Grosse, F. El Ghissassi, L. Benbrahim-Tallaa, N. Guha, C. Scoccianti, H. Mattock, K. Straif, Carcinogenicity of tetrachlorvinphos, parathion, malathion, diazinon, and glyphosate, The Lancet Oncology, 16 (2015) 490-491.

[25] J.P. Myers, M.N. Antoniou, B. Blumberg, L. Carroll, T. Colborn, L.G. Everett, M. Hansen, P.J. Landrigan, B.P. Lanphear, R. Mesnage, L.N. Vandenberg, F.S. vom Saal, W.V. Welshons, C.M. Benbrook, Concerns over use of glyphosate-based herbicides and risks associated with exposures: a consensus statement, Environmental Health, 15 (2016) 19.

[26] C. Nerozzi, S. Recuero, G. Galeati, D. Bucci, M. Spinaci, M. Yeste, Effects of Roundup and its main component, glyphosate, upon mammalian sperm function and survival, Scientific Reports, 10 (2020) 11026.

[27] J.V. Tarazona, D. Court-Marques, M. Tiramani, H. Reich, R. Pfeil, F. Istace, F. Crivellente, Glyphosate toxicity and carcinogenicity: a review of the scientific basis of the European Union assessment and its differences with IARC, Archives of toxicology, 91 (2017) 2723-2743.

[28] K. Gandhi, S. Khan, M. Patrikar, A. Markad, N. Kumar, A. Choudhari, P. Sagar, S. Indurkar, Exposure risk and environmental impacts of glyphosate: Highlights on the toxicity of herbicide co-formulants, Environmental Challenges, 4 (2021) 100149.

[29] H. Fingerhut, D.A. Lieb, 2025, Bayer backs broadened effort to shield popular weedkiller from claims it failed to warn of cancer, Jefferson City, Missouri, accessed 3 March 2025, https://apnews.com/article/bayer-roundup-glyphosate-pesticide-liability-cancer-7d7885e55e228fae8ed8ec7b207a65b8.

[30] J.P. Muñoz, E. Silva-Pavez, D. Carrillo-Beltrán, G.M. Calaf, Occurrence and exposure assessment of glyphosate in the environment and its impact on human beings, Environmental Research, 231 (2023) 116201.

[31] European Commission, 2022, Extension of the approval period of glyphosate, accessed January 30 2023, https://food.ec.europa.eu/plants/pesticides/approval-active-substances/renewal-approval/glyphosate_en.

[32] M. Garrido-Baserba, D.L. Sedlak, M. Molinos-Senante, I. Barnosell, O. Schraa, D. Rosso, M. Verdaguer, M. Poch, Using water and wastewater decentralization to enhance the resilience and sustainability of cities, Nature Water, 2 (2024) 953-974.

[33] K. Obaideen, N. Shehata, E.T. Sayed, M.A. Abdelkareem, M.S. Mahmoud, A.G. Olabi, The role of wastewater treatment in achieving sustainable development goals (SDGs) and sustainability guideline, Energy Nexus, 7 (2022) 100112.

[34] Y. Yang, X. Zhang, J. Jiang, J. Han, W. Li, X. Li, K.M. Yee Leung, S.A. Snyder, P.J.J. Alvarez, Which micropollutants in water environments deserve more attention globally?, Environmental Science & Technology, 56 (2022) 13-29.

[35] A.M. Meyer, C. Klein, E. Fünfrocken, R. Kautenburger, H.P. Beck, Real-time monitoring of water quality to identify pollution pathways in small and middle scale rivers, Science of The Total Environment, 651 (2019) 2323-2333.

[36] R. Annett, H.R. Habibi, A. Hontela, Impact of glyphosate and glyphosate-based herbicides on the freshwater environment, Journal of Applied Toxicology, 34 (2014) 458-479.

[37] E. Okada, M. Allinson, M.P. Barral, B. Clarke, G. Allinson, Glyphosate and aminomethylphosphonic acid (AMPA) are commonly found in urban streams and wetlands of Melbourne, Australia, Water Research, 168 (2020) 115139.

[38] M.J. Luján-Facundo, M.I. Iborra-Clar, J.A. Mendoza-Roca, M.I. Alcaina-Miranda, Pharmaceutical compounds removal by adsorption with commercial and reused carbon coming from a drinking water treatment plant, Journal of Cleaner Production, 238 (2019) 117866.

[39] P.E. Stackelberg, J. Gibs, E.T. Furlong, M.T. Meyer, S.D. Zaugg, R.L. Lippincott, Efficiency of conventional drinking-water-treatment processes in removal of pharmaceuticals and other organic compounds, Science of The Total Environment, 377 (2007) 255-272.

[40] Kompetenzzentrum Spurenstoffe BW, 2025, Kläranlagenausbau in Baden-Württemberg, accessed accessed on 30 May 2025, https://koms-bw.de/anlagen/.

[41] Federal Statistical Office, Öffentliche Wasserversorgung und Abwasserbeseitigung (1991, 1995, 1998, 2001, 2004), in: Fachserie 19 Umwelt, Reihe 2.1, Statistisches Bundesamt, 2009.

[42] S. Munirasu, M.A. Haija, F. Banat, Use of membrane technology for oil field and refinery produced water treatment—A review, Process Safety and Environmental Protection, 100 (2016) 183-202.

[43] R.R.Z. Tarpani, A. Azapagic, Life cycle costs of advanced treatment techniques for wastewater reuse and resource recovery from sewage sludge, Journal of Cleaner Production, 204 (2018) 832-847.

[44] S. Paul, W.F. Meggitt, P. Donald, Adsorption, mobility, and microbial degradation of glyphosate in the soil, Weed Science, 23 (1975) 229-234.

[45] H.A. Pereira, P.R.T. Hernandes, M.S. Netto, G.D. Reske, V. Vieceli, L.F.S. Oliveira, G.L. Dotto, Adsorbents for glyphosate removal in contaminated waters: a review, Environmental Chemistry Letters, 19 (2021) 1525-1543.

[46] S.R. Moller, A.F. Wallace, R. Zahir, A. Quadery, D.P. Jaisi, Effect of temperature on the degradation of glyphosate by Mn-oxide: Products and pathways of degradation, Journal of Hazardous Materials, 461 (2024) 132467.

[47] S.R. Moller, M.A. Campos, J.I. Rilling, R. Bakkour, A.J. Hollenback, M.A. Jorquera, D.P. Jaisi, Persistence and pathway of glyphosate degradation in the coastal wetland soil of central Delaware, Journal of Hazardous Materials, 477 (2024) 135238.

[48] N. Hosseini, M.R. Toosi, Removal of 2,4-D, glyphosate, trifluralin, and butachlor herbicides from water by polysulfone membranes mixed by graphene oxide/TiO_2 nanocomposite: study of filtration and batch adsorption, Journal of Environmental Health Science and Engineering, 17 (2019) 247-258.

[49] D.W. Kolpin, E.M. Thurman, E.A. Lee, M.T. Meyer, E.T. Furlong, S.T. Glassmeyer, Urban contributions of glyphosate and its degradate AMPA to streams in the United States, Science of The Total Environment, 354 (2006) 191-197.

[50] K.A. Lewis, J. Tzilivakis, D.J. Warner, A. Green, An international database for pesticide risk assessments and management, Human and Ecological Risk Assessment: An International Journal, 22 (2016) 1050-1064.

[51] J. Sheals, S. Sjöberg, P. Persson, Adsorption of glyphosate on goethite: molecular characterization of surface complexes, Environmental Science & Technology, 36 (2002) 3090-3095.

[52] M.A. Kamrin, J.H. Montgomery, Agrochemical desk reference, 2nd ed., CRC Press Boca Raton, 1997.

[53] C.R. Worthing, S.B. Walker, C. British Crop Protection, The pesticide manual : A world compendium, British Crop Protection Council, Thornton Heath, 1987.

[54] J.E. Franz, M.K. Mao, J.A. Sikorski, Glyphosate: A unique global herbicide, 06/12 ed., Washington, DC : American Chemical Society, 1997.

[55] A.L. Valle, F.C.C. Mello, R.P. Alves-Balvedi, L.P. Rodrigues, L.R. Goulart, Glyphosate detection: methods, needs and challenges, Environmental Chemistry Letters, 17 (2019) 291-317.

[56] A. Grandcoin, S. Piel, E. Baurès, Aminomethylphosphonic acid (AMPA) in natural waters: Its sources, behavior and environmental fate, Water Research, 117 (2017) 187-197.

[57] G. Obeid, G.O. Moraes, T.C. Penna, L.A. Schenberg, L.C. Ducati, T.C. Correra, Solvation effects on glyphosate protonation and deprotonation states evaluated by mass spectrometry and explicit solvation simulations, The Journal of chemical physics, 158 (2023) 054306.

[58] Z.W. Windom, M. Datta, M.M. Huda, M.A. Sabuj, N. Rai, Understanding speciation and solvation of glyphosate from first principles simulations, Journal of Molecular Liquids, 365 (2022) 120154.

[59] R. Loos, R. Niessner, Analysis of atrazine, terbutylazine and their N-dealkylated chloro and hydroxy metabolites by solid-phase extraction and gas chromatography–mass spectrometry and capillary electrophoresis–ultraviolet detection, Journal of Chromatography A, 835 (1999) 217-229.

[60] E.A. Oliveira Pereira, V. Freitas Melo, G. Abate, J.C. Masini, Determination of glyphosate and aminomethylphosphonic acid by sequential-injection reversed-phase chromatography: method improvements and application in adsorption studies, Analytical and Bioanalytical Chemistry, 411 (2019) 2317-2326.

[61] E. Worch, Eine neue Gleichung zur Berechnung von Diffusionskoeffizienten gelöster Stoffe, Vom Wasser, 81 (1993) 289–297.

[62] A.A. Ahmed, P. Leinweber, O. Kühn, Unravelling the nature of glyphosate binding to goethite surfaces by ab initio molecular dynamics simulations, Physical Chemistry Chemical Physics, 20 (2018) 1531-1539.

[63] J. Song, X.-M. Li, A. Figoli, H. Huang, C. Pan, T. He, B. Jiang, Composite hollow fiber nanofiltration membranes for recovery of glyphosate from saline wastewater, Water Research, 47 (2013) 2065-2074.

[64] C.A. Villamar-Ayala, J.V. Carrera-Cevallos, R. Vasquez-Medrano, P.J. Espinoza-Montero, Fate, eco-toxicological characteristics, and treatment processes applied to water polluted with glyphosate: A critical review, Critical Reviews in Environmental Science and Technology, 49 (2019) 1476-1514.

[65] P. Gros, A. Ahmed, O. Kühn, P. Leinweber, Glyphosate binding in soil as revealed by sorption experiments and quantum-chemical modeling, Science of The Total Environment, 586 (2017) 527-535.

[66] X. Yang, V. Silva, D.W.S. Tang, Pesticide transport under runoff-erosion potentially dominated by small sediments: A glyphosate and AMPA experiment, Journal of Hydrology, 661 (2025) 133633.

[67] I.B. Lima, I.G. Boëchat, M.D. Fernandes, J.A.F. Monteiro, L. Rivaroli, B. Gücker, Glyphosate pollution of surface runoff, stream water, and drinking water resources in Southeast Brazil, Environmental Science and Pollution Research, 30 (2023) 27030-27040.

[68] D. Mackay, Finding fugacity feasible, Environmental Science & Technology, 13 (1979) 1218-1223.

[69] D. Mackay, S. Paterson, Calculating fugacity, Environmental Science & Technology, 15 (1981) 1006-1014.

[70] R. Quilbé, A.N. Rousseau, P. Lafrance, J. Leclerc, M. Amrani, Selecting a pesticide fate model at the watershed scale using a multi-criteria analysis, Water Quality Research Journal, 41 (2006) 283-295.

[71] N. Suciu, T. Tanaka, M. Trevisan, M. Schuhmacher, M. Nadal, J. Rovira, X. Segui, J. Casal, R.M. Darbra, E. Capri, Environmental Fate Models, in: Global risk-based management of chemical additives II, 2013, pp. 47-71.

[72] S.G. Kilic, M.M. Aral, A fugacity based continuous and dynamic fate and transport model for river networks and its application to Altamaha River, Science of The Total Environment, 407 (2009) 3855-3866.

[73] D. Mackay, S. Paterson, B. Cheung, W.B. Neely, Evaluating the environmental behavior of chemicals with a level III fugacity model, Chemosphere, 14 (1985) 335-374.

[74] D. Mackay, S. Paterson, W.Y. Shiu, Generic models for evaluating the regional fate of chemicals, Chemosphere, 24 (1992) 695-717.

[75] T. Ntakirutimana, J. Guo, X. Gao, D.-c. Gong, Application of multimedia fugacity model to assess the environmental fate of benzo (a) pyrene, in, 2012.

[76] D. Mackay, A. Di Guardo, S. Paterson, C.E. Cowan, Evaluating the environmental fate of a variety of types of chemicals using the EQC model, Environmental toxicology and chemistry, 15 (1996) 1627-1637.

[77] International Union of Pure and Applied Chemistry, 2020, Pesticide Properties Database: Glyphosate (Ref: MON 0573), accessed 30 April 2025, https://sitem.herts.ac.uk/aeru/iupac/Reports/373.htm.

[78] Agriculture and food development authority, 2024, Glyphosate: Avoid the resistance risk!, accessed accessed on September 15 2025, https://teagasc.ie/news--events/daily/glyphosate-avoid-the-resistance-risk/.

[79] S. Aslam, Y. Jing, K.M. Nowak, Fate of glyphosate and its degradation products AMPA, glycine and sarcosine in an agricultural soil: Implications for environmental risk assessment, Journal of Hazardous Materials, 447 (2023) 130847.

[80] W. Li, K. Wang, P. Wang, P. Yang, S. Xu, J. Tong, Y. Zhang, Y. Yang, L. Han, M. Ye, S. Shen, B. Lei, B. Liu, Impact of glyphosate on soil bacterial communities and degradation mechanisms in large-leaf tea plantations, Journal of Hazardous Materials, 483 (2025) 136626.

[81] F. Botta, G. Lavison, G. Couturier, F. Alliot, E. Moreau-Guigon, N. Fauchon, B. Guery, M. Chevreuil, H. Blanchoud, Transfer of glyphosate and its degradate AMPA to surface waters through urban sewerage systems, Chemosphere, 77 (2009) 133-139.

[82] L. Torstensson, E. Börjesson, J. Stenström, Efficacy and fate of glyphosate on Swedish railway embankments, Pest Management Science, 61 (2005) 881-886.

[83] I. Hanke, I. Wittmer, S. Bischofberger, C. Stamm, H. Singer, Relevance of urban glyphosate use for surface water quality, Chemosphere, 81 (2010) 422-429.

[84] M. Schwientek, H. Rügner, S.B. Haderlein, W. Schulz, B. Wimmer, L. Engelbart, S. Bieger, C. Huhn, Glyphosate contamination in European rivers not from herbicide application?, Water Research, 263 (2024) 122140.

[85] H.H. Tolkamp, R. Hofman-Caris, Comment on “Glyphosate contamination in European rivers not from herbicide application?” By M. Schwientek, H. Rügner, S.B. Haderlein, W. Schulz, B. Wimmer, L. Engelbart, S. Bieger, C. Huhn; Water Research Volume 263, 1 October 2024, 122140, page 1–10, Water Research, 272 (2025) 122965.

[86] L. Engelbart, S. Bieger, K. Thompson, L. Fischer, T. Bader, M. Kramer, S.B. Haderlein, A.M. Röhnelt, P.R. Martin, D. Buchner, R. Bloch, H. Rügner, C. Huhn, In-situ formation of

glyphosate and AMPA in activated sludge from phosphonates used as antiscalants and bleach stabilizers in households and industry, Water Research, 280 (2025) 123464.

[87] A.M. Röhnelt, P.R. Martin, M. Athmer, S. Bieger, D. Buchner, U. Karst, C. Huhn, T.C. Schmidt, S.B. Haderlein, Glyphosate is a transformation product of a widely used aminopolyphosphonate complexing agent, Nature Communications, 16 (2025) 2438.

[88] S. Finckh, L.-M. Beckers, W. Busch, E. Carmona, V. Dulio, L. Kramer, M. Krauss, L. Posthuma, T. Schulze, J. Slootweg, P.C. Von der Ohe, W. Brack, A risk based assessment approach for chemical mixtures from wastewater treatment plant effluents, Environment International, 164 (2022) 107234.

[89] S. Finckh, S. Buchinger, B.I. Escher, H. Hollert, M. König, M. Krauss, W. Leekitratanapisan, S. Schiwy, R. Schlichting, A. Shuliakevich, W. Brack, Endocrine disrupting chemicals entering European rivers: Occurrence and adverse mixture effects in treated wastewater, Environment International, 170 (2022) 107608.

[90] G. Campbell, B.J. Tscharke, P. Prasad, E.R. Knight, T. Reeks, A. Jackson, K.V. Thomas, J.F. Mueller, S.L. Kaserzon, Occurrence and fate of glyphosate and AMPA in wastewater treatment plants in Australia, Science of The Total Environment, 969 (2025) 178964.

[91] A.K. Sarmah, K. Müller, R. Ahmad, Fate and behaviour of pesticides in the agroecosystem—a review with a New Zealand perspective, Australian Journal of Soil Research, 42 (2004) 125-154.

[92] N. Suciu, E. Russo, M. Calliera, G.P. Luciani, M. Trevisan, E. Capri, Glyphosate, glufosinate ammonium, and AMPA occurrences and sources in groundwater of hilly vineyards, Science of The Total Environment, 866 (2023) 161171.

[93] M. Feltracco, E. Barbaro, E. Morabito, R. Zangrando, R. Piazza, C. Barbante, A. Gambaro, Assessing glyphosate in water, marine particulate matter, and sediments in the Lagoon of Venice, Environmental Science and Pollution Research, 29 (2022) 16383-16391.

[94] I. Navarro, A. de la Torre, P. Sanz, N. Abrantes, I. Campos, A. Alaoui, F. Christ, F. Alcon, J. Contreras, M. Glavan, I. Pasković, M.P. Pasković, T. Nørgaard, D. Mandrioli, D. Sgargi, J. Hofman, V. Aparicio, I. Baldi, M. Bureau, A. Vested, P. Harkes, E. Huerta-Lwanga, H. Mol, V. Geissen, V. Silva, M.Á. Martínez, Assessing pesticide residues occurrence and risks in water systems: A Pan-European and Argentina perspective, Water Research, 254 (2024) 121419.

[95] J. Sanchís, L. Kantiani, M. Llorca, F. Rubio, A. Ginebreda, J. Fraile, T. Garrido, M. Farré, Determination of glyphosate in groundwater samples using an ultrasensitive immunoassay and confirmation by on-line solid-phase extraction followed by liquid chromatography coupled to tandem mass spectrometry, Analytical and Bioanalytical Chemistry, 402 (2012) 2335-2345.

[96] L. Carles, H. Gardon, L. Joseph, J. Sanchís, M. Farré, J. Artigas, Meta-analysis of glyphosate contamination in surface waters and dissipation by biofilms, Environment International, 124 (2019) 284-293.

[97] N. Tauchnitz, F. Kurzius, H. Rupp, G. Schmidt, B. Hauser, M. Schrödter, R. Meissner, Assessment of pesticide inputs into surface waters by agricultural and urban sources - A case study in the Querne/Weida catchment, central Germany, Environmental Pollution, 267 (2020) 115186.

[98] V. Silva, L. Montanarella, A. Jones, O. Fernández-Ugalde, H.G.J. Mol, C.J. Ritsema, V. Geissen, Distribution of glyphosate and aminomethylphosphonic acid (AMPA) in agricultural topsoils of the European Union, Science of The Total Environment, 621 (2018) 1352-1359.

[99] R.I. Bonansea, I. Filippi, D.A. Wunderlin, D.J.G. Marino, M.V. Amé, The fate of glyphosate and ampa in a freshwater endorheic basin: An ecotoxicological risk assessment, Toxics, 6 (2017).

[100] M.T.K. Tsui, L.M. Chu, Environmental fate and non-target impact of glyphosate-based herbicide (Roundup®) in a subtropical wetland, Chemosphere, 71 (2008) 439-446.

[101] R.H. Coupe, S.J. Kalkhoff, P.D. Capel, C. Gregoire, Fate and transport of glyphosate and aminomethylphosphonic acid in surface waters of agricultural basins, Pest Management Science, 68 (2012) 16-30.

[102] J. Rendon-von Osten, R. Dzul-Caamal, Glyphosate residues in groundwater, drinking water and urine of subsistence farmers from intensive agriculture localities: A survey in Hopelchén, Campeche, Mexico, Int J Environ Res Public Health, 14 (2017) 595.

[103] H. Horth, A. Gendebien, Review of glyphosate and AMPA in drinking water in selected European countries, in, 2008.

[104] W. Zhang, Y. Feng, L. Ma, J. An, H. Zhang, M. Cao, H. Zhu, W. Kang, K. Lian, A method for determining glyphosate and its metabolite aminomethyl phosphonic acid by gas chromatography-flame photometric detection, Journal of Chromatography A, 1589 (2019) 116-121.

[105] V. Toss, I. Leito, S. Yurchenko, R. Freiberg, A. Kruve, Determination of glyphosate in surface water with high organic matter content, Environmental Science and Pollution Research, 24 (2017) 7880-7888.

[106] C. Hao, D. Morse, F. Morra, X. Zhao, P. Yang, B. Nunn, Direct aqueous determination of glyphosate and related compounds by liquid chromatography/tandem mass spectrometry using reversed-phase and weak anion-exchange mixed-mode column, Journal of Chromatography A, 1218 (2011) 5638-5643.

[107] J.P.F. Tiago, S.L. C., B.R. E., d.P.G. P., F.O. and Silvério, Simultaneous and direct determination of glyphosate and AMPA in water samples from the hydroponic cultivation of eucalyptus seedlings using HPLC-ICP-MS/MS, Journal of Environmental Science and Health, Part B, 55 (2020) 558-565.

[108] E. Okada, T. Coggan, T. Anumol, B. Clarke, G. Allinson, A simple and rapid direct injection method for the determination of glyphosate and AMPA in environmental water samples, Analytical and Bioanalytical Chemistry, 411 (2019) 715-724.

[109] L. Carretta, A. Cardinali, E. Marotta, G. Zanin, R. Masin, A new rapid procedure for simultaneous determination of glyphosate and AMPA in water at sub μg/L level, Journal of Chromatography A, 1600 (2019) 65-72.

[110] M.A. Wirth, D.E. Schulz-Bull, M. Kanwischer, The challenge of detecting the herbicide glyphosate and its metabolite AMPA in seawater – Method development and application in the Baltic Sea, Chemosphere, 262 (2021) 128327.

[111] A. Royer, S. Beguin, J.C. Tabet, S. Hulot, M.A. Reding, P.Y. Communal, Determination of glyphosate and aminomethylphosphonic acid residues in water by gas chromatography with tandem mass spectrometry after exchange ion resin purification and derivatization: Application on vegetable matrixes, Analytical Chemistry, 72 (2000) 3826-3832.

[112] P. Rocío-Bautista, D. Moreno-González, A.B. Martínez-Piernas, J.F. García-Reyes, A. Molina-Díaz, Novel liquid chromatography/mass spectrometry-based approaches for the

determination of glyphosate and related compounds: A review, Trends in Environmental Analytical Chemistry, 36 (2022) e00186.

[113] Z.-X. Guo, Q. Cai, Z. Yang, Determination of glyphosate and phosphate in water by ion chromatography—inductively coupled plasma mass spectrometry detection, Journal of Chromatography A, 1100 (2005) 160-167.

[114] E. Börjesson, L. Torstensson, New methods for determination of glyphosate and (aminomethyl)phosphonic acid in water and soil, Journal of Chromatography A, 886 (2000) 207-216.

[115] K. Sato, J.-Y. Jin, T. Takeuchi, T. Miwa, K. Suenami, Y. Takekoshi, S. Kanno, Integrated pulsed amperometric detection of glufosinate, bialaphos and glyphosate at gold electrodes in anion-exchange chromatography, Journal of Chromatography A, 919 (2001) 313-320.

[116] A.-K. Schäfer, W. Vetter, M. Anastassiades, Improved analysis of glyphosate, aminomethylphosphonic acid, and other highly polar pesticides and metabolites via the quppe method by employing ethylenediaminetetraacetic acid and IC-MS/MS, Journal of Agricultural and Food Chemistry, 73 (2025) 2645-2652.

[117] Deutsche Institut für Normung, DIN 38407-22:2001-Deutsche Einheitsverfahren zur Wasser-, Abwasser- und Schlammuntersuchung - Gemeinsam erfassbare Stoffgruppen (Gruppe F) - Teil 22: Bestimmung von Glyphosat und Aminomethylphosphonsäure (AMPA) in Wasser durch Hochleistungs-Flüssigchromatographie (HPLC), Nachsäulenderivatisierung und Fluoreszenzdetektion (F 22), in, 2001.

[118] International Organization for Standardization, ISO 16308:2014-Water quality - Determination of glyphosate and AMPA - Method using high performance liquid chromatography (HPLC) with tandem mass spectrometric detection, in, 2014.

[119] E. Mallat, D. Barceló, Analysis and degradation study of glyphosate and of aminomethylphosphonic acid in natural waters by means of polymeric and ion-exchange solid-phase extraction columns followed by ion chromatography–post-column derivatization with fluorescence detection, Journal of Chromatography A, 823 (1998) 129-136.

[120] P.J. Martin, K. He, L. Blaney, S.R. Hobbs, Advanced Liquid Chromatography with Tandem Mass Spectrometry Method for Quantifying Glyphosate, Glufosinate, and Aminomethylphosphonic Acid Using Pre-Column Derivatization, ACS Environmental Science & Technology Water, 3 (2023) 2407-2414.

[121] Z. Shamsi, D. Buchner, S.B. Haderlein, Methods for pre-concentration and clean-up of glyphosate and aminomethylphosphonic acid from water samples: A review, TrAC Trends in Analytical Chemistry, 193 (2025) 118459.

[122] M.-X. Chen, Z.-Y. Cao, Y. Jiang, Z.-W. Zhu, Direct determination of glyphosate and its major metabolite, aminomethylphosphonic acid, in fruits and vegetables by mixed-mode hydrophilic interaction/weak anion-exchange liquid chromatography coupled with electrospray tandem mass spectrometry, Journal of Chromatography A, 1272 (2013) 90-99.

[123] A.K. Brown, A. Farenhorst, Quantitation of glyphosate, glufosinate, and AMPA in drinking water and surface waters using direct injection and charged-surface ultra-high performance liquid chromatography-tandem mass spectrometry, Chemosphere, 349 (2024) 140924.

[124] K. Chamberlain, A.A. Evans, R.H. Bromilow, 1-octanol/water partition coefficient (K_{ow}) and pKa for ionisable pesticides measured by apH-metric method, Pesticide Science, 47 (1996) 265-271.

[125] P. Avino, I. Notardonato, M. Russo, A review of the analytical methods based on chromatography for analyzing glyphosate in foods, in: Pests, weeds and diseases in agricultural crop and animal husbandry production, Intechopen 2020.

[126] F. Fang, R. Wei, X. Liu, Novel pre-column derivatisation reagent for glyphosate by high-performance liquid chromatography and ultraviolet detection, International Journal of Environmental Analytical Chemistry, 94 (2014) 661-667.

[127] T.M. Annesley, Ion suppression in mass spectrometry, Clinical chemistry, 49 (2003) 1041-1044.

[128] H. Mei, Y. Hsieh, C. Nardo, X. Xu, S. Wang, K. Ng, W.A. Korfmacher, Investigation of matrix effects in bioanalytical high-performance liquid chromatography/tandem mass spectrometric assays: Application to drug discovery, Rapid Communications in Mass Spectrometry, 17 (2003) 97-103.

[129] J.-P. Antignac, K. de Wasch, F. Monteau, H. De Brabander, F. Andre, B. Le Bizec, The ion suppression phenomenon in liquid chromatography–mass spectrometry and its consequences in the field of residue analysis, Analytica Chimica Acta, 529 (2005) 129-136.

[130] J. Yuan, J. Duan, C.P. Saint, D. Mulcahy, Removal of glyphosate and aminomethylphosphonic acid from synthetic water by nanofiltration, Environmental Technology, 39 (2018) 1384-1392.

[131] V.B. Kimbi Yaah, S. Ahmadi, J. Quimbayo M, S. Morales-Torres, S. Ojala, Recent technologies for glyphosate removal from aqueous environment: A critical review, Environmental Research, 240 (2024) 117477.

[132] J. Li, W.-J. Chen, W. Zhang, Y. Zhang, Q. Lei, S. Wu, Y. Huang, S. Mishra, P. Bhatt, S. Chen, Effects of free or immobilized bacterium stenotrophomonas acidaminiphila y4b on glyphosate degradation performance and indigenous microbial community structure, Journal of Agricultural and Food Chemistry, 70 (2022) 13945-13958.

[133] J. Gasperi, B. Laborie, V. Rocher, Treatment of combined sewer overflows by ballasted flocculation: Removal study of a large broad spectrum of pollutants, Chemical Engineering Journal, 211-212 (2012) 293-301.

[134] A.D. Villalobos-Lara, F.F. Rivera, J. Paramo-Vargas, Z. Gamiño-Arroyo, T. Ruiz-Vera, Experimental and CFD simulation of glyphosate removal by a filter-press electrocoagulation reactor, Journal of Environmental Chemical Engineering, 11 (2023) 111214.

[135] J. Margot, C. Kienle, A. Magnet, M. Weil, L. Rossi, L.F. de Alencastro, C. Abegglen, D. Thonney, N. Chèvre, M. Schärer, D.A. Barry, Treatment of micropollutants in municipal wastewater: Ozone or powdered activated carbon?, Science of The Total Environment, 461-462 (2013) 480-498.

[136] J. Altmann, A.S. Ruhl, F. Zietzschmann, M. Jekel, Direct comparison of ozonation and adsorption onto powdered activated carbon for micropollutant removal in advanced wastewater treatment, Water Research, 55 (2014) 185-193.

[137] S. Gidstedt, A. Betsholtz, P. Falås, M. Cimbritz, Å. Davidsson, F. Micolucci, O. Svahn, A comparison of adsorption of organic micropollutants onto activated carbon following chemically enhanced primary treatment with microsieving, direct membrane filtration and tertiary treatment of municipal wastewater, Science of The Total Environment, 811 (2022) 152225.

[138] R. Mailler, J. Gasperi, Y. Coquet, S. Deshayes, S. Zedek, C. Cren-Olivé, N. Cartiser, V. Eudes, A. Bressy, E. Caupos, R. Moilleron, G. Chebbo, V. Rocher, Study of a large scale powdered activated carbon pilot: Removals of a wide range of emerging and priority micropollutants from wastewater treatment plant effluents, Water Research, 72 (2015) 315-330.

[139] T. Fundneider, V. Acevedo Alonso, G. Abbt-Braun, A. Wick, D. Albrecht, S. Lackner, Empty bed contact time: The key for micropollutant removal in activated carbon filters, Water Research, 191 (2021) 116765.

[140] J. Guo, X. Song, R. Li, Q. Zhang, S. Zheng, Q. Li, B. Tao, Isolation of a degrading strain of Fusarium verticillioides and bioremediation of glyphosate residue, Pesticide Biochemistry and Physiology, 182 (2022) 105031.

[141] G. Xiao, R. Wen, Comparative adsorption of glyphosate from aqueous solution by 2-aminopyridine modified polystyrene resin, D301 resin and 330 resin: Influencing factors, salinity resistance and mechanism, Fluid Phase Equilibria, 411 (2016) 1-6.

[142] D.M. Jia, C.H. Li, A.M. Li, Effective removal of glyphosate from water by resin-supported double valent nano-sized hydroxyl iron oxide, RSC advances, 7 (2017) 24430-24437.

[143] Y. Tao, F. Fang, Q. Lv, W. Qin, X. He, Y. Zhang, Y. Zhou, X. Li, J. Li, Highly efficient removal of glyphosate from water by hierarchical-pore UiO-66: Selectivity and effects of natural water particles, Journal of Environmental Management, 316 (2022) 115301.

[144] S. Naghdi, E. Brown, M. Zendehbad, A. Duong, W. Ipsmiller, S. Biswas, M.C. Toroker, H. Kazemian, D. Eder, Glyphosate adsorption from water using hierarchically porous metal–organic frameworks, Advanced Functional Materials, 33 (2023) 2213862.

[145] H. Park, A. May, L. Portilla, H. Dietrich, F. Münch, T. Rejek, M. Sarcletti, L. Banspach, D. Zahn, M. Halik, Magnetite nanoparticles as efficient materials for removal of glyphosate from water, Nature Sustainability, 3 (2020) 129-135.

[146] Q. Chen, J. Zheng, Q. Yang, Z. Dang, L. Zhang, Insights into the glyphosate adsorption behavior and mechanism by a $MnFe_2O_4$@cellulose-activated carbon magnetic hybrid, ACS Applied Materials & Interfaces, 11 (2019) 15478-15488.

[147] G.A. Grant, P.R. Fisher, J.E. Barrett, P.C. Wilson, Removal of agrichemicals from water using granular activated carbon filtration, Water, Air, & Soil Pollution, 230 (2018) 7.

[148] B. Geysels, T. Hiemstra, J.E. Groenenberg, R.N.J. Comans, Glyphosate binding and speciation at the water-goethite interface: A surface complexation model consistent with IR spectroscopy and MO/DFT, Water Research, 273 (2025) 123031.

[149] B. Geysels, T. Hiemstra, A.W.P. Vermeer, J.E. Groenenberg, A mechanistic surface complexation model for glyphosate adsorption to ferrihydrite in competition with phosphate, Water Research, 288 (2026) 124634.

[150] P. Czupryński, M. Płotka, P. Glamowski, W. Żukowski, T. Bajda, An assessment of an ion exchange resin system for the removal and recovery of Ni, Hg, and Cr from wet flue gas desulphurization wastewater-a pilot study, RSC advances, 12 (2022) 5145-5156.

[151] E. Çermikli, F. Şen, E. Altıok, J. Wolska, P. Cyganowski, N. Kabay, M. Bryjak, M. Arda, M. Yüksel, Performances of novel chelating ion exchange resins for boron and arsenic removal from saline geothermal water using adsorption-membrane filtration hybrid process, Desalination, 491 (2020) 114504.

[152] F.T. Lange, B. Post, Occurrence of glyphosate and AMPA in German rivers and their behaviour in drinking water treatment, in: Seminar on Glyphosate and Water, Monsanto Europe, Brussels, 2000, pp. 19–20.

[153] P. Yu, X. Li, X. Zhang, H. Zhou, Y. Xu, Y. Sun, H. Zheng, Insights into the glyphosate removal efficiency by using magnetic powder activated carbon composite, Separation and Purification Technology, 254 (2021) 117662.

[154] H.N. Tran, Y.-F. Wang, S.-J. You, H.-P. Chao, Insights into the mechanism of cationic dye adsorption on activated charcoal: The importance of π–π interactions, Process Safety and Environmental Protection, 107 (2017) 168-180.

[155] X. Zhu, B. Li, J. Yang, Y. Li, W. Zhao, J. Shi, J. Gu, Effective adsorption and enhanced removal of organophosphorus pesticides from aqueous solution by Zr-based MOFs of UiO-67, ACS Applied Materials & Interfaces, 7 (2015) 223-231.

[156] C. Li, Y. Li, Q. Li, J. Duan, J. Hou, Q. Hou, S. Ai, H. Li, Y. Yang, Regenerable magnetic aminated lignin/Fe_3O_4/$La(OH)_3$ adsorbents for the effective removal of phosphate and glyphosate, Science of The Total Environment, 788 (2021) 147812.

[157] D.A. Gkika, A.C. Mitropoulos, G.Z. Kyzas, Why reuse spent adsorbents? The latest challenges and limitations, Science of The Total Environment, 822 (2022) 153612.

[158] B. Van Der Bruggen, C. Vandecasteele, T. Van Gestel, W. Doyen, R. Leysen, A review of pressure-driven membrane processes in wastewater treatment and drinking water production, Environmental Progress, 22 (2003) 46-56.

[159] M. Giagnorio, S. Steffenino, L. Meucci, M.C. Zanetti, A. Tiraferri, Design and performance of a nanofiltration plant for the removal of chromium aimed at the production of safe potable water, Journal of Environmental Chemical Engineering, 6 (2018) 4467-4475.

[160] G.K. Pearce, UF/MF pre-treatment to RO in seawater and wastewater reuse applications: a comparison of energy costs, Desalination, 222 (2008) 66-73.

[161] F. Prézélus, L. Tiruta-Barna, J.-C. Remigy, C. Guigui, Process-based LCA of ultrafiltration for drinking water production, Water Research, 199 (2021) 117156.

[162] H. Saitúa, F. Giannini, A.P. Padilla, Drinking water obtaining by nanofiltration from waters contaminated with glyphosate formulations: Process evaluation by means of toxicity tests and studies on operating parameters, Journal of Hazardous Materials, 227-228 (2012) 204-210.

[163] A. Loi-Brügger, S. Panglisch, G. Hoffmann, P. Buchta, R. Gimbel, C.J. Nacke, Removal of trace organic substances from river bank filtrate – performance study of RO and NF membranes, Water Supply, 8 (2008) 85-92.

[164] P. Xu, J.E. Drewes, C. Bellona, G. Amy, T.U. Kim, M. Adam, T. Heberer, Rejection of emerging organic micropollutants in nanofiltration-reverse osmosis membrane applications, Water environment research : a research publication of the Water Environment Federation, 77 (2005) 40-48.

[165] K. Kimura, S. Toshima, G. Amy, Y. Watanabe, Rejection of neutral endocrine disrupting compounds (EDCs) and pharmaceutical active compounds (PhACs) by RO membranes, Journal of Membrane Science, 245 (2004) 71-78.

[166] A.H.C. Van Bruggen, M.M. He, K. Shin, V. Mai, K.C. Jeong, M.R. Finckh, J.G. Morris, Environmental and health effects of the herbicide glyphosate, Science of The Total Environment, 616-617 (2018) 255-268.

[167] W. Guo, H.-H. Ngo, J. Li, A mini-review on membrane fouling, Bioresource Technology, 122 (2012) 27-34.

[168] B. Díez, R. Rosal, A critical review of membrane modification techniques for fouling and biofouling control in pressure-driven membrane processes, Nanotechnology for Environmental Engineering, 5 (2020) 15.

[169] A. Subramani, J.G. Jacangelo, Treatment technologies for reverse osmosis concentrate volume minimization: A review, Separation and Purification Technology, 122 (2014) 472-489.

[170] D. Feng, A. Soric, O. Boutin, Treatment technologies and degradation pathways of glyphosate: A critical review, Science of The Total Environment, 742 (2020) 140559.

[171] L. Borella, G. Novello, M. Gasparotto, G. Renella, M. Roverso, S. Bogialli, F. Filippini, E. Sforza, Design and experimental validation of an optimized microalgae-bacteria consortium for the bioremediation of glyphosate in continuous photobioreactors, Journal of Hazardous Materials, 441 (2023) 129921.

[172] S. Firdous, S. Iqbal, S. Anwar, Optimization and modeling of glyphosate biodegradation by a novel *Comamonas odontotermitis* P2 through response surface methodology, Pedosphere, 30 (2020) 618-627.

[173] J. Georgin, D. Stracke Pfingsten Franco, C. Gindri Ramos, H. Nguyen Tran, A. Benettayeb, G. Imanova, I. Ali, Recent advances in removing glyphosate herbicide and its aminomethylphosphonic acid metabolite in water, Journal of Molecular Liquids, 402 (2024) 124786.

[174] M. Priyadarshini, I. Das, M.M. Ghangrekar, L. Blaney, Advanced oxidation processes: Performance, advantages, and scale-up of emerging technologies, Journal of Environmental Management, 316 (2022) 115295.

[175] M.R. Assalin, S.G. De Moraes, S.C.N. Queiroz, V.L. Ferracini, N. Duran, Studies on degradation of glyphosate by several oxidative chemical processes: Ozonation, photolysis and heterogeneous photocatalysis, Journal of Environmental Science and Health, Part B, 45 (2009) 89-94.

[176] L. Chen, S. Zhou, Y. Xu, Y. Sun, H. Zheng, Effective glyphosate degradation through the combination of ozone/hydrogen peroxide oxidation and coagulation, Desalination and Water Treatment, 204 (2020) 377-387.

[177] Y. Chen, F. Wu, Y. Lin, N. Deng, N. Bazhin, E. Glebov, Photodegradation of glyphosate in the ferrioxalate system, Journal of Hazardous Materials, 148 (2007) 360-365.

[178] Y. Yang, Q. Deng, W. Yan, C. Jing, Y. Zhang, Comparative study of glyphosate removal on goethite and magnetite: Adsorption and photo-degradation, Chemical Engineering Journal, 352 (2018) 581-589.

[179] D. Chen, R. Zhao, H. Liu, H. Tian, Y. Tian, D. Huang, D. Johnson, Y. Huang, Selective photo-Fenton degradation of glyphosate using Schiff base metal complexes: Insights into metal-mediated pathways, Journal of Cleaner Production, 491 (2025) 144837.

[180] M.H. Tran, H.C. Nguyen, T.S. Le, V.A.D. Dang, T.H. Cao, C.K. Le, T.D. Dang, Degradation of glyphosate herbicide by an electro-Fenton process using carbon felt cathode, Environmental Technology, 42 (2021) 1155-1164.

[181] Y. Xie, R. Xiong, J. Li, W. Li, X. Yang, H. Tong, Insight into n-CaO_2/SBC/Fe(II) Fenton-like system for glyphosate degradation: pH change, iron conversion, and mechanism, Journal of Environmental Management, 333 (2023) 117428.

[182] N. Tran, P. Drogui, T.L. Doan, T.S. Le, H.C. Nguyen, Electrochemical degradation and mineralization of glyphosate herbicide, Environmental Technology, 38 (2017) 2939-2948.

[183] M.N. Chong, B. Jin, C.W.K. Chow, C. Saint, Recent developments in photocatalytic water treatment technology: A review, Water Research, 44 (2010) 2997-3027.

[184] F.-Y. Chen, Z.-Y. Wu, Z. Adler, H. Wang, Stability challenges of electrocatalytic oxygen evolution reaction: From mechanistic understanding to reactor design, Joule, 5 (2021) 1704-1731.

[185] T.F. Qahtan, T.O. Owolabi, O.E. Olubi, A. Hezam, State-of-the-art, challenges and prospects of heterogeneous tandem photocatalysis, Coordination Chemistry Reviews, 492 (2023) 215276.

[186] H. Chen, S. Chen, X. Quan, Y. Zhang, Structuring a TiO_2-based photonic crystal photocatalyst with Schottky junction for efficient photocatalysis, Environmental Science & Technology, 44 (2010) 451-455.

[187] J. Schneider, M. Matsuoka, M. Takeuchi, J. Zhang, Y. Horiuchi, M. Anpo, D.W. Bahnemann, Understanding TiO_2 photocatalysis: Mechanisms and materials, Chemical Reviews, 114 (2014) 9919-9986.

[188] A.L. Linsebigler, G. Lu, J.T. Yates, Jr., Photocatalysis on TiO_2 surfaces: Principles, mechanisms, and selected results, Chemical Reviews, 95 (1995) 735-758.

[189] P. Garcia-Muñoz, W. Dachtler, B. Altmayer, R. Schulz, D. Robert, F. Seitz, R. Rosenfeldt, N. Keller, Reaction pathways, kinetics and toxicity assessment during the photocatalytic degradation of glyphosate and myclobutanil pesticides: Influence of the aqueous matrix, Chemical Engineering Journal, 384 (2020) 123315.

[190] J.Q. Chen, Z.J. Hu, N.X. Wang, Photocatalytic mineralization of glyphosate in a small-scale plug flow simulation reactor by UV/TiO_2, Journal of Environmental Science and Health - Part B, 47 (2012) 579-588.

[191] S. Chen, Y. Liu, Study on the photocatalytic degradation of glyphosate by TiO_2 photocatalyst, Chemosphere, 67 (2007) 1010-1017.

[192] J. Löwenberg, A. Zenker, M. Baggenstos, G. Koch, C. Kazner, T. Wintgens, Comparison of two PAC/UF processes for the removal of micropollutants from wastewater treatment plant effluent: Process performance and removal efficiency, Water Research, 56 (2014) 26-36.

[193] C. Stoquart, P. Servais, P.R. Bérubé, B. Barbeau, Hybrid membrane processes using activated carbon treatment for drinking water: A review, Journal of Membrane Science, 411-412 (2012) 1-12.

[194] P. Awasthi, G.K. Agrahari, A. Patel, A. Singh, Hybrid membrane technology with renewably derived biological and photocatalytic systems for wastewater treatment, Biodegradation, 36 (2025) 77.

[195] R. Lyubimenko, O.I. Gutierrez Cardenas, A. Turshatov, B.S. Richards, A.I. Schäfer, Photodegradation of steroid-hormone micropollutants in a flow-through membrane reactor coated with Pd(II)-porphyrin, Applied Catalysis B: Environmental, (2021) 120097.

[196] E. Worch, Chapter 5 - Adsorption kinetics, in: Adsorption technology in water treatment: Fundamentals, processes, and modeling, De Gruyter, 2012, pp. 140-168.

[197] P.B. Trinh, A.I. Schäfer, Adsorption of glyphosate and metabolite aminomethylphosphonic acid (AMPA) from water by polymer-based spherical activated carbon (PBSAC), Journal of Hazardous Materials, (2023) 131211.

[198] K. Sen, N.K. Mondal, Glyphosate adsorptive behaviour using magnetic activated carbon: kinetics, isotherms, and DFT study, Biomass Conversion and Biorefinery, (2022).

[199] I. Herath, P. Kumarathilaka, M.I. Al-Wabel, A. Abduljabbar, M. Ahmad, A.R.A. Usman, M. Vithanage, Mechanistic modeling of glyphosate interaction with rice husk derived engineered biochar, Microporous and Mesoporous Materials, 225 (2016) 280-288.

[200] R. Chang, Chapter 11 - Intermolecular forces and liquids and solids, in: Chemistry, 10th edition, McGraw-Hill Education, 2009.

[201] Z. Adamczyk, Chapter 2 - Potential interactions among particles, in: Z. Adamczyk (Ed.) Particles at interfaces: Interactions, deposition, structure, Elsevier, Interface Science and Technology, 2006, pp. 15-196.

[202] K. Kendall, Adhesion: molecules and mechanics, Science, 263 (1994) 1720-1725.

[203] M. Nishio, Y. Umezawa, J. Fantini, M.S. Weiss, P. Chakrabarti, CH–π hydrogen bonds in biological macromolecules, Physical Chemistry Chemical Physics, 16 (2014) 12648-12683.

[204] C.R. Kennedy, S. Lin, E.N. Jacobsen, The cation-π interaction in small-molecule catalysis, Angewandte Chemie International Edition, 55 (2016) 12596-12624.

[205] A. Tkatchenko, L. Romaner, O.T. Hofmann, E. Zojer, C. Ambrosch-Draxl, M. Scheffler, Van der Waals interactions between organic adsorbates and at organic/inorganic interfaces, MRS Bulletin, 35 (2011) 435-442.

[206] M. Tagliavini, F. Engel, P.G. Weidler, T. Scherer, A.I. Schäfer, Adsorption of steroid micropollutants on polymer-based spherical activated carbon (PBSAC), Journal of Hazardous Materials, 337 (2017) 126-137.

[207] M. Tagliavini, P.G. Weidler, C. Njel, J. Pohl, D. Richter, B. Böhringer, A.I. Schäfer, Polymer-based spherical activated carbon – ultrafiltration (UF-PBSAC) for the adsorption of steroid hormones from water: Material characteristics and process configuration, Water Research, 185 (2020) 116249.

[208] Y. Yoon, P. Westerhoff, S.A. Snyder, Adsorption of ^{3}H-labeled 17-β estradiol on powdered activated carbon, Water, Air, and Soil Pollution, 166 (2005) 343-351.

[209] E. Partlan, K. Davis, Y. Ren, O.G. Apul, O.T. Mefford, T. Karanfil, D.A. Ladner, Effect of bead milling on chemical and physical characteristics of activated carbons pulverized to superfine sizes, Water Research, 89 (2016) 161-170.

[210] B. Böhringer, O. Guerra Gonzalez, I. Eckle, M. Müller, J.-M. Giebelhausen, C. Schrage, S. Fichtner, Polymer-based spherical activated carbons – From adsorptive properties to filter performance, Chemie Ingenieur Technik, 83 (2011) 53-60.

[211] H. Klefer, M. Munoz, A. Modrow, B. Böhringer, P. Wasserscheid, B.J.M. Etzold, Polymer-based spherical activated carbon as easy-to-handle catalyst support for hydrogenation reactions, Chemical Engineering & Technology, 39 (2016) 276-284.

[212] M. Fuerhacker, A. Dürauer, A. Jungbauer, Adsorption isotherms of 17β-estradiol on granular activated carbon (GAC), Chemosphere, 44 (2001) 1573-1579.

[213] J. Kim, Z. Cai, M.M. Benjamin, Effects of adsorbents on membrane fouling by natural organic matter, Journal of Membrane Science, 310 (2008) 356-364.

[214] C.-W. Li, Y.-S. Chen, Fouling of UF membrane by humic substance: Effects of molecular weight and powder-activated carbon (PAC) pre-treatment, Desalination, 170 (2004) 59-67.

[215] J. Wolters, M. Tagliavini, A.I. Schäfer, Removal of steroid hormone micropollutants by UF-PBSAC composite in presence of organic matter, Journal of Membrane Science, 592 (2019) 117315.

[216] K. Ebie, F. Li, Y. Azuma, A. Yuasa, T. Hagishita, Pore distribution effect of activated carbon in adsorbing organic micropollutants from natural water, Water Research, 35 (2001) 167-179.

[217] R. Guillossou, J. Le Roux, R. Mailler, C.S. Pereira-Derome, G. Varrault, A. Bressy, E. Vulliet, C. Morlay, F. Nauleau, V. Rocher, J. Gasperi, Influence of dissolved organic matter on the removal of 12 organic micropollutants from wastewater effluent by powdered activated carbon adsorption, Water Research, 172 (2020) 115487.

[218] F. Zietzschmann, E. Worch, J. Altmann, A.S. Ruhl, A. Sperlich, F. Meinel, M. Jekel, Impact of EfOM size on competition in activated carbon adsorption of organic micro-pollutants from treated wastewater, Water Research, 65 (2014) 297-306.

[219] S. Shao, L. Cai, K. Li, J. Li, X. Du, G. Li, H. Liang, Deposition of powdered activated carbon (PAC) on ultrafiltration (UF) membrane surface: influencing factors and mechanisms, Journal of Membrane Science, 530 (2017) 104-111.

[220] J.R. Ellerie, O.G. Apul, T. Karanfil, D.A. Ladner, Comparing graphene, carbon nanotubes, and superfine powdered activated carbon as adsorptive coating materials for microfiltration membranes, Journal of Hazardous Materials, 261 (2013) 91-98.

[221] M.N. Nguyen, P.B. Trinh, C.J. Burkhardt, A.I. Schäfer, Incorporation of single-walled carbon nanotubes in ultrafiltration support structure for the removal of steroid hormone micropollutants, Separation and Purification Technology, 264 (2021) 118405.

[222] A. Freixa, V. Acuña, J. Sanchís, M. Farré, D. Barceló, S. Sabater, Ecotoxicological effects of carbon based nanomaterials in aquatic organisms, Science of The Total Environment, 619-620 (2018) 328-337.

[223] L. Paredes, C. Alfonsin, T. Allegue, F. Omil, M. Carballa, Integrating granular activated carbon in the post-treatment of membrane and settler effluents to improve organic micropollutants removal, Chemical Engineering Journal, 345 (2018) 79-86.

[224] E. Worch, Chapter 6 - Adsorption dynamics in fixed-bed adsorbers, in: Adsorption technology in water treatment: Fundamentals, processes, and modeling, De Gruyter, 2012, pp. 169-193.

[225] H. Fan, M. Heiranian, M. Elimelech, The solution-diffusion model for water transport in reverse osmosis: What went wrong?, Desalination, 580 (2024) 117575.

[226] L. Wang, J. He, M. Heiranian, H. Fan, L. Song, Y. Li, M. Elimelech, Water transport in reverse osmosis membranes is governed by pore flow, not a solution-diffusion mechanism, Science Advances, 9 (2023) eadf8488.

[227] L.F. Villalobos, J. Zhang, M. Elimelech, Nanofiltration for circularity: Fit-for-purpose design and evaluation, One Earth, 6 (2023) 767-771.

[228] A.J.C. Semião, A.I. Schäfer, Removal of adsorbing estrogenic micropollutants by nanofiltration membranes. Part A—Experimental evidence, Journal of Membrane Science, 431 (2013) 244-256.

[229] S. Castaño Osorio, P.M. Biesheuvel, E. Spruijt, J.E. Dykstra, A. van der Wal, Modeling micropollutant removal by nanofiltration and reverse osmosis membranes: Considerations and challenges, Water Research, 225 (2022) 119130.

[230] Y. Yoon, P. Westerhoff, S.A. Snyder, E.C. Wert, Nanofiltration and ultrafiltration of endocrine disrupting compounds, pharmaceuticals and personal care products, Journal of Membrane Science, 270 (2006) 88-100.

[231] L.D. Nghiem, A.I. Schäfer, M. Elimelech, Pharmaceutical retention mechanisms by nanofiltration membranes, Environmental Science & Technology, 39 (2005) 7698-7705.

[232] Y. Cheng, H. Ding, Y. Liu, D. He, L.E. Peng, H. Matsuyama, M. Hu, X. Li, Fabrication of polyethersulfone/sulfonated polysulfone loose nanofiltration membranes for enhanced selectivity of pharmaceuticals and personal care products and minerals, Separation and Purification Technology, 337 (2024) 126466.

[233] R.-y. Fu, T. Zhang, X.-m. Wang, Rigorous determination of pore size non-uniformity for nanofiltration membranes by incorporating the effects on mass transport, Desalination, 549 (2023) 116318.

[234] V. Freger, Nanoscale heterogeneity of polyamide membranes formed by interfacial polymerization, Langmuir : the ACS journal of surfaces and colloids, 19 (2003) 4791-4797.

[235] X. Song, B. Gan, S. Qi, H. Guo, C.Y. Tang, Y. Zhou, C. Gao, Intrinsic nanoscale structure of thin film composite polyamide membranes: Connectivity, defects, and structure–property correlation, Environmental Science & Technology, 54 (2020) 3559-3569.

[236] E.E. Chang, C.-H. Liang, C.-P. Huang, P.-C. Chiang, A simplified method for elucidating the effect of size exclusion on nanofiltration membranes, Separation and Purification Technology, 85 (2012) 1-7.

[237] A.E. Yaroshchuk, Non-steric mechanisms of nanofiltration: superposition of Donnan and dielectric exclusion, Separation and Purification Technology, 22-23 (2001) 143-158.

[238] R. Epsztein, E. Shaulsky, N. Dizge, D.M. Warsinger, M. Elimelech, Role of ionic charge density in Donnan exclusion of monovalent anions by nanofiltration, Environmental Science & Technology, 52 (2018) 4108-4116.

[239] B. Van der Bruggen, J. Schaep, D. Wilms, C. Vandecasteele, Influence of molecular size, polarity and charge on the retention of organic molecules by nanofiltration, Journal of Membrane Science, 156 (1999) 29-41.

[240] R.S. Roth, L. Birnhack, M. Avidar, E.A. Hjelvik, A.P. Straub, R. Epsztein, Effect of solution ions on the charge and performance of nanofiltration membranes, npj Clean Water, 7 (2024) 25.

[241] L.D. Nghiem, A.I. Schäfer, M. Elimelech, Role of electrostatic interactions in the retention of pharmaceutically active contaminants by a loose nanofiltration membrane, Journal of Membrane Science, 286 (2006) 52-59.

[242] W.R. Bowen, J.S. Welfoot, Modelling the performance of membrane nanofiltration—critical assessment and model development, Chemical Engineering Science, 57 (2002) 1121-1137.

[243] Y.-A. Boussouga, H. Than, A.I. Schäfer, Selenium species removal by nanofiltration: Determination of retention mechanisms, Science of The Total Environment, 829 (2022) 154287.

[244] Y.-A. Boussouga, T. Okkali, T. Luxbacher, A.I. Schäfer, Chromium (III) and chromium (VI) removal and organic matter interaction with nanofiltration, Science of The Total Environment, 885 (2023) 163695.

[245] D.L. Oatley, L. Llenas, R. Pérez, P.M. Williams, X. Martínez-Lladó, M. Rovira, Review of the dielectric properties of nanofiltration membranes and verification of the single oriented layer approximation, Advances in Colloid and Interface Science, 173 (2012) 1-11.

[246] S. You, J. Lu, C.Y. Tang, X. Wang, Rejection of heavy metals in acidic wastewater by a novel thin-film inorganic forward osmosis membrane, Chemical Engineering Journal, 320 (2017) 532-538.

[247] V. Freger, Dielectric exclusion, an éminence grise, Advances in Colloid and Interface Science, 319 (2023) 102972.

[248] X. Zhai, S. Lin, X. Li, Z. Wang, The hidden role of the dielectric effect in nanofiltration: A novel perspective to unravel new ion separation mechanisms, Environmental Science & Technology, 58 (2024) 15874-15884.

[249] S. Bandini, D. Vezzani, Nanofiltration modeling: the role of dielectric exclusion in membrane characterization, Chemical Engineering Science, 58 (2003) 3303-3326.

[250] M. Manciu, E. Ruckenstein, The polarization model for hydration/double layer interactions: the role of the electrolyte ions, Advances in Colloid and Interface Science, 112 (2004) 109-128.

[251] B. Saliha, F. Patrick, S. Anthony, Investigating nanofiltration of multi-ionic solutions using the steric, electric and dielectric exclusion model, Chemical Engineering Science, 64 (2009) 3789-3798.

[252] A. Szymczyk, P. Fievet, Investigating transport properties of nanofiltration membranes by means of a steric, electric and dielectric exclusion model, Journal of Membrane Science, 252 (2005) 77-88.

[253] R. Wang, S. Lin, Pore model for nanofiltration: History, theoretical framework, key predictions, limitations, and prospects, Journal of Membrane Science, 620 (2021) 118809.

[254] A.E. Yaroshchuk, Dielectric exclusion of ions from membranes, Advances in Colloid and Interface Science, 85 (2000) 193-230.

[255] W. Liu, X.-M. Wang, D. Li, Y. Gao, K. Wang, X. Huang, Dominant mechanism of nanofiltration for chloride/sulfate ion separation in high salinity solutions: The quantification of pore size-influenced dielectric exclusion, Environmental Science & Technology, 59 (2025) 5848-5855.

[256] L.A. Richards, A.I. Schäfer, B.S. Richards, B. Corry, The importance of dehydration in determining ion transport in narrow pores, Small, 8 (2012) 1701-1709.

[257] M. Zocchi, R. Sommaruga, Microplastics modify the toxicity of glyphosate on Daphnia magna, Science of The Total Environment, 697 (2019) 134194.

[258] K. Boussu, C. Vandecasteele, B. Van der Bruggen, Relation between membrane characteristics and performance in nanofiltration, Journal of Membrane Science, 310 (2008) 51-65.

[259] Q. Guo, C. Zhou, Z. Ma, X. Yang, Fundamentals of TiO_2 photocatalysis: Concepts, mechanisms, and challenges, Advanced Materials, 31 (2019) 1901997.

[260] R.A. Deshpande, J. Navne, M.V. Adelmark, E. Shkondin, A. Crovetto, O. Hansen, J. Bachmann, R. Taboryski, Understanding the light induced hydrophilicity of metal-oxide thin films, Nature Communications, 15 (2024) 124.

[261] G.R. Buettner, The pecking order of free radicals and antioxidants: Lipid peroxidation, α-tocopherol, and ascorbate, Archives of Biochemistry and Biophysics, 300 (1993) 535-543.

[262] C.D. Vecitis, H. Park, J. Cheng, B.T. Mader, M.R. Hoffmann, Treatment technologies for aqueous perfluorooctanesulfonate (PFOS) and perfluorooctanoate (PFOA), Frontiers of Environmental Science & Engineering in China, 3 (2009) 129-151.

[263] J.M. Burns, W.J. Cooper, J.L. Ferry, D.W. King, B.P. DiMento, K. McNeill, C.J. Miller, W.L. Miller, B.M. Peake, S.A. Rusak, A.L. Rose, T.D. Waite, Methods for reactive oxygen species (ROS) detection in aqueous environments, Aquatic Sciences, 74 (2012) 683-734.

[264] S. Nonell, C. Flors, Steady-state and time-resolved singlet oxygen phosphorescence detection in the near-IR, in: S. Nonell, C. Flors, S. Nonell, C. Flors (Eds.) Singlet Oxygen: Applications in Biosciences and Nanosciences, The Royal Society of Chemistry, 2016, pp. 0.

[265] A.V. Demyanenko, A.S. Bogomolov, N.V. Dozmorov, A.I. Svyatova, A.P. Pyryaeva, V.G. Goldort, S.A. Kochubei, A.V. Baklanov, Singlet oxygen $^1O_2$ in photocatalysis on TiO_2. Where does it come from?, The Journal of Physical Chemistry C, 123 (2019) 2175-2181.

[266] S. Riaz, S.-J. Park, An overview of TiO_2-based photocatalytic membrane reactors for water and wastewater treatments, Journal of Industrial and Engineering Chemistry, 84 (2020) 23-41.

[267] M. Sun, H. Li, D.P. Jaisi, Degradation of glyphosate and bioavailability of phosphorus derived from glyphosate in a soil-water system, Water Research, 163 (2019) 114840.

[268] H. Li, A.F. Wallace, M. Sun, P. Reardon, D.P. Jaisi, Degradation of glyphosate by Mn-oxide may bypass sarcosine and form glycine directly after C–N bond cleavage, Environmental Science & Technology, 52 (2018) 1109-1117.

[269] Y. Chen, Y. Huang, H. Tian, L. Ye, R. Li, C. Chen, Z. Dai, D. Huang, Fluorine-doped $BiVO_4$ photocatalyst: Preferential cleavage of C−N bond for green degradation of glyphosate, Journal of Environmental Sciences, 127 (2023) 60-68.

[270] L.D. Freedman, G.O. Doak, The preparation and properties of phosphonic acids, Chemical Reviews, 57 (1957) 479-523.

[271] W. Ma, J. He, L. Han, C. Ma, Y. Cai, X. Guo, Z. Yang, Hydrophilic fraction of dissolved organic matter largely facilitated microplastics photoaging: Insights from redox properties and reactive oxygen species, Environmental Science & Technology, 58 (2024) 11625-11636.

[272] Y. Guo, Y. Zhang, G. Yu, Y. Wang, Revisiting the role of reactive oxygen species for pollutant abatement during catalytic ozonation: The probe approach versus the scavenger approach, Applied Catalysis B: Environmental, 280 (2021) 119418.

[273] S. Zhang, T. Hedtke, Q. Zhu, M. Sun, S. Weon, Y. Zhao, E. Stavitski, M. Elimelech, J.-H. Kim, Membrane-confined iron oxychloride nanocatalysts for highly efficient heterogeneous fenton water treatment, Environmental Science & Technology, 55 (2021) 9266-9275.

[274] S. Nandy, S.A. Savant, S. Haussener, Prospects and challenges in designing photocatalytic particle suspension reactors for solar fuel processing, Chemical Science, 12 (2021) 9866-9884.

[275] S. Kundu, N. Karak, Polymeric photocatalytic membrane: An emerging solution for environmental remediation, Chemical Engineering Journal, 438 (2022) 135575.

[276] N. Rosman, W.N.W. Salleh, M.A. Mohamed, J. Jaafar, A.F. Ismail, Z. Harun, Hybrid membrane filtration-advanced oxidation processes for removal of pharmaceutical residue, Journal of Colloid and Interface Science, 532 (2018) 236-260.

[277] D.D. Phan, F. Babick, M.T. Nguyen, B. Wessely, M. Stintz, Modelling the influence of mass transfer on fixed-bed photocatalytic membrane reactors, Chemical Engineering Science, 173 (2017) 242-252.

[278] M.d.l.M. Ballari, R. Brandi, O. Alfano, A. Cassano, Mass transfer limitations in photocatalytic reactors employing titanium dioxide suspensions: I. Concentration profiles in the bulk, Chemical Engineering Journal, 136 (2008) 50-65.

[279] R. Lyubimenko, A. Turshatov, A. Welle, P.G. Weidler, B.S. Richards, A.I. Schäfer, Enhanced photocatalytic efficiency via improved contact in a solar-driven membrane reactor for steroid hormone removal, Chemical Engineering Journal, 451 (2023) 138449.

[280] M.F.J. Dijkstra, A. Michorius, H. Buwalda, H.J. Panneman, J.G.M. Winkelman, A.A.C.M. Beenackers, Comparison of the efficiency of immobilized and suspended systems in photocatalytic degradation, Catalysis Today, 66 (2001) 487-494.

[281] S.S. Chin, K. Chiang, A.G. Fane, The stability of polymeric membranes in a TiO_2 photocatalysis process, Journal of Membrane Science, 275 (2006) 202-211.

[282] C.S. Raota, S. Lotfi, R. Lyubimenko, B.S. Richards, A.I. Schäfer, Accelerated ageing method for the determination of photostability of polymer-based photocatalytic membranes, Journal of Membrane Science, 686 (2023) 121944.

[283] J. Kim, K. Park, D.R. Yang, S. Hong, A comprehensive review of energy consumption of seawater reverse osmosis desalination plants, Applied Energy, 254 (2019) 113652.

[284] D. Mousel, L. Palmowski, J. Pinnekamp, Energy demand for elimination of organic micropollutants in municipal wastewater treatment plants, Science of The Total Environment, 575 (2017) 1139-1149.

[285] C. Echevarría, C. Valderrama, J.L. Cortina, I. Martín, M. Arnaldos, X. Bernat, A. De la Cal, M.R. Boleda, A. Vega, A. Teuler, E. Castellví, Hybrid sorption and pressure-driven membrane technologies for organic micropollutants removal in advanced water reclamation: A techno-economic assessment, Journal of Cleaner Production, 273 (2020) 123108.

[286] D.S. Saal, P. Arocena, A. Maziotis, T. Triebs, Scale and scope economies and the efficient vertical and horizontal configuration of the water industry: A survey of the literature, Review of Network Economics, 12 (2013) 93-129.

[287] T. Guo, J. Englehardt, T. Wu, Review of cost versus scale: water and wastewater treatment and reuse processes, Water science and technology : a journal of the International Association on Water Pollution Research, 69 (2014) 223-234.

[288] M. Krajewska, M.N. Nguyen, A.I. Schäfer, Interference of the real water matrix with micropollutant removal via advanced filtration: Insights from the Goreangab reservoir in Namibia, Environmental Science & Technology, 60 (2026) 8193-8204.

[289] P.B. Trinh, D.J. Mattern, A.I. Schäfer, Determination of glyphosate (GLY) and aminomethylphosphonic acid (AMPA) in water by direct injection liquid chromatography tandem mass spectrometry (LC-MS/MS), submitted to ChemSusChem, (2025).

[290] A.M. Botero-Coy, M. Ibáñez, J.V. Sancho, F. Hernández, Direct liquid chromatography–tandem mass spectrometry determination of underivatized glyphosate in rice, maize and soybean, Journal of Chromatography A, 1313 (2013) 157-165.

[291] C.S. Ho, C.W. Lam, M.H. Chan, R.C. Cheung, L.K. Law, L.C. Lit, K.F. Ng, M.W. Suen, H.L. Tai, Electrospray ionisation mass spectrometry: principles and clinical applications, Clinical Biochemist Reviews, 24 (2003) 3-12.

[292] M. Wilm, Principles of electrospray ionization, Molecular & Cellular Proteomics, 10 (2011) M111.009407.

[293] N. Fang, S. Yu, M.J. Ronis, T.M. Badger, Matrix effects break the LC behavior rule for analytes in LC-MS/MS analysis of biological samples, Experimental Biology and Medicine (Maywood), 240 (2015) 488-497.

[294] K. Müller, D. Zahn, T. Frömel, T.P. Knepper, Matrix effects in the analysis of polar organic water contaminants with HILIC-ESI-MS, Analytical and Bioanalytical Chemistry, 412 (2020) 4867-4879.

[295] Hellma GmbH & Co. KG, Safety data sheet: Hellmanex lll in: Hellma GmbH & Co. KG (Ed.), 2018.

[296] M. Anastassiades, A.-K. Wachtler, D.I. Kolberg, E. Eichhorn, H. Marks, A. Benkenstein, S. Zechmann, D. Mack, C. Wildgrube, A. Barth, I. Sigalov, S. Goerlich, D. Dörk, G. Cerchia, Quick method for the analysis of highly polar pesticides in food involving extraction with acidified methanol and LC- or IC-MS/MS Measurement I. Food of plant origin (QuPPe-PO-Method), Version 12.2, in: European Uion reference laboratory for pesticides requiring single residue methods, 2023.

[297] European Union reference laboratories for residues of pesticides, SANTE 11312/2021 v2: Analytical quality control and method validation procedures for pesticides residue analysis in food and feed, in, 2021.

[298] M. Posselt, A. Jaeger, J.L. Schaper, M. Radke, J.P. Benskin, Determination of polar organic micropollutants in surface and pore water by high-resolution sampling-direct injection-ultra high performance liquid chromatography-tandem mass spectrometry, Environmental Science: Processes & Impacts, 20 (2018) 1716-1727.

[299] A. Tan, S. Hussain, A. Musuku, R. Massé, Internal standard response variations during incurred sample analysis by LC–MS/MS: Case by case trouble-shooting, Journal of Chromatography B, 877 (2009) 3201-3209.

[300] SIELC, accessed in 2022, Obelisc N, https://www.sielc.com/Products_Obelisc_N.html, accessed 06-03 2020.

[301] B. Chen, M.G. Bartlett, Evaluation of mobile phase composition for enhancing sensitivity of targeted quantification of oligonucleotides using ultra-high performance liquid chromatography and mass spectrometry: Application to phosphorothioate deoxyribonucleic acid, Journal of Chromatography A, 1288 (2013) 73-81.

[302] Y. Hua, D. Jenke, Increasing the sensitivity of an LC–MS method for screening material extracts for organic extractables via mobile phase optimization, Journal of Chromatographic Science, 50 (2012) 213-227.

[303] R.B. Cole, Electrospray ionization mass spectrometry: Fundamentals, instrumentation and applications, 1999.

[304] R. Lyubimenko, B.S. Richards, A. Turshatov, A.I. Schäfer, Separation and degradation detection of nanogram-per-litre concentrations of radiolabelled steroid hormones using combined liquid chromatography and flow scintillation analysis, Scientific Reports, 10 (2020) 7095.

[305] T.L. Constantopoulos, G.S. Jackson, C.G. Enke, Effects of salt concentration on analyte response using electrospray ionization mass spectrometry, Journal of the American Society for Mass Spectrometry, 10 (1999) 625-634.

[306] T. Van Der Laan, T. Kloots, M. Beekman, A. Kindt, A.-C. Dubbelman, A. Harms, C.M. Van Duijn, P.E. Slagboom, T. Hankemeier, Fast LC-ESI-MS/MS analysis and influence of sampling conditions for gut metabolites in plasma and serum, Scientific Reports, 9 (2019) 12370.

[307] W. Skeff, C. Recknagel, D.E. Schulz-Bull, The influence of salt matrices on the reversed-phase liquid chromatography behavior and electrospray ionization tandem mass spectrometry detection of glyphosate, glufosinate, aminomethylphosphonic acid and 2-aminoethylphosphonic acid in water, Journal of Chromatography A, 1475 (2016) 64-73.

[308] F. Carnevale Neto, V. Pascua, D. Raftery, Formation of sodium cluster ions complicates liquid chromatography-mass spectrometry metabolomics analyses, Rapid communications in mass spectrometry : RCM, 35 (2021) e9175.

[309] US Environmental Protection Agency, 2016, Definition and procedure for the determination of the method detection limit, revision 2, accessed 08.08 2023, https://www.epa.gov/sites/default/files/2016-12/documents/mdl-procedure_rev2_12-13-2016.pdf.

[310] Deutsche Institut für Normung, DIN ISO 16308- Wasserbeschaffenheit - Bestimmung von Glyphosat und AMPA - Verfahren mittels Hochleistungs-Flüssigkeitschromatographie (HPLC) mit tandem-massenspektrometrischer Detektion, in, 2017.

[311] Y.-A. Boussouga, F. Sacher, A.I. Schäfer, Water quality of The Gambia River: A prospective drinking water supply, Science of The Total Environment, 878 (2023) 162794.

[312] P.B. Trinh, A.I. Schäfer, Corrigendum to “Adsorption of glyphosate and metabolite aminomethylphosphonic acid (AMPA) from water by polymer-based spherical activated carbon (PBSAC)”, Journal of Hazardous Materials, 470 (2024) 134136.

[313] M. Rafatullah, O. Sulaiman, R. Hashim, A. Ahmad, Adsorption of methylene blue on low-cost adsorbents: A review, Journal of Hazardous Materials, 177 (2010) 70-80.

[314] E. Worch, Chapter 8 - Desorption and reactivation, in: Adsorption technology in water treatment: Fundamentals, processes, and modeling, De Gruyter, 2012, pp. 253-263.

[315] Z. Lu, X. Liu, X. Zhu, H. Lu, Y. Ma, B. Zhang, S. Huang, M. Xiang, G. Hu, Y. Yu, Rational design of mixed-ligand metal–organic framework with dual emission signals for real-time visual detection and efficient adsorption of glyphosate in water, Journal of Hazardous Materials, 494 (2025) 138683.

[316] Y. Du, Z. Liu, F. He, Fabrication of a novel bifunctional magnetic nanocomposite for colorimetric detection and removal of glyphosate, Journal of Hazardous Materials, 484 (2025) 136772.

[317] F. Julien, M. Baudu, M. Mazet, Relationship between chemical and physical surface properties of activated carbon, Water Research, 32 (1998) 3414-3424.

[318] R.W. Stevens, Jr., R.V. Siriwardane, J. Logan, In situ fourier transform infrared (FTIR) investigation of CO_2 adsorption onto zeolite materials, Energy & Fuels, 22 (2008) 3070-3079.

[319] B.C. Smith, The C=O bond, Part III: Carboxylic acids, Spectroscopy, 33 (2018) 14–20.

[320] D.I. Hitchcock, The formal identity of Langmuir's adsorption equation with the law of mass action, Journal of the American Chemical Society, 48 (1926) 2870-2870.

[321] X. Guo, J. Wang, A general kinetic model for adsorption: Theoretical analysis and modeling, Journal of Molecular Liquids, 288 (2019) 111100.

[322] Y. Liu, L. Shen, From Langmuir kinetics to first- and second-order rate equations for adsorption, Langmuir : the ACS journal of surfaces and colloids, 24 (2008) 11625-11630.

[323] J. Weber Walter, J.C. Morris, Kinetics of adsorption on carbon from solution, Journal of the Sanitary Engineering Division, 89 (1963) 31-59.

[324] S. Lagergren, Zur theorie der sogenannten adsorption gelöster stoffe, Zeitschrift für Chemie und Industrie der Kolloide, 24 (1898) 1–39.

[325] Y.S. Ho, G. McKay, Pseudo-second order model for sorption processes, Process Biochemistry, 34 (1999) 451-465.

[326] K.Y. Foo, B.H. Hameed, Insights into the modeling of adsorption isotherm systems, Chemical Engineering Journal, 156 (2010) 2-10.

[327] E.C. Lima, A. Hosseini-Bandegharaei, J.C. Moreno-Piraján, I. Anastopoulos, A critical review of the estimation of the thermodynamic parameters on adsorption equilibria. Wrong use of equilibrium constant in the Van't Hoof equation for calculation of thermodynamic parameters of adsorption, Journal of Molecular Liquids, 273 (2019) 425-434.

[328] I. Langmuir, The adsorption of gases on plane surfaces of glass, mica and platinum, Journal of the American Chemical Society, 40 (1918) 1361-1403.

[329] H. Freundlich, Über die adsorption in lösungen, Zeitschrift für Physikalische Chemie, 57 (1907) 385 - 470.

[330] Y. Liu, Is the free energy change of adsorption correctly calculated?, Journal of Chemical & Engineering Data, 54 (2009) 1981-1985.

[331] A. Torres-Knoop, A. Poursaeidesfahani, T.J.H. Vlugt, D. Dubbeldam, Behavior of the enthalpy of adsorption in nanoporous materials close to saturation conditions, Journal of Chemical Theory and Computation, 13 (2017) 3326-3339.

[332] D.D. Do, Adsorption analysis: Equilibria and kinetics, Imperial college press, 1998.

[333] W. Rudzinski, W. Plazinski, Theoretical description of the kinetics of solute adsorption at heterogeneous solid/solution interfaces: On the possibility of distinguishing between the diffusional and the surface reaction kinetics models, Applied Surface Science, 253 (2007) 5827-5840.

[334] M.J. Sanchez Martín, M.V. Villa, M. Sánchez-Camazano, Glyphosate-hydrotalcite interaction as influenced by pH, Clays and Clay Minerals, 47 (1999) 777-783.

[335] L. Li, P.A. Quinlivan, D.R.U. Knappe, Effects of activated carbon surface chemistry and pore structure on the adsorption of organic contaminants from aqueous solution, Carbon, 40 (2002) 2085-2100.

[336] E. Worch, Chapter 7 - Fixed-bed adsorber design, in: Adsorption technology in water treatment: Fundamentals, processes, and modeling, De Gruyter, 2012, pp. 197-252.

[337] B. Li, Z. Lei, Z. Huang, Surface-treated activated carbon for removal of aromatic compounds from water, Chemical Engineering & Technology, 32 (2009) 763-770.

[338] Y. Li, C. Zhao, Y. Wen, Y. Wang, Y. Yang, Adsorption performance and mechanism of magnetic reduced graphene oxide in glyphosate contaminated water, Environmental science and pollution research international,, 25 (2018) 21036-21048.

[339] J.J. Alvear-Daza, A. Cánneva, J.A. Donadelli, M. Manrique-Holguín, J.A. Rengifo-Herrera, L.R. Pizzio, Removal of diclofenac and ibuprofen on mesoporous activated carbon from agro-industrial wastes prepared by optimized synthesis employing a central composite design, Biomass Conversion and Biorefinery, 13 (2022) 13197–13219.

[340] J. Comer, R. Chen, H. Poblete, A. Vergara-Jaque, J.E. Riviere, Predicting adsorption affinities of small molecules on carbon nanotubes using molecular dynamics simulation, ACS Nano, 9 (2015) 11761-11774.

[341] J. Zhou, N. Saeidi, L.Y. Wick, F.-D. Kopinke, A. Georgi, Adsorption of polar and ionic organic compounds on activated carbon: Surface chemistry matters, Science of The Total Environment, 794 (2021) 148508.

[342] M. Kah, G. Sigmund, F. Xiao, T. Hofmann, Sorption of ionizable and ionic organic compounds to biochar, activated carbon and other carbonaceous materials, Water Research, 124 (2017) 673-692.

[343] J.N. Israelachvili, The nature of van der waals forces, Contemporary Physics, 15 (1974) 159-178.

[344] E.M. Pérez, N. Martín, π–π interactions in carbon nanostructures, Chemical Society Reviews, 44 (2015) 6425-6433.

[345] H. Horth, K. Blackmore, Survey of glyphosate and AMPA in groundwaters and surface waters in Europe, in, Monsanto, 2009.

[346] M. Silva da Rocha, K. Iha, A.C. Faleiros, E.J. Corat, M.E.V. Suárez-Iha, Henry's law as a limit for an isotherm model based on a statistical mechanics approach, Journal of Colloid and Interface Science, 208 (1998) 211-215.

[347] B.M. Aumeier, H. Graul, A.-K. Müller, C. Lackmann, R. Wünsch, T. Wintgens, H. Hollert, M. Wessling, The hydrothermal solution for self-sustaining drinking water purification at point of use, Water Research, 170 (2020) 115338.

[348] M. Doğan, M. Alkan, Removal of methyl violet from aqueous solution by perlite, Journal of Colloid and Interface Science, 267 (2003) 32-41.

[349] V.J. Inglezakis, A.A. Zorpas, Heat of adsorption, adsorption energy and activation energy in adsorption and ion exchange systems, Desalination and Water Treatment, 39 (2012) 149-157.

[350] G. McKay, The adsorption of dyestuffs from aqueous solutions using activated carbon. III. intraparticle diffusion processes, Journal of Chemical Technology and Biotechnology. Chemical Technology, 33 (1983) 196-204.

[351] M.D. LeVan, G. Carta, C.M. Yon, Section 16: Adsorption and ion exchange, in: 8th (Ed.) Perry's chemical engineers' handbook, McGraw-Hill, 2008.

[352] P.B. Trinh, A.I. Schäfer, Removal of glyphosate (GLY) and aminomethylphosphonic acid (AMPA) by ultrafiltration with permeate-side polymer-based spherical activated carbon (UF–PBSAC), Water Research, 250 (2024) 121021.

[353] M. Tagliavini, A.I. Schäfer, Removal of steroid micropollutants by polymer-based spherical activated carbon (PBSAC) assisted membrane filtration, Journal of Hazardous Materials, 353 (2018) 514-521.

[354] A. Imbrogno, A.I. Schäfer, Comparative study of nanofiltration membrane characterization devices of different dimension and configuration (cross flow and dead end), Journal of Membrane Science, 585 (2019) 67-80.

[355] S. Lotfi, K. Fischer, A. Schulze, A.I. Schäfer, Photocatalytic degradation of steroid hormone micropollutants by TiO_2-coated polyethersulfone membranes in a continuous flow-through process, Nature Nanotechnology, 17 (2022) 417-423.

[356] E.M. Thurman, Aquatic humic substances, in: E.M. Thurman (Ed.) Organic geochemistry of natural waters, Springer Netherlands, Dordrecht, 1985, pp. 273-361.

[357] H.K. Shon, S. Vigneswaran, S.A. Snyder, Effluent organic matter (EfOM) in wastewater: Constituents, effects, and treatment, Critical Reviews in Environmental Science and Technology, 36 (2006) 327-374.

[358] S.N. Nam, G. Amy, Differentiation of wastewater effluent organic matter (EfOM) from natural organic matter (NOM) using multiple analytical techniques, Water Science & Technology, 57 (2008) 1009-1015.

[359] International Association for the Properties of Water and Steam, 2008, Release on the IAPWS formulation 2008 for the viscosity of ordinary water substance, accessed accessed on 30 April 2025, https://www.iapws.org/relguide/visc.pdf.

[360] S.Q. de Aguiar Filho, A.M.F. Costa, A.K. dos Santos Pereira, G.S. Cavallini, D.H. Pereira, Interaction of glyphosate in matrices of cellulose and diethylaminoethyl cellulose biopolymers: Theoretical viewpoint of the adsorption process, Journal of Molecular Modeling, 27 (2021) 272.

[361] M. Tagliavini, M.N. Nguyen, A.I. Schäfer, Predicting steroid hormone removal in a thin activated carbon layer coupled with ultrafiltration, Chemical Engineering Journal, 462 (2023) 142125.

[362] G.M. Walker, L.R. Weatherley, Adsorption of acid dyes on to granular activated carbon in fixed beds, Water Research, 31 (1997) 2093-2101.

[363] A. Imbrogno, A.I. Schäfer, Micropollutants breakthrough curve phenomena in nanofiltration: Impact of operational parameters, Separation and Purification Technology, 267 (2021) 118406.

[364] L.F. Greenlee, D.F. Lawler, B.D. Freeman, B. Marrot, P. Moulin, Reverse osmosis desalination: Water sources, technology, and today's challenges, Water Research, 43 (2009) 2317-2348.

[365] P.B. Trinh, M.N. Nguyen, Z. Futera, B. Minofar, M. Personeni, P.B. Petersen, A.I. Schäfer, The role of hydration in the removal of glyphosate (GLY) and aminomethylphosphonic acid (AMPA) by nanofiltration membranes, Nature Communications, 17 (2026) 3741.

[366] M.C. Dodd, N.D. Vu, A. Ammann, V.C. Le, R. Kissner, H.V. Pham, T.H. Cao, M. Berg, U. von Gunten, Kinetics and mechanistic aspects of As(III) oxidation by aqueous chlorine, chloramines, and ozone: Relevance to drinking water treatment, Environmental Science & Technology, 40 (2006) 3285-3292.

[367] L. Qing, J. Tao, H. Yu, P. Jiang, C. Qiao, S. Zhao, H. Liu, A molecular model for ion dehydration in confined water, AIChE Journal, 66 (2020) e16938.

[368] M. Nilsson, G. Trägårdh, K. Östergren, The influence of sodium chloride on mass transfer in a polyamide nanofiltration membrane at elevated temperatures, Journal of Membrane Science, 280 (2006) 928-936.

[369] Y.-H. Cai, A.I. Schäfer, Renewable energy powered membrane technology: Impact of solar irradiance fluctuation on direct osmotic backwash, Journal of Membrane Science, 598 (2020) 117666.

[370] E. Idil Mouhoumed, A. Szymczyk, A. Schäfer, L. Paugam, Y.H. La, Physico-chemical characterization of polyamide NF/RO membranes: Insight from streaming current measurements, Journal of Membrane Science, 461 (2014) 130-138.

[371] P. Atkins, J. DePaula, J. Keeler, Atkins' Physical Chemistry, Oxford University Press, Oxford, 2006.

[372] R. Shang, A.R.D. Verliefde, J. Hu, Z. Zeng, J. Lu, A.J.B. Kemperman, H. Deng, K. Nijmeijer, S.G.J. Heijman, L.C. Rietveld, Tight ceramic UF membrane as RO pre-treatment: The role of electrostatic interactions on phosphate rejection, Water Research, 48 (2014) 498-507.

[373] K. Nörtemann, J. Hilland, U. Kaatze, Dielectric properties of aqueous NaCl solutions at microwave frequencies, The Journal of Physical Chemistry A, 101 (1997) 6864-6869.

[374] D.G. Archer, P.-m. Wang, The dielectric constant of water and Debye-Hückel limiting law slopes, Journal of Physical and Chemical Reference Data, 19 (1990) 371-411.

[375] J.K. Bungay, Synthetic membranes: Science, engineering and applications, Springer Science & Business Media, 2012.

[376] J. Schaep, C. Vandecasteele, B. Peeters, J. Luyten, C. Dotremont, D. Roels, Characteristics and retention properties of a mesoporous γ-Al_2O_3 membrane for nanofiltration, Journal of Membrane Science, 163 (1999) 229-237.

[377] S.S. Sablani, M.F.A. Goosen, R. Al-Belushi, M. Wilf, Concentration polarization in ultrafiltration and reverse osmosis: a critical review, Desalination, 141 (2001) 269-289.

[378] G. Jonsson, C. Boesen, Polarization phenomena in membrane processes, Synthetic Membrane Process, (1984) 101-130.

[379] G.B. van den Berg, I.G. Rácz, C.A. Smolders, Mass transfer coefficients in cross-flow ultrafiltration, Journal of Membrane Science, 47 (1989) 25-51.

[380] A. Schäfer, A.G. Fane, T.D. Waite, Nanofiltration: Principles and Applications, Elsevier, 2005.

[381] M.C. Porter, Concentration polarization with membrane ultrafiltration, Product R&D, 11 (1972) 234-248.

[382] C.P. Koutsou, A.J. Karabelas, Shear stresses and mass transfer at the base of a stirred filtration cell and corresponding conditions in narrow channels with spacers, Journal of Membrane Science, 399-400 (2012) 60-72.

[383] C.K. Colton, K.A. Smith, Mass transfer to a rotating fluid. Part II. Transport from the base of an agitated cylindrical tank, AIChE Journal, 18 (1972) 958-967.

[384] W.M. Deen, Hindered transport of large molecules in liquid-filled pores, AIChE Journal, 33 (1987) 1409-1425.

[385] C.Y. Tang, Y.-N. Kwon, J.O. Leckie, Probing the nano- and micro-scales of reverse osmosis membranes—A comprehensive characterization of physiochemical properties of uncoated and coated membranes by XPS, TEM, ATR-FTIR, and streaming potential measurements, Journal of Membrane Science, 287 (2007) 146-156.

[386] L.D. Nghiem, Removal of emerging trace organic contaminants by nanofiltration and reverse osmosis, in, University of Wollongong, 2005.

[387] Y.-l. Liu, X.-m. Wang, H.-w. Yang, Y.F. Xie, Adsorption of pharmaceuticals onto isolated polyamide active layer of NF/RO membranes, Chemosphere, 200 (2018) 36-47.

[388] Lenntech, Chlorine tolerant spiral wound nanofiltration: Color removal membrane elements, in, 2002.

[389] G. Dagher, G. Saab, A. Martin, G. Couturier, P. Candido, L. Moulin, J.P. Croué, B. Teychene, Understanding and predicting the adsorption and rejection of pesticides and metabolites by hollow fiber nanofiltration membranes, Separation and Purification Technology, 330 (2024) 125323.

[390] K.Y. Koh, S. Zhang, J. Paul Chen, Incorporation of lanthanum particles to polyethersulfone ultrafiltration membrane for specific phosphorus uptake: Method comparison and performance assessment, Journal of Colloid and Interface Science, 601 (2021) 242-253.

[391] A.I. Schäfer, I. Akanyeti, A.J.C. Semião, Micropollutant sorption to membrane polymers: A review of mechanisms for estrogens, Advances in Colloid and Interface Science, 164 (2011) 100-117.

[392] Z. Jiang, X. Huang, Q. Wu, M. Li, Q. Xie, Z. Liu, X. Zou, Adsorption of sulfonamides on polyamide microplastics in an aqueous solution: Behavior, structural effects, and its mechanism, Chemical Engineering Journal, 454 (2023) 140452.

[393] M.M. Ngoma, M. Mathaba, K. Moothi, Effect of carbon nanotubes loading and pressure on the performance of a polyethersulfone (PES)/carbon nanotubes (CNT) membrane, Scientific Reports, 11 (2021) 23805.

[394] H. Rho, K. Chon, J. Cho, Surface charge characterization of nanofiltration membranes by potentiometric titrations and electrophoresis: Functionality vs. zeta potential, Desalination, 427 (2018) 19-26.

[395] C. Song, B. Corry, Intrinsic ion selectivity of narrow hydrophobic pores, The Journal of Physical Chemistry B, 113 (2009) 7642-7649.

[396] V. Pavluchkov, I. Shefer, O. Peer-Haim, J. Blotevogel, R. Epsztein, Indications of ion dehydration in diffusion-only and pressure-driven nanofiltration, Journal of Membrane Science, 648 (2022) 120358.

[397] R. Epsztein, R.M. DuChanois, C.L. Ritt, A. Noy, M. Elimelech, Towards single-species selectivity of membranes with subnanometre pores, Nature Nanotechnology, 15 (2020) 426-436.

[398] L.A. Richards, B.S. Richards, B. Corry, A.I. Schäfer, Experimental energy barriers to anions transporting through nanofiltration membranes, Environmental Science & Technology, 47 (2013) 1968-1976.

[399] M. Andreev, J.J. de Pablo, A. Chremos, J.F. Douglas, Influence of ion solvation on the properties of electrolyte solutions, The Journal of Physical Chemistry B, 122 (2018) 4029-4034.

[400] V. Wieser, L.L.E. Mears, R.D. Barker, H.-W. Cheng, M. Valtiner, Hydration forces dominate surface charge dependent lipid bilayer interactions under physiological conditions, The Journal of Physical Chemistry Letters, 12 (2021) 9248-9252.

[401] C. Lu, C. Hu, Z. Chen, P. Wang, F. Feng, G. He, F. Wang, Y. Zhang, J.Z. Liu, X. Zhang, J. Qu, Dehydration-enhanced ion-pore interactions dominate anion transport and selectivity in nanochannels, Science Advances, 9 (2023) eadf8412.

[402] P.B. Trinh, S. Liu, N.F. Himma, B. Fiser, A.I. Schäfer, Continuous-flow photocatalytic degradation of glyphosate and aminomethylphosphonic acid under simulated sunlight with TiO_2-coated poly(vinylidene fluoride) membrane, Advanced Functional Materials, 36, no. 21 (2026) e11431.

[403] M. Muneer, C. Boxall, Photocatalyzed degradation of a pesticide derivative glyphosate in aqueous suspensions of titanium dioxide, International Journal of Photoenergy, 2008 (2008) 197346.

[404] K.P. Gopinath, N.V. Madhav, A. Krishnan, R. Malolan, G. Rangarajan, Present applications of titanium dioxide for the photocatalytic removal of pollutants from water: A review, Journal of Environmental Management, 270 (2020) 110906.

[405] S. Banerjee, S.C. Pillai, P. Falaras, K.E. O'Shea, J.A. Byrne, D.D. Dionysiou, New insights into the mechanism of visible light photocatalysis, The Journal of Physical Chemistry Letters, 5 (2014) 2543-2554.

[406] J. Xie, C. Zhang, T. David Waite, Integrated flow anodic oxidation and ultrafiltration system for continuous defluorination of perfluorooctanoic acid (PFOA), Water Research, 216 (2022) 118319.

[407] S. Chai, G. Zhao, Y. Wang, Y.-n. Zhang, Y. Wang, Y. Jin, X. Huang, Fabrication and enhanced electrocatalytic activity of 3D highly ordered macroporous PbO_2 electrode for recalcitrant pollutant incineration, Applied Catalysis B: Environmental, 147 (2014) 275-286.

[408] Y. Horiuchi, T. Toyao, M. Takeuchi, M. Matsuoka, M. Anpo, Recent advances in visible-light-responsive photocatalysts for hydrogen production and solar energy conversion – from semiconducting TiO_2 to MOF/PCP photocatalysts, Physical Chemistry Chemical Physics, 15 (2013) 13243-13253.

[409] H.S. Zakria, M.H.D. Othman, R. Kamaludin, S.H. Sheikh Abdul Kadir, T.A. Kurniawan, A. Jilani, Immobilization techniques of a photocatalyst into and onto a polymer membrane for photocatalytic activity, RSC advances, 11 (2021) 6985-7014.

[410] H. Ji, W. Liu, F. Sun, T. Huang, L. Chen, Y. Liu, J. Qi, C. Xie, D. Zhao, Experimental evidences and theoretical calculations on phenanthrene degradation in a solar-light-driven photocatalysis system using silica aerogel supported TiO_2 nanoparticles: Insights into reactive sites and energy evolution, Chemical Engineering Journal, 419 (2021) 129605.

[411] S.M. Fernandes, B.T. Barrocas, J.V. Nardeli, M.F. Montemor, E. Maçoas, M.C. Oliveira, C.C.C.R. de Carvalho, A. Lauria, M. Niederberger, A.C. Marques, Maximizing photocatalytic efficiency with minimal amount of gold: Solar-driven TiO_2 photocatalysis supported by MICROSCAFS® for facile catalyst recovery, Journal of Environmental Chemical Engineering, 12 (2024) 112043.

[412] S. Amiri, M. Anbia, Insights into the effect of parameters and pathway of visible-light photodegradation of glyphosate and diazinon by C-TiO_2/clinoptilolite nanocomposite, Journal of Photochemistry and Photobiology A: Chemistry, 446 (2024) 115146.

[413] S. Liu, E. Véron, S. Lotfi, K. Fischer, A. Schulze, A.I. Schäfer, Poly(vinylidene fluoride) membrane with immobilized TiO_2 for degradation of steroid hormone micropollutants in a photocatalytic membrane reactor, Journal of Hazardous Materials, 447 (2023) 130832.

[414] ASTM G173-03, Standard tables for reference solar spectral Irradiances: direct normal and hemispherical on 37° tilted surface, in: ASTM International: West Conshohocken, PA, 2012, 2012.

[415] R. Lyubimenko, B.S. Richards, A.I. Schäfer, A. Turshatov, Noble-metal-free photosensitizers for continuous-flow photochemical oxidation of steroid hormone micropollutants under sunlight, Journal of Membrane Science, 642 (2022) 119981.

[416] K. Fischer, P. Schulz, I. Atanasov, A. Abdul Latif, I. Thomas, M. Kühnert, A. Prager, J. Griebel, A. Schulze, Synthesis of high crystalline TiO_2 nanoparticles on a polymer membrane to degrade pollutants from water, Catalysts, 8 (2018) 376.

[417] A. Schulze, M.F. Maitz, R. Zimmermann, B. Marquardt, M. Fischer, C. Werner, M. Went, I. Thomas, Permanent surface modification by electron-beam-induced grafting of hydrophilic polymers to PVDF membranes, RSC advances, 3 (2013) 22518-22526.

[418] G.V. Buxton, C.L. Greenstock, W.P. Helman, A.B. Ross, Critical review of rate constants for reactions of hydrated electrons, hydrogen atoms and hydroxyl radicals ($\cdot OH/\cdot O^-$) in aqueous solution, Journal of Physical and Chemical Reference Data, 17 (1988) 513-886.

[419] Y. Liu, H. Guo, Y. Zhang, X. Cheng, P. Zhou, J. Wang, W. Li, Fe@C carbonized resin for peroxymonosulfate activation and bisphenol S degradation, Environmental Pollution, 252 (2019) 1042-1050.

[420] C. Liang, J.H. Lei, Identification of active radical species in alkaline persulfate oxidation, Water Environment Research, 87 (2015) 656-659.

[421] Y. Yang, J.J. Pignatello, J. Ma, W.A. Mitch, Comparison of halide impacts on the efficiency of contaminant degradation by sulfate and hydroxyl radical-based advanced oxidation processes (AOPs), Environmental Science & Technology, 48 (2014) 2344-2351.

[422] J. Ma, Y. Yang, X. Jiang, Z. Xie, X. Li, C. Chen, H. Chen, Impacts of inorganic anions and natural organic matter on thermally activated persulfate oxidation of BTEX in water, Chemosphere, 190 (2018) 296-306.

[423] P.S. Rao, E. Hayon, Redox potentials of free radicals. IV. Superoxide and hydroperoxy radicals $\cdot O_2^-$ and $\cdot HO_2$, The Journal of Physical Chemistry, 79 (1975) 397-402.

[424] G.E. Adams, B.D. Michael, Pulse radiolysis of benzoquinone and hydroquinone. Semiquinone formation by water elimination from trihydroxy-cyclohexadienyl radicals, Transactions of the Faraday Society, 63 (1967) 1171-1180.

[425] X. Cheng, H. Guo, Y. Zhang, X. Wu, Y. Liu, Non-photochemical production of singlet oxygen via activation of persulfate by carbon nanotubes, Water Research, 113 (2017) 80-88.

[426] T. Wang, Z. Jiang, T. An, G. Li, H. Zhao, P.K. Wong, Enhanced visible-light-driven photocatalytic bacterial inactivation by ultrathin carbon-coated magnetic cobalt ferrite nanoparticles, Environmental Science & Technology, 52 (2018) 4774-4784.

[427] D. Papagiannaki, C. Medana, R. Binetti, P. Calza, P. Roslev, Effect of UV-A, UV-B and UV-C irradiation of glyphosate on photolysis and mitigation of aquatic toxicity, Scientific Reports, 10 (2020) 20247.

[428] C.P.M. Bento, X. Yang, G. Gort, S. Xue, R. van Dam, P. Zomer, H.G.J. Mol, C.J. Ritsema, V. Geissen, Persistence of glyphosate and aminomethylphosphonic acid in loess soil under different combinations of temperature, soil moisture and light/darkness, Science of The Total Environment, 572 (2016) 301-311.

[429] Y. Huang, Z. Li, K. Yao, C. Chen, C. Deng, Y. Fang, R. Li, H. Tian, Suppressing toxic intermediates during photocatalytic degradation of glyphosate by controlling adsorption modes, Applied Catalysis B: Environmental, 299 (2021) 120671.

[430] S.M. Ilina, P. Ollivier, D. Slomberg, N. Baran, A. Pariat, N. Devau, N. Sani-Kast, M. Scheringer, J. Labille, Investigations into titanium dioxide nanoparticle and pesticide interactions in aqueous environments, Environmental Science: Nano, 4 (2017) 2055-2065.

[431] M. Ndjeri, A. Pensel, S. Peulon, V. Haldys, B. Desmazières, A. Chaussé, Degradation of glyphosate and AMPA (amino methylphosphonic acid) solutions by thin films of birnessite electrodeposited: A new design of material for remediation processes?, Colloids and Surfaces A: Physicochemical and Engineering Aspects, 435 (2013) 154-169.

[432] S. Venditti, A. Kiesch, J. Hansen, Fate of glyphosate and its metabolite AminoMethylPhosponic acid (AMPA) from point source through wastewater sludge and advanced treatment, Chemosphere, 340 (2023) 139843.

[433] M. Sadatsharifi, D.W. Ingersoll, M. Purgel, The fate of a hazardous herbicide: a DFT-based ab initio study on glyphosate degradation, Environmental Science: Processes & Impacts, 23 (2021) 1018-1028.

[434] J.M. Herrmann, Heterogeneous photocatalysis: state of the art and present applications, Topics in Catalysis, 34 (2005) 49-65.

[435] Z. Wang, J. Liu, Y. Dai, W. Dong, S. Zhang, J. Chen, Dimethyl sulfide photocatalytic degradation in a light-emitting-diode continuous reactor: Kinetic and mechanistic study, Industrial & Engineering Chemistry Research, 50 (2011) 7977-7984.

[436] B. Byrne, J. Liu, K.W. Bowman, M. Pascolini-Campbell, A. Chatterjee, S. Pandey, K. Miyazaki, G.R. van der Werf, D. Wunch, P.O. Wennberg, C.M. Roehl, S. Sinha, Carbon emissions from the 2023 Canadian wildfires, Nature, 633 (2024) 835-839.

[437] W. Yan, C. Jing, Molecular insights into glyphosate adsorption to goethite gained from ATR-FTIR, two-dimensional correlation spectroscopy, and DFT study, Environmental Science & Technology, 52 (2018) 1946-1953.

[438] S. Doyle, M. Garvey, C. Fowley, Removal of glyphosate from water through adsorption onto goethite nanoparticles, Environmental Nanotechnology, Monitoring & Management, 20 (2023) 100839.

[439] S.G. Patra, A. Mizrahi, D. Meyerstein, The role of carbonate in catalytic oxidations, Accounts of Chemical Research, 53 (2020) 2189-2200.

[440] Y. Guo, J. Long, J. Huang, G. Yu, Y. Wang, Can the commonly used quenching method really evaluate the role of reactive oxygen species in pollutant abatement during catalytic ozonation?, Water Research, 215 (2022) 118275.

[441] R. Dennington, T.A. Keith, J.M. Millam, GaussView, Version 6.0, in, Semichem Inc., Shawnee Mission, KS, 2016.

[442] M. Narimani, G. da Silva, Thermal decomposition kinetics of glyphosate (GP) and its metabolite aminomethylphosphonic acid (AMPA), Environmental Science: Processes & Impacts, 22 (2020) 152-160.

[443] E. Okada, J.L. Costa, F. Bedmar, Adsorption and mobility of glyphosate in different soils under no-till and conventional tillage, Geoderma, 263 (2016) 78-85.

[444] B.C. Barja, M. dos Santos Afonso, Aminomethylphosphonic acid and glyphosate adsorption onto goethite: A comparative study, Environmental Science & Technology, 39 (2005) 585-592.

[445] L.D. Nghiem, A.I. Schäfer, M. Elimelech, Removal of natural hormones by nanofiltration membranes: Measurement, modeling, and mechanisms, Environmental Science & Technology, 38 (2004) 1888-1896.

[446] L.D. Nghiem, A.I. Schäfer, T.D. Waite, Adsorptive interactions between membranes and trace contaminants, Desalination, 147 (2002) 269-274.

[447] L.D. Nghiem, A.I. Schäfer, Adsorption and transport of trace contaminant estrone in NF/RO membranes, Environmental Engineering Science, 19 (2002) 441-451.

[448] A.I. Schäfer, L.D. Nghiem, A. Meier, P.A. Neale, Impact of organic matrix compounds on the retention of steroid hormone estrone by a 'loose' nanofiltration membrane, Separation and Purification Technology, 73 (2010) 179-187.